ROYAUME DU MAROC
Université Mohammed V - RABAT -
جامعة محمد الخامس – الرباط –
Faculté des sciences
كلية العلوم
CENTRE D'ETUDES DOCTORALES - SCIENCES ET TECHNOLOGIES

N° d'ordre **3236**

THESE

En vue de l'obtention du: ***DOCTORAT***

Structure de Recherche : Laboratoire de la Matière Condensée et Sciences Interdisciplinaires
Discipline : Physique Informatique
Spécialité : Matière condensée et modélisation des systèmes énergétiques

Présentée et soutenue le 23/07/2019 par :

Marwan LAKHAL

Hydrogen Storage Properties of Magnesium Hydride MgH_2 by ab initio Calculations and Kinetic Monte Carlo Simulations (KMC)

JURY

Hamid EZ-ZAHRAOUY	PES, Faculté des sciences, Université Mohammed V-Rabat	Président
Mohamed BALLI	PES, Université Internationale-Rabat	Examinateur
Abdelilah BENYOUSSEF	PES, Académie Hassan II des sciences et techniques-Rabat	Examinateur
Abdallah El KENZ	PES, Faculté des sciences, Université Mohammed V-Rabat	Examinateur/rapporteur
El Kebir HLIL	PES, Institut Neel, Université de Grenoble-France	Examinateur/rapporteur
Abdelmajid JEMNI	PES, Ecole nationale des ingénieurs de Monastir-Tunisie	Examinateur
Mohammed LOULIDI	PES, Faculté des sciences, Université Mohammed V-Rabat	Directeur

Année Universitaire: **2018/2019**

✉ Faculté des Sciences, avenue Ibn Battouta, BP. 1014 RP, Rabat –Maroc
☎ 00212(05) 37 77 18 76 🖷 00212(05) 37 77 42 61; http://www. fsr.um5.ac.ma

Acknowledgments

This thesis was carried out at the Laboratory of Condensed Matter and Interdisciplinary Sciences (LaMCScI) of Faculty of Science, University of Mohammed V-Rabat, Morocco under the supervision of Prof. **Mohammed LOULIDI**.

First, I would like to express my very great appreciation, deep gratitude and sincere thanks to my supervisor **Mohammed LOULIDI**, for his indispensable practical teaching and supervision, for all of the encouragements and supports that he gave me, on my research works, on my publications and the thesis write-up. I wish to thank you Prof. **Mohammed LOULIDI** for your patience in revising my papers and thesis, for providing invaluable insight and constructive criticism to the work I have done. It has truly been a great pleasure to work with you. It is a privilege to be your student.
I would like also to thank Prof. **Mohammed LOULIDI** for reviewing this Ph.D thesis.

I would also thank the thesis committee for reviewing my work and giving their insightful and useful comments. It is an honor for me that they agree to judge this work.

I would like to thank Prof. **Hamid EZ-ZAHRAOUY** from University Mohammed V-Rabat, Faculty of Science, to be the president of the jury members of this thesis.

I would like also to offer my thanks to Prof. **Abdallah EL KENZ** from University Mohammed V-Rabat, Faculty of Science, for reporting and reviewing this PhD thesis.

I would also like to extend my thanks to Prof. **El Kebir HLIL** from Institut Néel, Grenoble, France, for reporting and reviewing this PhD thesis.

I would like also to thank Prof. **Mohamed BALLI** from International University of Rabat, for reviewing my Ph.D thesis.

I would like to express my thanks to Prof. **Abdelilah BENYOUSSEF**, from Académie Hassan II des sciences et techniques of Rabat, for reviewing this thesis.

I would like also to express my thanks to Prof. **Abdelmajid JEMNI** from Ecole Nationale des Ingénieurs of Monastir, Tunisia, for reviewing this Ph.D thesis.

I would like to point out that this work was done as part of the activities of the hydrogen storage group of the Laboratory of Condensed Matter and Interdisciplinary Sciences (LaMCScI) composed of professors, doctors and PhD students. The obtained results and the published works are the result of many years of hard work, long hours of effort and deep reflection of each of the founding members of the team. I thank all the members of the hydrogen storage team whom without their expertise this project could not have been accomplished. My sincere thanks to them for their efforts, their support and their encouragement.

I would like to take this opportunity to express my sincere gratitude to Prof. **Omar MOUNKACHI**, Dr. **Mohammed BHIHI**, Dr. **Hicham LABRIM**, Dr. **Sufyan NAJI**, Prof. **Adil BELHAJ**, Dr. **Mustapha ABDELLAOUI**, **Mourad GARARA** and **Hind BENZIDI** for the interesting discussions, contributions, for their generous assistance and their friendship. My thanks also go to my LaMCScI's colleagues Dr. **Mourad BOUJNAH**, Dr. **Noureddine LAKOUARI**, Dr. **Zakaryaa ZARHRI**, Dr. **Adil MARJAOUI**, Prof. **Halima ZAARI**, **Anass SIBARI**, **Ahmed Al-SHAMI**, also to Prof. **Lahoucine BAHMAD**, Prof. **Mohammed HAMEDOUN**, Prof. **Outmane OUBRAM**, Dr. **Fadoua EL-YAHYAOUI**, Mme. **Karima ECHTIOUI** and **Abdrrahim TRALI**.

Finally, my gratitude goes to my two mothers and two fathers, my brother, my aunts and uncles, my cousins, to my friends and every people who helped and supported me in any way during my Ph.D studies.

Abstract

Actually, hydrogen is considered as one of the most promising energy carriers alternatively to the fossil fuels. However, the development of hydrogen faces a significant problem concerning its storage. Alternative were proposed including high pressure gas cylinders, liquid hydrogen, physisorption of hydrogen on materials with a high specific surface area, and hydrogen storage through hydrides, e.g. Magnesium hydrides. The latter is very promising due to its high hydrogen storage capacities.

In order to study the hydrogen storage in the magnesium hydride (MgH_2), understand the underlying physical mechanisms and provide approaches that improve its hydrogen storage properties and meet the DoE criterions, we carried out a theoretical investigations of the thermodynamic properties by using ab initio calculations (DFT) and the sorption kinetic properties by developing a Kinetic Monte Carlo simulation method (KMC).

The calculation results show that pure MgH_2 involves high stability, high desorption temperature and slow kinetic even at high pressure and temperature which agree with the experimental results founding in the literature. However, the simulations show that the addition of small amounts of Ti, V, Fe, Ni and Al, the nano-structuring from bulk to thin films and/or by applying a strain improves considerably its thermodynamic and kinetic properties.

Key words: Hydrogen storage; MgH_2; DFT; Kinetic Monte Carlo; Kinetic properties; Thermodynamic properties; activation energies.

Résumé

Récemment, l'hydrogène est considéré comme l'un des vecteurs énergétiques les plus prometteurs par rapport aux combustibles fossiles et le stockage de l'hydrogène dans des hydrures tel que l'hydrure de magnésium est très prometteur en raison de ses hautes capacités.

Afin d'étudier le stockage d'hydrogène dans l'hydrure de magnésium (MgH_2), de comprendre les mécanismes physiques sous-jacents et de proposer des approches qui améliorent ses propriétés de stockage d'hydrogène et répondent aux critères de la DoE, nous avons mené, dans cette thèse, une étude théorique des propriétés thermodynamiques à l'aide de calculs ab initio (DFT) et les propriétés cinétiques de sorption en développant un algorithme basé sur la méthode de simulation dite Monte Carlo cinétique (KMC).

Les résultats obtenus montrent que le MgH_2 pur a une haute stabilité, une température de désorption élevée et une cinétique d'ab/désorption d'hydrogène lente même à des pressions et températures élevées, ce qui est en accord avec les études expérimentales trouvé dans la littérature. Cependant, les simulations montrent que l'ajout de faible quantités de Ti, V, Fe, Ni et Al, la nano-structuration vers les nano-couches et/ou l'application de contraintes mécanique améliorent les propriétés thermodynamiques et cinétiques de MgH_2 sans trop influencer ces hautes capacités.

Mots clés: Stockage de l'hydrogène; MgH_2; DFT; Monte Carlo cinétique; Température de désorption; Enthalpie de formation; Energie d'activation.

Résumé détaillé

Comme il est bien connu, la technologie de stockage de l'hydrogène devient rapidement une alternative aux combustibles fossiles et le stockage de l'hydrogène dans des composés à l'état solide semble être la solution la plus pratique étant donné qu'il s'agit d'une méthode plus sûre que la compression à haute pression ou la liquéfaction à faible température. À cet égard, l'hydrure de magnésium est un composé potentiel pour le stockage de l'hydrogène à l'état solide en raison de ses capacités de stockage élevées gravimétrique ainsi que volumétrique ($7,66\%$ en poids et $110 g/l.H_2$ respectivement). Cependant, il souffre d'une cinétique lente et d'une température de décomposition élevée, ce qui limite son utilisation en tant que matériau pour les systèmes de stockage d'hydrogène embarqués.

Afin d'étudier le stockage de l'hydrogène dans l'hydrure de magnésium (MgH_2), de comprendre les mécanismes physiques sous-jacents et de proposer des approches qui améliorent ses propriétés de stockage de l'hydrogène tout en répondant aux critères de la *DoE*, nous avons mené une étude théorique des propriétés thermodynamiques en utilisant les calculs ab initio (DFT) et des propriétés cinétiques de sorption en développant un model basé sur la méthode de simulation dite Monte Carlo cinétique (KMC).

Premièrement, nous avons examiné les propriétés structurales et thermodynamiques de MgH_2 pur par principe de la DFT. Les résultats des calculs montrent que MgH_2 a une énergie de formation élevée et par conséquent une haute stabilité et une température de désorption élevée, ce qui est en accord avec les résultats expérimentaux trouvés dans la littérature. Par la suite, en étudiant la structure électronique de MgH_2, nous avons montré que cette stabilité élevée est due à la forte hybridation entre les atomes de magnésium et d'hydrogène et que l'ajout d'une petite quantité de $M= Al, Ti, V, Fe, Ni$, ou la nanostructuration en couches minces et/ou l'application des contraintes réduit considérablement cette hybridation, ce qui améliore les propriétés de stockage de l'hydrogène dans l'hydrure de magnésium sans influencer ces hautes capacités volumétrique et gravimétrique.

Deuxièmement, et pour la première fois pour ce matériaux, nous proposons un modèle pour étudier les propriétés cinétiques d'absorption et de désorption d'hydrogène de l'hydrure de magnésium pur et MgH_2 dopé avec différents métaux M ($M = Al, Ti, V, Fe$

et Ni) en utilisant les simulations de Monte Carlo cinétiques. Dans ces investigations numériques, les énergies d'activation calculées par la méthode DFT pour différents processus élémentaires sont implémentées dans notre algorithme. Ainsi, en définissant la relation entre le temps simulé et les pas de Monte Carlo, nous avons pu simuler la cinétique d'absorption/désorption de l'hydrogène de MgH_2 pure et dopé en fonction de la température et de la pression.
Les résultats obtenus montrent que MgH_2 pur a une cinétique lente, même à haute température, ce qui est dû d'une part au fait que l'hydrure de magnésium présente des énergies d'activation élevées de la dissociation des molécules H_2 et de la diffusion d'hydrogene, et d'autre part aux atomes d'hydrogène qui préfèrent diffuser le long des directions X et Y au lieu de se déplacer verticalement Puisque les énergies d'activation de la diffusion de l'hydrogène dans les plans (001) sont inférieures aux barrières d'énergie nécessaires pour les déplacements entre plans. De plus, nous avons montré que l'incorporation de petites quantités de Al, Ti, V, Fe et Ni dans MgH_2 diminué considérablement les barrières énergétiques nécessaires aux différents mécanismes et conduit par conséquent à une amélioration considérable de la cinétique de sorption du matériau.

De cette façon nous avons pu étudier les propriétés de stockage de l'hydrogène de MgH_2 et proposer des méthodes pour améliorer les propriétés thermodynamique et cinétique du composé tout en gardant les hautes capacités du matériau intactes. Suite à notre étude, nous remarquons que le dopage avec Ni présente les meilleures performances et constitue l'élément le plus approprié pour un meilleur stockage de l'hydrogène.

Contents

List of Figures

List of Tables

List of abbreviations

DoE	Department of Energy
CNTs	Carbon nanotubes
MOFs	Metal organic framework
TPES	Total primary energy supply
GHG	Greenhouse gas
PV	Photovoltaics
ICE	Internal combustion engine
PEM	proton exchange membrane
PEMFC	proton exchange membrane fuel cell
DMFC	Direct Methanol Fuel Cell
PAFC	Phosphoric Acid Fuel Cell
AFC	Alkaline Fuel Cell
SOFC	Solid Oxide Fuel Cell
MCFC	Molten Carbon Fuel Cell
COFs	Covalent organic frameworks
PIMs	Polymers of intrinsic micro-porosity
SWNT	Single wall structure
MWNT	Mmultiple wall structure
HCP	Hexagonal close-packed
DC	Direct current
RF	Radio frequency
UHV	Ultra-high vacuum
C_g	Gravimetric capacity
C_v	Volumetric capacity
wt.	Weight
T_{des}	Desorption Temperature
P	Equilibrium pressure
T	Temperature
R	The gas constant
E_a	Activation energy
K_β	Boltzmann constant
G	Free energy
ΔH	Heat of formation
ΔS	Entropy
E_{tot}	Energy total
DOS	Density of states
PDOS	Partial desnity of states
VB	Valence band
CB	Conduction band
TM	Transition metal

ab initio	First principal calculation
Ψ	Many-body wave function of electrons
$\hbar$	Planck's constant devised by 2π
e	Charge of the electron
m_e	Mass of the electron
M_I	Mass of the nucleus
Z_I	Charge of the nucleus
R_I	Position of the nuclei
r_i	Position of electron
T_e	Kinetic energies of the electrons
T_n	kinetic energies of the the nuclei
V_{int}	Internal potential
V_{ext}	External potential
V_{nn}	nucleus-nucleus potential
$n_H(z)$	Number of hydrogen in plan z
$n_S(z)$	Number of interstitial sites in plan z
$\rho(z)$	Density of Hydrogen in plan z
t_{eq}	Equilibrium time
t_f	Filling time
t_r	Relaxation time
V_{ee}	Electron electron potential
V_{KS}	Effective potential
$V_H(r)$	Hartree potential
$V_{xc}(r)$	Exchange-correlation potential
$\hat{H}$	Hamiltonian operator
Z	Partition function
LDA	Local density approximation
LSDA	Local Spin-Density approximation
GGA	Generalized gradient approximation
MC	Monte Carlo
MMC	Metropolis Monte Carlo
MCMC	Markov chain Monte Carlo
KMC	Kinetic Monte Carlo
ΔE	Energies difference
F	Hydrogen flux
M_{H_2}	Molecular mass of hydrogen
P_i	probability
R_i	The rate transition
R	Total rate transition
DFT	Density functional theory

Introduction

Energy is one of the basic requirements in our daily lives and the world's energy demand is continuously increasing over the years due to the ever-increasing growth in the human population as well as economic development [1, 2, 3]. At present, the most of energy demands are fulfilled by fossil fuels which are depleting at an alarming rate since fossil fuels are non-renewable sources of energy. In addition, fossil fuels are the main contributor of greenhouse gas emissions that have a negative impact on human health and environment in the long term. Hence, there is a critical need to develop alternative sources of energy in replacement of fossil fuels.

Renewable energy sources such as hydro, solar, geothermal, and wind sources, including bio-fuels are possible solutions for replacing fossil fuels [4]. However, for a more efficient use of renewable energy sources, in particular for transportation, there is great demand for means of energy storage (i.e. secondary energy) that allows on-demand release and mobility. Among the various kinds of secondary energy sources converted from various primary energy resources, hydrogen energy can be considered as one of the most potential alternative.

Hydrogen is the earth's most abundant element, non-toxic, renewable and zero carbon emission when used in proton exchange membrane (PEM) fuel cells [3, 5]. However, for broader and more conventional usage of hydrogen energy, a few limitations in its production, storage, and distribution need to be overcome [6, 7, 8]. The major disadvantage with hydrogen storage originates from the lower volumetric density of the hydrogen [9, 10]. Studies show that $1kg$ of hydrogen is equivalent to $2.75kg$ of gasoline, but when this ratio is considered as a volume, $1L$ of hydrogen is required for the same obtained energy from $0.27L$ of gas [11]. Much effort has been made to develop hydrogen storage systems that are safe, cost-effective, environmental-friendly and more importantly with high energy densities [12].

For optimal use of hydrogen, the anticipated gas storage characteristics are high gravimetric and volumetric densities, low sorption temperature and heat transfer, good reversibility, fast reaction kinetics and low cost [13]. Current technologies used for hydrogen storage include compression in gas cylinders, liquefaction in cryogenic tanks and adsorption/absorption into solid state compounds. Storage as compressed and liquefied

hydrogen involves high pressure [14] and very low temperature (cryogenic temperature) [15] respectively, additionally to high maintenance costs which limit their use for on-board storage application. Among the three types of hydrogen storage technologies, the storage of hydrogen in solid state compounds appears to be the most feasible solution since it is a safer and more convenient method compared to high-pressure compression and liquefaction technologies.

Generally, hydrogen storage in solid state material can be classified into two broad categories, namely physical adsorption and chemical absorption [16, 17, 18, 19, 20, 21]. In large surface and porous materials, the hydrogen molecules can be adsorbed on the surface and pores via physisorption through the van der Waals interactions. In metal hydrides, the hydrogen atoms are chemically bonded with metallic elements such as intermetallic hydrides, complex hydrides and elemental hydrides. These latter are potential compounds for solid-state hydrogen storage .

Among numerous candidates, Mg and its hydride (MgH_2) are considered as a highly promising material to store the hydrogen in terms of gravimetric and volumetric capacities [22]. However, because of its higher thermodynamic stability and sluggish hydrogen sorption kinetics, the sorption temperature is much higher than practical applications and the sorption time is long, limiting for practical usage [23].

A large number of studies have been carried out to provide strategies to tackle the limitations of Mg based hydrogen storage system and synthesize low-cost metal hydrides with low absorption/desorption temperatures, high gravimetric and volumetric hydrogen storage densities, good resistance to oxidation, good reversibility and cyclic ability, fast kinetics and reactivity, and moderate thermodynamic stability. In general, studies have shown that the hydrogen storage properties of magnesuim hydride can be improved by: (1) the addition of appropriate catalysts into the metal hydride, (2) alloying with other hydride, material or their oxides [24, 25, 26, 27, 28] and (3) reduction of the MgH_2 size (nano-structuring) [16, 29]. Despite the important scientific effort, a clear description of how these procedures enhance the thermodynamic and kinetic properties of MgH_2 is still missing. An understanding of the mechanisms by which additives and nano-structuring effectively change the properties of the Mg–H reaction may help guide the development of even more effective additives.

For this reason, we opted for a theoretical approach, based on numerical simulation calculations, to study the hydrogen storage properties of the magnesium hydride, to understand and explain the mechanisms that operate in it. These calculations are made using a combination of the first principle method, also called ab initio calculations (DFT), and kinetic Monte Carlo simulations (KMC). The first method is used to study the thermodynamic properties of MgH_2 while the second one allows us to simulate the kinetic of absorption and desorption of hydrogen.

This study is organized as follows:

- The first chapter is devoted to the presentation of the hydrogen properties from its production to the mode of use, reviewing the different types and methods of hydrogen storage focusing on the storage properties of magnesium hydride.
- The second chapter is devoted to introduce the theoretical frame that we use to study the magnesium's hydrogen storage properties namely ab initio calculations (DFT) and Kinetic Monte Carlo simulations (KMC).
- In chapter 3, firstly, we provide an examination of structural and thermodynamic properties of MgH_2 by first principal. The results of calculations based on density functional theory are quantitatively compared with the experimental values of heat of formation and desorption temperature of bulk MgH_2. Also, an investigation of the electronic structure (density of states) of the pure MgH_2 is done. Secondly, the influence of small amount of Al, Ti, V, Fe, Ni additive, the nano-structuring from bulk to thin films and/or to applying the strain features on the hydrogen-magnesium interaction are examined.
- In the last chapter, and for the first time for this material, we give a model based on kinetic Monte Carlo method to investigate the hydrogen diffusion in the pure magnesium hydride and MgH_2 doped with different concentration of Al, Ti, V, Fe and Ni. The effect of each elementary mechanism such as dissociation of H_2, adsorption, diffusion and desorption on the kinetic properties, that we characterized through density distribution of hydrogen, filling ratios, diffusion time, temperature and pressure, is analyzed.
- Finally we give a general conclusion and perspective.

Chapter 1

Hydrogen storage

Contents

1.1 Introduction

The significant growth of the human population and the rapid evolution of the industrial sectors are reflected in a continuous increase in the demand for energy [1, 2, 3]. However, the depletion of fossil resources and the growing concern to reduce greenhouse gas emissions must be taken into account. As a result, scientists are constantly seeking to develop energy systems that harness energy from renewable and sustainable sources such as solar, wind, wave, tidal or geothermal energy. Solar and wind energy are dependent on weather conditions. Wave energy is exploited in the oceans while geothermal energy is exploited from rocks in the Earth's crust, so both forms of energy are location-dependent [4]. For these reasons, there is a growing interest in hydrogen, which is an energy carrier considered ideal for mobile applications, with an energy density of $142MJ/kg$, about three times higher than petrol.

Hydrogen is renewable, abundant and is a clean fuel that releases only water vapor into the environment during combustion [3, 5]. The development of hydrogen energy systems involves three stages: production, storage and use. The methods of production and use are the subject of much research, but the stumbling block is the storage of hydrogen that must be profitable, safe, efficient and practical. This requires the search for a solution that encompasses the various fields of science and engineering in order to produce such systems [12].

A technique of hydrogen storage has to meet the DoE criterion for the volumetric and gravimetric density of the stored hydrogen and the reversibility criterion for the charging/discharging processes. Hydrogen storage materials must have the following characteristics: low absorption/desorption temperatures, rapid hydrogenation and high dehydrogenation rates, good reversibility and high storage volume densities [13]. In addition, any method of storage is not allowed to considerably increase the cost of hydrogen fuel. Conventional hydrogen storage technologies such as high-pressure compression at about $70MPa$ [14], liquefaction at cryogenic temperatures ($77K$) [15] are impractical for this purpose, and a more feasible alternative is to store hydrogen in solid form by either absorption in metal hydrides or adsorption on high surface area materials such as carbon nanotubes ($CNTs$) and metal organic framework ($MOFs$) systems [13].

This chapter deals with a bibliographic study of the energy vector that is hydrogen, these characteristics, its production as well as its storage. An overview is given for the storage methods available today with respect to the progress made recently and problems still there. We will focus specifically on hydrogen storage in the solid state and more precisely in magnesium hydride. We will deal with the problems of this form of storage and solutions already proposed.

1.2 Hydrogen as a renewable energy carrier

One of the major challenges of the 21 century is keeping up with the growth in global energy demand due to increasing population and rising standards of living. For instance, in 2011, $15TW$ energy was consumed by approximately seven billion people world-wide. By 2050, these numbers are expected to escalate to $30TW$ and nine billion people, respectively [30]. Figure 1.1 demonstrates world's fuel shares of total primary energy supply ($TPES$), electricity generation, and the resulting CO_2 emissions. From Figure 1.1, it can be seen that 85% of the global energy supply was met by fossil fuels in 2011 [31].

However, because of their limited nature and non-homogeneous distribution, fossil fuels are not expected to keep up with the increase in energy demand. Also, fossil fuel reserves are getting less accessible as the easily accessible ones are consumed, and the prices of fossil fuels keep increasing due to accessibility loss and political uncertainties of the countries holding world's fossil fuel supplies [16]. Along with economic issues, greenhouse gas (mainly CO_2) emissions as a result of fossil fuel utilization, and their contribution to global warming, have been raising serious environmental concerns.

Therefore, switching to a non-fossil fuel energy source could greatly reduce the CO_2 related emissions and their adverse effect on global warming. Reducing the dependence on fossil fuels and minimizing environmentally harmful emissions can be achieved by sustainable energy sources such as solar, wind, wave, tidal or geothermal energy.

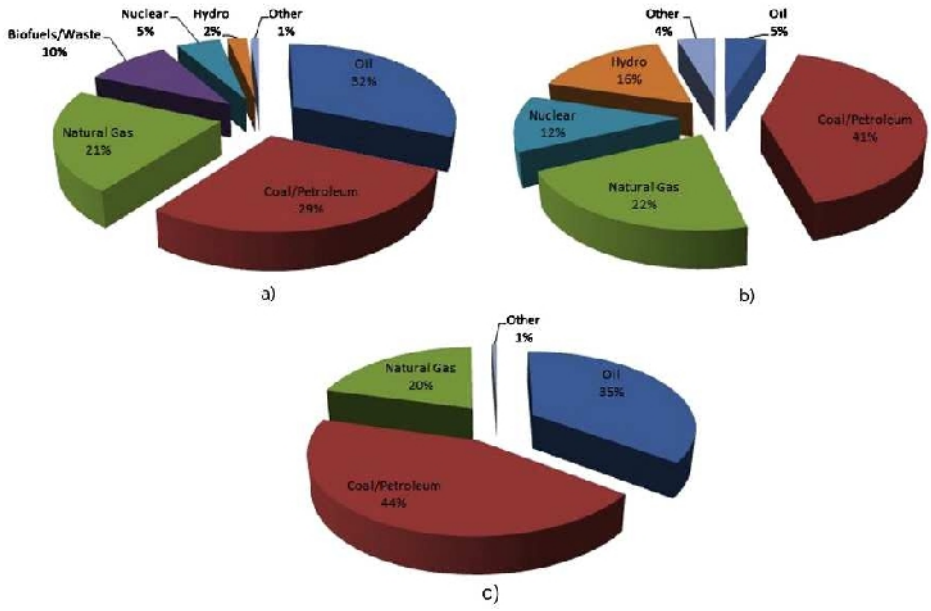

Figure 1.1: World's fuel shares of (a) total primary energy supply ($TPES$), (b) electricity generation, and (c) CO_2 emissions in 2011 (Other includes geothermal, solar, wind, heat, and waste etc)[32].

The variable nature of renewable energy sources such as solar and wind power does not match with the nearly constant use of energy. This means that renewable energy has to be stored on a large scale, which for electricity is not trivial. Typically, electricity is converted to chemical energy by storage in batteries. The energy density of batteries is, however, relatively low. For instance, the gravimetric energy density of Li-ion batteries is typically $1MJ/kg$, while that of gasoline is $45MJ/kg$ [33].
Hydrogen, on the other hand, has an even higher energy density of $142MJ/kg$. This energy density enables a car equipped with a fuel cell and $5kg$ of H_2 to drive about $500km$, while for the same trip a normal car would require about $20kg$ ($25l$) of gasoline. It is a primary candidate for future energy application, due to its higher chemical energy when compared to other fossil fuels. Table 1.1 represents the comparative energy values of different fuels [16]. It shows that the chemical energy of hydrogen is approximately three times higher than those of petroleum fuels such as gasoline, kerosene, and diesel oil.

Fuel	**Phase**	**Chemical energy** (MJ/kg)
Hydrogen	gas	141.79
Methane	gas	55.50
Ethane	gas	51.88
Propane	gas	50.35
Butane	gas	49.85
Ethanol	liquid	29.85
Gasoline	liquid	45.58
Kerosene	liquid	45.42
Diesel oil	liquid	45.00
Coal	solid	25.58
Wood (dry)	solid	21.14
Peat (dry)	solid	22.09

Table 1.1: Chemical energy values of various fuels, adapted from [16].

The use of hydrogen as a renewable energy carrier is summarized in the hydrogen cycle [32], shown in Figure 1.2. Once produced in a sustainable way (combination of solar electricity and water electrolysis), hydrogen generates electricity during fuel cell operations, leaving water vapor as the only exhaust gas, without any other greenhouse gases or harmful emissions [34, 35]. However, for broader and more conventional usage o hydrogen energy, a few limitations in its production, storage, and distribution need to be overcome [6, 7, 8]. The major disadvantage with storage of hydrogen originates from its lower volumetric density [9, 10].

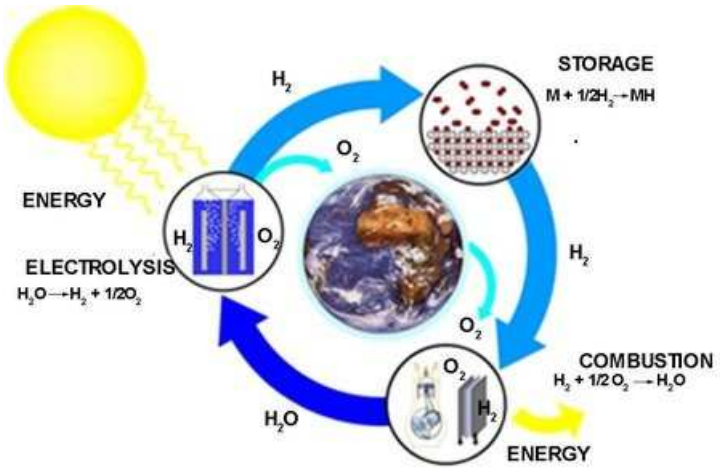

Figure 1.2: The closed hydrogen cycle (adapted from [36])

1.3 Hydrogen production

As an abundant element, hydrogen can be found in many substances in nature (i.e. fresh and sea water, biomass, hydrogen sulfide, and fossil fuels). In order to produce hydrogen with zero or low environmental impact (*green hydrogen*), all CO_2 and other pollutants must be processed (i.e. separated or sequestrated) when hydrogen is extracted from fossil fuels. Thermal, electrical, photonic, and biochemical energy are the primary energy sources to generate hydrogen [37].

Among the possible hydrogen production methods studied in the literature, natural gas steam reforming is the most commonly used process, resulting heavy greenhouse gas (GHG) emissions [37]. In order to remove the adverse effects of fossil fuel utilization on the environment, human health, and the climate, hydrogen should be produced from clean and abundant sources with environmentally benign methods [38, 39]. This concept is called as *green hydrogen production*.

Green hydrogen technologies are not quickly accessible with sensible effectiveness and expense. For instance, studies on effectiveness and cost of photovoltaics PV electrolysis for large and small scale hydrogen production show that PV electrolysis is currently expensive ($>5\$/kg$ for H_2) and it cannot reach high conversion efficiency (with energy and energy efficiency less than 5%) [40].

Table 1.2 shows an overview and brief description of hydrogen production methods along with their primary energy and material sources. The electrical and thermal energy can be generated from fossil fuels (has to be processed to be considered as *clean*), renewable energies (i.e. solar, wind, hydro, wave, ocean, and thermal), biomass, nuclear, or recovered energy. The photonic energy comes from solar irradiation, while biochemical energy is recovered from organic matter. In addition to the four major primary sources listed in Table 1.2 (electrical, thermal, biochemical, and photonic), there are also hybrid

forms of energy such as electrical-thermal, photonic-biochemical, and electrical-photonic.

Methods	Source		Brief description
	Primary energy	Material	
Electrolysis	Electrical		Water Direct current is used to split water into O_2 and H_2 (electrochemical reaction)
Plasma arc decomposition		Fossil fuels	Cleaned natural gas is passed through plasma arc to generate H_2 and carbon soot
Thermolysis	Thermal	Water	Thermal decomposition of water (steam) at temperatures over $2500K$
Thermochemical proc./ Water splitting		Water	Cyclical chemical reactions (net reaction: water splitting into H_2)
Biomass conversion		Biomass	Thermocatalytic conversion
Gasification			Conversion of biomass into syngas
Reforming			Conversion of liquid biomass (biofuels) into H_2
PV electrolysis	Photonic	Water	PV panels are used to generate electricity
Photocatalysis			Water is split into H_2 by using the electron-hole pair generated by the photocatalyst
Photoelectrochemical method			A hybrid cell simultaneously produces current and voltage upon absorption of light
Dark fermentation	Biochemical	Biomass	Biological systems are used to generate H2 in the absence of light
High temperature electrolysis	Electrical+ Thermal	Water	Electrical and thermal energy are used together to drive water splitting at high temperatures
Hybrid thermochemical cycles			Electrical and thermal energy are used together to drive cyclical chemical reactions
Coal gasification			Conversion of coal into syngas
Fossil fuel reforming			Fossil fuels are converted to H_2 and CO_2
Biophotolysis	Photonic+ Biochemical	Biomass+ Water	Biological systems (microbes, bacteria, etc.) are used to generate H_2
Photofermentation			Fermentation process activated by exposure to light
Artificial photosynthesis			Chemically engineered systems mimic photosynthesis to generate H_2
Photoelectrolysis	Electrical+ Photonic	Water	Photoelectrodes and external electricity are used to drive water electrolysis

Table 1.2: Overview of hydrogen production methods by primary energy and material source [31].

1.4 Transforming hydrogen to energy

Hydrogen is attractive as a clean or zero emission fuel of the future. During power generation only water is formed as the oxidation product of hydrogen. Hydrogen can principally be utilized in two different modes for power generation. It can be used either in an internal combustion engine (ICE) to produce mechanical power or in a fuel cell to produce electrical power for automotive applications [41]. Among several other kinds of

fuel cells, the *PEM* or proton exchange membrane fuel cell (*PEMFC*) is attractive due to its high chemical to electrical energy conversion efficiency and high power density [42]. While in the *PEM* fuel cell, the hydrogen reacts with oxygen and only water and heat are produced, the use of hydrogen in *ICEs* additionally produce nitrogen oxides (NO_x) due to combustion of a hydrogen–air mixture. Although both the hydrogen fuel cells and *ICEs* are the main contending technologies for vehicular applications, the fuel cells are superior in terms of cleaner air quality. In addition, in a vehicle the fuel cell can function with $50-60\%$ efficiency by electrochemical means whereas the efficiency of the *ICEs* is limited by the Carnot cycle (which is $\sim$ 25 per cent for combustion of an hydrogen–air mixture)[43]. Moreover, the hydrogen fuel cell vehicle efficiencies are $\sim 2-3$ times greater than that of conventional gasoline-based *ICEs* and even $1.5-2$ times greater than diesel–electric hybrids [44]. Considering the above, *PEMFCs* have great potential to emerge as a practical technological solution for power in the transport sector.

1.4.1 Fuel cell operation

In a fuel cell the chemical energy is converted into electrical energy [45]. Similar to any typical battery systems, the fuel cells are composed of an anode, cathode, and an electrolyte (Figure 1.3).

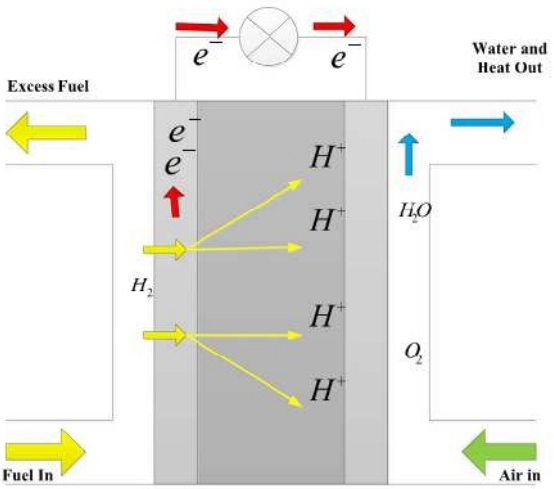

Figure 1.3: Schematic of fuel cell [46].

The electrochemical process at the anode is the oxidation of hydrogen, while the oxygen from air is reduced to water at the cathode. The protons produced during oxidation pass through the electrolyte to reach the cathode and the electron released travels through an external circuit and produces an electrical current.
Generally, the fuel is pure hydrogen or contains some hydrogen gases like methanol, ethanol and natural gases. The oxidants are pure oxygen or contains gases like air or

halogens like chlorine [47, 48, 49]. Fuel cells are mainly classified according to the electrolyte and types of fuel used. The main categories of fuel cells available in the market are explained below [46].

1.4.1.1 Proton Exchange Membrane Fuel Cells (*PEMFC*)

Acid polymer is used as the electrolyte and pure hydrogen is used as fuel. The operating temperature of the *PEMFC* is below $100°C$. Now a day, this fuel cell is popular and widely used in vehicle application.

1.4.1.2 Direct Methanol Fuel Cell (*DMFC*)

In *DMFC*, the polymer membrane used as an electrolyte, and the fuel used is methanol. The operating temperature of *DMFC* is below $60°C$ and it is mainly used for portable power applications below $259W$.

1.4.1.3 Phosphoric Acid Fuel Cell (*PAFC*)

In *PAFC*, The liquid phosphoric acid is used as the electrolyte and pure hydrogen is used as the fuel. The operating temperature is around $180°C$. These types of fuel cell are particularly used as stationary power generators and which is not efficient electrically.

1.4.1.4 Alkaline Fuel Cell (*AFC*)

Here, alkaline solutions are used as electrolyte of fuel cell and pure hydrogen is used as fuel. The operating temperature is about $70°C$. This type fuel cell is mainly used as standalone power generators.

1.4.1.5 Solid Oxide Fuel Cell (*SOFC*)

This type of fuel cells is widely used as stationary power generator and its operating temperature is around $1000°C$. The solid ceramic electrolyte like zirconium oxide and syn-gas type of fuels are used in this fuel cell.

1.4.1.6 Molten Carbon Fuel Cell (*MCFC*)

Here, Molten carbonate salt suspended in a porous ceramic matrix is used as the electrolyte and hydrocarbon is used as fuel. The operating temperature is around $650°C$ and which is mainly used for high power application.

The Fuel cells have a variety of advantages when compared to conventional power sources like internal combustion engine and other renewable energy sources. The major advantages are enlisted below:

- As compared to other power source fuel cell has higher efficiency.
- Noise free operation.
- It has pollution free completely, since water is the repercussion instead of CO_2 emission from the fuel cell.
- It has lesser maintenance, since there are no moving parts.
- The Fuel cell is economical because it does not need any fossil fuel to operate.

Although hydrogen is an attractive option as a sustainable fuel, it is mostly present in nature in a bound form as a compound and needs to be isolated, or generated, and stored before it can be used. Therefore, hydrogen storage itself constitutes a major challenge for the hydrogen economy.

1.5 Hydrogen storing methods

Research on hydrogen storage is being done on a larger scale in order to develop safe, reliable, compact and cost-effective materials which can be used for fuel cell technology. Like any other product, hydrogen must be packaged, transported, stored and transferred, to bring it from production to final use. The main technological problem of a viable hydrogen economy is its storage and so far, finding a cost-effective method of storing hydrogen remains an indomitable challenge. Hydrogen must be made more energy dense to be useful for transportation. However, the solutions to the hydrogen storage problem are surfacing at a fast pace. Scientists are researching innovative ways to store hydrogen[17].

The hydrogen economy requires both mobile and stationary hydrogen storage systems to thrive. The mobile division is thought to be the higher quantity consumer of hydrogen in the future hydrogen economy [18, 50, 51, 52, 53, 54]. However, both mobile and stationary storage systems have their peculiar requirements and challenges.
Concerning stationary applications, hydrogen storage issues of weight and volume are not as much serious compared to mobile applications. Stationary hydrogen storage systems can take up more space, function at high temperatures and pressures and feature spare capacity to offset sluggish kinetics. Even so, inadequate materials for storage tanks is a major technical setback against the development of stationary hydrogen storage systems. On the other hand, mobile applications hydrogen storage requirements are way exhaustive in contrast to stationary applications [50, 52, 55].

1.5.1 *DoE* criteria

The US Department of Energy (*DoE*) goals for hydrogen storage requirements for mobile applications identifies the significance of both gravimetric and volumetric capacity of storage. Here, the *gravimetric capacity* of storage refers to the quantity of hydrogen gas a given weight of storage material can generate while *volumetric capacity* of storage conveys the quantity of hydrogen gas contained in a given volume of storage material. High values of both parameters are greatly desired for suitable hydrogen storage. However, if storage is too heavy, the range of the vehicle will be restricted and if storage is too voluminous, the luggage space will be restricted as well. In other words, effective balance must be ensured.
Table 1.3 shows an overview of some of the new *DoE* technical system goals for on-board hydrogen storage for light-duty fuel cell vehicles beginning from 2020 [1].

Storage parameter	**Unit**	**2020**	**2025**	**Ultimate**
Storage capacities				
System-based gravimetric capacity	kgH_2/kg system	0.045	0.055	0.065
System-based volumetric capacity	kgH_2/l system	0.030	0.040	0.050
Storage system cost (and fuel cost)	$\$/kWh$ net $\$/kgH_2$	10 333	9 300	8 266
Durability/Operability				
Min/Max delivery temperature	$°C$	-40/85	-40/85	-40/85
Cycle life (1/4 tank to full)	cycles	1500	1500	1500
Min. delivery pressure from tank	bar	5	5	5
Max delivery pressure from tank	bar	12	12	12
Charging/Discharging rates System fill time (for $4-10kg$)	min	3-5	3-5	3-5
Fuel purity (H_2 from storage)	$\%H_2$	Meet or exceed applicable standards		

Table 1.3: Overview of some selected parts of the *US-DoE* technical system goals for on-board hydrogen storage for light-duty fuel cell vehicles, (data adapted from [1].

Requirements for on-board hydrogen storage include [9, 50, 52, 53, 56, 19, 57, 58, 59, 60]:

- low operating pressure
- low operating temperature
- fast kinetics of hydrogen uptake/release
- low heat of formation to minimize the energy necessary for hydrogen release
- low heat dissipation during the exothermic hydride formation
- limited energy loss during charge and discharge of hydrogen

- multi-cycle reversibility of hydrogen uptake/release
- high stability against oxygen and moisture for long cycle life
- low cost of recycling and charging infrastructures
- high safety under operating conditions and public acceptance

Hydrogen could be stored in multiple ways, though with their identified strengths and weaknesses [61]. There are two types of hydrogen storage methods available depending on the size of storage and area of application (Figure 1.4) namely conventional methods (or physical storage), to store hydrogen involve compression of gas and liquefaction, and solid-state materials where hydrogen is absorbed or adsorbed on these materials [16, 17, 18, 19, 20, 21].
In next sections, an overview is given for the storage methods available today with respect to the progress made recently and the problems that encounter.

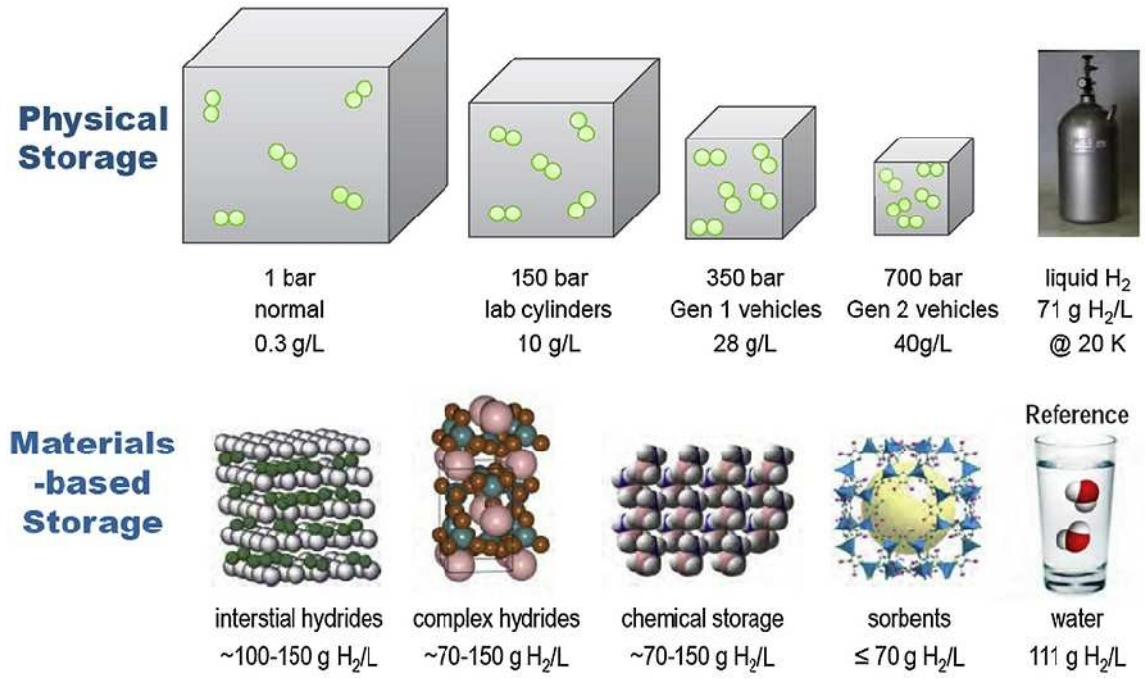

Figure 1.4: Hydrogen storage systems [62]

1.5.2 Compressed hydrogen

The most established hydrogen storage system is physical storage in the form of pressurized hydrogen gas in high pressure gas cylinders. Because of the very low density of hydrogen ($0.089 kg/m^3$) its storage requires high pressure [1] between $35 MPa$ and $70 MPa$. Compressed hydrogen is a highly efficient methodology for hydrogen storage

($\sim 30 - 40g/l$) and the energy density considering volumetric increase with the pressure increase of the gas. However, between 11 and 13% of the hydrogen energy content is affected negatively by pressurizing [63]. Due to its extreme lightness, there are chances that under high-pressure hydrogen leakage from containing vessels may ensue [1].

Pressure vessel usage for H_2 storage was first reported in 1880. The hydrogen was stored in wrought iron vessels at $12MPa$ [14]. Currently, the compressed hydrogen can be stored in 4 different types of pressures vessel presented in Figure 1.5:

- Type I metallic pressure vessel is mostly use for industrial applications with pressure of $20 - 30MPa$. This type has a limitation in storage efficiency, it can only able to store about $1wt.\%$ of H_2.
- Type II where the cylindrical part of the vessel is wrapped with fiber resin composite;
- Type III and type IV is a fully composites materials based pressure vessel (design by $COPV$ [64]) as shown in Figure 1.6, in which the composites is either made of plastic or carbon fibers embedded in polymer matrix (filament winding).
  The characterization between type III and type IV is in the mechanical resistance, usually more than 5% is contributed by liner, commonly metal liner, for type III pressure vessel; for Type IV pressure vessel, the liner is mainly polymer and is seldom an extremely thin metal [14].

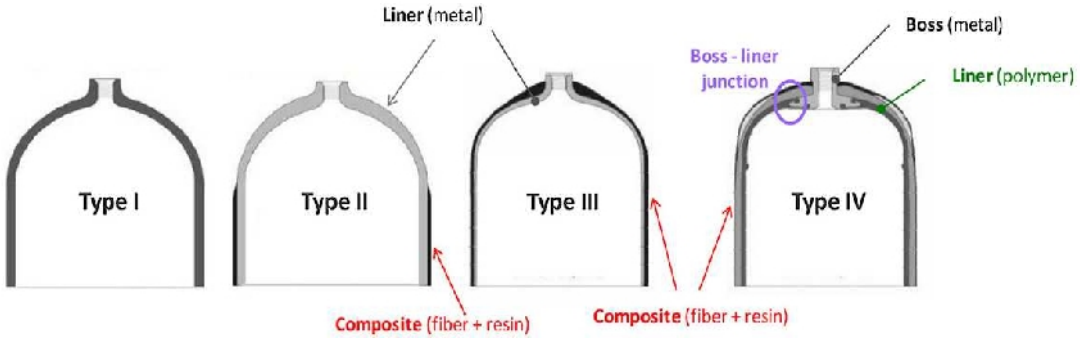

Figure 1.5: Different types of hydrogen compressed tank [14].

The ideal material characteristics for high pressure vessel are [60]: high tensile strength, low density and does not react with hydrogen or allows it to diffuse. Today's commercially available vessels can achieve an average hydrogen content of $1 - 2wt.\%$ at pressures of about $20 - 25MPa$ [65] but composite pressure tanks up to $70MPa$ have also been successfully developed, reaching a gravimetric storage density of $6wt.\%$ and a volumetric storage density of $30g/l$ [66]. These values still do not meet the two US Department of Energy targets, which set the ultimate gravimetric and volumetric capacity for hydrogen automotive systems at $50g/l$ and $6.5wt.\%$ respectively. More than to two

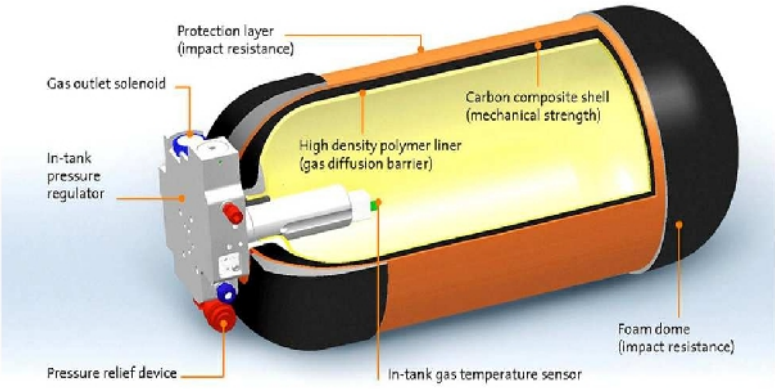

Figure 1.6: Type IV pressure vessel for compressed hydrogen storage [64].

obstacles discussed, cost is considered the greatest barrier [9]. It is largely contributed to the carbon fiber composing the tank with a large contribution from assembly and some for binding. Even if the cost is lowered, there is concern that high-pressure tanks will not be accepted by the general public because they are perceived as unsafe [1, 9, 17, 54, 19, 60, 67].

1.5.3 Liquefied hydrogen

Another advanced technology and conventional technique of storing H_2 is by liquefying the hydrogen at $-253°C$. Storage as liquid comes with a higher density. Liquid hydrogen has a density of about $71g/l$ at its normal boiling point of $20K$, which is approximately 1.8 times the density of hydrogen pressurized up to $70MPa$ at $288K$. However, this process is intensive energy and time consuming, and the energy content lost estimated as 40% in contrast to energy lost for compressed hydrogen, about 10%. [14, 68, 69]. Thus, special double-walled vessels furnished with good insulation systems are essential to mitigate heat leakage.

Another H_2 storing technique is by using a *cryo-compressed* storage method, where both properties of compressed gaseous hydrogen and cryogenic hydrogen systems are combined. This method is used to minimize the *boil-off* rate of hydrogen and at the same time, maintain a high energy density. Cryo-compressed vessel must be able to store hydrogen at cryogenic temperature ($20K$) and high pressure, at least $30MPa$ as presented in Figure 1.7 [15].

More compact and lighter cryogenic pressure vessels, therefore, provide better safety advantages than compressed hydrogen vessels. However, the persistent boil-off of hydrogen and too much energy required for liquefaction restrict the potential use of liquid hydrogen storage systems to applications that require high energy density as well as uses where hydrogen cost does not matter, and its consumption is within a short time, examples include air and space and automotive applications [4, 70, 71, 72, 73].

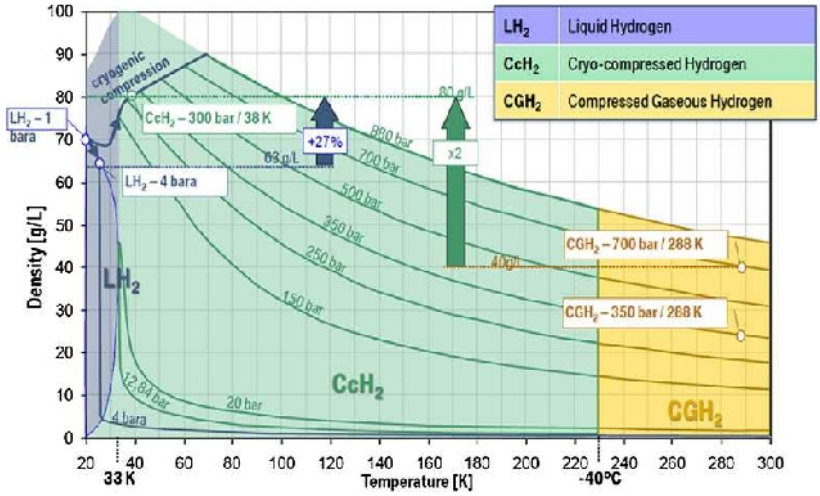

Figure 1.7: Temperature versus hydrogen density curve for compressed hydrogen, liquid hydrogen and cryo-compressed hydrogen; respectively [15].

1.5.4 Solid state storage system

In view of a hydrogen economy, storage systems need to be very safe, efficient, economical, light and compact. On the other hand, due to the safety problems involved with conventional methods (compression of hydrogen and liquefaction), it is obvious that hydrogen storage needs a more technical breakthrough, probably in the most feasible option in contrast to pressurized hydrogen gas and cryogenic liquid Hydrogen. Specifically, for a fuel cell vehicle, storage of enough hydrogen onboard is a major hurdle to cross [9, 48, 53, 74, 75, 76, 77, 78].

hydrogen storage system is expected to possess high gravimetric and volumetric capacity to realize techno-economically viable hydrogen-based vehicular applications. To achieve this goal much attention is currently being given to storing hydrogen in solid-state materials. A solid storage material that satisfied the *US-DoE* target capacities (Table 1.3) and has favorable hydrogen uptake–release characteristics within the functional temperature window of *PEM* fuel cells would be ideal [79].

Storage of hydrogen in the solid state is divided into two categories depending on the nature of bonding between the solid and hydrogen which is stored either by *physisorption* or *chemisorption* [16, 9, 19, 80, 81].

In physisorption, hydrogen molecules are adsorbed on surfaces of porous solids by van der Waals interactions such as in carbon-based materials, carbon nanotubes, fibers, fullerenes, activated carbon, zeolites, metal-organic frameworks (*MOFs*) as well as covalent organic frameworks (*COFs*) and more recently polymers of intrinsic micro-porosity (*PIMs*). The hydrogen can then be liberated whenever required by thermal stimulation or any other suitable technique. Although the reversibility and fast kinetics make these materials nice-looking options, low hydrogen storage capacity at ambient conditions and the re-

quirement of extremely low temperatures for high hydrogen storage capacity place appalling constraints on the use of these materials as it touches on the practical application [9, 48, 19, 60, 69, 82, 83].
On the other hand, chemisorption is in form of atomic hydrogen chemically reacting with solids to form hydrides (metallic, intermetallic, complex and chemical hydrides). The capture and release of hydrogen on these materials involves molecular adsorption, diffusion, chemical bonding and Van der Waals attraction and dissociation[84, 85]
In the next subsections a brief description will be given for some materials suitable for hydrogen storage in solid-state.

1.5.4.1 Carbon Nanotubes

Carbon Nanotubes ($CNTs$) are microscopic tubes of carbon [86] with two nanometers thickness across that can store hydrogen in their microscopic pores or within the tube structures (Figure 1.8). Nanotubes have single ($SWNT$) or multiple wall structure ($MWNT$), multiple adsorption sites, high packing density and possess an estimated capacity of $6wt.\%$ [87]. Experimental data on hydrogen adsorption was determined that the gravimetric storage density for $SWNT$ at ambiante temperature is in a range of $5-10wt.\%$[87].

Multi-walled Nanotubes ($MWNTs$) possess superior physical, chemical and mechanical properties plus large surface areas making them promising H_2 storage physical adsorbents. $MWNTs$ provide several sites such as the exterior walls, space between the nanotubes, tube channels, and interstitial space in the lattices for physical adsorption of H_2. The initial investigations for H_2 storage on bare $MWNTs$ disclosed that weak interactions between the $MWNTs$ and H_2 are not sufficient for efficient H_2 uptake. Surface modifications and, decoration with metals/metal oxides are some of the strategies used to improve the H_2 storage capacity of $MWNTs$ [88, 89, 90].
Chen et al. [91] reported that Li-doped and K-doped multi-walled Nanotubes show an uptake capacity of $20wt.\%$ and $14wt.\%$, respectively, among which the K-doped $MWNTs$ are chemically unstable, whereas the Li-doped $MWNTs$ are chemically stable but require elevated temperatures (473 to $673K$) for maximum adsorption and desorption of H_2.

The hydrogen capacity of nanotubes varies with its preparation and processing uncertainties and synthetic purity, the release temperature of hydrogen, the metal clustering and the stability of the materials. For this reason, the use of nanotubes becomes a limitation because it is not well adjusted for storing a high capacity of H_2. Also, it requires more modifications in preparation and processing methods to achieve the high target of hydrogen capacity [62].

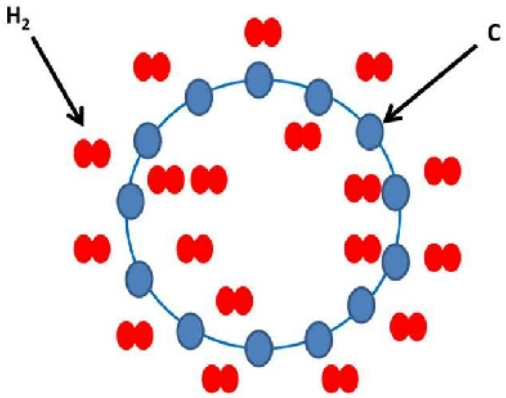

Figure 1.8: Absoption in carbon nanotube [62].

1.5.4.2 Metal-organic frameworks

Metal-organic frameworks (*MOFs*) (also known as coordination frameworks, coordination network materials, or coordination polymers) are among the widely investigated examples of materials for hydrogen storage that operate via physisorption [92].
MOFs are porous architectures built from metal ions/clusters and organic linkers (Figure 1.9). Their high surface areas of up to $6000 m^2/g$, permanent porosity, tunable pore sizes, rigidity, structural flexibility and thermal stability make them as promising materials for H_2 storage [93, 94, 95]. The pore dimensions of *MOFs* are suitable for the kinetic diameter of H_2 (2.89Å), which suits the easy entry of H_2 into their structures[13].

An example of *MOFs* structure is shown in Figure 1.9. On each of the corners, is a cluster $[OZn_4(CO_2)_6]$ of an oxygen-centred Zn_4 tetrahedron bridged by six carboxylates of an organic linker (Zn are blue polyhedrons, O red spheres and C black spheres). The large yellow sphere represents the largest sphere that would fit in the cavities without touching the van der Waals atoms of the frameworks.

Hydrogen uptake studies on a series of *MOFs* (*IRMOF*-1, -6, -11, -20, -74, *MOF*-177, and *HKUST*-1) reveal that saturation uptake correlates with the surface area and varied widely with the saturation pressure reaching a strikingly high capacity of 6.7 and $7.1 wt.\%$ in *IRMOF*-20 and *MOF*-177 at saturation pressures of 70 and $80 bar$ (at $77K$), respectively [96]. It has been demonstrated in *MOFs* that high surface area and pore volume are approximately proportional to the amount of stored hydrogen [96, 97, 98].

Recently, covalent-organic frameworks (*COFs*, where the organic structural building units are held together by strong covalent bonds, (e.g. $C-C$, $C-O$, $B-O$, and $Si-C$) have been found to be promising candidates for hydrogen storage because of their low density and ultrahigh porosity [100, 101, 102, 103, 104]. In *COF*-8 an excess hydrogen uptake of $10 wt.\%$ has been found experimentally at $77K$ and $100 bar$ [104]. These values are significantly higher than the highest values reported in *MOFs* ($7 wt.\%$ in *MOF*-177

and 7.1$wt.\%$ in MOF-5), although the pressure employed is quite high at $77K$ [96, 105].

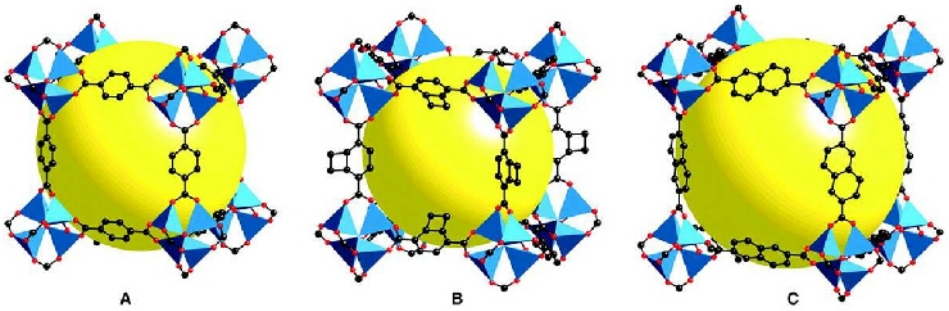

Figure 1.9: Single crystal x-ray structures of: A) MOF-5, B) $IRMOF$-6 and C)$IRMOF$-8[99].

Scientists are giving tremendous attention to MOF for hydrogen storage due to their acquiescent in designing, extraordinary permanent porosity, large pore volume and exhibition of highly hydrogen storage capacities from 0.6 to 13$wt.\%$ uptake experimentally and 16$wt.\%$ theoretically at low temperature of $77K$ (liquid nitrogen temperature) [106, 107, 108, 109, 110, 111]. However, very low hydrogen uptakes ($< 1wt.\%$) have been reported for a wide range of $MOFs$ at room temperature [112, 113, 114, 115]. As the van der Waals forces that are responsible for physisorption are weak, the hydrogen storage capacities of adsorbents are low at room temperature. It has been shown from theory that in order to maintain high hydrogen storage capacity at room temperature an isostermic heat of hydrogen adsorption of $15 - 25kJ.mol^{-1}$ is required of the material [116].

In summary, the small enthalpy change (heat of adsorption) in physically adsorbing $MOFs$ offers a huge advantage for fast kinetics and reversibility. Heats of adsorption vary with the type of metal, framework topology, surface area, and pore size, and hence the extent of hydrogen adsorption in MOF materials can be influenced by manipulating these parameters [117, 118]. Therefore, the exploration of new $MOFs$ and developing an understanding of adsorption mechanisms are very important steps towards optimizing the hydrogen storage properties of $MOFs$ at near ambient conditions.

1.5.4.3 Metal hydrid

A metal hydride is technically formed via a chemical reaction but acts like a physical storage method [50, 119, 120]. In metal hydride tank, hydrogen molecules bond into metal under moderate temperature and pressure, usually between 3 and 30atm, much lower than compressed gas tanks. This makes the system safer than any other solutions since hydrogen gas leakage cannot be spontaneous or the tank contains it by itself [57, 63, 104, 119]. However, metal hydride tanks are comparatively very heavy, but weight should not be a challenge for stationary and some other applications, especially for small storage. And once their weight issue is solved by discovering novel light materials, incorporating

them in mobile application will be more probable. Moreover, they have comparatively high hydrogen volumetric energy densities, good storage efficiency, and can uptake/release hydrogen with a slight change in pressure, which make them one of the most promising solutions [9, 63, 119].

According to authors of many works [50, 57, 60, 121, 122], metal hydrides are produced by the interaction of hydrogen with different metals, either pure or alloy (in granular form or particles) resulting in solid-state storage under moderate temperature and pressure which gives them the crucial safety advantage above gaseous and liquid storage systems. A key contributing factor to a wide usage of metal hydrides in the field of hydrogen storage is their huge capacity to accommodate a significant amount of hydrogen in their structures [119, 122, 123, 124]. It is possible to pack more atoms of hydrogen into a metal that forms a hydride lattice than into the same volume of liquid hydrogen. When such metal is brought in contact with gaseous hydrogen, the hydrogen molecules are first adsorbed onto the surface of the material and if enough energy is added to the system, the hydrogen molecules dissociate into hydrogen atoms, then diffuses into the bulk and occupy the interstitial sites of the metal crystal lattice and forms a *solid solution* with a lesser amount of hydrogen (α phase). As more energy is added to the system, the hydrogen content increases, a *hydride phase* (β phase) appears which allows the metal to absorb hydrogen in larger amounts and grows until the metal becomes saturated with hydrogen [60, 119, 123, 125], see Figure 1.10 .

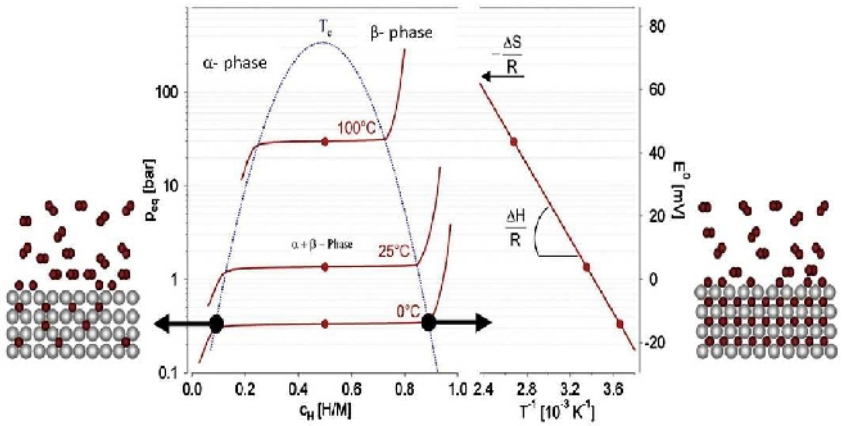

Figure 1.10: Pressure-composition-isotherms diagram for the formation of hydrides [1].

As a comparison with conventional methods, the hydrogen storage density of magnesium hydride ($6.5 Hatoms/cm^3$) is way higher than hydrogen gas ($0.99 Hatoms/cm^3$) or liquid hydrogen ($4.2 Hatoms/cm^3$). That confirms that the volumetric density of hydrogen can be increased by the solid state hydrogen storage system. Thus, metal hydride storage is considered a safe volume-efficient storage system for on board applications [50, 57, 121, 123, 126, 127, 128].

Ozturk and Demirbas [53], Sahaym and Norton [119] and Zaluski et al. [129] described metal hydrogenation as the formation of metal hydrides by hydrogen absorption usually accompanied by the release of heat. In this way, as hydrogen gas is absorbed in these metal particles pressure builds up in the tank. However, for decomposition and dehydrogenation process equal amount of heat must be added to the metal hydride. These processes are continuously repeatable, and reversible metal hydrides can, therefore, be used for the storage of heat and hydrogen. Charging and discharging of the hydride tank can be performed as many times as possible in as much as the hydride material does not become contaminated [50, 121, 130, 131].
Depending on the thermodynamics of the reaction, different temperatures apply to different metal hydrides. A typical reversible interaction between metal/alloy and hydrogen can be written as:

$$M + \frac{x}{2}H_2 \longleftrightarrow MH_x + Q \tag{1.1}$$

where M is a metal, an intermetallic alloy, or a solid solution; x is the number of hydrogen, MH_x is the formed hydride and Q is the heat of reaction. A simplified model of hydrogen storage in a metal hydride is given in Figure 1.11 below.

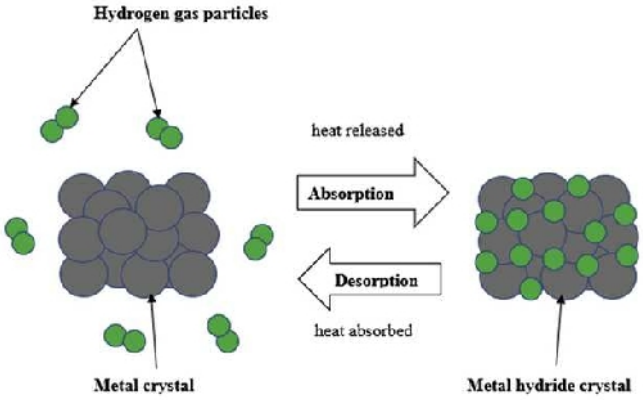

Figure 1.11: A simplified model of a metal hydride hydrogen storage [1].

Prabhukhot et *al.* [50] and Ozturk et *al.* [131] reported that both the thermodynamic and kinetic conditions are the essential requirement that must be met for hydrogen storage to occur. Under this circumstance, a metal exposed to hydrogen gas absorbs hydrogen until equilibrium is reached. There are various reaction steps that kinetically may prevent a hydrogen-storing system to reach its thermodynamic equilibrium of hydrogen storage within a reasonable time. The reaction rate of a metal-hydrogen system is, therefore, a function of pressure and temperature. Hydrogen storage in metal hydrides comprises a few mechanistic steps and depends on some parameters. Essentially, the surface of the metal must be able to dissociate the hydrogen molecule and permit easy mobility of

hydrogen atoms to be able to store hydrogen. Different metals have different abilities to dissociate hydrogen depending on their surface structures, morphologies, and purities.

According to David [73], Lai et *al.* [83] and Khafidz et *al.* [125],metal hydrides can be categorized into low-temperature hydrides and high-temperature hydrides based on the temperature of absorption/desorption of hydrogen. Hydrogen is bound via covalent bonding in the low-temperature hydrides, and the metal hydride consists of high molecular weight material which exhibits fast kinetics and low hydrogen equilibrium pressures because of their low heat of reaction. These metal hydrides are mostly intermetallic alloy or solid solution hydrides operating at ambient to moderate temperatures. Whereas on the other hand, hydrogen is usually ionically bound in the high-temperature hydrides, and the metal hydride consists of low molecular weight material. Although the high temperature restricts the choice of high-temperature hydrides, they have been found to possess relatively higher hydrogen storage capacities than the low-temperature hydrides.

Metal hydrides appear to be the safest method of storing hydrogen since metal hydrides can be operated at relatively low temperatures and pressures typical of fuel cell vehicles and the release of hydrogen from metal hydrides is an endothermic process [132]. Hydrogen can be released from metal hydrides either by an increase in temperature rise or a decrease in external pressure [133].
However, there are a number of issues associated with hydrogen storage in metal hydrides, i.e. slow reaction kinetics, low reversibility and high dehydrogenation temperatures [134]. Nowadays, research is still ongoing to synthesize metal hydrides which will fulfill the targets for hydrogen storage systems set by the *US-DoE* for on-board vehicular applications, a brief summary was given in Table 1.3.
At present, the main alloying materials for metal hydrides are:

- Intermetallic compounds (AB_5, AB_2, AB, and A_2B), which has a hydrogen storage capacity of 1.5, 2.0, 1.8 and 3.0$wt.\%$, respectively [135]. Solid solution alloys are also available such as vanadium-based solid solution alloys and Mg-based alloys, which have a hydrogen storage capacity of approximately 2 and 5$wt.\%$ respectively [135].

- Metallic hydrides (also called element hydrides or metal hydrides) composed of lightweight elements such lithium (Li), boron (B), nitrogen (N), magnesium (Mg) and aluminium (Al) have shown great potential for use as hydrogen storage materials [136].

- Complex hydrides which are the only group of metal hydrides having high volumetric and gravimetric hydrogen storage densities [137].

Some features of these metal hydrides will be given in next sections.

1.5.4.4 Intermetallic compounds

Intermetallic compounds have gained prominence in recent years due to their widespread use in the development of hydrogen-absorbing metal alloys [138]. The applications of intermetallic compounds are numerous, which include hydrogen storage systems, nickel metal hydride ($NiMH$) for battery electrodes, hydrogen purification systems, hydrogen sensors and catalysts, heat pumps, as well as cooling systems [139].

Intermetallic compounds are attractive for the development of metal hydrides since they are capable of absorbing large quantities of hydrogen. Moreover, they are available in abundance and they come in a variety of compositions. In general, hydrogen reacts with intermetallic compounds, producing crystalline or amorphous solid solutions of hydrogen in the respective compounds or in the hydrides formed [140]. The resultant hydrides are called intermetallic hydrides and their common formula is $A_mB_nH_x$.

The properties of the intermetallic compounds are determined by the interaction between the interstitial hydrogen atoms and the metal atoms and therefore, they are largely dependent on the crystal structure of the compounds. AB_5 ($CaCu_5$ structure), AB_2 (Laves phase), AB ($CsCl$ relative structure), A_2B and vanadium-based solid solution alloys are among the important types of intermetallic compounds [141]. It has been shown that AB_5, AB_2, and A_2B type alloys have excellent hydrogen absorbing properties [142]. The properties of some of the most common intermetallic hydrides are summarized in Table 1.4.

Intermetallic compound	**Intermetallic hydride**	**Hydrogen storage capacity (wt.%)**	**Temperature at 1 bar ($^\circ C$)**
$LaNi_5$	$LaNi_5H_6$	1.37	295
$FeTi$	$FeTiH_2$	1.89	185
Mg_2Ni	Mg_2NiH_4	3.59	255
$ZrMn_2$	$ZrMn_2H_2$	1.77	440

Table 1.4: Properties of some of the most common intermetallic metal hydrides [135])

However, the use of intermetallic hydrides is rather limited for on-board vehicular applications since intermetallic hydrides have low hydrogen storage capacities by weight, slow kinetics, and complicated activation procedure. It is not possible to attain a hydrogen storage capacity greater than $3wt.\%$ based on the intermetallic hydrogen storage materials currently available [138]. Thus, much effort has been made to optimize the composition, morphology and size distribution of the metal hydride particles, modify the hydride particles surface and optimize the surface oxides via various synthesis routes in order to achieve a good compromise between degradation, kinetics and hydrogen storage capacity of the intermetallic hydrides [143]. Based on the chemical formula $A_mB_nH_x$, the partial substitution of A, B or both will alter the hydrogenation kinetics and equilibrium

pressure of the metal hydride without affecting its hydrogen storage capacity [144].

1.5.4.5 Complex hydride

The main disadvantage of conventional metal hydrides such as intermetallic hydrides is their low gravimetric hydrogen storage capacities [145]. Complex hydrides composed of light elements such as lithium (Li), bor (B) and sodium (Na) have gained significance as hydrogen storage materials since conventional metal hydrides are mostly composed of heavy elements. Lightweight complex hydrides emerge as potential candidates for hydrogen storage applications due to their high hydrogen storage capacities (up to $18 wt.\% H_2$ for $LiBH_4$), high hydrogen storage densities, as well as mild dehydrogenation pressures and temperatures [146]. The gravimetric storage capacity and dehydrogenation temperatures for some selected complex hydrides are shown in Table 1.5.

Complex compound	**Desorption temperature** T_{des} $(°C)$	**Hydrogen storage capacity (wt.%)**
$LiBH_4$	380	18.4
$NaBH_4$	400	10.6
KBH_4	500	7.4
$LiAlH_4$	125	9.5
$NaAlH_4$	210	7.4
$KAlH_4$	270	5.7
$Mg(AlH_4)_2$	140-200	9.3
$Ca(BH_4)_2$	320	11.5

Table 1.5: Dehydrogenation temperature and gravimetric storage capacities of complex hydrides [79, 147, 22]

Group III complex hydrides such as alanates and borohydrides are able to bond four hydrogen atoms with an alkali metal, ionic compound or partially covalent compound [148]. Even though complex hydrides have high energy densities, they are difficult to handle safely and they may decompose according the a cascade of reaction into highly stable elements, which are very challenging to refuel with hydrogen on board a motor vehicle [149]. More importantly, most of these complex hydrides do not fulfill the targets set by the United States Department of Energy since they have high thermodynamic stability and slow kinetics during hydrogen cycling [150].
However, these problems can be compensated to a certain extent by thermodynamic destabilization, which involves the addition of a new element into the system by means of cation or anion substitution, or the addition of reactive hydride composites. Nanoconfinement or the addition of catalysts can also be used for thermodynamic destabilization[151].

1.5.4.6 Chemical hydrides

Differ than conventional metal hydrides, chemical hydrides are typically composed of lighter elements [152]. This result in higher gravimetric hydrogen storage capacities, along with ease of hydrogen release which is similar to complex hydrides [153]. Chemical hydrides can exist in either solid or liquid state, and can be heated directly, passed through a catalyst containing reactor, or combined with water (i.e. hydrolysis) or other reactants to produce hydrogen. Unlike reversible complex hydrides, chemical hydrides are irreversible and generally intended as *one-way single-use* fuels. Besides, the left-over by-product must be removed from the vehicle for off-board regeneration [154]. Among chemical hydrides, ammonia borane is reported as a potential material for hydrogen storage due to its high hydrogen capacity.

Ammonia borane (NH_3BH_3 or simply known as AB) has garnered considerable attention from scientists and researchers due to their favorable properties which can be exploited for on-board hydrogen storage applications [155]. According to Lee and McKee [156], NH_3BH_3 has high hydrogen content up to $19.6wt.\%$ and it is really stable in basic or neutral aqueous solutions. However, NH_3BH_3 suffers from a number of disadvantages: (1) NH_3BH_3 hydrolyzes easily in acids [156], (2) the synthesis of NH_3BH_3 is a complex process, and (3) the decomposition of NH_3BH_3 results in the formation of B_2H_6 impurities. In spite of these drawbacks, NH_3BH_3 is still one of the leading materials for hydrogen storage with assured stability [157]. The exothermic decomposition of NH_3BH_3 is a multi-step reaction which is given by equation 1.2 to equation 1.4 [158]:

$$xNH_3BH_3(s) \rightarrow [NH_2BH_2]_x + xH_2 \tag{1.2}$$

$$[NH_2BH_2]_x \rightarrow [NHBH]_x + xH_2 \tag{1.3}$$

$$[NHBH]_x \rightarrow BN + xH_2 \tag{1.4}$$

In addition, the rate of hydrogen released from NH_3BH_3 is sluggish at moderate temperatures below $373K$. The hydrogen gets entrapped by the discharge of harmful by-products due to energy barriers and side reactions. Various techniques have been proposed and implemented to overcome these issues, which include the addition of catalysts or chemical promoters which will improve the hydrolysis reactions, as well as chemical modifications of NH_3BH_3 by the substitution of its amine protonic hydrogen with metal cations [155].

Among several options presented so far, solid-state storage systems based on metal hydrides have been recognized as one of the most feasible solutions to store hydrogen in

hydrogen-powered systems. However, there exist serious challenges with using hydrides. Hydrides violently react with moist air and can cause skin or eyes irritation. Also, impurities will be absorb during the H_2 uptake in the tanks which is troublesome to counter and recycle. This problem results in the reduction of the tank's lifetime as a result of the impurities occupying the spaces that were occupied by hydrogen. Additionally, the existence of air and O_2, hydrides require high temperature to desorb H_2, which is an indication of slow desorption kinetics and reactivity [159, 160]. For complex hydrides, the safety handling of the hydride is difficult as it may decompose to form highly stable elements [149].

1.6 Summary

The hydrogen storage technology is rapidly emerging as a fast alternative to fossil fuels but it needs further improvements in terms of infrastructure and applications which in turn depends on the energy density, storage capacity, efficient hydrogen storing system, least safety requirements and finally low investment cost. Hydrogen economy cannot be attained through a single route as there are many variables that are taken into consideration in order to achieve the target of attaining a clean and renewable economy which would depend entirely on hydrogen.

Compressed hydrogen storage is beneficial for fuel purpose but requires a high pressure tank which limits their use while liquid hydrogen offers high volumetric energy density but fails as being an energy extensive method. Corrosion is another problem that occurs due to the formation of ice around the tank that leads to boil off. On the other hand, hydrogen has been adsorbed on porous systems (physisorption) which possess high gravimetric capacity, fast hydrogen adsorption and desorption cycles. Problems like metal clustering, adsorption at low temperature or high pressure and weak interaction with the H_2 molecules limits their use. Also, metal hydrides (chemical storage) offer high gravimetric capacity but require high pressure and temperature for hydride formation and hydrogen release. A comparison of properties, benefits and limitations of the different hydrogen storage methods is given in Table 1.6.

Among the methods of hydrogen storage reviewed in this chapter, storage in metal hydrides seems an interesting method due to its high safety under operating conditions and the high gravimetric capacity that some hydrides exhibit. An overview of the storage materials developed through the Centers of Excellence of the US Department of Energy H_2 storage program is presented in Figure 1.12.

Parameters	Compressed storage	Liquid storage	Chemical storage	Physisorption
Gravimetric capacity ($wt.\%$)	13	Varies	<18	20
Volumetric capacity ($Kg.m^{-3}$)	<40	70.8	150	20
Temperature (K)	273	21.5	$373-573$	Varies
Pressure (bar)	800	1	1	100
System cost ($\$kW/h$)	$12-16$	6	$8-16$	100/60
Method of storage	Compressed gas storage	Cryogenic storage	Chemical storage	Physical adsorption by porous materials
Benefits	Lightweight, highly beneficial for fuel purpose, occupies smaller space and energy effective	Volumetrically and gravimetrically efficient, long term hydrogen storage	High storage density and low reactivity and short storage time	Fully reversible process, no accumulation of impurities, fast cycle life and refilling time
limitations	Requires high-pressure cylinder, volumetrically and gravimetrically inefficient	Requires compressed tanks, suffers from large energy loss due to liquefaction and boil off process and high tank cost	Reacts violently with moist air, cumbersome to handle, absorption of impurities, lack of reversibility, desorption at elevated temperature and slow kinetics of dehydrogenation	Clustering problem, requires low temperature or exceedingly high pressure and shows weak interaction with the H_2 molecule

Table 1.6: Comparison between the various hydrogen storage methods [17].

From Figure 1.12, Mg based hydrides can be considered as an efficient hydrogen storage. Magnesium (Mg) and its alloys received greater attention due to their highly H_2 storage capacity by weight $7.66wt.\%$ and as well as being inexpensive material [22], also their hydrides have an excellent quality for functional properties which are heat-resistance, vibration absorbing, reversibility and recyclability [161]. However, it suffers from slow kinetics and a high decomposition temperature and several approaches have been adopted to improve its performance. In next section we will focus on this attractive material.

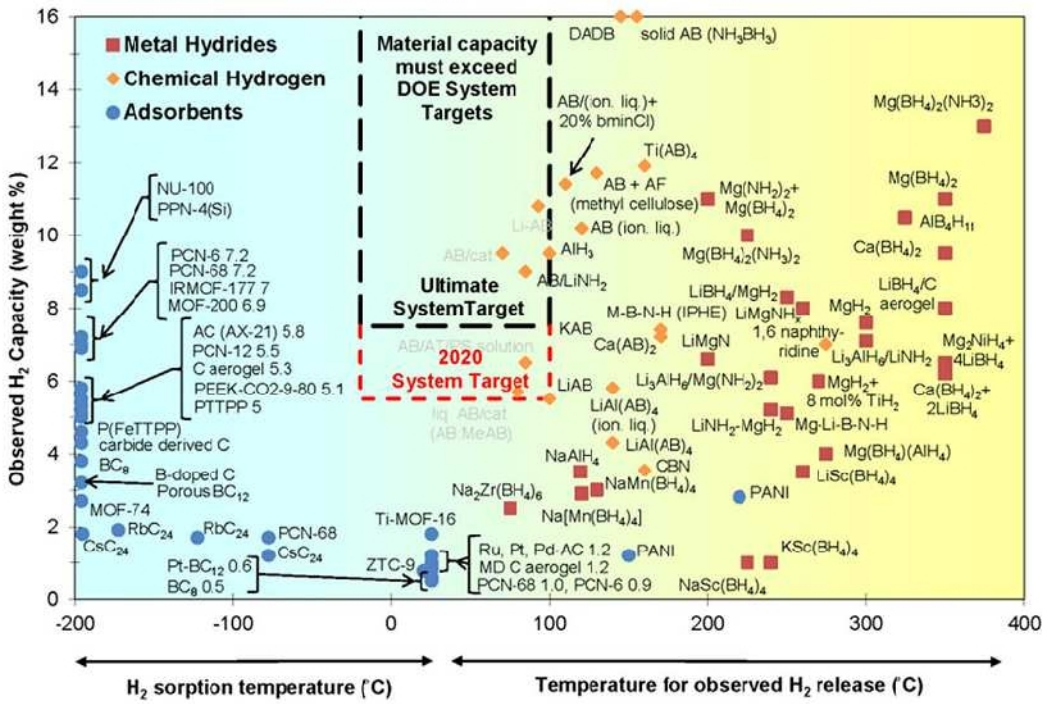

Figure 1.12: Gravimetric hydrogen capacity and sorption temperature of various hydrogen storage materials [162].

1.7 Magnesuim hydride MgH_2

Mg is one of the most efficient metals to store hydrogen in various metal hydride forms, such as intermetallic hydrides (Mg_2NiH_x), complex hydrides ($Mg(AlH_4)_2$, $Mg(BH_4)_2$) and elemental hydride (MgH_2). Among them, elemental hydride revealed an advantages of having higher volumetric (110 H/l) and gravimetric (7.6$wt.\%$) hydrogen capacities than intermetallic hydrides, and higher reversibility than the complex hydrides [23, 163, 164]. However, it has not been widely adopted commercially, mainly because of its high thermodynamic stability, high desorption temperature and slow hydrogen sorption (both absorption and desorption) kinetics [23].

Several studies have attempted to overcome the thermodynamic and kinetic limitations of MgH_2 for the past few decades. Common areas of study included the reduction of MgH_2 size [16, 29] and the employment of novel catalysts. At present, many types of catalyst materials, such as metals [24, 165, 25], metal oxides [25, 166, 167, 168, 169], alloys [26, 170, 171, 172], carbon-based structures [27, 173, 174, 175], and other compounds [28, 176, 177], were employed with MgH_2 to accelerate the sorption kinetics and decrease the desorption temperature. However the progress made to date is not enough in the catalyzed Mg/MgH_2 to meet the *US-DoE* requirements [23].

1.7.1 Properties of MgH_2

1.7.1.1 Structural properties of MgH_2

Mg is the ninth most abundant element in the universe and lightly packed ($1.738 g/cm^3$) solid material [178]. The element is a group-2 alkaline earth metal with a hexagonal close-packed crystal structure, and is a potential candidate to store hydrogen.
Magnesium forms a stoichiometric dihydride MgH_2 which crystallizes in two polymorphic forms. Stable at ambient conditions, α-MgH_2 has a tetragonal TiO_2 rutile-type structure. This hydride, at high applied pressures exceeding $0.39 GPa$ ($3.9 kbar$) [179], transforms into a metastable, at normal conditions, γ-MgH_2 which crystallizes with an orthorhombic α-PbO_2-type structure. A β-MgH_2 cubic modified CaF_2 structure has been also reported, observed experimentally using in situ synchrotron diffraction, which is stable at very high pressure [179]. More structural details are given in Table 1.7.

During hydrogenation, the hexagonal close-packed (HCP) lattice of magnesium expands and leads to a transformation into the deformed body-centred cubic sub-lattice. Because of the deformation, this sub-lattice becomes tetragonal for α-MgH_2 and orthorhombic for γ-MgH_2. In what follows we are interested in the rutile-phase (stable) of this compound.

Type of hydride	**Space group symmetry and type**	**Unit cell parameters** (Å)	**Atomic coordinates**	**Shortest distances** (Å)		**Size of interstice**
				D_{Mg-H}	D_{H-H}	r_{int} (Å)
$\alpha - MgH_2$	$P4_2/mnm$ TiO_2	a = 4.5025 c = 3.0123	2Mg in 2a: 0,0 ,0 4 H in 4f: 0.306 , x ,0	1.948	2.471	Δ:0.35
$\beta - MgH_2$	Pa3 Deformed CaF	a = 4.6655	4 Mg in 4c: 0 ,0 ,0 8 H in 8c: 0.3429 , x , x	1.906	2.489	Δ:0.37
$\gamma - MgH_2$	Pbcn $\alpha - PbO_2$	a = 4.5051 b = 5.4197 c = 4.9168	4 Mg in 4a: 0 , 0.3313 , 8 H in 8d: 0.273 , 0.109 , 0.079	1.915	2.489	Δ:0.34

Table 1.7: Crystal structure data for $\alpha - MgH_2$, $\beta - MgH_2$ and $\gamma - MgH_2$ [180].

1.7.1.2 Thermodynamic and kinetic properties of MgH_2

As for the other conventional hydrides, the equilibrium pressure of the $\alpha(Mg\text{-}HCP) \longleftrightarrow \beta(MgH_2\text{-rutile})$ transition (Figure 1.10) is given by the Van't Hoff equation[180]:

$$\ln\left[\frac{P}{P_0}\right] = \frac{\Delta H}{RT} - \frac{\Delta S}{R} \tag{1.5}$$

where ΔH and ΔS are, respectively, the formation enthalpy and entropy, P_0 is the equilibrium pressure, T is the temperature and R is the gas constant.

Magnesium hydride is considered to be a stable hydride, with a heat of formation of $-74.5 kJ/mol.H2$ and entropy variation of $-0.135 kJ/mol.H$. Figure 1.13 shows the variation of plateau pressure as a function of temperature for magnesium hydride.

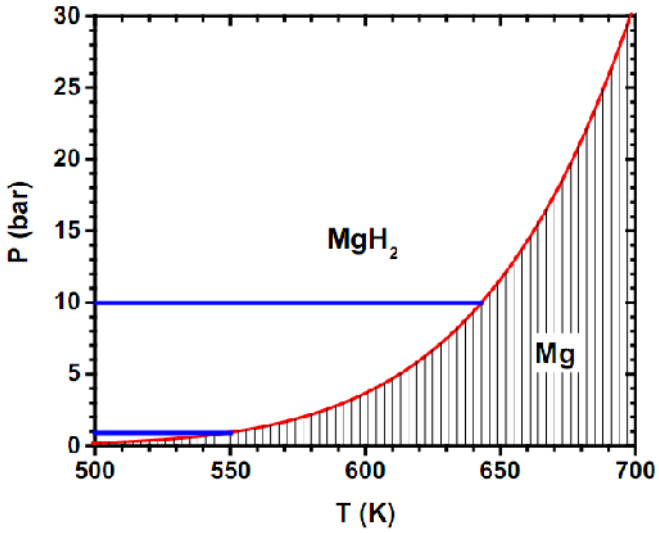

Figure 1.13: Temperature dependence of the dissociation pressure of MgH_2 [180].

One can see that to desorb hydrogen under $1bar$ of pressure, magnesium hydride has to be heated to at least $550K$. Similarly, magnesium could not absorb hydrogen below a pressure of $10bar$ if the temperature is higher than about $640K$ [180]. It is thus clear that magnesium hydride could only operate at high temperature. The challenge is thus to reduce its temperature of operation while keeping as much as possible its high hydrogen storage capacity.

The reaction of Mg with hydrogen involves a number of different steps, such as physisorption, dissociation and chemisorption, the diffusion of hydrogen into subsurface sites and bulk lattice sites and finally the nucleation and growth of the hydride phase. During desorption, Mg itself has to be nucleated and hydrogen atoms have to diffuse to the subsurface and surface and recombine there to hydrogen molecules, which have to be physically desorbed back into the gas phase. The overall hydrogen sorption kinetics is determined by the slowest step in this reaction chain [181]. While the diffusion constant of hydrogen in Mg has been found to be of the order of $10^{-13}m^2/s$ at $300K$, H-diffusion in MgH_2 is found to be at least three orders of magnitude lower [176]. Hence, it is expected that the sorption kinetic in magnesium hydride is significantly slow.
There are three factors that inhibit the hydrogen absorption/desorption kinetics of Mg[182]:

- The first factor is the formation of a magnesium oxide (MgO) layer, resulting from oxidation of the Mg surface. This layer forms a barrier which cannot be penetrated by hydrogen. However, the MgO layer can be broken down by performing several cycles of annealing at $\sim 673K$, which is a form of heat treatment, in both vacuum and hydrogen environments.

- The second factor is the limited dissociation rate of the hydrogen molecules on the Mg surface. However, the dissociation rate can be improved by the addition of a

small amount of catalyst.

- The third factor is the low hydrogen mobility of the magnesium hydride (MgH_2) phase, which hinders further hydrogen absorption when the catalysed Mg begins to absorb hydrogen [183].

Much effort has been made to overcome the thermodynamic and kinetic limitations of MgH_2 [184]. A number of techniques have been devised to achieve this goal, which includes alloying, surface modifications, doping the materials with catalysts, as well as the development of nano-crystalline and amorphous Mg-based alloys [185, 186]. In the subsequent sections, we explain some of these approaches.

1.7.2 Improvements on the thermodynamic and kinetic properties of MgH_2

1.7.2.1 Improvement on surface properties and mechanical ball-milling

A critical factor for hydrogen absorption by metals is the metal surface, which activates dissociation of hydrogen molecules and allows easy diffusion of hydrogen into the bulk. Diffusion is not the limiting step initially because no material has been reacted and there are sufficient active sites available [187], but chemisorption is the slowest step for pure Mg at this point [188]. As the reaction progresses, hydrogen diffusion takes place and the hydride layer grows, producing a nearly impermeable layer. Diffusion through this hydride layer becomes the rate-limiting step in the hydride formation process [188]. In addition to formation of a compact hydride layer, exposure to oxygen also lowers absorption rates due to the formation of a highly stable oxide layer [159]. Andreasen et al. [189] have reviewed the kinetics in terms of apparent activation energies and apparent prefactors of Mg-based hydrides. It was suggested that variations in apparent activation energies correlate with the presence of MgO surface layer inhibiting diffusion of hydrogen. Thus, oxidized samples show large apparent activation energies and well activated samples show smaller activation energies.

The ball-milling creating fresh surfaces during processing is an economic process that is widely applied to metal hydrides to achieve good surface properties [22]. The main effects of ball-milling are increased surface area, formation of micro/nano-structures and creation of defects on the surface and in the interior of the material. The induced lattice defects may aid the diffusion of hydrogen in materials by providing many sites with low activation energy of diffusion. The induced micro-strain assists diffusion by reducing the hysteresis of hydrogen absorption and desorption [190]. The increased surface contact during ball-milling leads to fast kinetics of hydrogen transformations. It is possible

to control properties of the store material, according to specific applications. These include changing the alloy composition, surface properties, micro-structures and grain size by ball-milling without the additional cost of catalyst and with minimal loss of storage capacity[191].

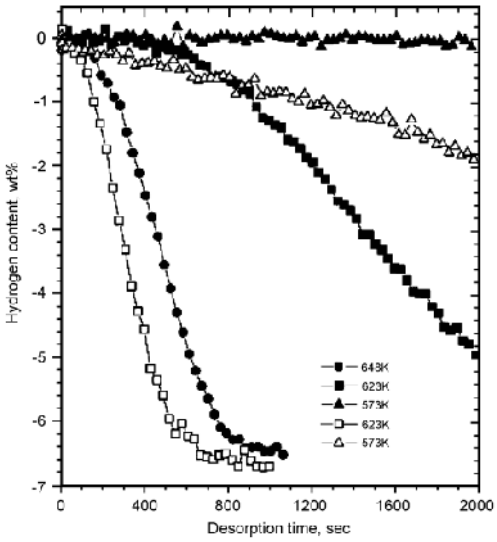

Figure 1.14: Hydrogen desorption curves of unmilled MgH_2 (solid symbols) and ball-milled (hollow symbols) MgH_2 under a hydrogen pressure of $0.15bar$ [192].

Huot et al. [191] investigated the structural difference between milled and unmilled MgH_2. The specific surface area is decreased by milling 10-fold. Faster hydrogen desorption kinetics, reduction in activation energy and enhanced kinetics observed for the milled MgH_2 compared to the unmilled one are seen in Figure 1.14. The activation energies for desorption were measured as 120 and $156kJ/mol$ for the milled and unmilled powders, respectively.

Thus, mechanochemical synthesis using ball milling of magnesium hydride with and without additives and alloying metals has been employed to produce defect-enhanced potential hydrogen storage materials [180]. The high pressure, high energy impacts of the balls and vial walls repeatedly compress, fracture and cold-weld the powder particles. This can significantly reduce both powder and grain (crystallite) size, break the oxide layer on magnesium powder and provide fresh surfaces, as well as dispersing additives through the composite materials [180].

1.7.2.2 Catalysis and alloying with other elements

Catalysis is the process of enhancing the sorption kinetics of hydrogen of metal hydride systems that facilitates dissociation of hydrogen molecules or recombination of hydrogen atoms rapidly and effectively [1]. Lots of experiment and theoretical studies have

indicated that the catalysts, whether mixed as additives or doped as alloying components, could control the following factors to accelerate the hydrogen absorption rate of metal hydrides [192]:

- the rate of hydrogen dissociation at the surface of metal hydrides;
- the capability of hydrogen to penetrate from the surface of metal hydrides which is typically covered by an oxide layer into metal;
- the rate of hydrogen diffusion into the bulk metal and through the metal hydrides already formed.

Effective catalysts, even added in small amounts enhance the formation of a hydride in reasonable extent. Palladium is a good catalyst for hydrogen dissociation reaction. The hydriding properties are enhanced by catalysis through nano-particles of Pd located on magnesium surface [159]. The reactivity of palladium after exposure to oxygen is recovered during exposure to hydrogen because of the easy decomposition of palladium oxide [193]. However, high cost of palladium is the main disadvantage for the industrial applications [22]. Zaluski et al. [194] have also reported on the Hydrogen molecules have a strong affinity for nickel and readily dissociate and adsorb onto surface-layer nickel clusters [195, 196]. Through the addition of 1% of nickel to magnesium, Holtz and Imam [197] achieved a 50% increase in hydrogen capacity, a decrease in the temperature for the onset of hydrogenation from 275 to $175°C$, and a lowering of the dehydrogenation onset temperature from 350 to $275°C$.
In addition to Pd and Ni, Ge can be used for the catalysis of hydrogenation kinetics [198]. The presence of Ge decreases the hydride decomposition temperature in a range from 50 to $150C$, depending on the catalyst amount. But the catalytic effect of Ge disappears after few hydrogen absorption/desorption cycles [198].
Vanadium also acts as a catalyst for the dissociation of hydrogen molecules. It was also reported using V as a catalyst, hydrogen capacity can be increased up to $5.8wt.\%H_2$ while the thermodynamic parameters of MgH_2 were not altered [199], as shown in Figure 1.15. Titanium and vanadium block the oxidation of the alloy surface, and therefore, increase the discharge capacity over multiple cycles [200]. A nano-crystalline $Mg1.9Ti0.1Ni$ alloy shows good absorption kinetics at room temperature [201].

Experimentally, some transition metal atoms were identified to be doped into MgH_2 lattices and replaced the Mg ions to form new phases, which resulted in the enhanced dehydrogenation kinetics or lowered desorption temperature. For example, Chen et al. [202] found that the $MgH_2 - Fe$ composite, with the formative new phases FeH_4/FeH_2, had the maximum amount of hydrogen released within 5 min at $340°C$.

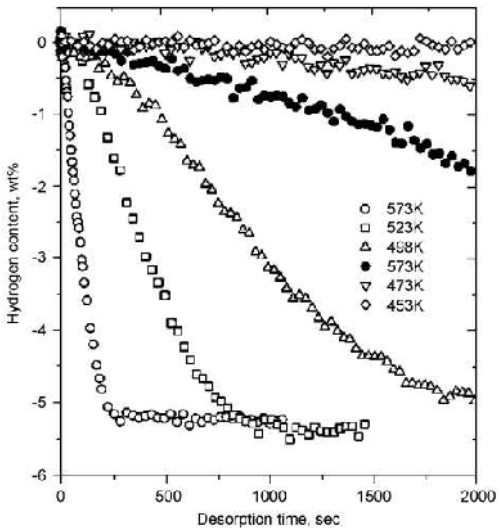

Figure 1.15: Hydrogen desorption curves of mechanically milled MgH_2 at $5\%V$ composite (hollow symbols) and MgH_2 (solid symbols) under $0.15bar$ [192].

Eskandarany et al. [203] reported that the $MgH_2 - 5.5wt\%Ni$ composite, prepared by gradual doping Ni particles into MgH_2 powders, was a reversible hydrogen storage material with a cyclic capacity of $5.5wt.\%H_2$ over 100 cycles at $275°C$. Furthermore, Chen et al. [204] reported that the $MgH_2-4wt\%Ni$ nano-fibres nanocomposite dehydrogenated completely ($7.02wt.\%H_2$) within only 11 min at $325°C$.

Metal oxides can also be used as catalysts material such as V_2O_5 [205] and Cr_2O_3 [206, 207]. These metal oxides can be acted as the refining agents during milling process, which are conducive to reducing the crystalline size and activation energy of MgH_2. More importantly, the catalysts play a decisive role in improving the de/hydrogenation ability of MgH_2 by attaching them on MgH_2 surface and/or reacting with MgH_2 to form some new phases. For instance, after ball-milling of MgH_2 with ZrO_2 for 20 h, $MgH_2 - 5wt\%ZrO_2$ exhibited a lower activation energy for the hydrogenation reaction. Notably, this composite had a hydrogen storage capacity of $6.73wt.\%H_2$ at $423K$ within $100s$ and still absorbed $4.0wt.\%$ H_2 under room conditions ($298K$) [208].

1.7.2.3 Nanostructuring (2D and 3D)

Subsequently, researchers demonstrated the advantages of pursuing dimensional investigations on Mg/MgH_2 for kinetic and thermodynamic changes. According to authors of many works [16, 209, 210, 211, 212], metal clusters stability and reactivity are a function of their size, especially in the nanoscale range, which presents a new area of practical solid-state hydrogen storage. Nano-materials generally have substantially distinct properties in contrast to the coarse-grained counterparts because of their increased surface area, shorter diffusion distances and multiplied grain boundary atoms.

Generally, the Mg and MgH_2 bulk particles were transformed to $3D$ nano-structured particles by employing the top down mechanical (ball) milling technique, using various types of ball mills [213, 214, 215, 216]. During the ball milling process, nano-structured building blocks are formed by the controlled mechanical attrition of the larger particles. The ball milling technique was used to decrease the crystallite size, particle size, defects on the surface, and distribution o catalyst materials on Mg/MgH_2 in Mg-based hydrogen storage materials [137, 213, 217].

Many efforts have already been made to decrease the particle size of Mg/MgH_2 through various ball milling techniques [213, 214, 215, 216]. Most of these studies reported that the ball milled Mg/MgH_2 particle size decreased to the sub-micron scale. Tian et al. [218] reported that the average particle size of ball milled TiC catalyzed MgH_2 was in the range of $200 - 400nm$, while the average size of Mm-oxide catalyzed Mg/MgH_2 was reported to have decreased to $< 1\mu m$ [213]. Pourabdoli et al. [219] prepared $50nm$ to $1\mu m$ sized Mg particles through a mechanical milling process with catalyst additives.

Figure 1.16 represents the isothermal desorption kinetic curves of (a) MgH_2 at 350 °C, (b) ball milled MgH_2 at 350°C and catalyzed MgH_2 at various temperatures (c) 250°C, (d)300°C, (e) 350°C, and (f)380°C. As seen in Figure 1.16, at constant temperature and pressure the isothermal desorption kinetics of nano-size MgH_2 is comparatively faster than that of the larger-sized particles [219]. Similarly, a noticeably lower onset desorption temperature (105°C lower), from 410°C for the bulk material to 305°C for the ball milled catalyzed MgH_2, is observed [220]. This considerable change is due to the decrease in the particle sizes and occurrence of new active surfaces of Mg/MgH_2.

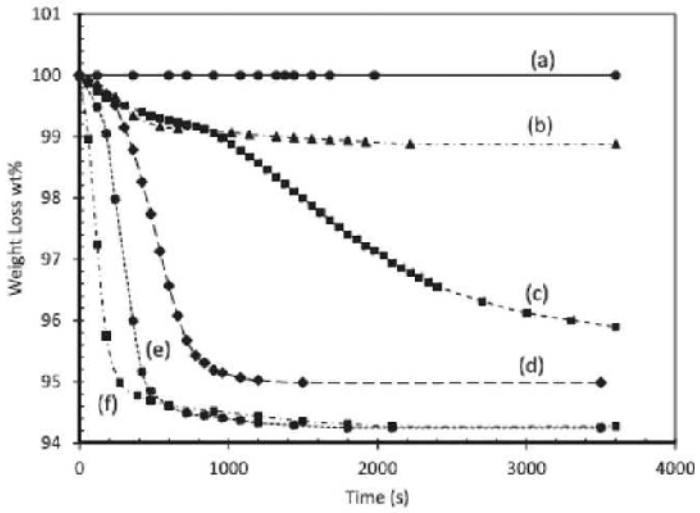

Figure 1.16: Isothermal hydrogen desorption kinetic curves of (a) as-received MgH_2. (b) ball milled MgH_2 (without catalyst) (e) ball milled MgH_2 (with catalyst) at 350°C, and (c), (d), (f) ball milled MgH_2 (with catalyst) at 250, 300, 380°C, respectively [16].

Decreasing the particle sizes to $3D$ nano-structures through the mechanical milling process is one of the known ways to increase the feasibility for further on board applications. Nevertheless, the $3D$ smaller-sized particles, with or without catalyst, were only helpful to enhance the hydrogen sorption reaction kinetics, but not the significant changes in ΔH and ΔS [215]. In this regard, to further continue research in this field, $2D$ dimensional was made to change the thermodynamic stability of the MgH_2 system.

$2D$ nano-structured materials can be prepared by externally controlling the synthesis of the desired structure. The preferred $2D$ nano-structured material for hydrogen storage properties is a Mg-based thin film [29, 221]. The $2D$ nano-structured Mg films were synthesized through different feasible techniques such as electron beam evaporation [29, 222], direct current (DC) and radio frequency (RF) magnetron sputtering deposition [220], and plasma sputter and pulsed laser deposition [221]. Relatively, the thickness of Mg film can have a ranging from micro- to nano-size, due to the externally applied conditions of divergent deposition techniques. For instance, Mg films with an approximate thickness of $100nm$ were prepared through ultra-high vacuum (UHV) sputtering techniques [220]. Barawi et al. [29] prepared various thicknesses (between 45 and $900nm$) of Mg films on SiO_2 substrates, through e-beam evaporation.

The thickness also plays a major role in the hydrogen absorption kinetics of Mg films due to the interface effects between the SiO_2 substrate and the Mg film. Tan et al. [222] synthesized the $4wt\%Fe$-doped Mg thin film on Al_2O_3 and Si substrate by an e-beam evaporation technique. They have found that the ΔH and ΔS of the Mg system, together with its thermodynamic stability, significantly decreased when using Fe-doped Mg film. The reported ΔH of the Mg film for hydrogen absorption and desorption is 42.7 ± 3.2 and $66.9 \pm 4.1 kJ/mol$, respectively [222]. In brief, these reported studies show that the ΔH of hydrogen absorption and desorption of $3D$ bulk Mg/MgH_2 are 73.9 ± 0.7 and $77.7 \pm 0.8 kJ/mol$, respectively [215], and are considerably higher than those of the as-prepared $2D$ nano-structured Mg/MgH_2 film. In the same way, the isothermal hydrogen absorption kinetics of Mg-based thin film is $56 \pm 3 kJ/mol$ [222].
The dimensional changes on Mg films have essentially improved the sorption kinetics and thermodynamic changes in Mg due to the thickness and surface properties of $2D$ nano-structured film.

1.8 Conclusion

Hydrogen fuels are an attractive alternative source of energy since they are clean, non-toxic and renewable, making them suitable for use as substitutes for petroleum-derived fuels in vehicular applications. However, the greatest challenge in making hydrogen fuel-based transportation a norm in the future lies in the development of safe, compact, portable and cost-effective hydrogen storage systems with high energy densities for on-board vehicular applications. Conventional hydrogen storage technologies such as high-pressure compression at about $70MPa$, liquefaction at cryogenic temperatures ($77K$) are impractical for this purpose, and a more feasible alternative is to store hydrogen in solid form by either absorption in metal hydrides or adsorption on high surface area materials such as carbon nanotubes ($CNTs$) and metal organic framework ($MOFs$) systems.

MgH_2 is a promising hydrogen storage material due to its high volumetric and gravimetric hydrogen storage capacities (Table 1.8.), low cost and abundance of Mg element. However, the undesirable thermodynamics, sluggish kinetics, less environmental stability and poor cycle properties of Mg/MgH_2 limits its practical application. According to the previous reports, both catalysis and nano-structuring (nano-sizing) are considered as the most promising options for address these issues to form the future clean, renewable, alternative and sustainable energy storage systems.

System	**Density** (g/cm^3)	**H atoms per unit volume** ($\times 10^{22}/cm^3$)	**Weight** $\%H$
Gas	0.008	0.5	100.0
Liquid H_2	0.07	4.2	100.0
H_2O (liquid)	1.0	6.7	11.2
MgH_2	1.4	6.7	7.6

Table 1.8: Comparison of gravimetric and volumetric hydrogen capacity between MgH_2 and other modes and system (adapted from [224]).

Many researchers have studied the effects of various kinds of catalysts including metals and oxides on hydrogen storage properties of MgH_2. Based on the experimental studies, the metal catalysts doped in MgH_2 will generate lots of defects and/or newly phases, as well as facilitate the formation and decomposition of $Mg-H$ bonds, leading to an enhanced de/hydrogenation kinetics of MgH_2. However, the addition of metal catalysts will inevitably lower the total hydrogen storage capacity of MgH_2 due to the nature of heavy element of metals. Recently, the alternative $2D$ nano-structured MgH_2 such as MgH_2 thin films can be prepared through viable synthetic techniques. The activation energy and formation heat values are significantly lowered to MgH_2 nano-films when compared to bulk MgH_2 structure. All efforts to downscale the Mg/MgH_2

particle/crystallite size to the nano-metre range are extremely positive in improving the kinetics of the reaction with hydrogen.

Several theoretical calculations were performed to study $3D$ Mg/MgH_2 properties with and without various kinds of catalysts materials, but few studies were made on other advanced structures such as Mg films. Moreover the observed catalytic mechanism is still not adequately explained.

Then, through methods (chapter 2) such as ab-initio calculations and Monte Carlo simulations we propose a model to simulate and study the thermodynamic (chapter 3) and kinetic (chapter 4) properties of MgH_2. Moreover, substitution and nano-structuring approaches to tune the thermodynamic and kinetic problematic of MgH_2 are presented.

Chapter 2

Thermodynamics and kinetics from the first principle

Contents

2.1 Introduction

The thermodynamic and kinetic properties of solids are macroscopic properties that are collectively determined by the underlying atomic interactions. An understanding of these macroscopic properties requires an understanding of the environment and behavior of atoms that form the solids. This means that in theory, we should solve the quantum mechanical equations that govern the behavior of these elementary particles in solids to understand the thermodynamic and kinetic properties. However, this is extremely difficult in practice. Fortunately, statistical mechanics serves as a bridge between the atomic-scale description of solids and their macroscopic properties, and allows the prediction of thermodynamic and kinetic properties from the first principle.
In last decades, some approaches have been developed to predict qualitatively or quantitatively the thermodynamic and kinetic properties. This chapter is dedicated to describe the methods and procedures used for this purpose: ab-initio calculations that will allow us to determine the structural and thermodynamic properties of our systems including the formation energy and desorption temperature and the Kinetic Monte Carlo simulations that will be used to reproduce the kinetics of hydrogen ab/desorption in our hydrides.

2.2 The procedure to predict thermodynamics and kinetics

It is well known in statistical mechanics that the macroscopic thermodynamic and kinetic properties of a solid are the weighted mean of the values of the specific property within each micro-state as the solid samples. Each micro-state s has an energy E_a associated with it which is an eigenvalue of the Schrodinger equation of the solid. The weight, according to the statistical mechanics then, is the probability that a system is in a particular state s, and is given by [225, 226]:

$$P_s = \frac{\exp(-E_a/K_\beta T)}{Z} \tag{2.1}$$

where K_β is the Boltzmann constant, T is the temperature and Z is the partition function defined as:

$$Z = \sum_s \exp(-E_a/K_\beta T) \tag{2.2}$$

Equation 2.1 represents a distribution function that assigns the relative importance of different micro-states in the determination of thermodynamic averages and reflects the fraction of time that a solid resides in each micro-state. In this way, the average thermo-

dynamic properties can be evaluated as:

$$A = \sum_s A_s P_s \tag{2.3}$$

where A is a macroscopic thermodynamic quantity and A_s is the value of that quantity when the solid is in micro-state s. Also, a prediction of phase stability requires a comparison of free energies of different phases at finite temperature. The free energy G of a system for example is formally related to the partition function Z according to equation[226]:

$$G = -K_\beta T \ln(Z) \tag{2.4}$$

The knowledge of E_a for all excited states s of the solid, which includes configurational, vibrational, and electronic excitation are required to the evaluation of equation 2.1 to equation 2.4.

In the systems studied in this thesis, the degrees of freedom of configuration arise from all the possible ways of distributing hydrogen on the interstitial sites of the metal hosts in the MgH_2 system and all the possible arrangements of the dopant atoms M ($M = Al, Ti, V, Fe$ and Ni) in the doped systems. Vibrational and electronic excitations are often neglected in studies of thermodynamic and kinetic properties by first principle in multi-component solids [227, 228, 229, 230, 231, 232, 233, 234, 235], so, in this thesis, we will neglect the electronic excitation for the the studied compounds and we will study thermodynamic properties without vibration.

The energies of activation E_a must be calculated from the first principle, but as the number of excitations is very important, it is necessary to resort to a simple model which allows us the computation of the energies for different configurations. Once energy barriers are calculated, a statistical physics technique such as Kinetic Monte Carlo simulations (KMC) can be used to evaluate kinetic properties at finite temperature.
Thus, the methods used in this thesis to calculate the thermodynamic and kinetic properties by DFT calculations and KMC simulations in MgH_2 and M doped MgH_2 systems can be divided into next steps:

- First, the total energies are calculated by first principles for the pure MgH_2 and M doped MgH_2 systems for various concentration and various doping atoms ($M = Al, Ti, V, Fe$ and Ni).

- By using these energies the thermodynamic properties of the different compounds are deducted in particular heat of formation and decomposition temperature.

- Then, we calculate a variety of total energies for various arrangements of hydrogen atoms in the Mg host.

- These energies are then used to calculate the activation barriers for dissociation, diffusion and adsorption process.

- Finally, the energy barriers are implemented in Monte Carlo algorithm to calculate the kinetic properties of our hydrides.

2.3 Total energies by first principle

Total energies are essential data for any analysis of phase stability and diffusion and must be calculated from the first principles at $0K$ by solving the Schrodinger equation independent of multi-body time:

$$\hat{H}\Psi = E\Psi \tag{2.5}$$

where Ψ is the many-body wave function of electrons, E is the total energy of solid, and $\hat{H}$ is the Hamiltonian operator for the whole system of electrons and nuclei, which is defined as:

$$\hat{H} = -\sum_i \frac{\hbar^2 \bigtriangledown_i^2}{2m_e} - \sum_I \frac{\hbar^2 \bigtriangledown_I^2}{2M_I} + \frac{1}{2}\sum_{i \neq j} \frac{e^2}{\mid r_i - rj \mid} + \frac{1}{2}\sum_{I \neq J} \frac{Z_I Z_J e^2}{\mid R_I - R_J \mid} - \sum_{i,I} \frac{Z_I e^2}{\mid r_i - R_I \mid} \tag{2.6}$$

where, $\hbar$ is Planck's constant devised by 2π, e and m_e denote the charge and the mass of a stationary electron, M_I and Z_I indicate respectively the mass and the charge (atomic number) of the nucleus (ion) and R_I and r_i stand for the positions of the nuclei and the electrons respectively.
In this expression, the first and the second terms correspond to the kinetic energies of the electrons (T_e) and the nuclei (T_n) while the reminder terms indicate, respectively, the Coulomb interactions of electron-electron (internal potential V_{int}), nucleus-electron (external potential V_{ext}) and nucleus-nucleus (V_{nn}). So the Hamiltonian describing the solid simply reads as:

$$\hat{H} = T_e + T_n + V_{int} + V_{nn} + V_{ext} \tag{2.7}$$

And the corresponding time independent Schrodinger equation with this Hamiltonian is given by:

$$\hat{H}\Psi(R_I, r_i) = E\Psi(R_I, r_i) \tag{2.8}$$

By solving exactly the last equation, all the macroscopic properties of the solid, in principle, would be determined. However, this kind of solution is a very hard task or even impossible for most cases. Indeed, this difficulty of solution is related, essentially, to the Coulomb many body terms V_{int} and V_{nn}. So, some approximations for this problem, depending on some physical considerations are required. Some of them will be briefly explained in next sections.

2.3.1 Born-Oppenheimer approximation

The first approximation was introduced by Born-Oppenheimer in 1927 [236]. In this approach, the many body wave function Ψ of the coupled nuclei-electrons system can be separated as result of the huge difference in motion between the nuclei and the electrons. Its validity is based on the fact that the mass of the nuclei, except in the case of the lightest elements, are generally four to five orders of magnitude, much larger than the mass of the electrons. Therefore their kinetic energy T_n, which is inversely proportional to the mass of the nucleus M_I, is relatively small and can be then ignored.
Consequently, the nuclei can be considered as $frozen$ at fixed positions R_I and the nucleus-nucleus Coulomb interaction term V_{nn} (the fourth term in the Hamiltonian) becomes just a classical constant E_n and the total Hamiltonian then simplifies to:

$$\hat{H} \simeq T_e + V_{int} + V_{ext} + E_n \simeq H + E_n \tag{2.9}$$

Under this assumption, the many body wave function Ψ can be then expressed as a product of the electron wave function and the nuclear wave function:

$$\Psi(R_I, r_i) = \psi(R_I, r_i)\psi_n(R_I) \tag{2.10}$$

This involves that the many electron wave function Ψ depends explicitly on the electronic degrees of freedom r_i while it depends upon the nuclear positions R_I as parameters but not as variables. So, the electronic Hamiltonian and the corresponding Schrodinger equation are given by:

$$H = T_e + V_{int} + V_{ext} \tag{2.11}$$

$$H\psi(r_1, r_2, ...) = E_e\psi(r_1, r_2, ...) \tag{2.12}$$

The total energy E_{tot} is then the sum of E_e and the constant nucleus-nucleus Coulomb interaction energy E_n that comes from the constant potential energy V_{nn}:

$$E_{tot} =< H > +E_n = E_e + E_n \tag{2.13}$$

It is important to note, from the electronic Hamiltonian equation 2.11, that the specific information of the system is completely determined by the third term V_{ext} (i.e. the number of electrons N, and the charges Z_I and positions R_I of the nuclei). However, the first two terms can be considered universal, due to the fact they are entirely independent on the kind of the system. Additionally, Born-Oppenheimer approximation is also called adiabatic because it separates the lattice vibrations problem from the electronic ones.

2.3.2 Wave Function Approaches

Electronic structure methods, which are the numerical solutions of the equation 2.12, are distinct from other forms of modeling because they are first-principles in nature. These methods of calculations contain no external parameters other than a most basic description of the system. The fundamental classification of these calculations of matter can be made according to the quantity that is being calculated. In fact, several methods are developed, that aim either to compute the electron wave function or the electron density. There are many methods where the object of the calculation is to compute the full electron wave function that will be the subject of the following sections.

2.3.2.1 Hartree approximation

Hartree proposed to simplify solving the many-electron problem by considering the electrons as non-interacting particles (i.e independent particle model) and each electron then has its own individual wave function [237]. Consequently, the Schrodinger equation 2.12 can be written as a one-electron equation and the many-electron wave function can be expressed as a product of all one-electron wave functions:

$$\psi(r_1, r_2, ...r_N) = \prod_{i=1}^{N} \psi(r_i) \tag{2.14}$$

According to the variational principle in quantum mechanics which states that for any *trail* wave function Φ the minimal approximate energy E corresponding to this wave function is given by:

$$E[\phi] = \frac{<\phi|H|\phi>}{<\phi|\phi>} \geq E_0 \tag{2.15}$$

where E_0 is the ground state energy solution of the Schrodinger equation, when $E[\phi] = E_0$ then Φ is the gound state wave function. By applying this principle with the wave function in Hartree form and the Hamiltonian equation 2.12 the Hartree equation can be written as:

$$\left[-\sum_i \frac{\nabla_i^2}{2} - \sum_I \frac{Z_I}{\mid r_i - R_I \mid} + \sum_{j \neq i} \int dr_j \psi_j^*(r_j) \frac{1}{\mid r_i - r_j \mid} \psi_j(r_j)\right] \psi_i(r_i) = \epsilon_i \psi_i^*(r_i) \tag{2.16}$$

Due to this approximation each independent electron i, moves in an effective potential, representing the attractive Coulomb interaction term of the nuclei and the average effect of the repulsive Coulomb interactions of the other electrons that can be given by the integration over their densities. For this reason, this approximation is called a mean field approach in which the complicated many-body problem, due to the Coulomb many

body term V_{ee}, is replaced by n simpler problems in a mean field potential.

Since the effective potential for each wave function depends on the solution of all other wave functions, this problem (equation 2.16) is, in principle, self-consistent with N simultaneous integro-differential equations and then its solution can be achieved iteratively.

2.3.2.2 Hartree-Fock approximation

In Hartree approach, the electron spins and their fermionic nature are excluded in Hartree wave function and then the Pauli principle is not satisfied as well. In fact, this many-electron wave function, for electron as Fermi particles, must be antisymmetric by exchange of electrons:

$$\psi(r_1, r_2, ...r_j, r_k, ...r_N) = -\psi(r_1, r_2, ...r_k, r_j, ...r_N) \tag{2.17}$$

In order to incorporate the fermionic nature of electrons into the many-electron wave function $\psi(r_i)$ and to guarantee its antisymmetry, Fock assumed that this many-electron wave function should be, approximately, expressed by a single Slater determinant [238, 239] instead of the product in Hartree approach, as follows:

$$\psi(r_1\sigma_1...r_N\sigma_N) = \frac{1}{\sqrt{N!}} \begin{vmatrix} \phi_1(r_1\sigma_1) & \phi_2(r_1\sigma_1) & ... & \phi_N(r_1\sigma_1) \\ . & . & . & . \\ . & . & . & . \\ . & . & . & . \\ \phi_1(r_N\sigma_N) & \phi_2(r_N\sigma_N) & ... & \phi_N(r_N\sigma_N) \end{vmatrix} \tag{2.18}$$

where, N is the total number of electrons and the coefficient $(1/\sqrt{N!})$, is simply a normalization factor. In this determinant, each column and each line correspond, respectively, to a certain one-electron state, and a certain position in space. The interchanging of two electrons is equivalent to the interchanging of the corresponding two lines or columns in the determinant, which changes its sign (the wave function is antisymmetric). Moreover, this wave function representation ensures that the Pauli principle is satisfied, i.e. if two lines or columns are identical (two electrons have the same quantum state) then the determinant vanishes.

The corresponding Hartree-Fock equation is, also, derived from the variational principle by looking for the minimum of the many-electron Schrodinger equation 2.12 with

this single Slater determinant. This equation can be written as:

$$\left[-\sum_i \frac{\nabla_i^2}{2} - \sum_I \frac{Z_I}{\mid r_i - R_I \mid} + \sum_j \int dr_j \phi_j^*(r_j) \frac{1}{\mid r_i - r_j \mid} \phi_j(r_j)\right] \phi_i(r_i) - \sum_j \left[\int dr_j \phi_j^*(r_j) \frac{1}{\mid r_i - r_j \mid} \phi_j(r_j)\right] \phi_j(r_j) = \epsilon_i \phi_i^*(r_i) \tag{2.19}$$

This equation has one extra term compared with the mean field equation of Hartree, the last one called the *exchange potential* term which describes the effects of exchange between electrons that is included in Hartree–Fock many-electron wave function.
The solution procedure of these equations is similar to the iterative self-consistent method that is outlined in Hartree approach.

2.3.2.3 Beyond Hartree-Fock approaches

Even though the Hartree–Fock approximation includes the electron spins and provides an exact description of electron exchange, the electrons correlation property is entirely ignored (i.e. each electron is affected by the motion of other electron in the system). The energy associated with this approach, consequently, must be different from the exact energy by an energy difference that is called the correlation energy.

Therefore, many approaches which are more sophisticated and accurate than Hartree-Fock method were developed to include such energy. These approaches often described the electron correlation by mixing the wave function with some configurations in which the electrons are excited or promoted from lower energy to higher energy orbitals.

Furthermore, these methods are divided into groups based on the number of Slater determent that can be used. The first group uses a single Slater determinant as the reference wave function and excitation are made from that wave function. The methods belonging to this group are known as post-Hartree-Fock methods such as the configuration interaction (CI) [240], coupled cluster (CC) [241], Moller–Plesset perturbation theory (MP) [242], and the quadratic configuration interaction (QCI) approach [243]. Another methods that used more than one Slater determinant are the N-electron valence state perturbation theory ($NEVPT$) [244], multi-configurational self-consistent field ($MCSCF$) and the multi-reference single and double configuration interaction ($MRDCI$) methods[245]. All these methods, are potentially very accurate, however they are currently applied for small system due to their high computational cost that increases rapidly with system size.

2.3.3 Density Functional Theory

Density functional theory (DFT) is one of the most powerful, popular and successful quantum mechanical tools that solve the many-electron problem obtained from Born-Oppenheimer approximation in previous section (equation 2.12).
The basic concept of this method is to deal with a formulation of this many-electron problem that involves the total density of electrons instead of using the many-electron wave function without any loss of information. In fact, a huge simplification can be made by reducing the many-electron problem of N electrons with $3N$ degrees of freedom to 3 degrees of freedom only. It turns out that such a method will be as accurate as beyond Hartree-Fock approaches but with a low computational cost.
Consequently, physical and chemical properties of large molecular and solid systems can be, possibly, calculated and could challenge, quantitatively, the experimental ones.

Before going through this method, it would be useful first to give some basic definitions. Generally, the term functional means a function of a function which is in this case the total electron density. This total electron density for a system of electrons is defined from the wave functions as follows:

$$n(r) = \sum_{i=1}^{N} \int ... \int dr_1 ... dr_N \psi^*(r_1, ..., r_N) \delta(r_i - r) \psi(r_1, ..., r_N) \tag{2.20}$$

And the integral of this density over all space provides the total number of electrons:

$$\int n(r) dr = N \tag{2.21}$$

This density is also a non-negative function with the property:

$$n(r \longrightarrow \infty) = 0 \tag{2.22}$$

The following sections are devoted to explain, briefly, the original density functional theory of Thomas–Fermi-Dirac, the basic aspects of the modern density functional theory including Hohenberg-Kohn theorems, Kohn-Sham one-electron equations (that put this theory into practice) and the exchange-correlation approaches. The calculation methods, which are used in this thesis and some technical and related details, are discussed later on.

2.3.3.1 Thomas-Fermi-Dirac approach

The earliest method of density functional theory was proposed in 1927 by Thomas [246] and Fermi [247]. In their method, the total energy is represented, by terms defining the kinetic energy, the Coulomb interactions of electron-electron (internal potential V_{int}), nucleus-electron (external potential V_{ext}), as an explicit functional of the total density of electrons.

$$E_{TF}[n] = \frac{3}{10}(3\pi^2)^{2/3}\int drn(r)^{5/3} + \int drV_{ext}n(r) + \frac{1}{2}\int drdr'\frac{n(r)n(r')}{\mid r - r' \mid} \tag{2.23}$$

The original Thomas and Fermi formulation ignored the exchange and correlation between the electrons that has been added latter by Dirac in 1930 [248] who defined the local exchange approximation term. The energy functional, for electrons in an external $V_{ext}(r)$ potential, is written using Thomas–Fermi–Dirac approach as:

$$E_{TFD}[n] = E_{TF}[n] - \frac{3}{4}\left(\frac{3}{\pi}\right)^{1/3}\int drn(r)^{4/3} \tag{2.24}$$

The ground state energy and density will be determined by minimizing the functional $E[n]$ in this equation for all possible $n(r)$ in which the integral of the density over all space provides the total number of electrons.
The electronic density, in this approach, assumed to be local at any given point like a density of non-interacting electrons in a homogenous gas. That means that only one or two points of the density are required to get the terms in the equation, which makes a very efficient calculation with a low computational cost.

Several important improvements on this method are given by Weizsacker in 1935 who introduced the effects of inhomogeneous electron gas [249] and Wigner in 1938 who formulated an expression for the electrons correlation [250].
This approach has been applied to equations of state of element [251] but it was unable to predict some essential physical and chemical findings such as shell structures of atoms and binding of molecules.

2.3.3.2 The Hohenberg-Kohn theorems

The modern density functional theory has been, formally, established in 1964 by the two central Hohenberg-Kohn theorems [252]. The first theorem indicates that the many-electron wave function, as a fundamental and complicated quantity in quantum mechanics, can be replaced in the many-electron problem by the ground state electron density without any loss of information.
The second one defines a variational principle for an energy functional, which depends

on the ground state electron density, rather than the many-electron wave function. This variational principle is almost the equivalent of the standard variational principle in quantum theory.
The two theorems can be stated as follows:

- **Theorem 1**: For any system of interacting particles in an external potential $V_{ext}(r)$, the potential $V_{ext}(r)$ is determined uniquely, except for a constant, by the ground state density $n_0(r)$.

- **Theorem 2**: A universal functional for the energy $E[n]$ in terms of the density $n_(r)$ can be defined, valid for any external potential $V_{ext}(r)$. For any particular $V_{ext}(r)$, the exact ground state energy of the system is the global minimum value of this functional and the density that minimizes the functional is the exact ground state density $n_0(r)$.

In order to get more explanations and implications from these theorems, it is important to remind that the first two terms in the electronic Hamiltonian (equation 2.11) are completely universal. However, the third term, the external potentia V_{ext}, which is associated with the parameters N, R_I, Z_I, uniquely specifies this Hamiltonian. As result from this unique specification, the many-electrons wave function and the included information for all ground and excited states will be determined.

In fact, the three parameters N, R_I, Z_I, which are required for the unique specification of the Hamiltonian can be deduced from the ground state electron density making the first theorem feasible.
Firstly, as noted before, the total number of electrons N can be provided by integrating the density over all space. Secondly, at the positions of the nuclei R_I the density has maxima which are closely to the charge Z_I of these nuclei [253].

Therefore, the first theorem implies that the ground state electron density uniquely determines this external potential V_{ext} and as an immediate consequence from this theorem is that any property of the system can be completely, specified as a unique functional (i.e. a function of a function which is the electron density in this case) of the exact ground state electron density.

In this way, the ground state energy functional associated with the electronic Hamiltonian can be written as follows:

$$E_{HK}[n] = T_e[n] + E_{int}[n] + E_{ext}[n] = F_{HK}[n] + \int n(r)V_{ext}dr \tag{2.25}$$

$$F_{HK}[n] = T_e[n] + E_{int}[n] \tag{2.26}$$

where $E_{HK}[n]$ denotes the Hohenberg-Kohn functional which is universal for any many-electron system and contains the functionals of the kinetic energy and the electron-electron interaction terms.
However, the major problem now is only how to find such ground state density. The second theorem tackles this problem effectively by indicating that the $E_{HK}[n]$ reaches its global minimum value for the corresponding exact ground state electron density associated with V_{ext}. This theorem is nothing more than the variational principle:

$$E_{HK}[n] = F_{HK}[n] + \int n(r)V_{ext}dr \geq E_0 \tag{2.27}$$

It should be mentioned that the Hohenberg- Kohn formulation works at $T = 0K$. An extension and generalization have been made by Mermin in 1965 [254] on this formulation to finite temperature canonical and grand canonical ensembles. However, such extension has not been widely used due to the difficulty of constructing good approximate functionals for the entropy. Other popular and powerful extensions of Hohenberg-Kohn formulation are spin and time-dependent density functional theory.

Moreover, although the Hohenberg-Kohn theorems indicate that the electron density can rigorously be considered the central quantity of the many-electron problem, they are pure theorems of existence and give any information about constructing the functionals and finding such exact electron density.
However, these major issues can be treated in light of the ingenious Kohn-Sham ansatz which is the subject of the following section.

2.3.3.3 Kohn-Sham equations

Kohn and Sham [255] introduced, in 1965, the notion that the true density for the system of interacting electrons with a particular external potential V_{ext} may be identical with the density for a reference system of non-interacting electrons moving in an effective potential V_{KS} from all other electrons. In other words, the problem of solving the difficult interacting many-electron system is mapped to solve an auxiliary system of non-interacting electrons in the effective potential V_{KS} having the same ground state density. In this way, Kohn-Sham approach leads to independent electron equations which can be solved exactly by numerical means. Actually, the calculations are performed on the auxiliary system of non-interacting electrons with an exact kinetic energy T_{KS} and an effective

local potential V_{KS} described by the Hamiltonian:

$$H_{KS} = T_{KS} + V_{KS} \tag{2.28}$$

$$T_{KS} = -\frac{1}{2}\sum_{i}^{N} < \phi_i \mid \nabla^2 \mid \phi_i > \tag{2.29}$$

For this system the classical Coulomb interaction term of the electronic density interacting with itself can be defined by Hartree energy E_H as:

$$E_H[n] = \frac{1}{2}\int dr dr' \frac{n(r)n(r')}{\mid r - r' \mid} \tag{2.30}$$

By applying the first Hohenberg–Kohn theorem to this system, there exists a unique energy functional:

$$E_{KS}[n] = T_{KS}[n] + \int V_{KS}(r) n_{KS}(r) dr \tag{2.31}$$

where the ground state electron density $n_{KS}(r)$ of this system, which is identical with the interacting one $n(r)$, can be expressed as:

$$n_{KS}(r) = \sum_{i}^{N} \mid \phi_i(r) \mid^2 = n(r) \tag{2.32}$$

The N occupied orbitals satisfy the Schrodinger-like equations are given by the N lowest energy solutions of:

$$\left[-\frac{\nabla^2}{2} + V_{KS}(r)\right] \phi_i(r) = E_i \phi_i(r); E_1 \leq E_2 \leq ... \tag{2.33}$$

These equations are called the Kohn-Sham equations and the ground state wave function is just a Slater determinant of the N orbitals, the so-called Kohn–Sham orbitals. The main problem now is to determine the form $V_{KS}(r)$ that must take in order that the ground state electron density (equation 2.32) is fulfilled.

For a system of N interacting electrons in an external potential V_{ext}, Kohn and Sham introduced the following approach to rewrite the Hohenberg–Kohn ground state energy functional of the interacting many-electron problem as:

$$E_{KS}[n] = T_{KS}[n] + \int V_{ext}(r) n(r) dr + E_H[n] + E_{xc}[n] \tag{2.34}$$

where this equation incorporates all the difficult many-electron terms into an exchange-correlation functional of the density as:

$$E_{xc}[n] = T_e[n] + T_{KS}[n] + (E_{int}[n] - E_H[n]) \tag{2.35}$$

These last equations show that $E_{xc}[n]$ must be a functional, since the right-hand sides of these equations are functionals. In fact, this universal functional $E_{xc}[n]$ contains everything that is unknown about the real system. It represents the difference of the kinetic and Coulomb interaction energy terms between the interacting and non-interacting systems.
According to the second Hohenberg–Kohn theorem, the density $n(r)$ that minimizes the functionals is the ground-state density. Thus by taking the variation of the equation 2.31 and equation 2.32 with respect to the electron density, the resulting Kohn-Sham one-electron equations are rewritten as:

$$\left(-\frac{\nabla^2}{2} + V_{ext} + V_H(r) + V_{xc}\right)\phi_i(r) = E_i\phi_i(r) \tag{2.36}$$

where $V_H(r)$ and $V_{xc}(r)$ are Hartree and the exchange-correlation potentials, respectively.

We can highlighting a few points about the Kohn–Sham ansatz:

- Firstly, it provides an explicit algorithm to calculate the ground state energy and density of the interacting system.
- Secondly, it is formally exact, supposing that the exact exchange-correlation potential V_{xc} is provided.
- Additionally, the solution of the interacting N-electron problem is given in terms of non-interacting electrons in an external potential V_{KS} which is an extremely useful simplification.

Consequently, it is relatively easy to solve for Kohn–Sham orbitals (a Slater determinant of N orbitals) even for a big system with a few hundreds electrons. In analogy with Hartree approach, the solutions of the Kohn-Sham equations equation 2.36, have to be found self-consistently, the only difference being the presence of the exchange-correlation potential term.
In fact, an initial trial electron density can be chosen, for example, as a superposition or perturbation of atomic densities to find a trial form V_{KS}. The Kohn-Sham equations can now be solved and the orbitals $\Phi_i(r)$ then give the electron density according to equation 2.32 above to find the next iteration for $n(r)$. When this cycle has been repeated

a sufficient number of times that no further changes occur (or the difference between two successive densities is no larger than a predefined criterion), then a solution for $n(r)$ has been found and self-consistency is reached.
An additional advantage of this approach is the simultaneous introduction of useful tools for physical interpretation including the electronic charge density, the density of states and the electronic band structure of the system.

2.3.3.4 The exchange-correlation energy

Although the Kohn–Sham ansatz is formally exact and provides an exact expression for the total energy, unfortunately it introduces the central problem of DFT which is the unknown form of the universal exchange-correlation functional V_{xc}.
From a practical viewpoint, approaches of this functional are unavoidable to solve the Kohn-Sham equations. In fact, many approximations have been devised to get an explicit form for this functional among them the local density approximation LDA and the generalized gradient approximation GGA. These two are the most widely used approximations in solid state physics. In this section, the approximate expressions for exchange-correlation functional including LDA and GGA are briefly presented.

2.3.3.5 The Local Density Approximation

The first and simplest approximation for the exchange-correlation energy functional is the Local Density Approximation LDA [256, 257]. In fact, the mean idea behind this approximation is revealed from a homogeneous electron gas. In the LDA approximation, it is assumed that the local exchange-correlation energy per electron depends on the local density, and this energy equals to the exchange-correlation energy per electron of a uniform electron gas having same density. The total exchange-correlation energy E_{xc} can be then given by summing the contributions of each point in space as:

$$E_{xc}^{LDA}[n] = \int n(r) E_{xc}[n(r)] dr \tag{2.37}$$

In this equation, $E_{xc}[n(r)]$ stands for the exchange-correlation energy per electron of a homogeneous electron gas of density $n(r)$.

The LDA is more accurate for systems having slowly varying densities [255], as the assumed density is locally a constant.
The accuracy of this simple approximation almost leads to a correct picture of binding trends, structural parameters, vibrational energies, phonon spectra, bond lengths and other properties across the periodic table. Most of these properties are predicted correctly, or with a systematic deviation. However this approximation underestimates the

band gap, and also overestimates the binding energy of solids and molecules which leads usually, to an underestimation of the bond lengths [256].

This approximation can be extended to treat magnetic cases, by taking into account the spin-polarization of the material and it is then called the Local Spin-Density Approximation $LSDA$:

$$E_{xc}^{LSDA}[n_\uparrow, n_\downarrow] = \int n(r) E_{xc}[n_\uparrow(r), n_\downarrow(r)] dr \tag{2.38}$$

2.3.3.6 The Generalized Gradient Approximation

In real materials the density varies in space, so a logical improvement of LDA approximation would be to include also extra information of this rate of change in the functional. This can be achieved by adding gradient terms. This approach is called the gradient-expansion approximation GGA [257, 258, 259].
This approximation goes beyond LDA by including not only the information about the density at a specific point ($n(r)$) but also by introducing the density in the local vicinity through the dependence on the gradient ($\nabla n(r)$). Consequently, the non-homogeneity of the true electron density is taken into account within this approximation and the exchange-correlation energy functional is then given as:

$$E_{xc}^{GGA}[n] = \int n(r) E_{xc}[n(r), \nabla n(r)] dr \tag{2.39}$$

The current generalized gradient approximations (GGA) seem to provide reliable results for all main types of chemical bonds binding energies...etc than LDA and are popular in computational physics and chemistry.
There are various forms of GGA functionals that are used in many different calculations. Two widely used are the form of Perdew and Wang ($PW91$) [260] and the form of Perdew-Burke-Enzerhof (PBE) [261]. In this thesis, we used $GGA - PBE$ for all calculations.

2.3.4 Electronic structure of solids

In order to apply DFT to real crystals, the Kohn-Sham equations should be solved for all these particles present in the system (A regular three dimensional ($3D$) solid contains almost 10^{24} electrons and ions per cm^3). This task is computationally an impossible. Therefore, to solve this problem, the periodicity of the crystal must be used.
According to the periodic symmetry of crystal, the calculation problem can be significantly, reduced to only those electrons and ions that are contained only in the *unit cell*. By solving the Kohn-Sham Hamiltonian for the atoms in this unit cell, the electron eigen-

states for solid can be calculated.

According to the Bloch theory, the electrons move in a periodic potential rather than a free space. This potential is generated by the periodicity of the solid and is invariant by translation. Therefore, the effective potential V_{KS}, in the Kohn-Sham equation will be periodic for all lattice vectors R of the crystal and can be written as:

$$V_{KS}(r) = V_{KS}(r + R) \tag{2.40}$$

Bloch's theorem states that the eigenstates Φ of a one-electron Hamiltonian has the form of a plane wave times a lattice-periodic function $u_{nk}(r)$ as follows:

$$\Phi_{nk}(r) = \exp(ikr)u_{nk}(r) \tag{2.41}$$

Here, k denotes the wave vector that is chosen in the first Brillouin zone due to the translational symmetry, n stands for the band index which labels different solutions for a given k.
For all R in the crystal the lattice-periodic function is written as

$$u_{nk}(r + R) = u_{nk}(r) \tag{2.42}$$

Another equivalent form of Bloch's theorem is also given by:

$$\Phi_{nk}(r + R) = \exp(ikr)\Phi_{nk}(r) \tag{2.43}$$

The energy values are periodic also in the reciprocal space, so if $E_n(K)$ is an energy eigenvalue, then $E_n(K+G)$ is also an eigenvalue for all vectors G of the reciprocal lattice.

In case of large systems, the spectrum of k-points is quasi continuous therefore, an integration over k is required to calculate properties such as the density or energy of the system. According to Bloch's theorem the problem of infinitely many-electrons has been converted to a problem of infinitely many k-points inside the first Brillouin zone (due to the symmetry). As the wave functions of closely located k-points are nearly identical, a small region can be sampled by one single k-point. It is sufficient, generally, to solve the Kohn-Sham equations in a unit cell, using only a finite discrete number of k-points, and the electronic part of the total energy can be then calculated to a good approximation. This leads to bands of eigenvalues and energy gaps where no eigenstates can be there. By taking the symmetry of the system into account, the number of k-points can be further decreased by restricting the k-points to the so-called irreducible Brillouin zone. The required number of k-points that is needed to get a good description of a system depends

not only on the type and size of such system, but also particularly on the studied property. For example in isolators case only a few k-points are required as all bands are filled, while for metals more points are needed for bands that cross the Fermi level. Therefore, the convergence of any calculation should be checked with respect to the k-point grid.
Different schemes are developed in order to sample appropriately the Brillouin zone with a set of k-points that give the best estimate of the full integral such as the most widely scheme proposed by Monkhorst and Pack in 1976 [262].

There are several methods for calculating the electronic structure in material. All these methods can be, essentially, categorized in three basic types. There are no fundamental disagreements: all agree when applied carefully and taken to convergence. Indeed, each one leads to instructive, complementary ways to understand electronic structure and each can be developed into a general framework for accurate calculations. Furthermore, each one has its advantages and pitfalls.
The common point of these methods is the solution of Kohn-Sham equations in self consistent way. However, their specificities are given in the representation of the potential, electronics density and, especially, the mono electronic Kohn-Sham orbitals. Some of these calculation methods are schematized on Figure 2.1.

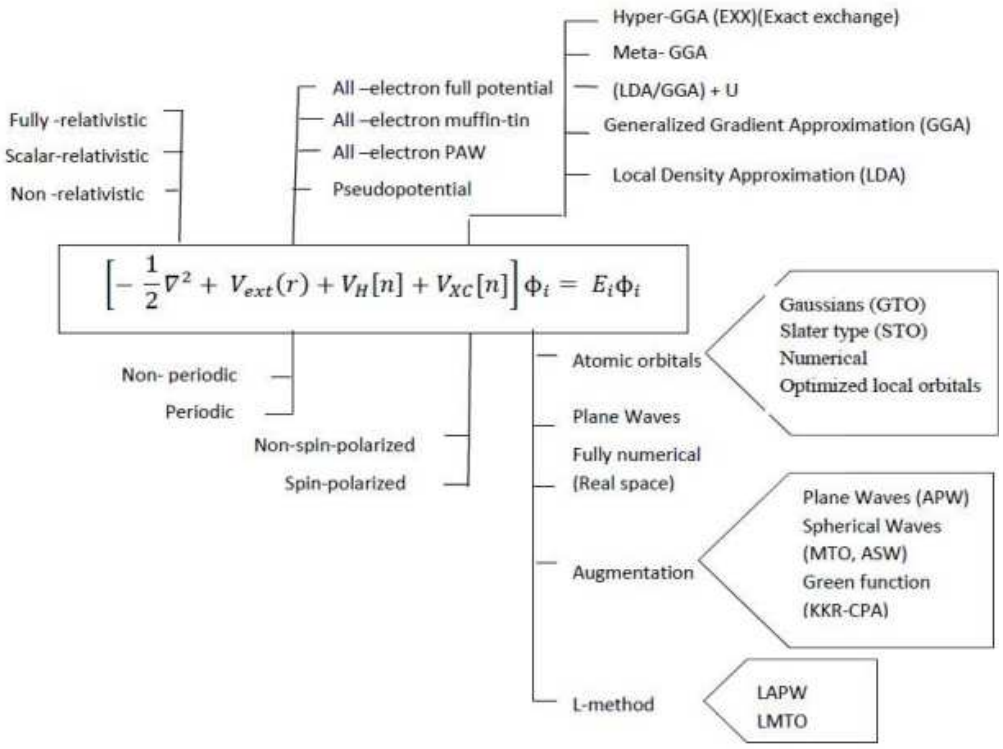

Figure 2.1: Schematic representation of the different calculation methods based on DFT

In chapter 3, somme of the above DFT methods will be used to study the electronic structures of the pure and doped MgH_2 and evaluate the hybridization between

the different elements composing the systems and interpret the stability of the studied hydrides.

2.3.5 Equilibrium Position of Atoms: The Force Theorem

Another practical and important task is the equilibrium position of atoms in the material, so in order to determine the equilibrium geometry of a system, it is necessary to calculate the forces on the nuclei in this system. The particular set of equilibrium position that minimizes the total energy is found when all forces are vanishing. Therefore the derivative of the total energy with respect to the ionic positions must be calculated and this should be zero for the equilibrium position:

$$F_I = -\frac{\partial E_t}{\partial R_I} = 0 \tag{2.44}$$

These forces can be calculated by applying the force theorem stated by Hellmann [263] and Feynman [264]:

$$-\frac{\partial E_t}{\partial R_I} = -\left\langle \frac{\partial \psi}{\partial R_I} \mid H \mid \psi \right\rangle - \left\langle \psi \mid \frac{\partial H}{\partial R_I} \mid \psi \right\rangle - \left\langle \psi \mid H \mid \frac{\partial \psi}{\partial R_I} \right\rangle - \frac{\partial E_n}{\partial R_I} \tag{2.45}$$

According to the variation principle, the first and the third term on the right vanish and the only non-zero terms come from the explicit dependence of the nuclear positions this equation can be written as:

$$F_I = -\frac{\partial E_t}{\partial R_I} = -\left\langle \psi \mid \frac{\partial H}{\partial R_I} \mid \psi \right\rangle - \frac{\partial E_n}{\partial R_I} \tag{2.46}$$

The force is independent on the pure electronic terms and it is given upon the following terms:

$$F_I = -\int n(r)\frac{\partial Vext(r)}{\partial R_I}dr - \frac{\partial E_n}{\partial R_I} \tag{2.47}$$

From this expression, it is clear that, the forces on the nuclei only depend on the ground state electron density and the positions of the other nuclei and can be then calculated if the electron density is known.

2.3.6 FPLO code

In this thesis, we perform the first-principle total energy calculations with the $FPLO9.00-34$ ab initio simulation package [265, 266] based on the all-electron full-potential local-orbital minimum-basis scheme in which all the electrons are explicitly used in the computation within a full-potential, which means that there is no shape restriction

to the potential, as in pseudopotentials and muffin-tin based methods. This all-electron method is considered among the most accurate schemes for band structure calculations of crystalline solids. In this part, the electronic structure method used to calculate the electronic structure in this thesis is briefly presented.
$FPLO$ code is based on the optimized $LCAO$ method [267], in which the Kohn-Sham orbitals are projected on local atomic orbitals and these orbitals are written in terms of radial functions and spherical harmonics as:

$$\varphi_{s\nu}(r-R-s) = \psi_s^{\nu}(\mid r-R-s \mid)Y_{\nu}(r-R-s) \tag{2.48}$$

where, R stands for a Bravais vector, s is a site vector in the unit cell, and ν is a multi-index which is denoted either by the non-relativistic quantum numbers as $\nu = (n, l, m_l)$ or by the relativistic ones as $\nu = (n, k, \mu)$.
The periodic boundary conditions grant that the Bloch functions Φ_{kn} are eigenfunctions of the Kohn-Sham Hamiltonian:

$$\phi_{kn} = \sum_{R,s,\nu} C_{s\nu}^{kn} \varphi_{s\nu}(r-R-s)\exp(ik(R+s)) \tag{2.49}$$

These Bloch functions are used in the self-consistent Kohn-Sham ansatz which leads to a matrix equation with an eigenvalue problem. It should be emphasized that in the case of too small basis, its completeness is achieved by adding more states. Moreover, the core states are assumed to be orthogonal to each other, so the overlap between core states of distinct sites is neglected. However, semi-core, and valence states may have a non-zero overlap. Due to this distinction between core, semi-core, and valence states, the diagonalization effort is, effectively, reduced.
Recalling that, the matrix diagonalization scales as the cube of the matrix size. Consequently, this method can achieve high accuracy relies on a relatively small number of basis states in comparison with plane-wave based codes, which use a high number of plane waves to get such accuracy.

The essential feature which allows for the use of a minimum basis is that the basis is not fixed in the course of iterations, instead it is adjusted to the actual effective crystal potential in each iteration step and it is even optimized in the course of iterations. In fact, all non-core orbitals are compressed by adding to the crystal potential, spherically, averaged around the site center s, a confining potential:

$$\nu^{conj} = (\frac{r}{r_0})^4 \tag{2.50}$$

with,

$$r_0 = \left(\frac{x_0 r_{NN}(s)}{2} \right)^{3/2} \tag{2.51}$$

Here, $r_{NN}(s)$ is the nearest neighbor distance, and x_0 denotes the parameter which is optimized in every iteration step. The parameters x_0 and $r_{NN}(s)$ are determined by minimizing the total energy. There are two main effects of this potential: firstly, the counterproductive long tails of basis orbitals are suppressed and secondly, the orbital resonance energies are pushed up, providing the optimal curvature of the orbitals and avoiding insufficient completeness of the local basis.
The resulting potential and density are expanded in spherical harmonics at each lattice site s, as follows:

$$\nu(r) = \sum_{R+s,\nu} \nu_{s\nu}(\mid r - R - s \mid) Y_\nu(r - R - s) \tag{2.52}$$

$$n(r) = \sum_{R+s,\nu} n_{s\nu}(\mid r - R - s \mid) Y_\nu(r - R - s) \tag{2.53}$$

This method of calculation will be used firstly to obtain the thermodynamic properties such as the equilibrium parameters, heat of formation and the decomposition temperature of the studied systems (chapter 3) and afterwards calculated the energy barriers which will be implemented in the Kinetic Monte Carlo algorithm (KMC) to simulate the diffusion kinetics of hydrogen in pure and doped magnesium hydride (chapter 4). The next part will be dedicated to Monte Carlo method.

2.4 Monte Carlo method

Monte Carlo is a wide term that covers a numerous family of approaches with one simple central idea in common: the resolution of complex problems using random numbers. Given the versatility of the concept, it is no surprise that Monte Carlo based approaches have gained popularity in computational chemistry and materials science [268], most prominently for the simulation of ensemble properties using Metropolis Monte Carlo, or methods derived from the latter. In addition to equilibrium properties, the Monte Carlo idea can also be exploited to tackle dynamical properties. In this sense, a number of approaches emerged over the decades under different names, until the term kinetic Monte Carlo (KMC) became universally used in this context.
Nowadays KMC is a popular tool to describe a variety of phenomena related to e.g. transport (diffusion), structures and properties of materials (e.g. crystal growth) or equilibrium and non-equilibrium chemistry (catalysis). KMC is an essential method to bridge

the gap between the microscopic world (elementary processes such as atomistic diffusion jumps or the making and breaking of chemical bonds) and the meso- to macroscopic world (e.g. a diffusion constant or a reaction rate).

2.4.1 Conventional Monte Carlo simulation

Monte Carlo (MC) methods are a class of numerical algorithms that use randomness in sampling. They are used in many cases of applied mathematics, including finance [269], infrastructure [270], medicine [271, 272], physics [273] and chemistry [274], or to solve purely deterministic problems by taking random samples from a probability distribution. One thing in common for these algorithms is that they are run for many iterations and use the law of large numbers and other properties to get the results [275].

Ordinary MC may have problems when used in many physical and chemical processes, because of large size or complex probabilities. In these cases, the Markov Monte Carlo chain ($MCMC$) is better suited, where random sampling comes from a Markov chain, the probability of each variable depends on its closest predecessor, with a desired stationary distribution. One common way to this is Metropolis-Hastings Monte Carlo (MMC)[276, 277].

2.4.1.1 Markov chain

Markov chains are a fundamental feature of any Monte Carlo algorithm so it is necessary to give at least an elementary explanation of the concept here.
A Markov process is one that only depends on the intial state of the system and does not need any information about the past to make a prediction about the future [278]. $MCMC$ generates a sequence of events that satisfy the condition of being a Markov process. This property states that the probability of selecting a value for the next event depends only on the value of current event. It is much more common to see a Markov process in physics because it usually does not matter how a system arrived at a state. If the intial state is provided a prediction can be made about the future of the system. For example, given position and momentum of a particle, the equations of motion can be used to determine all of its future position and momentum states.

Let us consider an evolving statistical set (for example a crystal in which atoms diffuse). Call $\{X_i\}$, the system configuration in step i. We can define in $\{X_i\}$, transitions (a transition is an elementary process that the system can undergo in the configuration i). In the case of an alloy, the processes to be considered are of a physico-chemical nature (dissolution, oxidation, etc.) likely to occur at the atomic level. The realization of a transition (for example the diffusion of an atom) brings the system from one configuration $\{X_i\}$ to another configuration $\{X_{i+1}\}$. The evolution of the system is of Markovian type

if the sequence of configurations $\{X_i\}$ verifies the following properties [279, 280]:

- Each $\{X_i\}$ configuration of the system depends only on the previous $\{X_{i-1}\}$,
- Each new configuration $\{X_i\}$ of the system belongs to the configuration space $\{X\}$, i.e. the set of feasible configurations: $\{X_1, X_2, ..., X_n\}$
- If $P_{ij}(X_i \to X_j)$ is the transition probability of the system from the state X_i to the state X_j, the process keeps the total probability, that is to say $\sum P_{ij}(X_i \to X_j) = 1$

$[P_{ij}]$ is the system transition matrix for a given configuration. An element P_{ij} of the matrix gives the transition probability $P_{ij}(X_i \to X_j)$ of a state i to a state j. An *ergodic* Markov chain is a string in which each state can be reached from another state.
The probability of the system being in the configuration i at time t is called $W(i,t)$. The *Markovian* process implies that the probability of going from a configuration i at time t to a configuration j at time $t+1$, does not depend on the configurations of the system for earlier times. Call $P(i \to j)$, the transition probability $i \to j$. The evolution equation of the system is given by the following master equation:

$$W(i,t+1) = W(i,t) + \sum_j [P(j \to i)W(j,t) - P(i \to j)W(i,t)] \tag{2.54}$$

There are additional properties that must be fulfilled for the sample mean to converge to the expected value.

2.4.1.2 Ergodic theorem

The Ergodic theorem for Markov chains [279, 280] states some properties for which the sample mean of the Markov chain converges almost surely to the expected value. These properties ensure that the transition rates are independent of time, that all states are reachable from any starting state and that there is no periodicity in when states are reached [281].

Let X be the set of all possible values for the stochastic variables.

Definition 1: A Markov chain is time-homogeneous if:

$$P(X_{i+1} = b \mid Xi = a) = T_{ab}; \quad \forall i \quad \forall a, b \in X \tag{2.55}$$

for some stochastic matrix T.

Definition 2: A probability density function π is a stationary distribution with respect

to a transition matrix T if:

$$\pi T = \pi \quad \text{or} \quad \text{equivalently} \quad \sum_{a \in X} \pi_a T_{ab} = \pi_b \quad \forall b \in X \tag{2.56}$$

Definition 3: A Markov chain is irreducible if $\forall a, b \in X \ \exists t \geq 0$such that

$$P(X_t = b \mid X_0 = a) > 0 \tag{2.57}$$

Definition 4: A Markov chain is aperiodic if $\forall a \in X$

$$gcd[t \mid P(X_t = a \mid X_0 = a) > 0] = 1 \tag{2.58}$$

where *gcd* denotes the greatest common divisor.

The aperiodicity ensures that there are no regular repetitions of how many steps the chain must take to be able to return to a given starting variable.

Definition 5: A sequence of random variables $\{X_i\}$ is said to converge almost surely to a value X if:

$$P\left(\lim_{i \to \infty} X_i = X\right) = 1 \tag{2.59}$$

Almost surely convergence is denoted by

$$X_i \xrightarrow{a.s.} X \tag{2.60}$$

With these properties defined the Ergodic theorem can be stated

Theorem 1: If $\{X_i\} = \{X_0, X_1, ..., X_n\}$ is an irreducible, time-homogeneous, discrete Markov chain with stationary distribution π then:

$$\frac{1}{n} \sum_{i=1}^{n} f(X_i) \xrightarrow{a.s.} E[f(x)] \tag{2.61}$$

as $n \to \infty$, where $x \sim \pi$ for any bounded function $f : X \to \Re$. Furthermore if (X_i) aperiodic then $P(X_n = x \mid X_0 = x_0 \to \pi(x) \ \forall x, x_0$.

Definition 6: An irreducible, aperiodic, time-homogeneous, discrete Markov chain is called an Ergodic Markov chain.

As the sample mean of a $MCMC$ converges to the expected value of the function over its stationary distribution, the chain must be constructed so that the stationary distribution is the desired sample distribution. A property that helps in the construction is

detailed balance.

Definition 7: A probability density function π on X satisfies detailed balance with respect to a transition matrix T if $\forall a, b \in X$.

$$\pi_a T_{ab} = \pi_b T_{ba} \tag{2.62}$$

A probability density function that satisfies detailed balance is also a stationary distribution since:

$$\pi_a T_{ab} = \pi_a T_{ba} \Rightarrow \sum_{a \in X} \pi_a T_{ab} = \sum_{a \in X} \pi_b T_{ba} = \pi_b \tag{2.63}$$

A method to construct a Markov chain with desired stationary distribution is Metropolis algorithm explained in the next section.

2.4.1.3 Metropolis algorithm

The purpose of this section is to expose the algorithmic principle of this method by given a concrete example.
The most famous Monte Carlo technique in physics is the Monte Carlo Metropolis technique named after its inventor [276, 282]. A two-dimensional network of *Ising spins* is the most widespread illustration, the objective in this example being to obtain the most stable system existing.

- Starting from an arbitrary initial configuration, the system evolves according to established rules cited above. The choice of Monte Carlo is to converge the total energy of the system to a maximum or minimum value depending on the case considered. For the Ising model, the event chosen to tend towards a convergence is the spin reversal.

- A site (spin) is chosen randomly in the initial configuration.

- If the chosen event (i.e. spin reversal) allows the system to gain energy, i.e. $\Delta E = E_{new\,configuratuin} - E_{old\,configuratuin} < 0$, then the event is realized.

- In the opposite case, if $\Delta E > 0$, the Monte Carlo Metropolis rather than simply rejecting the event, submits it to an *Acceptance* criterion denoted A, that is to say a probability of being accepted, determined statistically and therefore realistically,

by the expression Maxwell-Boltzman:

$$A = \exp\left(-\frac{\Delta E}{K_\beta T}\right) \tag{2.64}$$

where K_β is the Boltzman constant and T is the temperature. To decide, a random number ξ distributed niformly in the range [0,1] is generated, then the event is accepted if $\xi \leq A$ and it is refused if $\xi > A$ as shown in Figure 2.2.

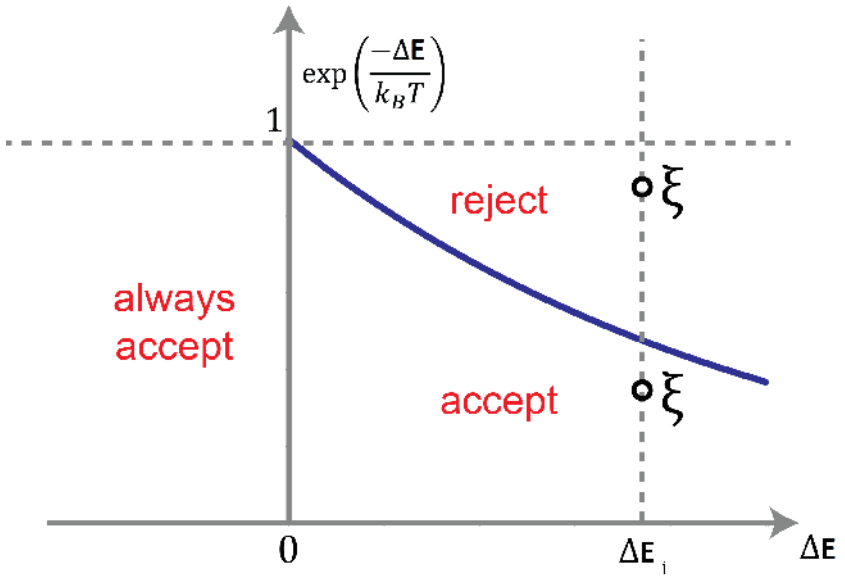

Figure 2.2: Schematic representation of the acceptance in Metropolis Monte Carlo algorithm.

The loop thus is repeated (Monte Carlo steps) until the parameter considered has reached the desired value or convergence (the total energy in the case of Ising model).

Despite the effectiveness of this algorithm MMC, in some numerical simulations in materials physics, the Metropolis algorithm has some limitations:

- The rejection rate during the pulling of transitions can sometimes be high, which can lead to a considerable slowdown in the evolution of the process.
- The time taken into account is a number of iterations and does not correspond to a real time. So, it gives no information on how the system evolves over time.

For simulations of a process over time, Kinetic Monte Carlo (KMC) is used by using transition rates as probabilities in the formation of the Markov chain [283, 284].

2.4.2 Kinetic Monte Carlo simulation

The Monte Carlo simulation mentioned above is used to predict the equilibrium thermodynamic properties. It allows to manage a KMC time which can be connected to the experimental time, thus allowing a comparison with the experimental kinetics. In order to investigate the kinetic properties such as hydrogen diffusion in MgH_2 as a function of time, kinetic Monte Carlo simulation is a powerful tool.

The statistical concept under the kinetic Monte Carlo is a continuous-time Markov chain, more specifically, a Poisson process. In this Poisson process the individual hop occurs instantaneously and the time between two successive hops is exponentially distributed with the mean $1/\Gamma_{tot}$, where Γ_{tot} is defined as [285]

$$\Gamma_{tot} = \sum_i \Gamma_i \tag{2.65}$$

where Γ_i is the migration frequency of hop i and Γ_{tot} is the sum of all individual probabilities Γ_i.
For a specific hop, we can calculate the migration probability Γ_i within the harmonic transition state theory [286], which gives:

$$\Gamma_i = \nu_{0i} \exp\left(-\frac{\Delta E_a(i)}{K_\beta T}\right) \tag{2.66}$$

where ν_{0i} is the vibration prefactor for hop i, $E_a(i)$ is the activation energy for hop i required to move the hopping atom(s) from the initial stable state to the activated state; k is Boltzmann's constant and T is the absolute temperature in degrees Kelvin.
In contrast to the Metropolis method in which changes are related to random variations of positions that do not necessarily have a precise physical meaning, the KMC is based on the identification of the basic physical processes that may occur in the system. Each of these processes is associated with activation energy (sometimes called the energy barrier). In our study, this barrier represents the energy which must be provided to:

- a molecule of hydrogen to be adsorbed at the surface of the host Mg.
- a hydrogen atom to diffuse between two interstitial sites, or leave the system (MgH_2).

Activation energy can be thought of as the magnitude of the potential barrier separating minima of the potential energy pertaining to the initial and final thermodynamic states as shown in Figure 2.3.

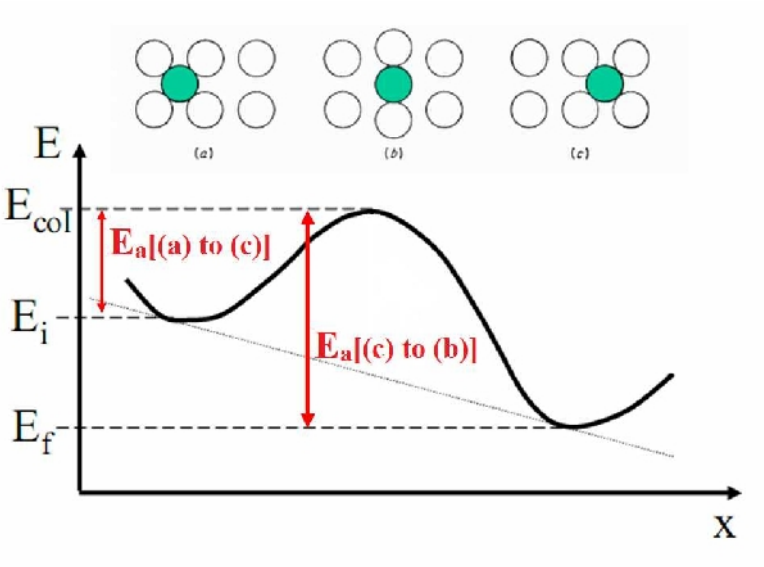

Figure 2.3: Activation energies of atom diffusing between two interstitial sites.

The attempt frequency ν_0 for a specific hop is calculated as:

$$\frac{\prod_{i=1}^{3N-3} \nu_i}{\prod_{i=1}^{3N-4} \nu_i^*} \tag{2.67}$$

where N is the number of sites involved in the hop ($N = 2$ if the hop involves one atom and one vacancy, $N = 3$ if the hop involves two atoms and one vacancy), ν_i is the normal vibration frequency at the stable state and ν_i^* is the normal vibration frequency at the activated state.
According to the stochastic theory, each individual hop will occur with the possibility:

$$P_i = \frac{\Gamma_i}{\Gamma_{tot}} \tag{2.68}$$

In the simulation, the time Δt between two consecutive hops can be defined as:

$$\Delta t = -\frac{\ln v}{\Gamma_{tot}} \tag{2.69}$$

where v is a uniformly distributed random variable between $(0, 1]$. It can be easily proved that Δt, which is defined by equation 2.69, is an exponentially distributed random variable with the mean $1/\Gamma_{tot}$.

For the realization of this type of Monte Carlo code, one must know in advance the physico-chemical elementary reactions that interact in the studied system. In the case

of diffusion of hydrogen in MgH_2 these events or elementary process are: adsorption, dissociation, diffusion and desorption.
The knowledge of the mechanisms involved in the evolution of the system is the main difficulty of this type of code. The ab initio calculations allow us the collect of data needed to create this list of mechanisms and then implement it in the algorithm. These data are used as input parameters.
A limitation of KMC is that the real reaction rates for the involved steps is hard to calculate, as these systems may be very complex. Instead different estimates of the activation energy barrier are used [287, 258, 289]. In chapter 4 we will see how we can calculate barriers energies of the different mechanisms that the system involves and the detailed model used to simulate the kinetics of ab/desoption of hydrogen in the pure and doped MgH_2.

2.4.2.1 KMC algorithm

The practical implementation of the KMC algorithm is very simple and it is given as follows:

- Make a list of possible processes for the system to escape the current state, with associated rate Γ_i:
- calculate the cumulative function Γ_{tot};
- draw two random numbers u, $v \in]0,1]$;
- extract process q, which has to fulfill the constraint:

$$\sum_{i=1}^{q} \Gamma_i \geq u\Gamma_{tot} \geq \sum_{i=1}^{q-1} \Gamma_i \tag{2.70}$$

- execute randomly drawn process;
- update clock: $t \leftarrow t - \ln(v)/\Gamma_{tot}$

The KMC algorithm flowchart is shown in Figure 2.4:

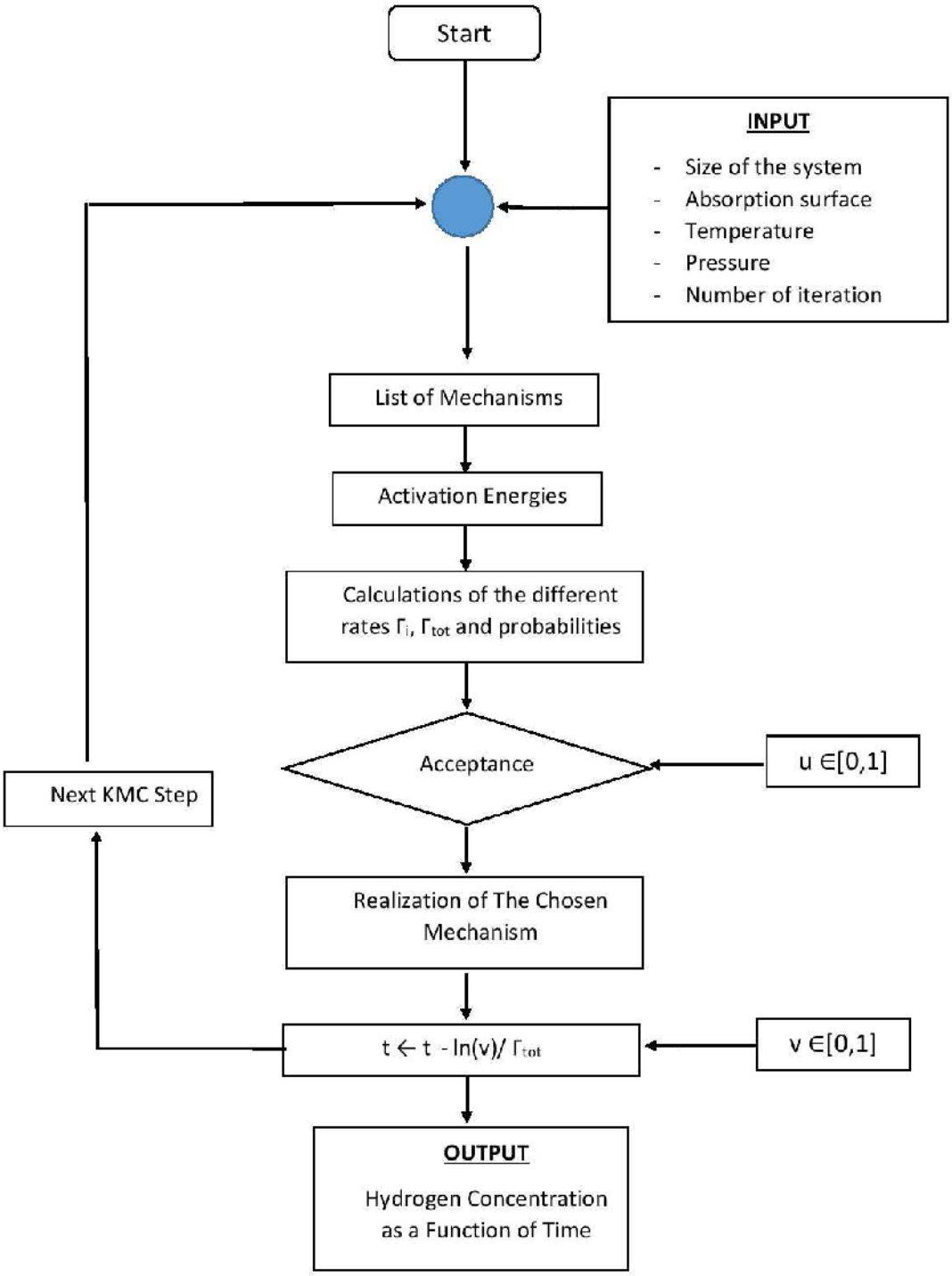

Figure 2.4: KMC algorithm flowchart.

2.5 Conclusion

In this chapter, we have outlined the different methods used in this thesis to study the thermodynamic and kinetic properties of MgH_2 namely ab-initio calculations and Kinetic Monte Carlo simulations.

By using DFT calculations, the total energies are calculated for the pure MgH_2 and M doped MgH_2 systems for various concentration and various doping atoms (M =Al, Ti, V, Fe and Ni) then the structural (equilibrium positions and parameters) and thermodynamic properties (stability and desorption temperature) are deduced (chapter3).

Thereafter, we proposed a model to simulate the absorption and desorption kinetics of the pure magnesium hydride and to study the effect of the dopant elements (Al, Ti, V, Fe and Ni) on its kinetics properties (chapter 4). For this purpose, the activation energies for the different elementary process such as adsorption, dissociation, diffusion and desorption are needed and are calculated by first principles.

Chapter 3

Study of the thermodynamic properties of magnesium hydride by ab-initio calculation

Contents

3.1 Introduction

Up to day, magnesium hydride is one of the most attractive materials for hydrogen storage applications due to its high gravimetric and volumetric capacities $7.65wt.\%$ and $110g.H_2/l$, respectively [60, 290, 209, 291, 292]. However, this material shows slow hydrogen absorption/ desorption kinetics as well as high stability and high dissociation temperature $573-673K$. These characteristics reduce its application regarding its use as a hydrogen storage material [291, 293].

Various attempts were made in order to improve magnesium hydrogen absorbing-desorbing characteristics. Experimentally, it was shown that the ball-milling with a small amount of transition metals (TM) or their oxides drastically accelerate the hydrogen kinetics. Moreover, they reduce also the decomposition temperature of the hydride [291, 292, 294, 295, 296].

On the other hand, several theoretical calculations were performed to clarify and understand the relevant mechanism dealing with the alloying effects on the thermodynamic properties on magnesium hydride [297, 298, 299, 300, 301, 302, 303, 304, 305, 306]. Unfortunately the observed catalytic mechanism is still not adequately explained.

In this chapter, a study of hydrogen storage properties of Magnesium Hydride by first principle calculation is proposed to study and understand the mechanisms that operate in this material and that make it very stable thermodynamically.

The stability of the studied compound is estimated by computing the heats of formation and desorption temperature. The obtained results are supported by an analysis of the density of states (DOS).

Thereafter, a substitution approach to tune the problematic of MgH_2's thermodynamic is presented. Ab initio calculation were used to investigate the effect of the substitution of magnesium by $M = Al, Ti, V, Fe$ and Ni inside MgH_2 lattice. In addition, the vibrational, thermodynamics properties and electronic structure were investigated to explore the mechanical stability and the possibility of lowering the hydrogen desorption temperature of substituted magnesium hydride structure.

3.2 Thermodynamic properties of the pure MgH_2 from DFT method

3.2.1 Computational method

In order to determinate the different properties of the studied material, ab initio calculations based on the all-electron full-potential local-orbital minimum-basis scheme $FPLO9.00-34$ [265, 266] was used to solve the Kohn-Sham equations using the scalar-

relativistic and the full four-component relativistic schemes. The parameterization of the exchange-correlation energy was done within the generalized gradient approximation GGA [261]. To ensure a high accuracy in our calculation, self-consistent criteria for both the energy and the density with precisions of 10^{-8} Ha and 10^{-6} $Ha^{-1}.\text{Å}^{-3}$ respectively are used. A mesh of $(12 \times 12 \times 12)$ $k-points$ in the irreducible part of the first Brillouin zone was used in our calculations. The total energy is calculated using the scalar-relativistic scheme, for all configurations.

The hydride MgH_2 crystallizes in the rutile-type structure ($P4_2/mnm$, space group $N°136$) at ambient conditions [307]. The primitive cell (Figure 3.1) has two Mg atoms, one at the corner and the other in the centre of the cell at $(1/2, 1/2, 1/2)$ plus four hydrogen atoms at $(x, x, 0)$, $(-x, -x, 0)$, $(1/2 - x, 1/2 + x1/2)$ and $(1/2 + x, 1/2 - x, 1/2)$ with $x = 0.304$. The lattice parameters used, in our calculation before relaxation, are the experimental values $a = 4.501$Å and $c = 3.01$Å [307].

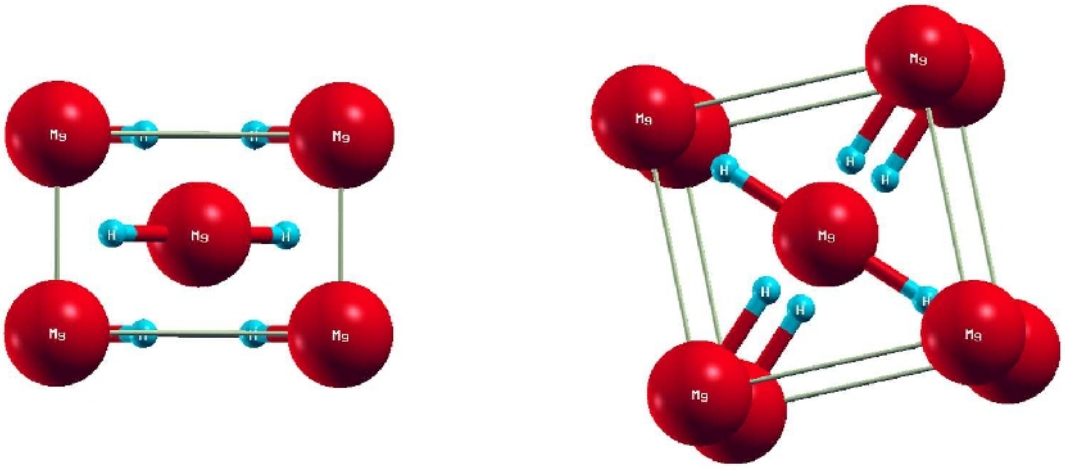

Figure 3.1: Crystal structure of MgH_2 in primitive cell

3.2.2 Thermodynamic properties of MgH_2

3.2.2.1 Equilibrium lattice parameters

Before discussing the thermodynamics of MgH_2 structure, which include desorpotion temperature and formation heat, firstly its equilibrium lattice parameters are determined using the relaxation method. Indeed, the MgH_2 structure is optimized by evaluating the total energy as function of unit cell volume, Figure 3.2. Using GGA approximation and fitting the obtained values with respect to a generic polynomial of the

second order, the equilibrium parameters which correspond to the minimum energy are $a = b = 4.5094$Å and $c = 3.0163$Å. They are in good agreement with those cited in the literature [307, 308].

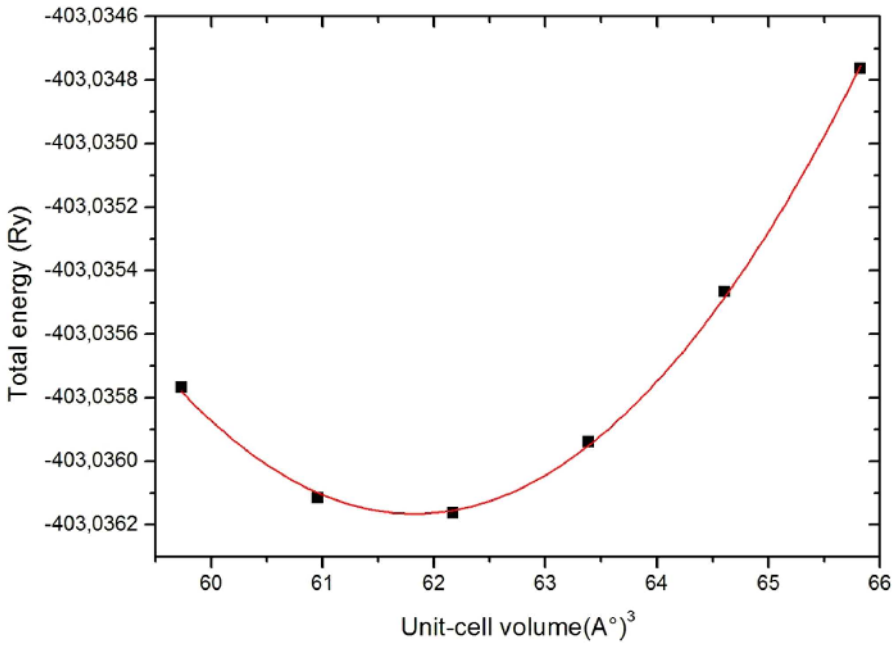

Figure 3.2: Total energy as a function of unit cell volume of MgH_2

3.2.2.2 Heat formation and decomposition temperature

The heat of formation (ΔH) is the most important thermodynamic parameter used to identify and classify hydrogen storage materials. This is due to the fact that it can be used to determine if the predicted phases are likely to be stable or not ($\Delta H < 0$ hydride is stable and vice versa).The ΔH of hydride can be defined as the difference between the total energies of products and reactants [300]:

$$\Delta H = \Sigma E_{tot}(products) - \Sigma E_{tot}(reactants) \tag{3.1}$$

To get the enthalpy of formation (ΔH) of the pure MgH_2, the following reaction (equation 3.2) related to the formation of the hydride is considered:

$$Mg + H_2 \rightarrow MgH_2 \tag{3.2}$$

To calculate ΔH related to the reaction of formation (equation 3.2), the total energies of the pure element Mg and the hydrogen molecule are subtracted from the total energy of

MgH_2 hydride obtained from the relaxation method:

$$\Delta H = E_{tot}(MgH_2) - E_{tot}(Mg) - E_{tot}(H_2) \tag{3.3}$$

The total energies of the pure element Mg and H_2 are obtained using the parameters listed in the Table 3.1.
The molecule of hydrogen is simulated by putting the center of the molecule in the center of a giant cube of parameter $a = 30$Å, to reduce the interaction between the molecules, while respecting the distance of 0.74Å which separates the centers of the two H atoms, see Figure 3.3.

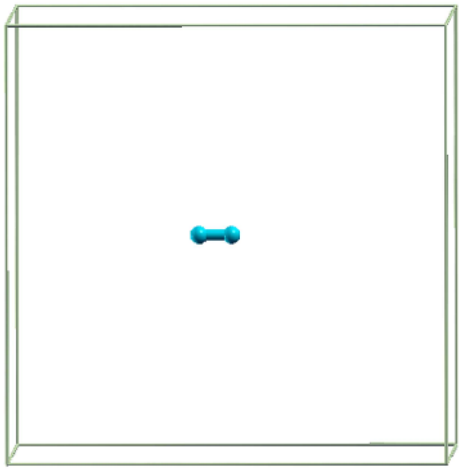

Figure 3.3: Molecule of hydrogen isolated in a cube with $a = 30$Å.

Element	**Space group**	**Crystalline structure**	**Parameters** (Å)	**Total energy** ($Ry/f.u$)	
				Our calculation	**Literature**
Mg	194-$P63/mmc$	Hcp	$a = b = 3.21$ $c = 5.21$ [310]	-400.6683	-400.6670 [308] -400.6675[305]
H_2	$P1$	molecule	0.74Å as molecular distance	-2.33	2.32 [297, 309]

Table 3.1: Structural parameters and total energies of Mg element and H_2 molecule.

As shown in Table 3.1, using DFT calculation, the total energies of hydrogen molecule and Mg pure are in good agreement with those reported in theoretical works [297, 309]. This confirms the validity of our model.
Moreover, the calculated heat of formation of MgH_2 (equation 3.3) is -63.18 $kJ/mol.H_2$. It is close to some calculated theoretical values -62.301 $kJ/mol.H_2$ [296], -75.99 $kJ/mol.H_2$ [297], -69.51 $kJ/mol.H_2$ [299], -82 $kJ/mol.H_2$ [311]. On the other hand, our result is close also to the experimental values -76.15±9.2 $kJ/mol.H_2$ obtained in ref.28. We think that this small difference is due to DFT method calculations.

To get the decomposition temperature T_{des}, we use the well known thermodynamical relation:

$$\Delta G = \Delta H - T\Delta S \tag{3.4}$$

where ΔG denotes the change in free energy. Since ab initio calculations operate at $T = 0K$, then $\Delta G = 0$ and the decomposition temperature can be estimated using:

$$T_{des} = \frac{\Delta H}{\Delta S} \tag{3.5}$$

During heating, the entropy change of the solid is very small compared to that of the gas, so the entropy change during the decomposition reaction is primarily due to the H_2 evolution. At the standard pressure and temperature, for most simple metal hydrides, the entropy is taken to be $\Delta S = \Delta S(H_2) = 130.7 J/mol.K$, corresponding to the entropy change due to a mole of gas transforming into the solid [307]. For most of the dehydrogenation reactions, it is estimated that ΔS is in the range of $95 J/mol.K < \Delta S < 140 J/mol.K$ [312].
Taking the above value of ΔH and the value of the entropy $130.7 J/mol.K$ obtained at standard temperature and pressure [307], we get $T_{des} = 482.52K$. It is in agreement with other values reported in [297, 308].

System	**Parameters**		**Volume**	**Formation enthalpy**	**Desorption temperature**	**Gravimetric capacity**	**Volumetric capacity**
	$a = b$(Å)	c(Å)	(Å^3)	$(kJ/mol.H_2)$	(K)	$(wt.\%)$	$(g.H_2/l)$
MgH_2	4.5094	3.0163	61.34	-63.18	482.52	7.66	109.52

Table 3.2: Summary of the obtained results.

As shown in the Table 3.2, magnesium hydride has high gravimetric and volumetric capacities ($7.66 wt\%$ and $109.52 g.H_2/l$ respectively) which make it a very promising material for hydrogen storage. However, MgH_2 has a high energy of formation ($-63.18 kJ/mol.H_2$) and high decomposition temperature ($482.53K$) making it thermodynamically stable which prevents its application for mobile hydrogen storage.
This high stability will be confirmed by vibrational properties and electronic structure investigations in next sections.

3.2.2.3 Lattice dynamic stability

To further study the mechanical stability of MgH_2 compound, first-principles phonon calculations are carried out using the software PHONOPY [313]. The phonon density of states is presented in Figure 3.4. According to harmonic approximation, this is possible when all the phonons have real and positive frequencies. Negative or imaginary frequencies of phonons indicate that crystal is dynamically unstable [313]. In our present study,

from Figure 3.4 little bit negative frequencies are observed for the pure MgH_2 compound. This means that the compound is mechanically stable. The phonon density of state shows three branches of optical phonons separated from the phonon branches of lower frequencies. The reason for separation of these branches is from the lower mass H present in the compound. The peak in the lower energy region corresponds to the acoustic branches in the dispersion plot. The next separated higher energy peaks represent the coupled optical phonon branches.

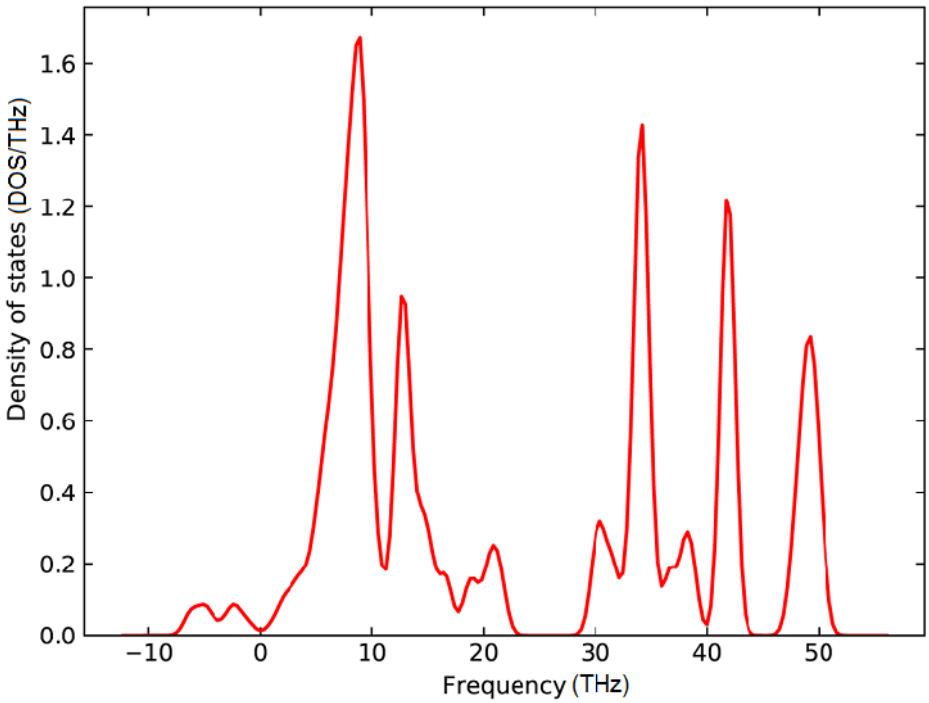

Figure 3.4: Phonon density of states of MgH_2.

3.2.2.4 Lattice Thermodynamic properties

Knowledge of the thermodynamic properties is essential for studying crystal, for that the thermodynamic parameters of (MgH_2) such entropy (S) and internal Energy (E) constant-volume specific heat(C_V) as a function of temperature are determined through quasi-harmonic approximation (QHA) using the phonopy package [313] then Gibbs free energy G is computed through the obtained internal energy E and entropy S. The calculated values at temperature from $0K$ to $1500K$ are illustrated in Figure 3.5.

The thermodynamic stability of a crystal structure depends on the Gibbs free energy. This is the minimum free energy of a crystal structure where the unit cell is allowed to change in response to temperature. The smaller the values of Gibbs free energy, the better the thermal stability of material will be. In our case, the free energy is found to be positive ($90KJ/mol$) at $0K$ and decreases with increasing temperature while the entropy

increases in same temperature range, see Figure 3.5.
It can be seen from Figure 3.5 that the lattice heat capacity increases slowly with the temperature in the initial stage. The lattice heat capacity approaches almost linear when the temperature exceeds $600K$.

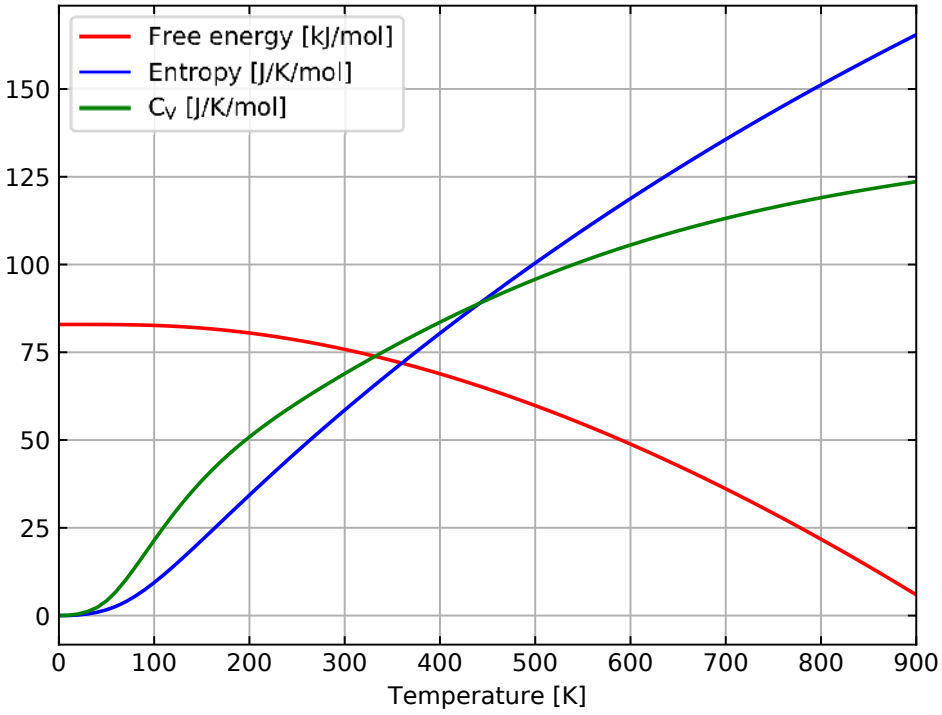

Figure 3.5: Gibss free energy, entropy and C_V for MgH_2 as function of temperature.

3.2.3 Electronique structure

The electronic structure calculations are performed to obtain density of states (DOS) which is the main tool used to elucidate the chemical bonding characteristics of the studied systems and therefore understand and explain the both high stability and desorption temperature in MgH_2. For this purpose, the total (DOS) and the partial ($PDOS$) densities of electronic states of MgH_2 were calculated and plotted and Figure 3.6.

On one hand, the electronic structure of the pure MgH_2 is non-metallic with the energy gap of $3.745eV$ (Figure 3.7), which is smaller than the experimental value $5.16eV$ [314] or $5.6eV$ [315] while it is closer to the theoretical value $3.6eV$ reported in [304]. We believe that this difference between the experimental results and our calculation is due to the GGA approximation which overestimates the interaction energies between the states of Mg and H atoms. Thus, it leads to a large valence band (VB) and a smaller band gap.

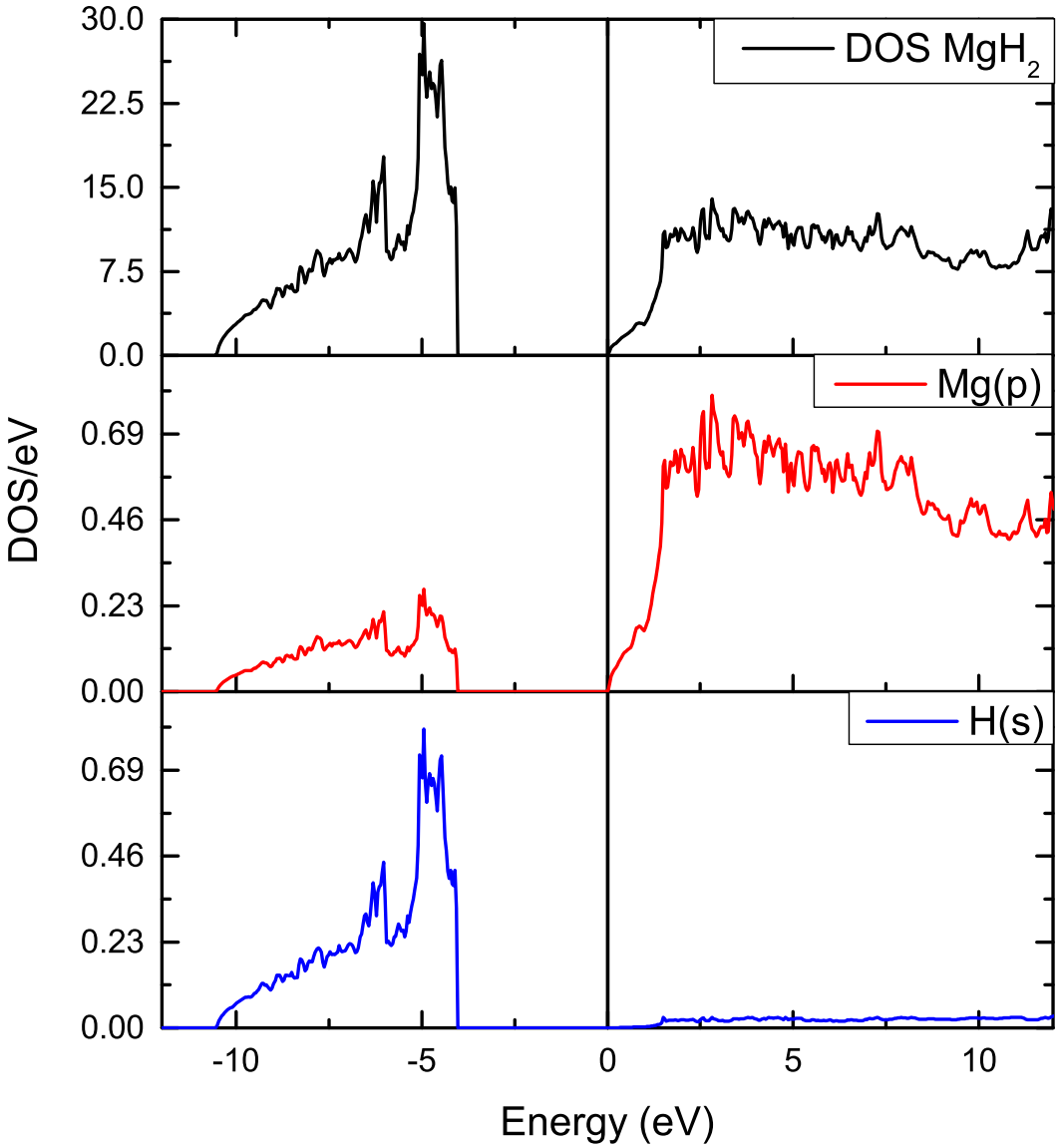

Figure 3.6: Total and partial DOS for the pure MgH_2.

It is well known that first-principles calculation based on the density functional theory suffers from the errors in the calculated band-gap.

On the other hand, it follows that there are two parts in the valence band (VB). In the first part, the band with energy range from $-7eVRy$ to $-3.8eV$ is called $highVB$ composed mainly of strongly hybridized $H-s$ and $Mg-3p$ states. The second part concerns the band energy ranging from $-11eV$ to $-7eV$ which is called $lowerVB$ originating almost from $Mg-s$ and $H-s$ states. While the contribution of the lowest conduction band (CB) is fully from $Mg-p$, $Mg-s$ and few $H-s$ states.

This indicates that there is a strong hybridization between the H and Mg atoms which can explain the high heat of formation obtained in section 3.2.2.2 and consequently high stability and high decomposition temperature.

So to reduce this stability, we have to find a way to reduce this strong hybridization between $Mg - H$, which we will try to explore in the next section by studying the effect of substitution by Al and transition metal like Ti, V, Fe and Ni.

3.3 Effect of doping in hydrogen storage properties of MgH_2

The aim of this part is to study, using first principles calculations, the hydrogen storage properties of MgH_2 doped with different metal M (M = Al,Ti,V, Fe and Ni) in order to reduce the strong hybridization between magnesium and hydrogen and consequently reduce the high desorption temperature.

3.3.1 The model

To perform such computations, calculations are carried out using a supercell containing 15 Mg atoms, 1 M atom ($M = Al, Ti, V, Fe$ and Ni) and 32 H atoms, denoted henceforth as $Mg_{15}M_1H_{32}$ as shown in Figure 3.7. This choice corresponds to an M doped concentration of 6.25%.The lattice parameters used in all calculation are the relaxed parameters see Table 3.3.

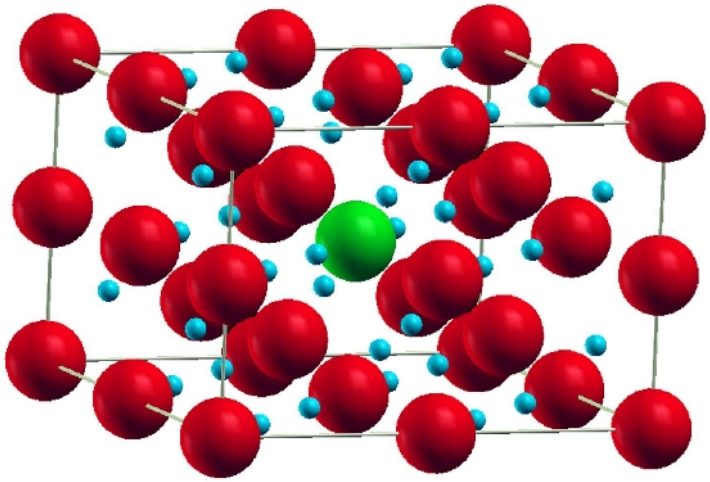

Figure 3.7: Supercell presented $Mg_{15}M_1H_{32}$; red atoms are Mg, H atoms are the bleu sphere and M is in green.

3.3.2 Thermodynamic properties of doped MgH_2 from DFT method

In order to study the thermodynamics properties of $Mg_{0.9375}M_{0.0625}H_2$ (M= Al, Ti, V, Fe and Ni) systems including heat of formation and desorption temperature, we first determine the equilibrium lattice parameters using the relaxation method. Indeed, we optimize the $Mg_{0.9375}M_{0.0625}H_2$ structures by evaluating the total energy as function of super-cell volume. The results of relaxed parameters, volume and storage capacities are listed in Table 3.3.

Systems	**Parameters**		**Volume** ($Å^3$)	**Cg** ($wt\%$)	**Cv** ($g.H_2/l$)	**Elements**	**Molar mass** (g/mol)
	a and **b** (Å)	**c** (Å)					
MgH_2 super-cell	9.0188	6.0272	490.245	7,660	109.619	Mg	24.3
$Mg_{0.9375}Al_{0.0625}H_2$	9, 0616	6, 0599	497.594	7,611	108.000	Al	27
$Mg_{0.9375}Ti_{0.0625}H_2$	8, 9416	5, 9796	478.082	7,253	112.408	Ti	47.9
$Mg_{0.9375}V_{0.0625}H_2$	9, 0020	6, 0200	487.837	7,203	110.160	V	51
$Mg_{0.9375}Fe_{0.0625}H_2$	8, 9416	5, 9796	478.082	7,127	112.408	Fe	55.8
$Mg_{0.9375}Ni_{0.0625}H_2$	8, 9719	5, 9999	482.962	7,081	111.272	Ni	58.7

Table 3.3: The lattice parameters and hydrogen storage quantities of $Mg_{0.9375}M_{0.0625}H_2$ ($M = Al, Ti, V, Fe$ and Ni.)

It follows from the obtained results (Table 3.3) that the addition of M atoms generates a small variation of the lattice parameters leading to an expansion of volume in the case of Mg substitution by Al, and a contraction when the Mg is substituted by transition metal Ti, V, Fe and Ni.
The expansion of the volume leads to a small decreases in the volumetric capacity of $MgH_2 : Al$ from 109.619 to $108 g.H_2/l$, while the volume contraction leads to an increase in volumetric capacities for MgH_2 doped Ti, V, Fe and Ni.
Contrariwise, the substitution of Mg by $M = Al, Ti, V, Fe$ and Ni decreases slightly the gravimetric capacities since the molar mass of M atoms are greater than that of Mg, but the acquired capacities remain in the standards proposed by the DOE [316, 317].

To calculate the heat of formation and the desorpotion temperature, we consider the following reaction related to the formation of the substituted compounds $Mg_{0.9375}M_{0.0625}H_2$ ($M = Al, Ti, V, Fe$ and Ni) which reads as:

$$0.9375Mg + 0.0625M + H_2 \longrightarrow Mg_{0.9375}M_{0.0625}H_2 \tag{3.6}$$

And we subtract the total energies of the pure element Mg, the atom M ($M = Al, Ti, V, Fe$ and Ni) and the hydrogen molecule from the one of $Mg_{0.9375}M_{0.0625}H_2$ obtained from re-

laxation method:

$$\Delta H = E_{tot}(Mg_{0.9375}M_{0.0625}H_2) - 0.9375E_{tot}(Mg) - 0.0625E_{tot}(M) - E_{tot}(H_2) \quad (3.7)$$

Using the value of total energies reported in Table 3.1 and Table 3.4, the resulting heats of formation of the studied system are listed in Table 3.5. Thus, the decomposition temperatures, which are presented in Table 3.5, were obtained by using the equation 3.5 and taking the value of the entropy $\Delta S = 130.7 J/mol$ [307].

Elements	**Crystalline structure**	**Total Energy** $(Ry/u.f)$
Al	fcc	-485.643646
Ti	hcp	-1707.633885
V	bcc	-1898.644689
Fe	bcc	-2545.56838
Ni	fcc	-3041.671468

Table 3.4: Crystalline structure and total energies of substitution elements.

It is shown, in one hand, that $\Delta H = -62.76 kJ/mol.H_2$ for MgH_2 super-cell is close to the one measured previously for MgH_2 unit cell. On the other hand, the addition of the element ($M = Al, Ti, V, Fe$ and Ni) to MgH_2 reduces its tability, which can lead to an improvement of the dehydrogenation temperature. This agrees well with the trend observed experimentally [297] and theoretically [297, 299]. More than, this improvement effect occurs in the following order Ti, Al, Fe, V, Ni and without unduly influenced the hydrogen storage capacities. Especially for hydride magnesium doped with 6.25% of Ni, the temperature of decomposition decreases to a value equal to $313.42K$ (see Table 3.5).

Systems	ΔH $(KJ/mol.H_2)$	T_{des} (K)
MgH_2 super-cell	-62.76	461.49
$Mg_{0.9375}Al_{0.0625}H_2$	-47.95	352.55
$Mg_{0.9375}Ti_{0.0625}H_2$	-51.42	378.07
$Mg_{0.9375}V_{0.0625}H_2$	-43.60	320.60
$Mg_{0.9375}Fe_{0.0625}H_2$	-44.97	330.68
$Mg_{0.9375}Ni_{0.0625}H_2$	-42.62	313.42

Table 3.5: Heat of formation and dehydrogenation temperature of studied compounds.

3.3.3 Electronic structure of doped systems

The density of state has been used to analyze and explain the effect of the addition of M elements ($M = Al, Ti, V, Fe$ and Ni) on both the stability and desorption temperature in $Mg_{1-x}M_xH_2$, $x = 0.0625$. For this purpose, the total (DOS) and the partial ($PDOS$) densities of electronic states of MgH_2 doped with M metals were calculated and plotted in Figure 3.8 to Figure 3.10.

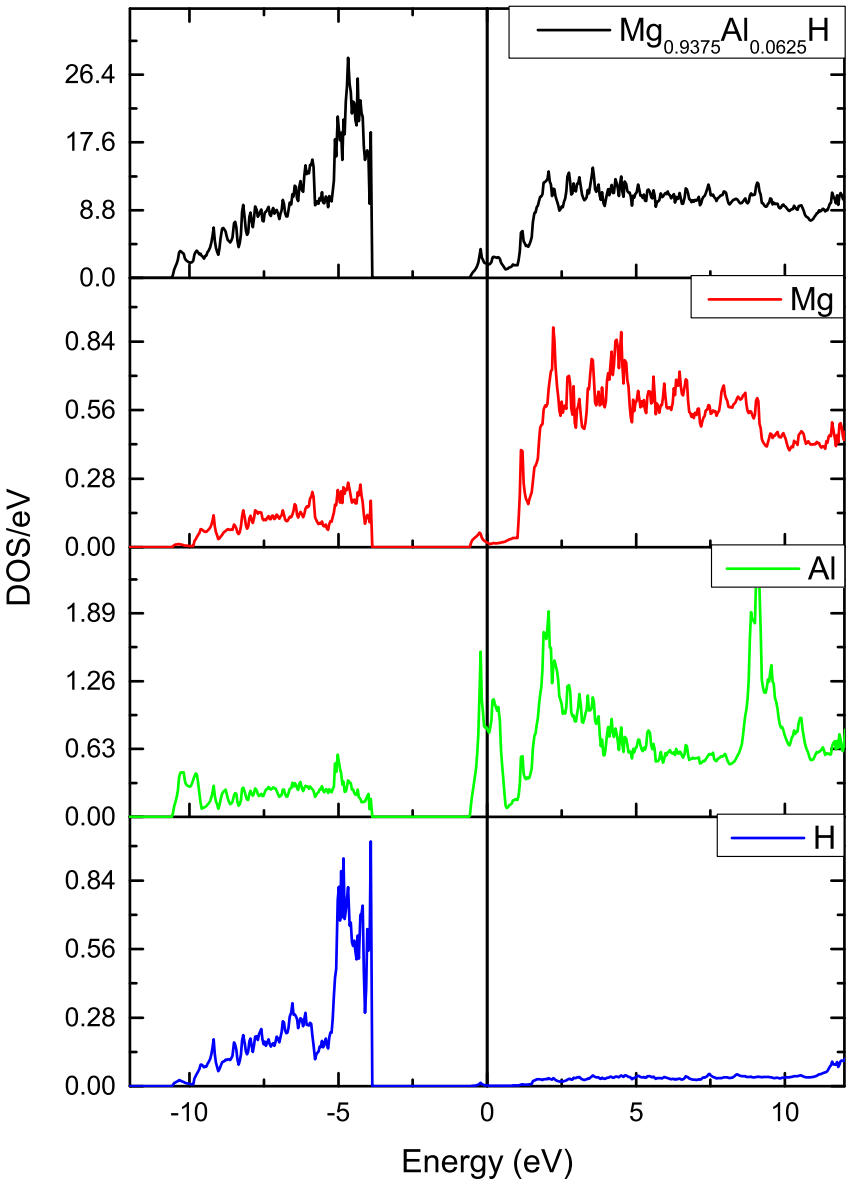

Figure 3.8: Total and partial DOS for $Mg_{0.9375}Al_{0.0625}H_2$.

The electronic structure of $Mg_{0.9375}M_{0.0625}H_2$ ($M = Al, Ti, V, Fe$ and Ni) shows

that the states of d orbitals of transition metal TM $(Ti, V, Fe$ and $Ni)$ and p states of Al are localized in the band gap. The main contribution to the total DOS comes form the M elements. In addition of hybridization $Mg - H$, there is a weak hybridization on the one hand between $TM(d)$ and $H(s)$ (Figure 3.9 and Figure 3.10) on the other hand between $Al(p)$ and $H(s)$ orbitals (Figure 3.8) unlike the pure MgH_2 where is mainly composed a single strong hybridization between the H and Mg atoms occurs (Figure 3.6). Moreover, no hybridization between TM and Mg atoms has been observed, while a weak hybridization between $Al(p)$ and Mg occurs.

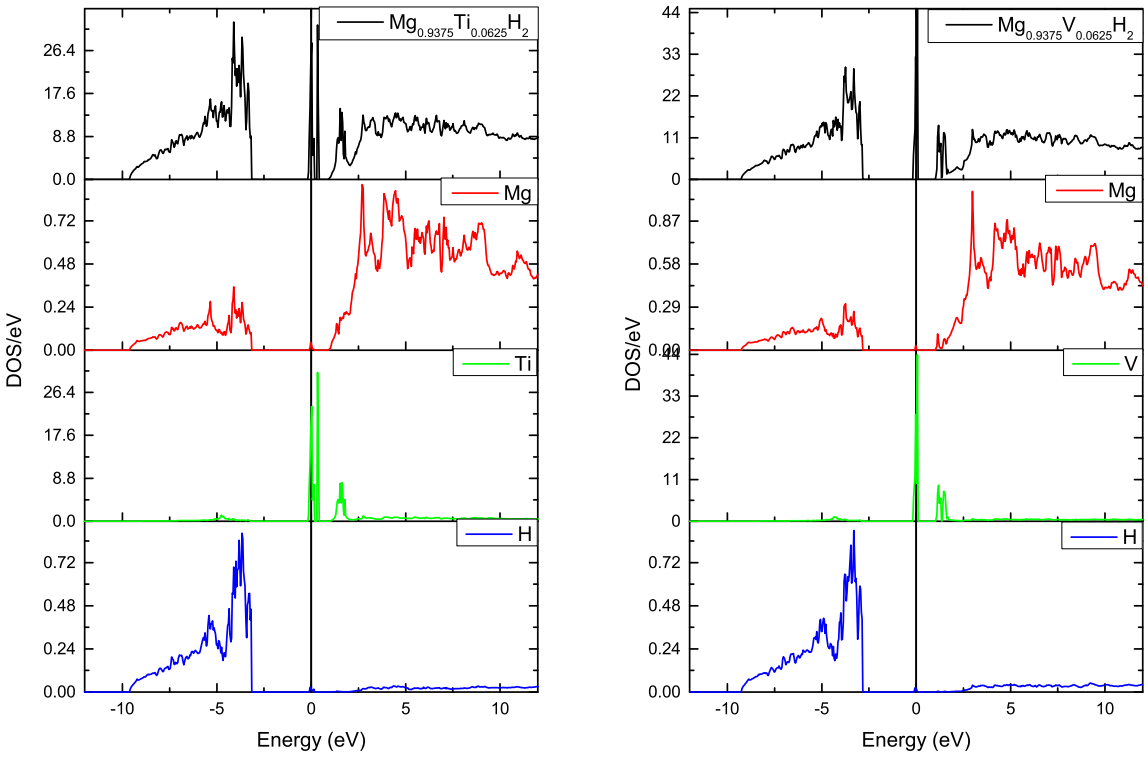

Figure 3.9: Total and partial DOS for $Mg_{0.9375}Ti_{0.0625}H_2$ and $Mg_{0.9375}V_{0.0625}H_2$.

This ascertainment is in agreement with the results of section 3.3.2, where the addition of Al and TM $(Ti, V, Fe$ and $Ni)$ in MgH_2 decreases the stability and the desorption temperature of the mixtures. We note that the MgH_2 doped Ni material exhibits the heigest density of state near the Fermi level.

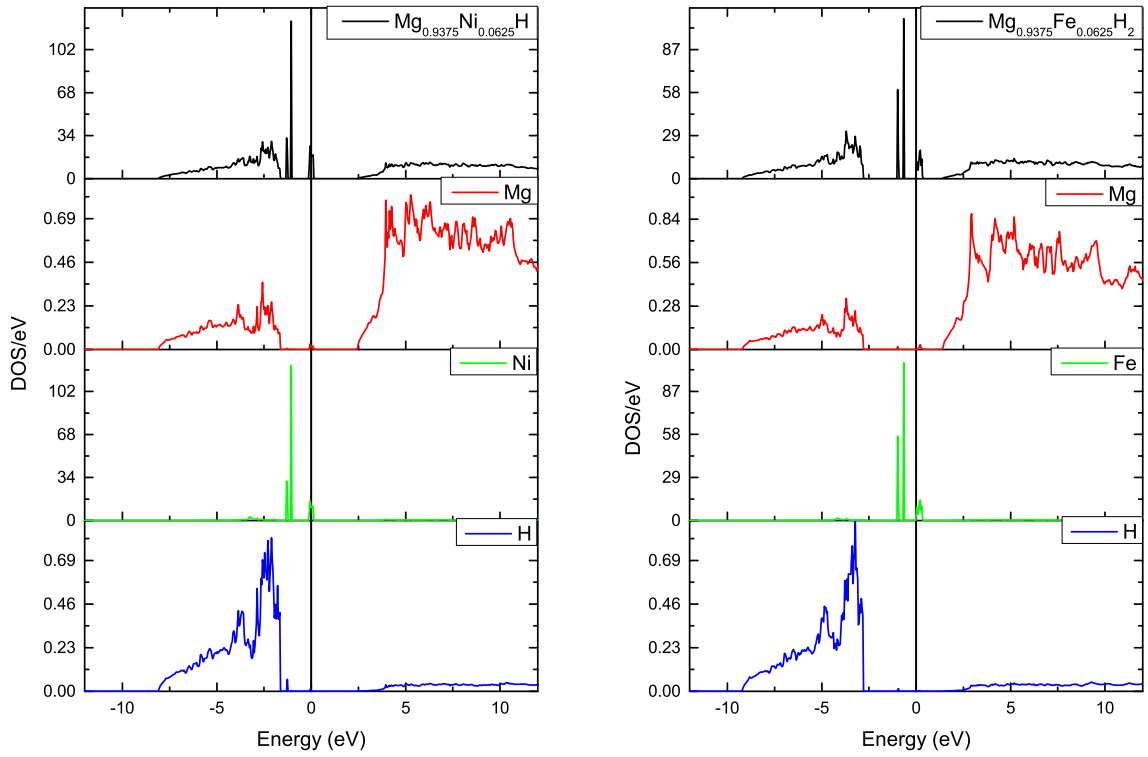

Figure 3.10: Total and partial DOS for $Mg_{0.9375}Ni_{0.0625}H_2$ and $Mg_{0.9375}Fe_{0.0625}H_2$.

3.3.4 Effect of doping concentration in thermodynamic properties

In this part, we propose to study the effect of the concentration of the doping element on the formation energy and desorption temperature. For this purpose the super-cell denoted $Mg_{14}M_2H_{32}$ illustrated in Figure 3.11 is considered. It contains 32 H atoms, 14 Mg atoms and 2 M atoms ($M = Al, Ti, V, Fe$ and Ni) positioned in the positions $0., 0., 0.$ and $0.5, 0.5, 0.5$ respectively, corresponding to an M doped concentration of 12.5%.

The formation reaction (equation 3.8) of $Mg_{0.875}M_{0.125}H_2$ ($M = Al, Ti, V, Fe$ and Ni) is considered and the heat formation is calculated according the equation 3.11.

$$0.875Mg + 0.125M + H_2 \longrightarrow Mg_{0.875}M_{0.125}H_2 \tag{3.8}$$

$$\Delta H = E_{tot}(Mg_{0.875}M_{0.125}H_2) - 0.875E_{tot}(Mg) - 0.125E_{tot}(M) - E_{tot}(H_2) \tag{3.9}$$

The resulting heats of formation and desorption temperature are listed in Table 3.6.

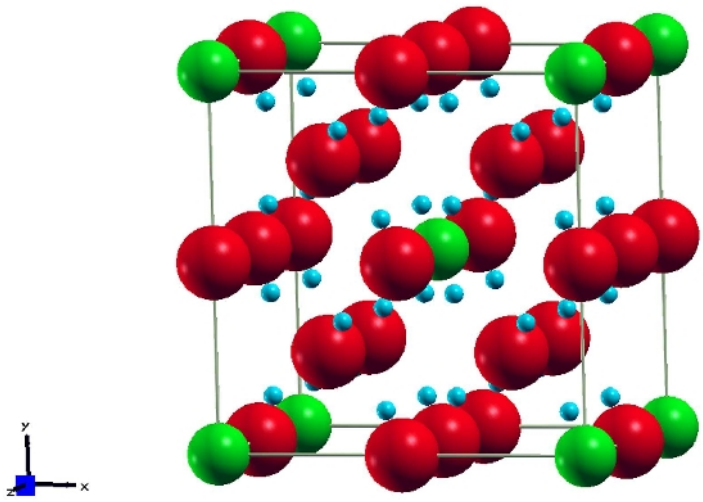

Figure 3.11: Super-cell presented $Mg_{14}M_2H_{32}$; red atoms are Mg, H atoms are the bleu sphere and M is in green.

A comparison of the results of both concentration 6.25% and 12.5% is required, so the heat of formation and desorption temperature formation of $Mg_{1-x}M_xH_2$ according to the x concentration of the substitution are plotted in Figure 3.12 and Figure 3.13 respectively.

Systems	ΔH $(KJ/mol.H_2)$	T_{des} (K)
$Mg_{0.875}Al_{0.125}H_2$	-33.49096514	246.257097
$Mg_{0.875}Ti_{0.125}H_2$	-40.42841536	297.26776
$Mg_{0.875}V_{0.125}H_2$	-24.81962365	182.497233
$Mg_{0.875}Fe_{0.125}H_2$	-27.40775187	201.527587
$Mg_{0.875}Ni_{0.125}H_2$	-23.06708948	169.610952

Table 3.6: Heat of formation and desportion temperature of $Mg_{0.875}M_{0.125}H_2$ where $M = Al, Ti, V, Fe$ and Ni.

It is shown in Figure 3.12 and Figure 3.13 that when the concentration is increased, the heat of formation increase linearly with a specific slope for each dopant, see Table 3.7. Consequently for each doped element concentration, the stability and the desorption temperature decrease compared to those of the pure MgH_2 ($x = 0\%$). In fact the hydrogen capacities are influenced by the addition of materials with a heavy mass compared to that of Mg, see Figure 3.14.

It follows, that the value of the heat of formation and decomposition temperature can be controlled by varying the concentrations of the doped elements to reach the optimum range $289 - 393K$ for the practical use of a $PEMFC$ [317].

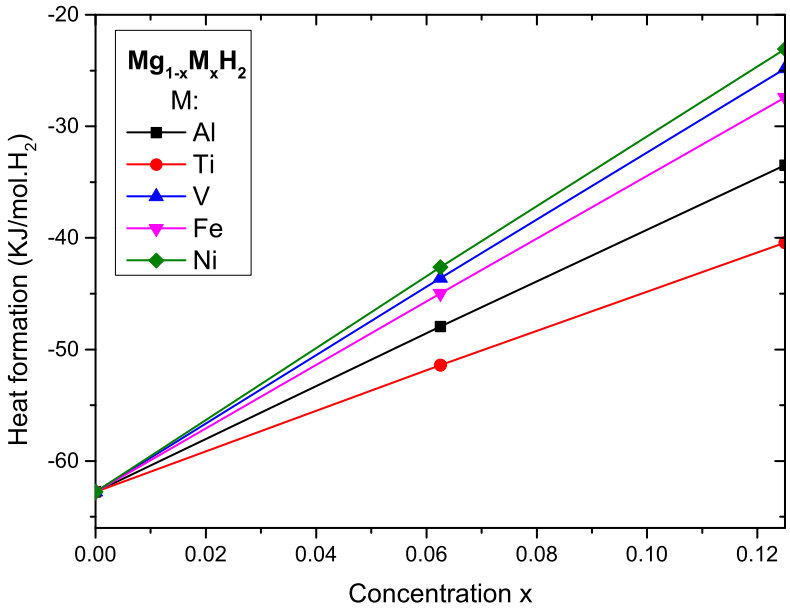

Figure 3.12: Energies of formation of $Mg_{1-x}M_xH_2$ according to the x concentration of the substitution.

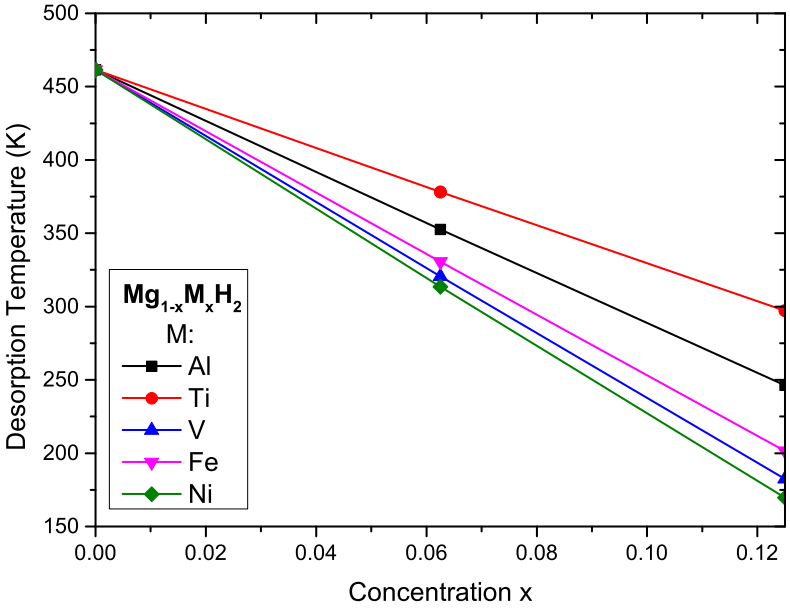

Figure 3.13: Desorption temperature of $Mg_{1-x}M_xH_2$ according to the concentration x of the substitution.

The linear variation of the formation enthalpies as function of the dopant concen-

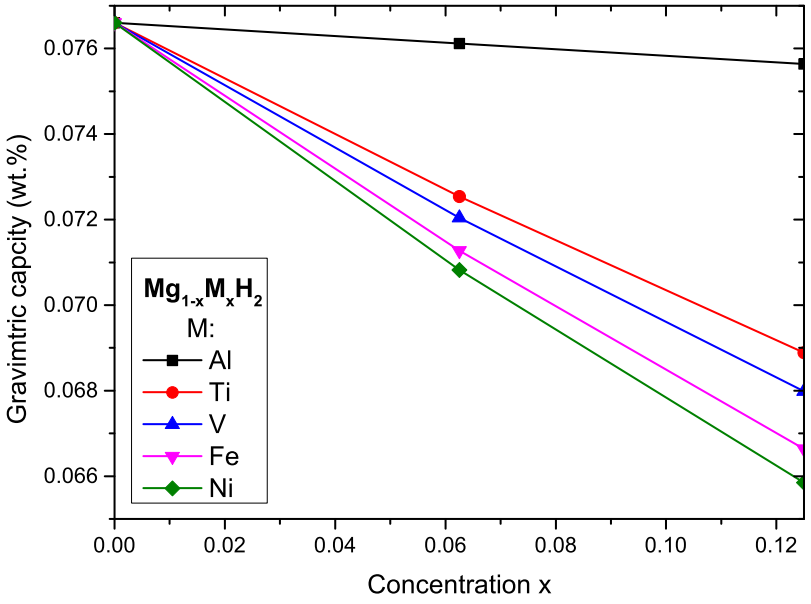

Figure 3.14: Gravimetric capacities of $Mg_{1-x}M_xH_2$ according to the concentration x of substitution

tration x can be described according to the equation 3.10 where the specific slope for each dopant element is given in Table 3.7.

$$\Delta H = -62.7 + Slope \times x \tag{3.10}$$

For optimal use, it is advisable to use a hydrogen storage material whose energy of formation is about $-40 KJ/mol.H_2$ [317]. By introducing this value into equation 3.10 and using the calculated slop values (Table 3.7), we can determine the concentration of each element that allows us to reach the optimal enthalpy. The resulted concentrations and the corresponding capacities are listed in Table 3.7.

Systems	**Slope** ($KJ/mol.H_2$)	**Standard error**	**Concentration x**	**Cg** ($wt.\%$)
$Mg_{1-x}Al_xH_2$	234.18	1.66	0.097	7.58
$Mg_{1-x}Ti_xH_2$	178.68	1.65	0.127	6.87
$Mg_{1-x}V_xH_2$	303.55	1.75	0.075	7.11
$Mg_{1-x}Fe_xH_2$	282.84	1.04	0.08	6.99
$Mg_{1-x}Ni_xH_2$	317.57	2.68	0.071	7.01

Table 3.7: Concentrations x and gravimetric capacities corresponding to ΔH = -40 $KJ/mol.H_2$.

It can be noticed that the gravimetric capacities are preserved above the DOE target for 2025 [1] and round the DOE ultimate target (Table 1.3) even though MgH_2 is doped with heavy elements. Following our study, we remark that the Ni presents the smallest concentration and then it is the most appropriate element for better hydrogen storage.

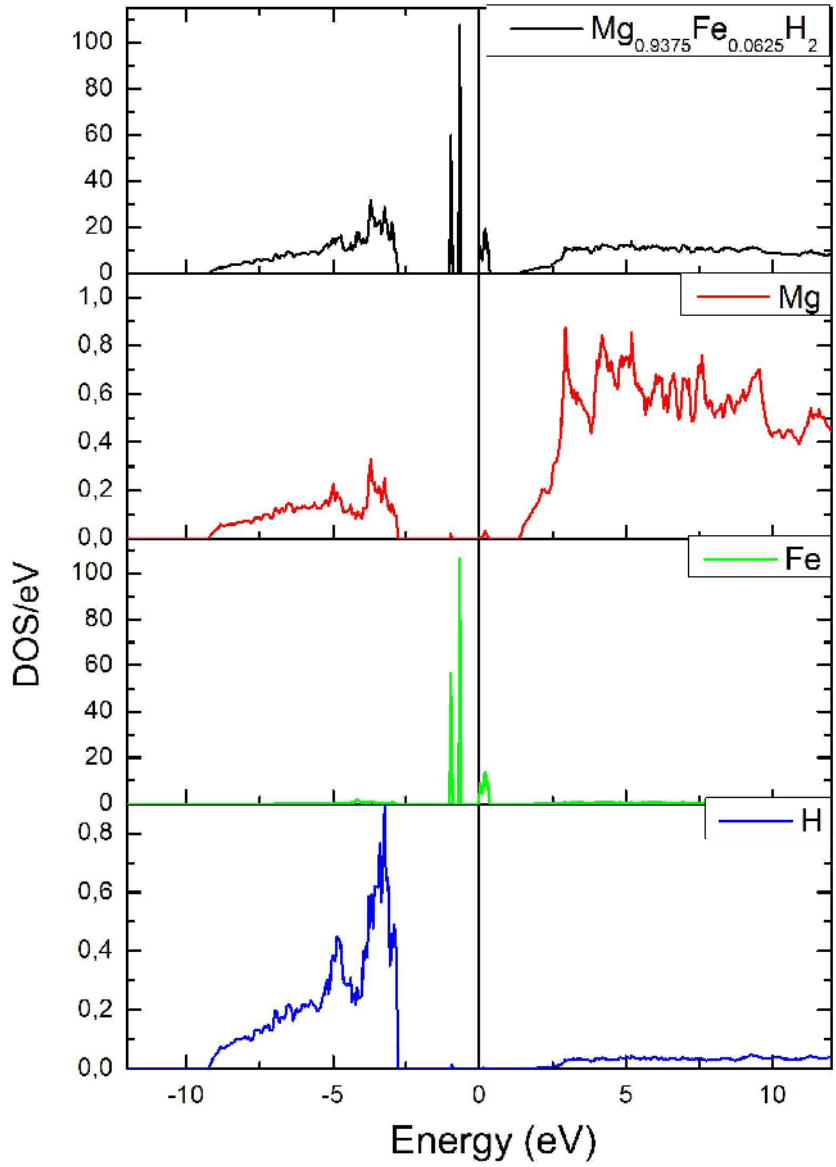

Figure 3.15: Total and partial DOS of $Mg_{1-x}Fe_xH_2$ where $x = 12.5\%$ as a concentration of substitution.

The electronic structure of $Mg_{0.875}M_{0.125}H_2$ shows the same behavior observed when MgH_2 is doped with 6.25% of M with one significant difference which is the density states of M atoms.

As an example, it is observed in the DOS of $Mg_{0.875}Fe_{0.125}H_2$ shown in Figure 3.15 that the states intensity of substitution element are higher then those observed for the concentration 0.0625 (Figure 3.10), which means that there are more M atoms that have a weak bond with H and suddenly hydrogen is released more easily which leads to an improvement in the thermodynamic properties of the hydride. The same things are observed for the other elements Al, Ti, V and Ni. These findings are in good agreement with the calculated values of heat of formation and desorption temperature listed in Table 3.6.

3.4 Nano-structuration effect in the thermodynamic properties of MgH_2

Nowadays, it is well known that nanostructuring materials leads to new physical phenomena and/or improve their physical properties. Experimentaly, MgH_2 based thin films shows improved hydrogen sorption performance than MgH_2 bulk [215, 29, 318, 319, 320, 321, 322, 323, 324, 325, 326, 327]. Lu H-B et *al.* [215] reported that ΔH of hydrogen absorption and desorption of bulk Mg/MgH_2 are 73.9±0.7 and 77.7±0.8 kJ/mol respectively and are considerably higher than those of $2D$ nanostructured Mg/MgH_2 film. Barawi et *al.* [29] and Baldi et *al.* [318] found that the thickness plays a major role in the hydrogen absorption kinetics of Mg films due to the interface effects between substrate and the Mg film. Even more, studies conducted over a decade or so [321, 322], showed that $50-100nm$ thick MgH_2 based thin films reduced stability. Thus, the improved dehydrogenation properties of Mg/MgH_2-based nanocomposites mentioned above certainly depend on the interface misfit and strain energy [323, 324, 325, 326, 327]. However, the origins of the tuned thermodynamics and kinetics properties of MgH_2 with different size and under strain have not been systematically investigated.
To address these issues, the properties of the nanostructured MgH_2 thin film and the effect of biaxial strain are studied using first principles calculations.

3.4.1 Size dependent thermodynamic properties

The effect of nanostructuring on the thermodynamic properties of MgH_2 was investigated by studying the size dependent hydrogen desorption in Mg hydride thin films with different thickness ($1nm, 4nm, 5nm$ and $22nm$, Figure 3.16).

The magnesium hydride thin films are modeled by considering a $(3\times3\times z)$ supercell with different size along Z direction. Periodic boundary conditions are applied along the X, $Y-$directions and a vacuum of 35Å was used along $Z-$direction to isolate the system of layers, see Figure 3.16.

The total energies of Mg and MgH_2 thin films are calculated. Therefore, the heat of formation can be deduced following the equation 3.11 for thin film model and the corresponding desorption temperature by using equation 3.5:

$$\Delta H = E_{tot}(MgH_2)_{nano} - E_{tot}(Mg)_{nano} - (n/2)E_{tot}(H_2), \tag{3.11}$$

where n is the number of H atoms contained in MgH_2 thin film.

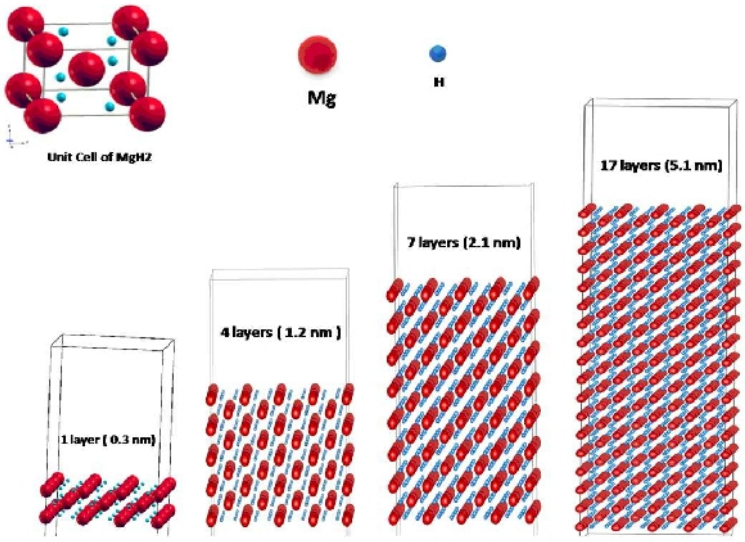

Figure 3.16: Structures of bulk and MgH_2 thin films.

The effect of the size of MgH_2 on the sorption temperatures and enthalpy of formation are shown in Figure 3.17.

By reducing the size, a significant enhancements in both heat of formation and sorption temperature are observed from $-0.715eV/H_2$; $542K$ for the bulk to $-0.56eV/H_2$, 414.75 and $-0.515eV/H_2$, $380K$ corresponding to $22nm$ and $1nm$ thickness, respectively. These results are in line with the reported findings[16, 29, 328, 329]. Krozer et *al.* [329] showed that Mg thin film has smaller heat of formation $60.3 \pm 6.7kJ/mol.H_2$ than the bulk MgH_2. Barawi et *al.* [29] reported that the desorption temperatures $T_{des} = 435°C$ are slightly lower ($\Delta T \sim 58°C$) in thickest hydrogenated films ($d < 150nm$). Such a result confirms that the size's change of MgH_2 films improves the sorption and thermodynamic properties of Mg due to the thickness and surface properties of $2D$ nanostructured film.

By assuming that sorption behavior of the thin films along the Z axis, it is necessary, for efficient hydrogen storage, to aim for nanometer sizes of thin layers. The remaining axis(X, Y) may be reserved for the application of a stress on MgH_2 thin films with $22nm$ thickness in order to investigate the effect of such a stress on de/hydrogenation properties.

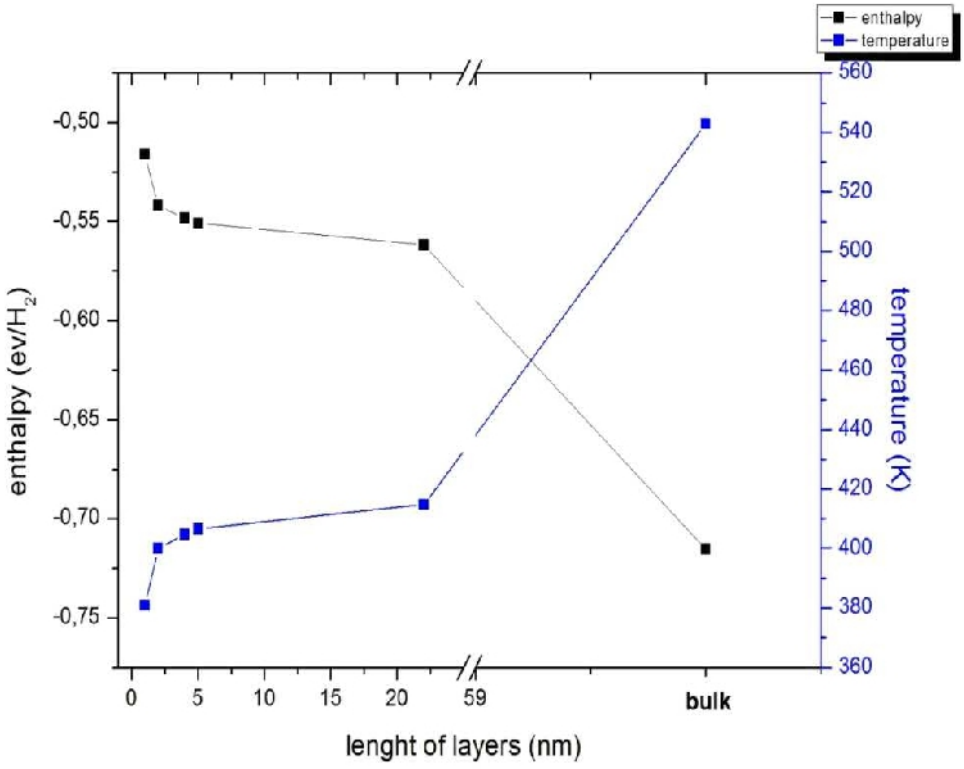

Figure 3.17: Variation of sorption temperatures and enthalpy *vs* thickness of the MgH_2.

3.4.2 Strained MgH_2 thin film properties

In order to simulate the extrinsic effect of the stresses which can be observed experimentally by the mismatch, a biaxial tensile/compressive strains are applied to the $22nm$ thin film along the [100] and [010] direction according to the equation 3.12 [330, 331, 332].

$$\varepsilon_{xx}(\%) = \varepsilon_{yy}(\%) = \frac{a(b) - a_0(b_0)}{a_0(b_0)}, \tag{3.12}$$

where the lattice constants $a(b)$ of $MgH_2(22nm)$ supercell are restricted to different values ranging from -2.7% to 1.8% by step of 0.1%; $a_0(b_0)$ are the equilibrium lattice constants. The c parameter is obtained by relaxing atomic positions under each strain. Figure 3.18 shows the stability of $22nm$ MgH_2 thins film system under strain.

The maximum of stability was found for the relaxed parameters and this stability is reduced considerably when we apply the strain. Even more, the lattice constant c increases under biaxial compressive strain while it decreases under the tensile one.

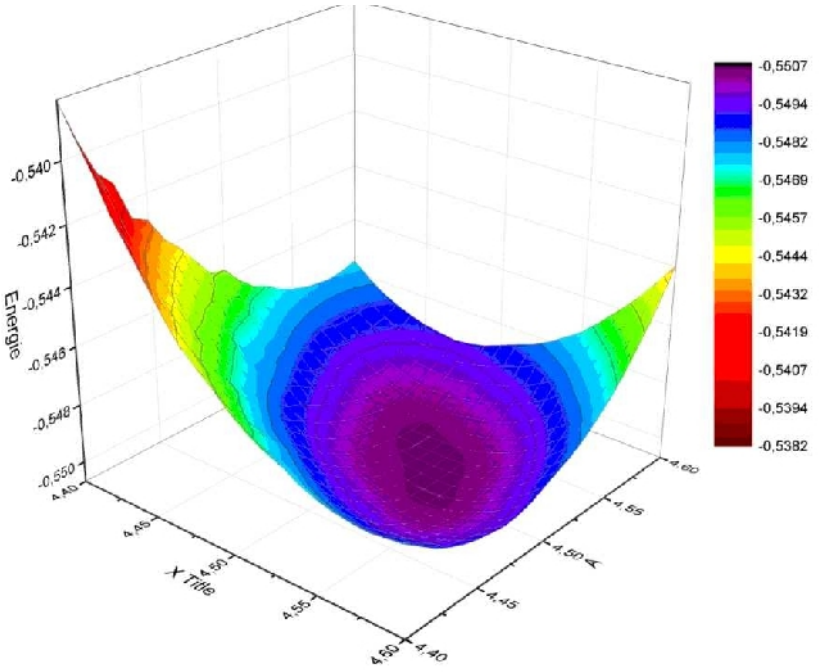

Figure 3.18: The effect of stress (variation of lattice a and b) on the stability of MgH_2 thin film (thickness $22nm$).

Figure 3.19 shows the calculated c/a ratio and cell volume of MgH_2 ($22nm$ thickness) under biaxial strains. Based on the two indexes, the lattice distortion of strained MgH_2 can be evaluated.

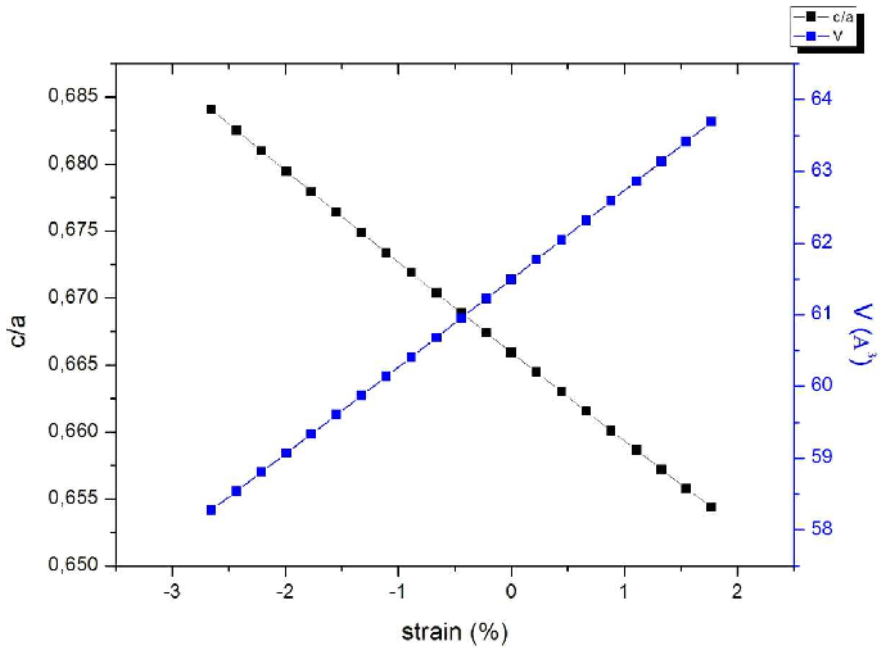

Figure 3.19: Calculated c/a and cell volume V as a function of biaxial strain in MgH_2 thin film.

Under biaxial compressive strain, the lattice constant of MgH_2 along Z axis direction is elongated, which results in an increasing ratio c/a relative to that of strain-free state (0.667). The maximal ratio of c/a reaches 0.684 for a compressive strain of -2.7%. Comparatively, the lattice of MgH_2 along Z axis direction shrinks under biaxial tensile strain, yielding a decreasing ratio of c/a relative to that of strain-free state. A minimum of 0.6543 is obtained at a tensile strain of $+1.8\%$. As MgH_2 expands or contracts under biaxial tensile or compressive strain its cell volume increases or decreases nearly linearly as the magnitude of strain as shown Figure 3.19. So it can be derived that either biaxial tensile or compressive strain is likely to cause structural deformation of MgH_2 crystal, or its lattice distortion becomes severe with increasing magnitude of biaxial strain.

The effect of strain on the thermodynamic properties of MgH_2 thins films (thickness of $22nm$) can be summarized in Figure 3.20. This figure shows that the application of the strain on MgH_2 thin films systems reduces its stability compared to that of strain-free one, which can improve its storage properties. This can be understood as follows: in the case of compressive strain, the distance between atoms is too small; this can lead to a strong interaction and therefore reduces the stability of the system. On the other hand, the H atoms can diffuse easily when we apply a tensile strain and consequently a decrease of the heat of formation.

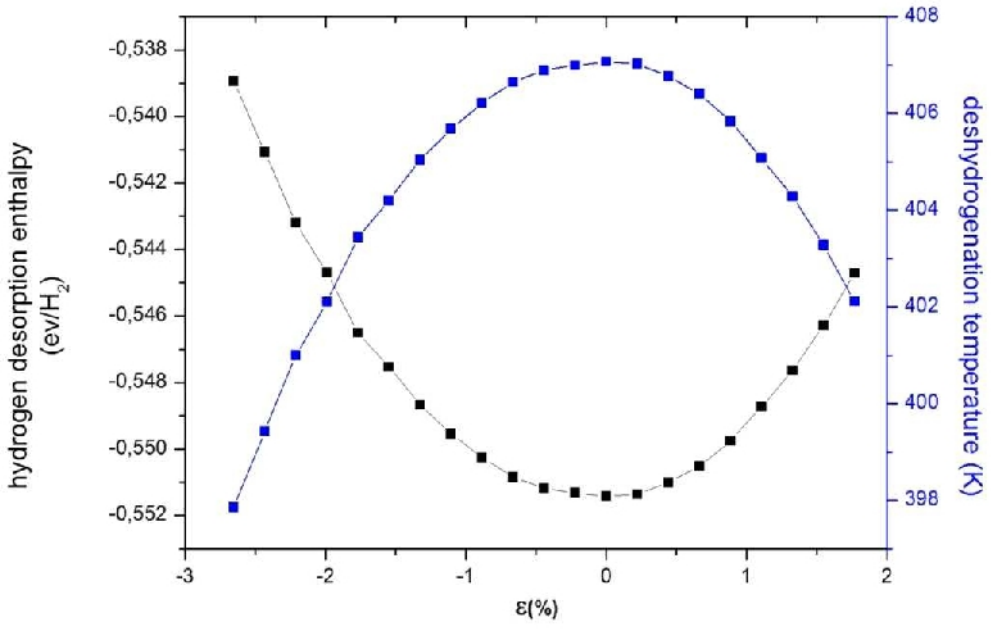

Figure 3.20: Formation enthalpies and desorption temperatures of MgH_2 thins films ($22nm$) as a function of strain ε.

The obtained results are partially comparable with the ones found by J.Zhang [330]

who states that strain lowers the enthalpy and decomposition temperature of the bulk MgH_2. Furthermore, the decrease observed in the case of the compressive strain is totally different than that of tensile one, whereas in our work both strain (compressive and tensile) symmetrically decrease the heat formation and desorption temperature for strained $MgH_2(22nm)$ thin film relative to the free strain. The finding behaviors are similar to the results of Benzidi et *al.* [332], who showed that the free strain $LiBH_4$ involves a high stability that is lowered by applying biaxial tensile or compressive strain, which leads to a decreasing of the hydrogen desorption enthalpy of $LiBH_4$ compound.
Finally, due to the contribution of strain, the stability and the decomposition temperature for strained MgH_2 thin film hydride are reduced relative to that of strain free system, which is a great enhancement of MgH_2 storage properties. The calculation results of this study show that T_d decreases significantly with increasing magnitude strain to a value equal to $398K$ which is close to the optimum range $289 - 393K$ for the practical use of a $PEMFC$ [317].

In conclusion, the nanostructuring of the bulk added to a biaxial strain applied a beneficial improvement to the storage properties of MgH_2. So, the stress concept validated via numerous experiments [323, 324, 325, 326, 327] could have general implications on destabilization of other types of metal hydrides for H_2 storage application.

3.5 Conclusion

First-principles calculations were used to investigate the mechanical stability, storage capacities, heat of formation and temperature of desorption in the pure MgH_2 and $Mg_{1-x}M_xH_2$ ($x = 0.0625$ and 0.125; $M = Al, Ti, V, Fe$ and Ni) systems. Using the DFT method, we have shown on the one hand that the doped MgH_2 system improves the thermodynamic properties of the material as summarized in what follow:

- The pure MgH_2 has high gravimetric and volumetric storage capacities (7,660 $wt.\%$ and 109.619 $g.H_2/l$ respectively).
- The pure MgH_2 presents a high stability (-62,018 $kJ/mol.H_2$) and a high decomposition temperature (483,521 K).
- The obtained values are in agreement with those obtained experimentally and theoretically in other works.
- The stability and the decomposition temperature reduce considerably when doping MgH_2 with a small amount of TM ($TM = Ti, V, Fe$ and Ni) and Al.
- The high stability of the pure MgH_2 is due to the strong hybridization between Mg and H atoms. Such hybridization is reduced by the addition of a small amount of

$M = Al, Ti, V, Fe$ and Ni, which improves the hydrogen storage properties of the magnesium hydride.

Following our study, we remark that the Ni presents the highest performances and is the most appropriate element for better hydrogen storage.
On the other hand we have shown that at nanoscale:

- The nanostructuring from bulk to thin films improves considerably its thermodynamic properties. $\Delta H = -0,56eV/mol.H_2$ and $T_d = 414,75K$ for a thickness of $22nm$.

- The biaxial tensile or compressive strain tends to lead to the structural deformation of MgH_2 crystal, and the lattice distortion becomes severe with increasing magnitude of strain.

- Due to the contribution of strain energy, the stability and the decomposition temperature for strained MgH_2 thin film hydride are reduced relative to that of strain free system, which is beneficial for the improvement of the dehydrogenation properties of MgH_2.

In this chapter, a complete study of the MgH_2 storage properties hase been realized namely: the storage capacities, stability and desorption temperature. We have explained what makes based magnesium hydride materials thermodynamically stable and the role of additives in improving their properties.

The kinetics of absorption and desorption of hydrogen inside MgH_2, which remains to be studied, are relevant properties for potential applications. Many experimental studies have addressed the subject and show that these materials exhibits a slow hydrogenation/dehydrogenation kinetics but to the best of our knowledge, there are no theoretical investigation performed previously and the mechanism which causes this slow kinetic is still not adequately explained.

Chapter 4

Simulation of the kinetics of hydrogen diffusion in MgH_2 and its derivatives by kinetic Monte Carlo method

Contents

4.1 Introduction

The kinetics of absorption and desorption of hydrogen inside MgH_2 are relevant properties for potential applications, but to the best of our knowledge, there are no theoretical investigation performed previously. So, the aim of this work is to present numerical investigations of the hydrogen storage ab/desorption kinetic properties for the pure MgH_2 and MgH_2 doped with different metal M ($M = Al, Ti, V, Fe$ and Ni) by combining density-functional theory (DFT) and Kinetic Monte Carlo (KMC) simulations. In particular, we dealt with the different mechanism appearing in ab/desorption phenomena. To perform such computations, the activation energies for different elementary processes and thermodynamical quantities, that we need, were computed by using DFT method. Taking into account of all the calculated quantities of interest, we study hydrogen diffusion in magnesium hydride (such as dissociation of H_2, adsorption, diffusion and desorption) using KMC simulations. The effect of each elementary mechanism on the diffusion that we characterized through density distribution of hydrogen, filling ratios, diffusion time, temperature and pressure is analyzed. It is worth noting that this numerical method is adopted to study the time of ab/desorption in MgH_2.

4.2 Model and computational methods

In this section, we describe details of our model based on kinetic Monte Carlo method (KMC) [333], and its application to the investigation of hydrogen diffusion in magnesium hydride.

4.2.1 Kinetic Monte Carlo calculation

In this computation program, the activation energies calculated by DFT method are implemented in our algorithm to determine the rate transition of each elementary process. By defining the relation between simulated time and Monte Carlo steps, we can predict the hydrogen diffusion time (ad/desorption time) in our systems as function of temperature and pressure.
In our model, we consider a supercell containing 160 magnesium atoms and 320 hydrogen atoms, Figure 4.1. In terms of Miller indices, the surface on which hydrogen will be adsorbed or desorbed is given by (001), Figure 4.2. Periodic boundary conditions were considered along $X-$ and $Y-$directions as shown in Figure 4.3.

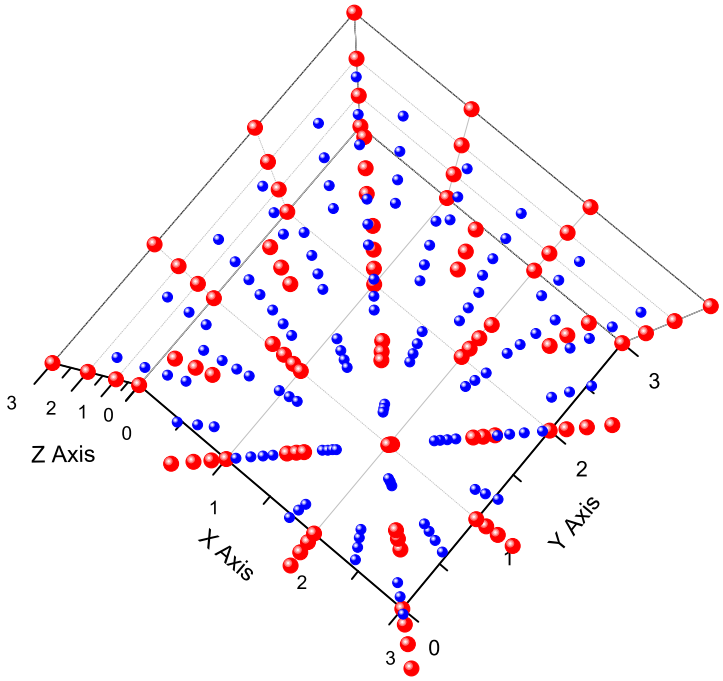

Figure 4.1: MgH_2 in $3 \times 3 \times 3$ supercell. Mg atoms are red spheres while the blue ones are H atoms.

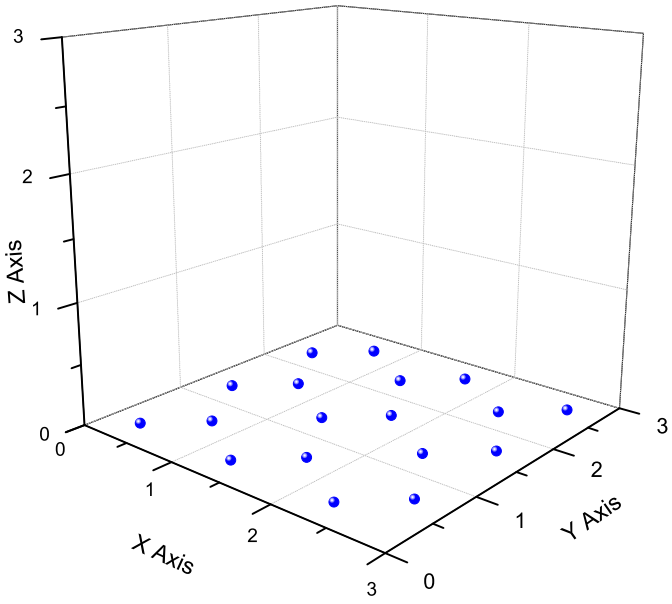

Figure 4.2: The surface (001) on which hydrogen will be adsorbed or desorbed.

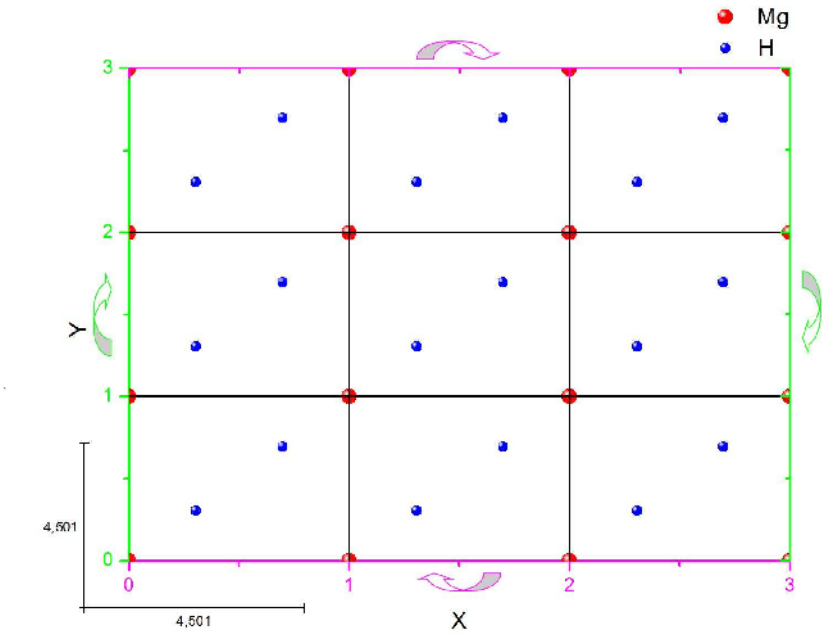

Figure 4.3: Periodic boundary conditions along $X-$ and $Y-$directions

We assume that the gas phase is an ideal gas composed of hydrogen atoms and thus fully described by partial pressures P_{H_2} and temperature T. The rate of hydrogen flux can be obtained using the kinetic theory of gases providing (F) the amount of gas hitting the unit area of a surface per unit time $(particles/m^2.s)$ [334]:

$$F = \frac{P_{H_2}}{\sqrt{2\pi m_{H_2} K_\beta T}} \tag{4.1}$$

where m_{H_2}, K_β are the mass of hydrogen, and Boltzmann constant, respectively.

Absorption and desorption of hydrogen in hydride metals can be done according to three steps. There are known by adsorption/desorption, dissociation and diffusion.
In order to study the absorption, we consider initially a supercell containing only the magnesium atoms, Figure 4.4. Then the interstitial sites will be occupied by H atoms at each Monte Carlo steps. Such filling of H atoms is based on the above three mentioned processes.
The adsorption of H_2 is followed by its decomposition in two H atoms. For such decomposition, one needs to introduce energy barriers controlling the dissociation processes. The calculations we performed show that the barrier energy of H_2 dissociation at the surface (001) of Mg atoms is of order $0.8eV$. It is in good agreement with the energy barriers $0.75 - 1.18eV$ obtained in the literature [311, 335, 336].

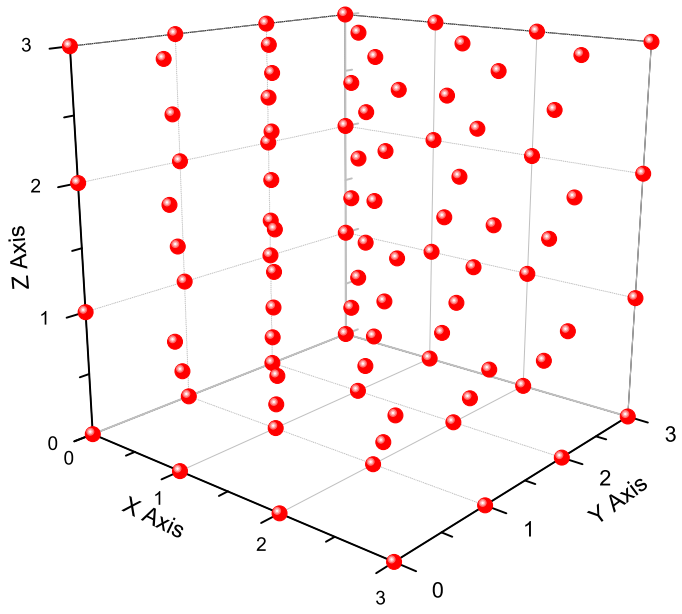

Figure 4.4: Super-cell containing only Mg atoms

After dissociation, the diffusion processes take place. In this step, the H atoms can move from an interstitial site to another one. In fact, each hydrogen atom has eleven nearest neighbors ($N.N$): seven in the same plane, two in the upper adjacent plane and the remaining two ones are located at the lower adjacent plane (Figure 4.5).

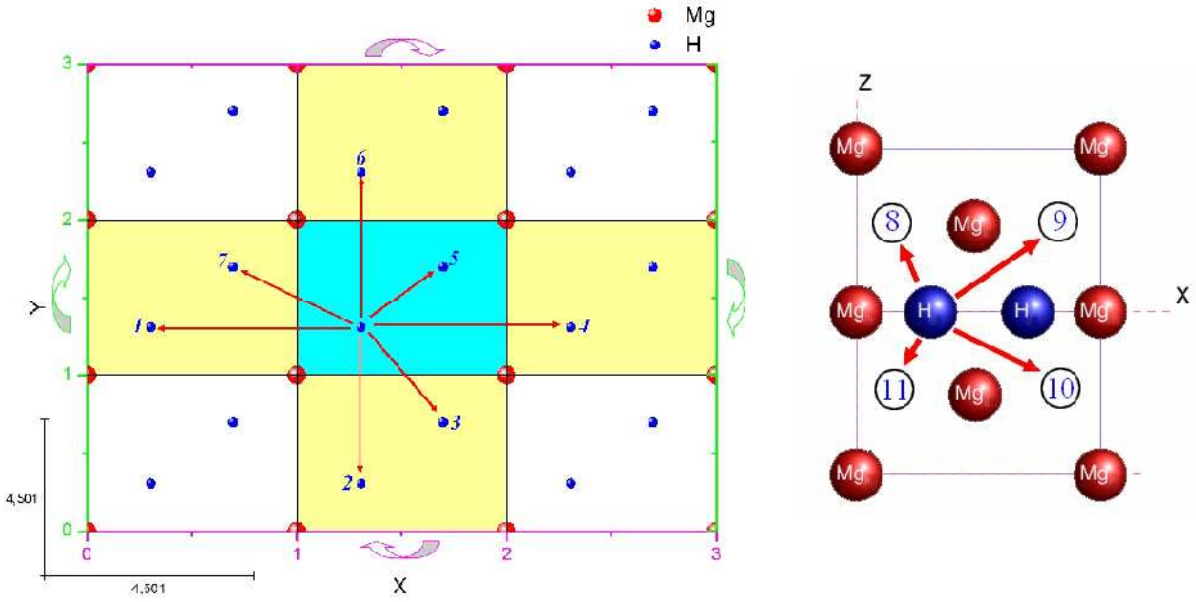

Figure 4.5: Representative scheme of neighbors sites. Left denotes the seven neighbors in the same plane; right shows the four neighbors in the other planes.

In our developed algorithm, various possible events including processes of diffusion to the free neighbors, adsorption and desorption are considered. The mentioned events are randomly selected at each KMC step with a probability P_i:

$$P_i = \frac{R_i}{R} \tag{4.2}$$

The rate transition R_i associated to the i^{th} jump process and the total rate transition R are given respectively by:

$$R_i = \nu_0 \exp\left(-\frac{E_i^a}{K_\beta T}\right) \tag{4.3}$$

$$R = \Sigma_{i=1}^{N} R_i \tag{4.4}$$

where ν_0 is the jump frequency (usually set to $10^{13} Hz$) and E_i^a the activation energy of i^{th} jump process taken from first-principles calculations (see section 4.2.2).
The time of hydrogen atoms displacement is incremented by Δt, which is defined as the inverse of the total rate transition:

$$\Delta t = -\frac{\ln(u)}{R} \tag{4.5}$$

where u is a uniformly distributed random variable between $0 < u \leq 1$.

4.2.2 Density functional theory calculations

In order to calculate energy barriers for the different process, we have used ab-initio calculations based on the all-electron full-potential local-orbital minimum-basis scheme $FPLO9.00-34$ [265, 266] to solve the Kohn-Sham equations using the scalar-relativistic and the full four-component relativistic schemes. The parameterization of the exchange-correlation energy was done within the generalized gradient approximation GGA [261]. To ensure a high accuracy in our calculation, self-consistent criteria for both the energy and the density with precisions of 10^{-8} Ha and 10^{-6} $Ha^{-1}.\text{Å}^{-3}$ respectively are used. A mesh of $(12\times12\times12)$ and $(6\times6\times6)$ $k-points$ in the irreducible part of the first Brillouin zone was used in our calculations for the pur MgH_2 and M doped MgH_2, $M = Al, Ti, V, Fe$ and Ni. The energy barrier are calculated using the scalar-relativistic scheme, for all configurations.

To calculate the activation energies, all hydrogen possible configuration have to be determined. However, in the unit cell model four atoms may move to empty neighbors. To reach the different possible arrangements of H atoms, we should break the usual symmetry $P4_2/mnm$ settings down to the standard setting $P1(1)$ by translating the Wyckoff position coordinates.

Based on this symmetry breaking and using combinatorial calculation, we obtain 304 H atom configurations. The activation energies were obtained from the maximal energy appearing in the possible paths between the initial position and the final one while the energy formation and the desorption temperature have been calculated in $P4_2/mnm$ settings (chapter 3).

4.3 Results and discussions

4.3.1 Kinetic Monte Carlo study of the pur MgH_2

To apply Monte Carlo calculations for studying the kinetic properties of the studied compound, we should calculate and implement the activation energies. These quantities are obtained using the DFT method based on ab-intio calculations.

4.3.1.1 Activation energies

For later use in Monte Carlo simulations, energy barriers (more than 300 activation energies) were computed. Four situations among them are illustrated in Figure 4.6 and Figure 4.7.

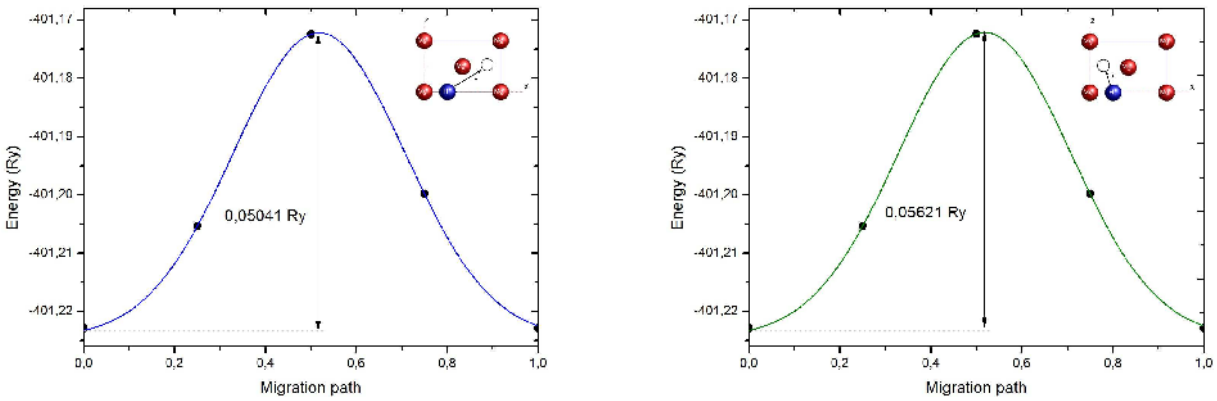

Figure 4.6: Energy barrier for an H atom diffusing between two parallel plans.

Particularly, we have found that the energies depend on the surrounding hydrogen atoms and the target-interstitial sites. The barriers get enlarged by increasing the hydrogen atom number in the system.

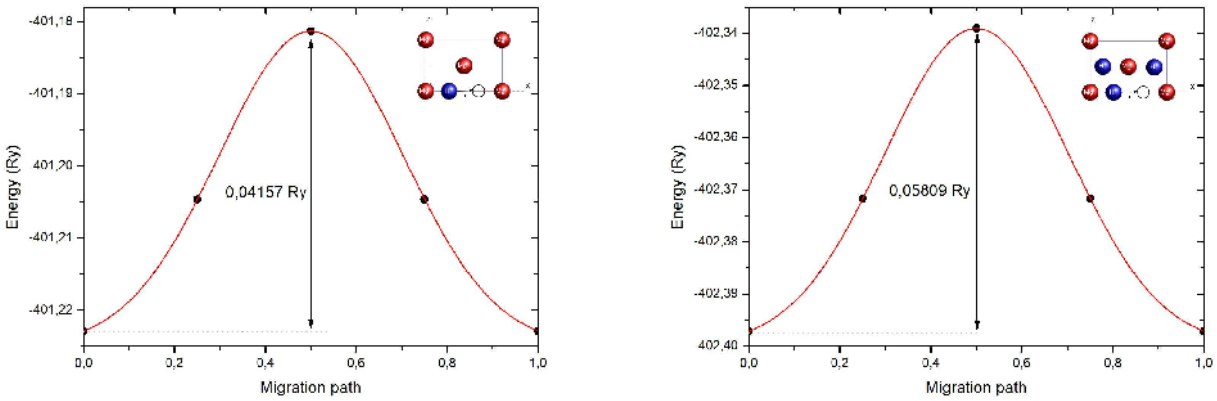

Figure 4.7: Energy barrier for an H atom diffusing between two interstitial sites along the same paths and different configurations.

Indeed, DFT calculations reveal that the energies corresponding to planar motion (001) hydrogen atoms are lower than the energies associated with the motion between two parallel plans. Therefore, hydrogen atom prefer to diffuse along X and Y directions instead of moving vertically, which may affect the kinetics of the material.

4.3.1.2 Absorption/desorption times of the pur MgH_2

Having determined the activation energies of the diffrent process in MgH_2 structure using DFT method, we incorporate all calculated quantities in the KMC method to study the kinetic properties of the magnesium hydride material.
In order to determine the responsible mechanism of hydrogen storage in magnesium hydride in conformity with the observed behavior in the experiment, we have used several elementary events (adsorption, surface diffusion, diffusion along $X-$, $Y-$ and $Z-$direction, and desorption). Along our numerical analysis, we have observed that all the mentioned mechanisms are necessary to reproduce the behaviour obtained experimentally in literature [292, 337].
In Figure 4.8 and Figure 4.9, we present respectively the amount of the absorbed and the desorbed hydrogen calculated (in $wt.\%$) as a function of the reaction time using the following equation:

$$\rho_m = \frac{xM_{H_2}}{xM_{H_2} + M_{Mg}} 100 \tag{4.6}$$

where M_{H_2}, M_{Mg} are the molar mass of hydrogen and magnesium respectively and where x is the rate of hydrogen atoms placed in the supercell.

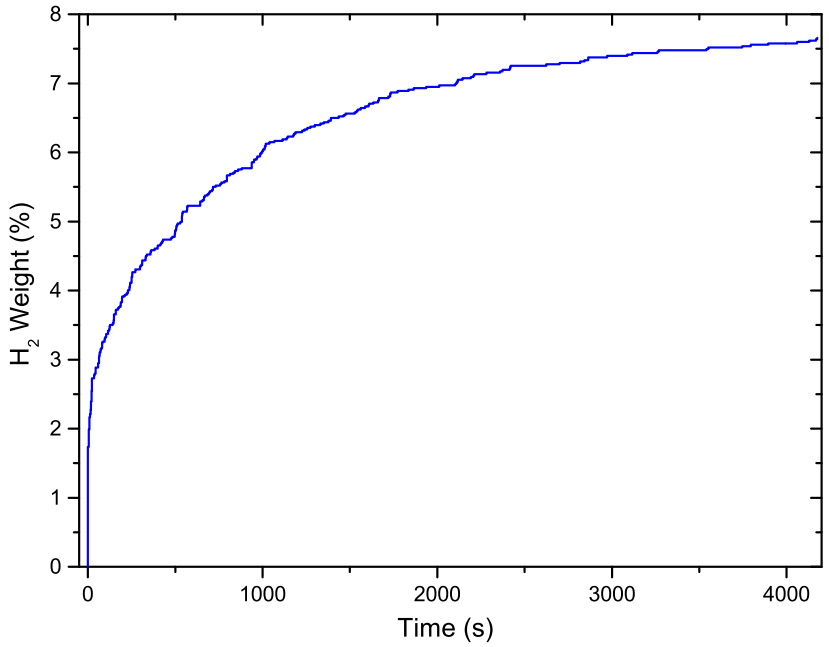

Figure 4.8: Simulation of absorption kinetic for the pure MgH_2 at $633K$ and $10bar$.

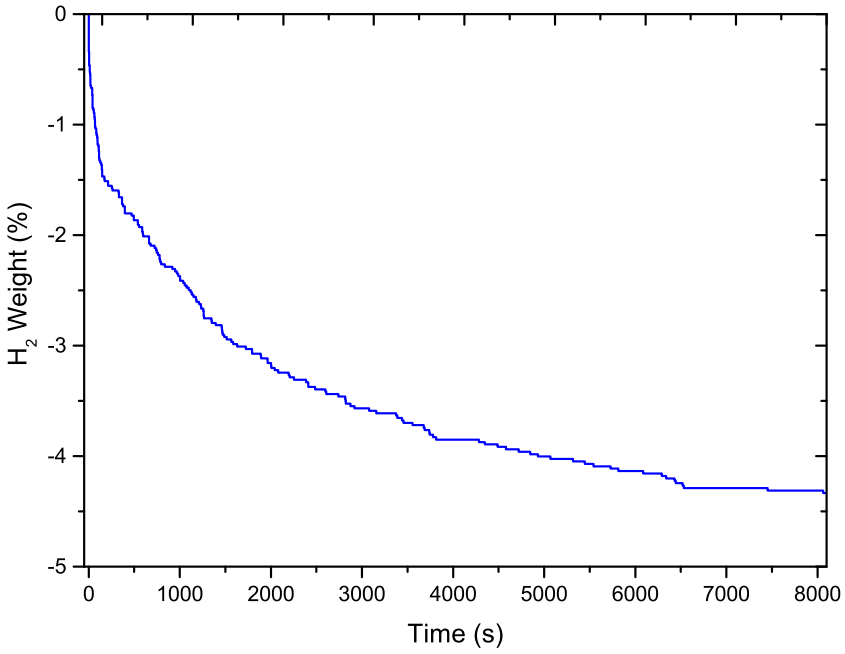

Figure 4.9: Kinetic of desorption for MgH_2 at $633K$ and $1bar$.

Both absorption and desorption kinetics exhibit a behavior quite similar to that observed in experimental results with a very small quantitative difference, which is due to the used pressure values being smaller or higher than the experimental ones [292, 337].

Depending on the initial conditions and to the initial pressure applied on the adsorption surface (001), the rate of hydrogen absorption in our material increases rapidly with respect to time. Once the number of the hydrogen atoms in the system becomes substantial, the activation energies increase. Then, the H atoms move with difficulties to the empty sites. For this reason the amount of hydrogen increases slowly as a function of time until reaching a limit equal to the gravimetric capacity of MgH_2 ($\rho = 7.65wt.\%$) where all the empty interstitial sites in the supercell are occupied by hydrogen atoms.

For the desorption process, the system does not completely desorbs all hydrogen atoms which prefer to move inside rather leaving the system. In order to discharge all hydrogen atoms, one needs a high vacuum, which cannot be realized within our numerical simulations. The maximal value of dehydrogenation, which depends on the temperature and the applied pressure, remains a little bit constant for a while. It follows that the kinetic of desorption of the hydrogen of our system is very slow in contrast to the absorption mechanism.

It follow that the behavior of ab/desorption of the pur MgH_2 agree perfectly with the experimental results [292, 337] and the suggested material has slow kinetics even at high temperature and pressure due to the high activation energies of hydrogen diffusion that the material exhibits.

4.3.1.3 Temperature effect in the kinetic of MgH_2

The effect of the temperature on such behavior is represented in Figure 4.10 and Figure 4.11 for temperature values running from $600K$ to $630K$ with a step of $10K$.

It is shown clearly that higher temperatures lead to significantly improved hydrogenation as well as dehydrogenation kinetics since the reaction speed increases by increasing the temperature. After a period of $4000s$, the tank already reaches the rate of saturation for a temperature of $630K$, while it hardly exceeds the half size at $600K$.

Thus, the filling time depends on the temperature. It decreases exponentially with respect to the temperature as shown in Figure 4.12.

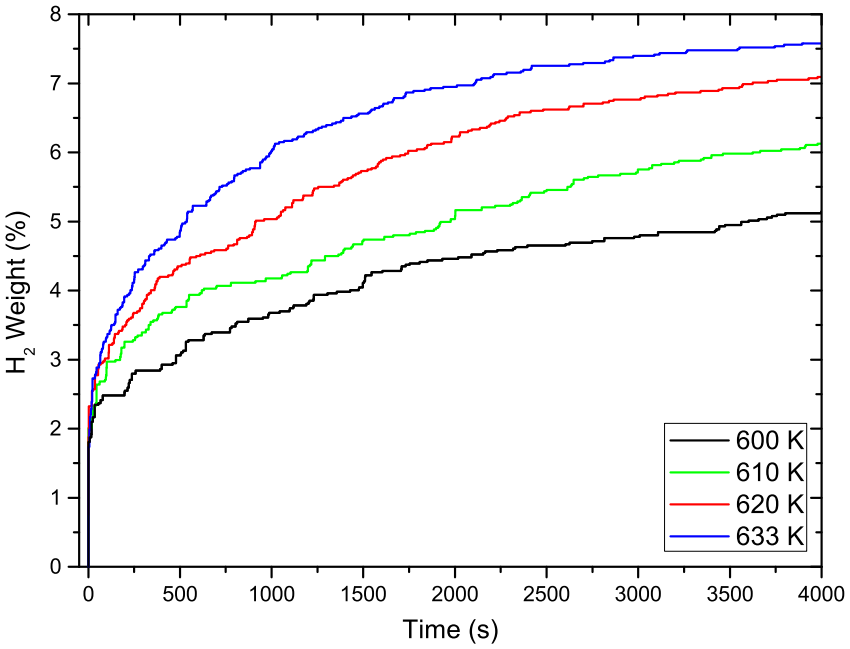

Figure 4.10: MgH_2 Hydrogenation kinetic at different temperature and $10bar$.

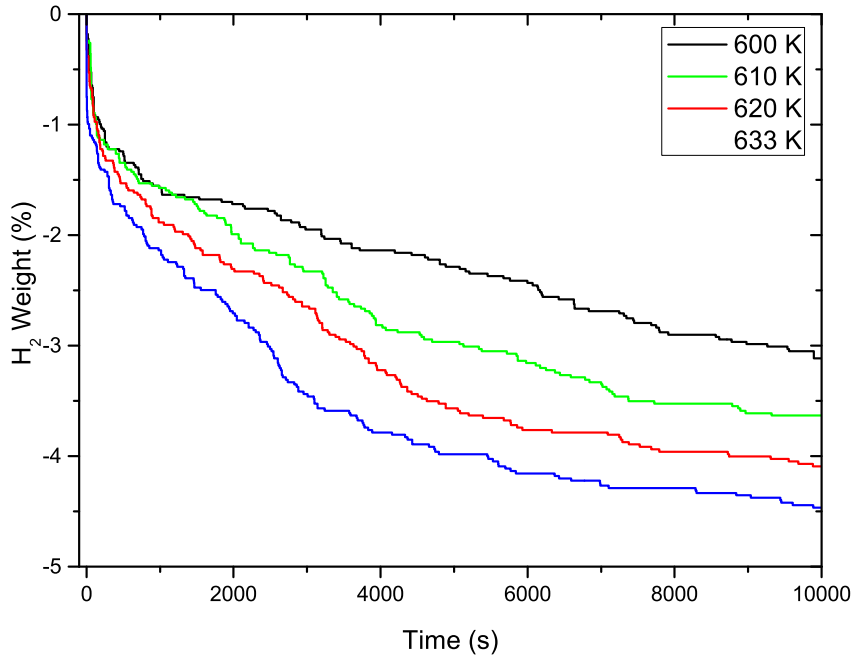

Figure 4.11: Dehydrogenation kinetic of MgH_2 at different temperature and $1bar$.

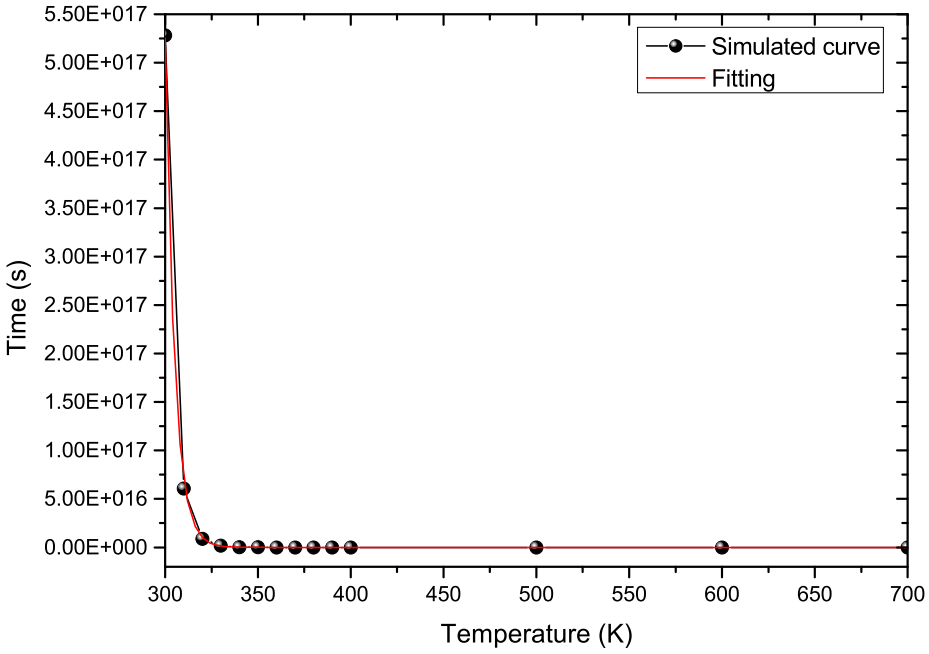

Figure 4.12: Filling time as a function of temperature for $10bar$. Black dots denote the simulation data while the fitted curve is in red.

4.3.1.4 Equilibrium time

To characterize the equilibrium in our system, the density for each plan ($z = 0, z = 0.25, \ldots z = 1$) is calculated at each Monte Carlo step by:

$$\rho(z) = \frac{n_H(z)}{n_S(z)} \tag{4.7}$$

where $n_H(z)$ represents the number of residing hydrogen and where $n_S(z)$ is the total number of interstitial sites appearing in the plan z. The system is considered to be in an equilibrium state when the density $\rho(z)$ is uniform; i.e almost the same in all plans z. The equilibrium time, t_{eq} required to reach such equilibrium phase for different hydrogen concentration is the sum of the filling time t_f (the necessary time to introduce the chosen concentration of hydrogen) and the relaxation time t_r (the necessary time to have a homogeneous distribution of hydrogen in the system).

We show, in Figure 4.13, that t_{eq} increases with respect to the hydrogen concentration until reaching a maximal value corresponding to a concentration of hydrogen atoms close to 90% then it goes down.

The same behavior was observed for different values of temperature (see Figure 4.14 and Figure 4.15). The increase of t_{eq} is completely obvious. More the hydrogen concentration

is high more we need large time t_f to fill the tank. On the other hand, the necessary barriers for the displacement of hydrogen atoms get larger by increasing the hydrogen rate leading to an increment of the relaxation time t_r.

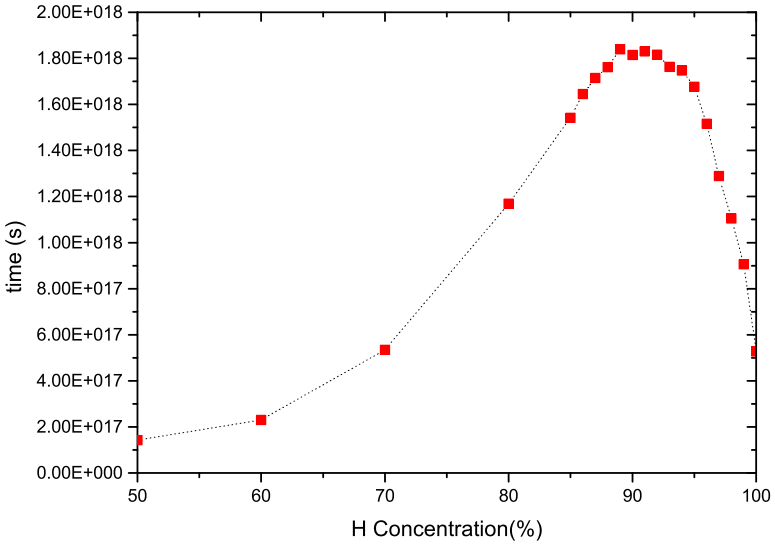

Figure 4.13: Equilibrium time as a function of hydrogen concentration for $300K$. Dotted lines are plotted for clearness.

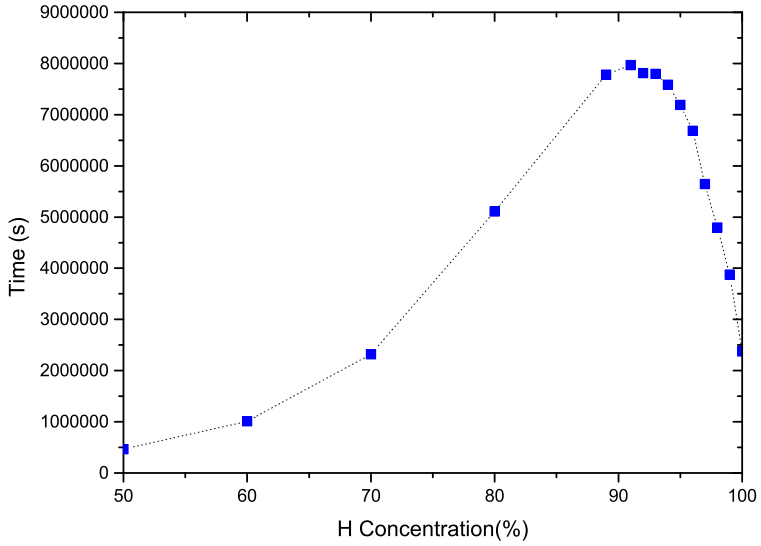

Figure 4.14: Equilibrium time as a function of hydrogen concentration at $500K$.

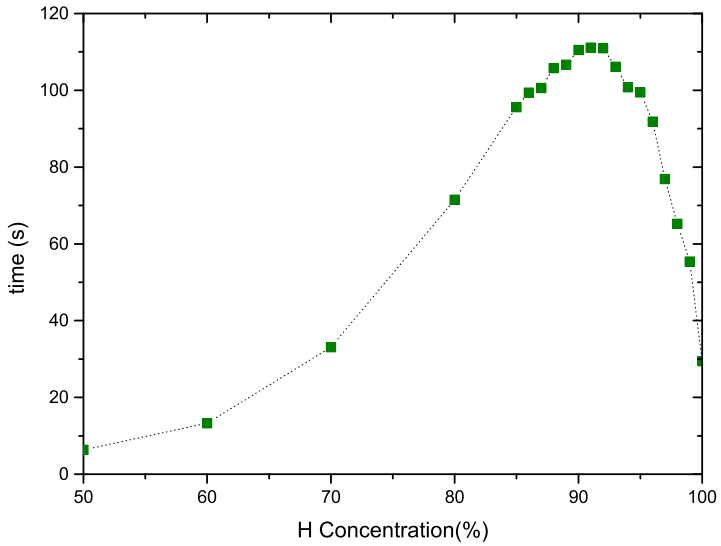

Figure 4.15: Equilibrium time as a function of hydrogen concentration at $700K$.

We expect that the observed maximum is due to the collision of hydrogen atoms with the upper wall (z_{max}) since the boundary conditions were applied only on X and Y directions and not on the Z direction. It turns out that the decrease of t_{eq} is due to the decrease of t_r which vanishes for $x = 100\%$ ($t_{eq} = t_f$). Thus, t_r vanishes when all interstitial sites in the supercell are occupied by hydrogen atoms.

4.3.2 Effect of doping in the kinetic of ab/desorption of MgH_2

In Chapter 3, we have made a complete study of the storage properties of MgH_2 when it is doped with a small amount of TM ($TM = Ti, V, Fe$ and Ni) and Al and we have shown that doping has a good impact on the improvement of the stability and the decomposition temperature of the material. In addition to that, in section 4.3.1 we have explained why this hydrid has a slow kinetic.
In this part, we will invistigate the doping affects on the energies activation of hydrogen diffusion and the reaction kinetic of MgH_2.

4.3.2.1 Activation energies for the diffusion of H atoms

We have computed a large number of energy barriers among them two situations are illustrated in Figure 4.16 and Figure 4.17.

For the same path of diffusion, we find that the H barrier energies with the M atoms ($M = Al, Ti, V, Fe$ and Ni) are less than that inside the pure MgH_2. This finding suggests that the H atoms are trapped more stably inside MgH_2 than the $Mg_{0.9375}M_{0.0625}H_2$ alloys.

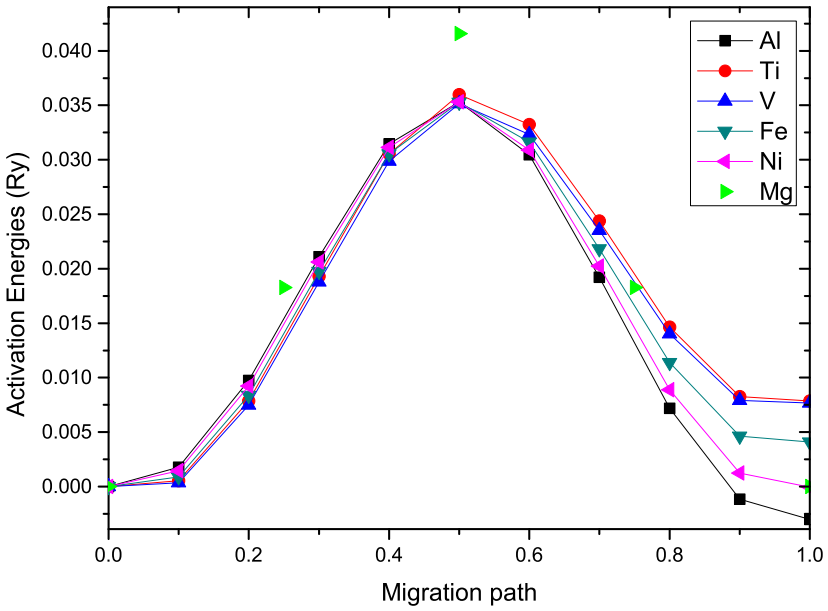

Figure 4.16: Energy curves for an H atom diffusing in different mixture of $Mg_{0.9375}M_{0.0625}H_2$ ($M = Al, Ti, V, Fe$ and Ni): Motion planar.

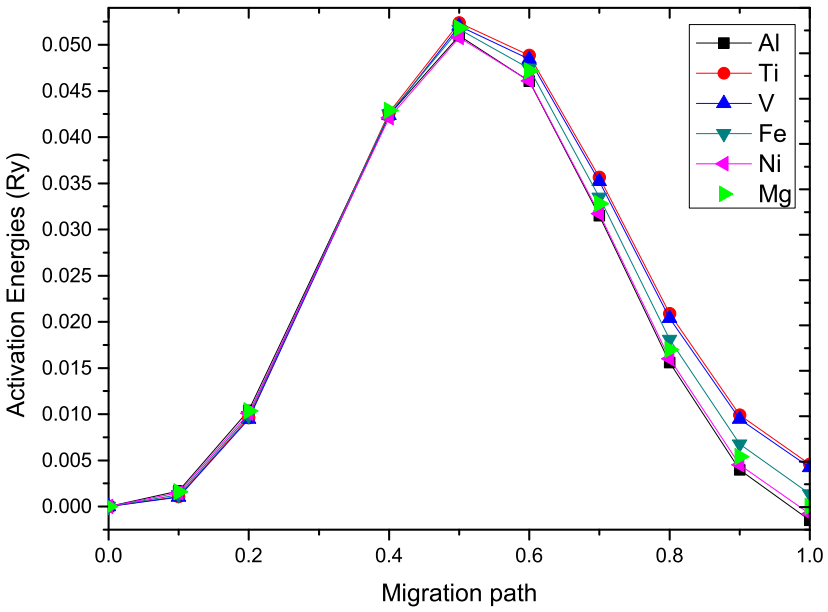

Figure 4.17: Energy barrier of inter-planar motion for an H atom diffusing, between two interstitial sites localized at different plans, in $Mg_{0.9375}M_{0.0625}H_2$ ($M = Al, Ti, V, Fe$ and Ni).

In other words, incorporation of small quantity of Al, Ti, V, Fe or Ni into magnesium hydride can efficiently reduce the interaction between interstitial H atoms and Mg host and thus reduce the stability of the systems, which in in agreement with the results reported in section 3.3.2 in chapter 3.
The minimum energy required for a chemical reaction to occur can be represented by the activation energy (E_a). The value of this energy can reflect the difficulty of the chemical reaction. In general, the lower activation energy corresponds to the faster reaction rate. So, the reduction of activation energy means the better hydrogen de/absorption kinetics of MgH_2 [341].

4.3.2.2 Activation barrier for the dissociation of H_2

The activation barriers for the dissociation of H_2 were calculated by DFT calculations in $Mg_{0.9375}M_{0.0625}H_2$ alloys ($M = Al, Ti, V, Fe$ and Ni), and a comparison of the obtained results with those of the pure MgH_2 is made and listed in the Table 4.1.

Systems	H_2 **dissociation** (eV)
MgH_2	0.8
$Mg_{0.9375}Al_{0.0625}H_2$	0.31
$Mg_{0.9375}Ti_{0.0625}H_2$	0.37
$Mg_{0.9375}V_{0.0625}H_2$	0.34
$Mg_{0.9375}Fe_{0.0625}H_2$	0.36
$Mg_{0.9375}Ni_{0.0625}H_2$	0.32

Table 4.1: Dissociation energy of H_2.

We remark that the barrier of dissociation of H_2 molecule in the pure MgH_2 are higher than those in MgH_2 doped with 6.25% of Al, Ti, V, Fe and Ni. Therefore the doping in MgH_2 decreases considerably the energy necessary for H_2 dissociation and this can play a crucial role in improving the hydrogenation kinetics of the hydride.
Having determined all the barrier energies that we need using DFT method, we move to apply kinetic Monte Carlo techniques to study kinetic properties as described below.

4.3.2.3 Ab/desorption times of the doped MgH_2 by Kinetic Monte Carlo simulation

The amount of absorbed hydrogen as a function of reaction time calculated (in wt. %) for MgH_2 and $Mg_{0.9375}M_{0.0625}H_2$ ($M = Al, Ti, V, Fe$ and Ni) is shown in Figure 4.18. Starting from an empty cell, the rate of hydrogen filled in our material exhibits a fast increasing with respect to time of absorption. Such behavior is due to the initial conditions and the initial pressure applied on the adsorption surface. Once the number of

hydrogen atoms increases in the system, the activation energies increase and then the H atoms move with difficulties to the empty sites. For this reason, after a while from the beginning the amount of hydrogen augments slowly as function of time until reaching for each system a maximal value, which is the gravimetric capacity of the material.
As a result, our KMC simulations show that the absorption kinetic of different doped materials $Mg_{0.9375}M_{0.0625}H_2$ at temperature $400K$ and pressure $10bar$ is very fast compared to the absorption in MgH_2 at high temperature and pressure $(633K, 10bar)$. This is due to the fact that H barrier energies with the M atoms ($M = Al, Ti, V, Fe$ and Ni) are lower than that inside the pure MgH_2.

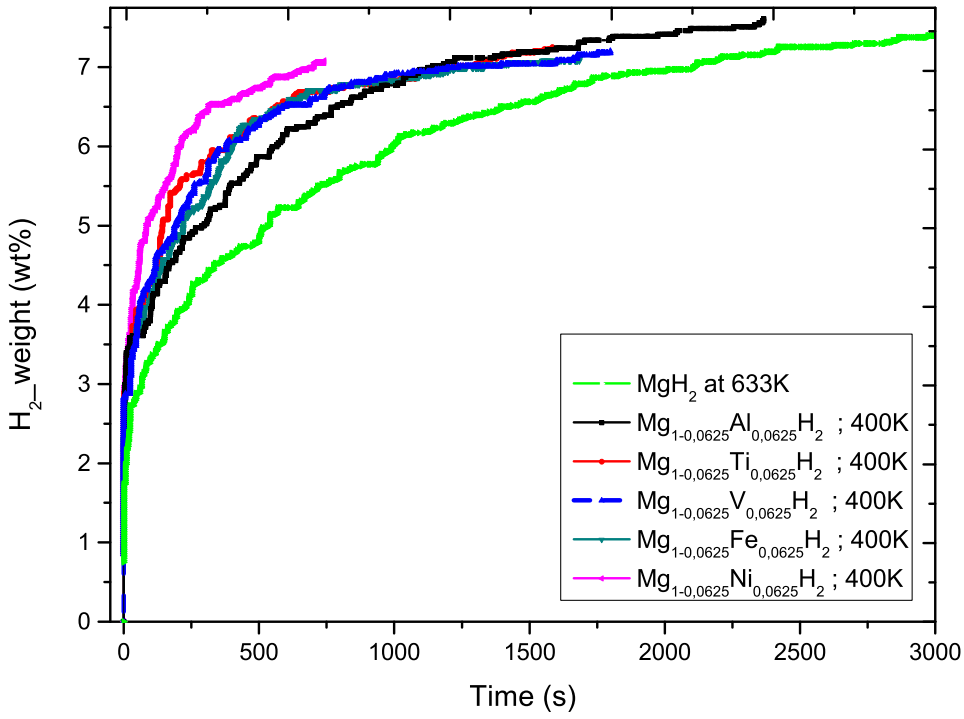

Figure 4.18: Simulation charging kinetic for the pure MgH_2 at $633K$ and $Mg_{0.9375}M_{0.0625}H_2$ ($M = Al, Ti, V, Fe$ and Ni) at $400K$, under $10bar$.

The average filling time for the pure and doped MgH_2 materials, which is computed by using random Monte-Carlo sampling, is represented in Figure 4.19. It follows clearly from this figure that the additive M element leads to significantly improved hydrogenation kinetics even at low temperature.

For the desorption process, the addition of M atoms in MgH_2 improve the kinetic of desorption at low temperature but the system does not completely desorbs all hydrogen atoms which prefer to move inside rather leaving the system (see Figure 4.20). In order to discharge all hydrogen atoms, one needs a high vacuum that we cannot realize within

our KMC simulations.

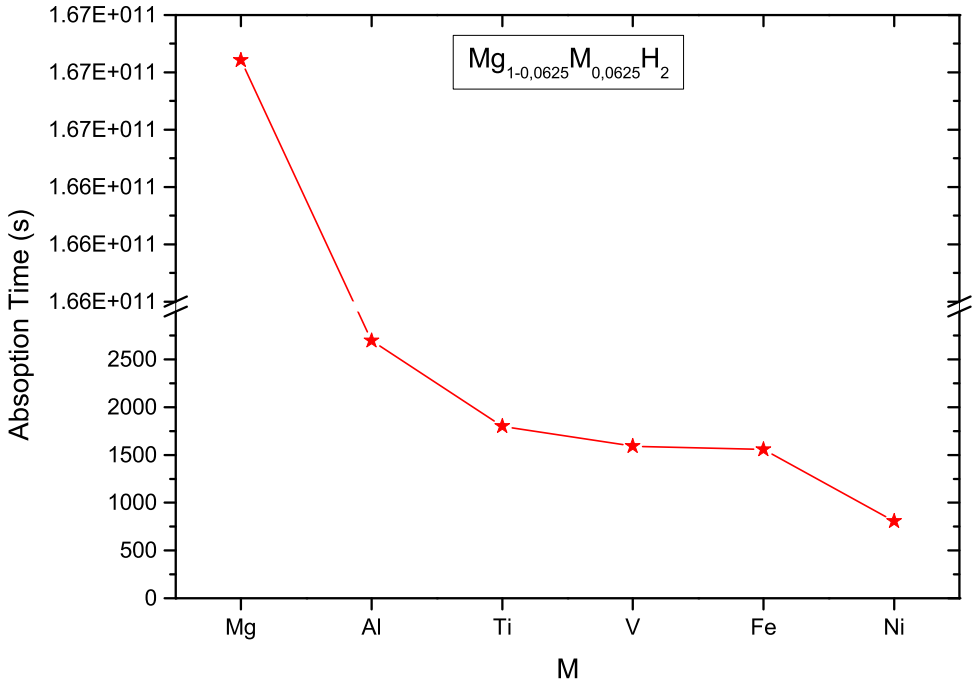

Figure 4.19: The average of filling time at $400K$ and $10bar$ for the pure MgH_2 and $Mg_{0.9375}M_{0.0625}H_2$ ($M = Al, Ti, V, Fe$ and Ni).

Both absorption and desorption kinetics exhibit a behavior quite similar to that observed in the experimental results with a quantitative difference, which is due to the used pressure and temperatures values being smaller or higher than the experimental ones and to the specific conditions of various experiments (its desorption was measured in vacuum, under He flow,...etc)[292, 297, 25]. A comparison of the simulated results with some experimental works found in the literature is given in the Table 4.2.

Systems components	Hydrogen absorption	Hydrogen desorption	Ref.
$MgH_2 - 10wt\%Fe$	20 bar, 350°C, 6.3 wt.%/4.2 min	Onset temperature: $\sim$ 170°C	[342]
$Mg_{0.9375}Fe_{0.0625}H_2$	10 bar, 127°C, 7.12 wt.%/25 min	1 bar, 127°C, 2.1 wt.%/50 min	our cal.
$MgH_2 - 10wt\%Ni$	20 bar, 350°C, 6.2 wt.%/2 min	Onset temperature: $\sim$ 130°C	[342]
$MgH_2 - 5.5wt\%Ni$	10 bar, 50°C, 3.9 wt.%/300 min 10 bar, 250°C, 5 wt.%/0.5 min	200 mbar, 250°C, 5.8 wt.%/21 min 200 mbar, 270°C, 5.8 wt.%/9 min	[203] [203]
$Mg_{0.9375}Ni_{0.0625}H_2$	10 bar, 127°C, 7.08 wt.%/13 min	1 bar, 127°C, 3.3 wt.%/50 min	our cal.
$MgH_2 - 5wt\%V$	1 MPa, 300°C, 6.0 wt.%/30 min	0.01 MPa, 300°C, 5.6 wt.%/40 min	[343]
$Mg_{0.9375}V_{0.0625}H_2$	10 bar, 127°C, 7.2 wt.%/28 min	1 bar, 127°C, 2.2 wt.%/50 min	our cal.
$MgH_2 - 10wt\%MnFe_2O_4$	30 atm, 200°C, 4.3 wt.%/10 min	1 atm, 320°C, 4.6 wt.%/10 min	[344]
$MgH_2 - 7mol\%\ MnFe_2O_4$		1 bar, 300°C, 5.05 wt.%/60 min	[345]
$MgH_2 - 10wt\%CeCl_3$	30 atm, 280°C, 5.6 wt.%/10 min	Onset temperature: 300°C	[346]
$MgH_2 - 20wt\%Fe_3S_4$	3 MPa, 423 K, 3.41 wt.%/20 min	0.001 MPa, 633 K, 4.01 wt.%/21 min	[347]

Table 4.2: A comparison with representative experiments related to catalysis effects on kinetic hydrogen properties of MgH_2.

We note that upon hydrogenation of magnesium a number of structural phase transitions occur [338, 339, 340], but it is not easy to simulate within the chosen approach a phenomenon that is accompanied by such phase transitions. To do it, a statistical model that combines both kinetic and phase transition is needed, which will be the subject of a future works.

However, alloying MgH_2 with small amounts of transition metals ($TM = Ti, V, Fe$ and Ni) and Al may accelerate the kinetic of absorption/desorption without reducing much its high hydrogen capacity (Table 3.3). We point out that the MgH_2 doped Ni presents the fastest ab/desorption kinetic since it exhibits the lowest energy barriers and gives better dehydrogenation thermodynamical quantities. This finding is quite similar to the experimental behavior found by Shang et *al.* [297] who showed that the kinetics of desorption varies with the type of the alloying elements and the addition of Ni shows the highest kinetics, with maximum hydrogen desorption, followed by Al, Fe, Nb, Ti and Cu, whereas both the as-received MgH_2 and the milled MgH_2, show relatively slow kinetics compared with the alloyed mixtures.

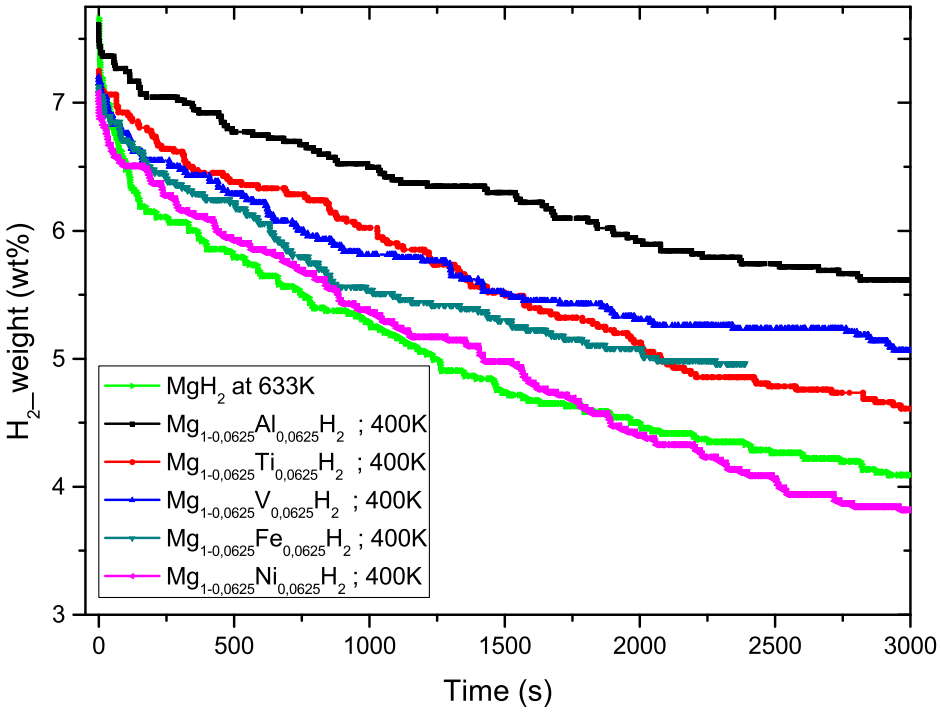

Figure 4.20: Simulation discharging kinetic for the pure MgH_2 at $633K$ and $Mg_{0.9375}M_{0.0625}H_2$ ($M = Al, Ti, V, Fe$ and Ni) at $400K$, under $1bar$.

4.3.2.4 Effect of concentration

As for the study of the effect of concentration on thermodynamic properties of MgH_2 discussed in section 3.3.4 in chapter 3, we will explore such effect on its absorption kinetic. The results of KMC simulation of tank fill times are shown in Figure 4.21.

Note that the concentration of the dopant has a good effect on reducing the absorption time of hydrogen. The acceleration of absorption for a concentration of 12.5% is slight compared to the case of doping with a concentration of 6.25%. This is due to the fact that the diffusion barriers in the case of doping with 12.5% of M are slightly lower than those of MgH_2 doped whit $x = 0.0625$ of $M = Al, Ti, V, Fe$ and Ni.

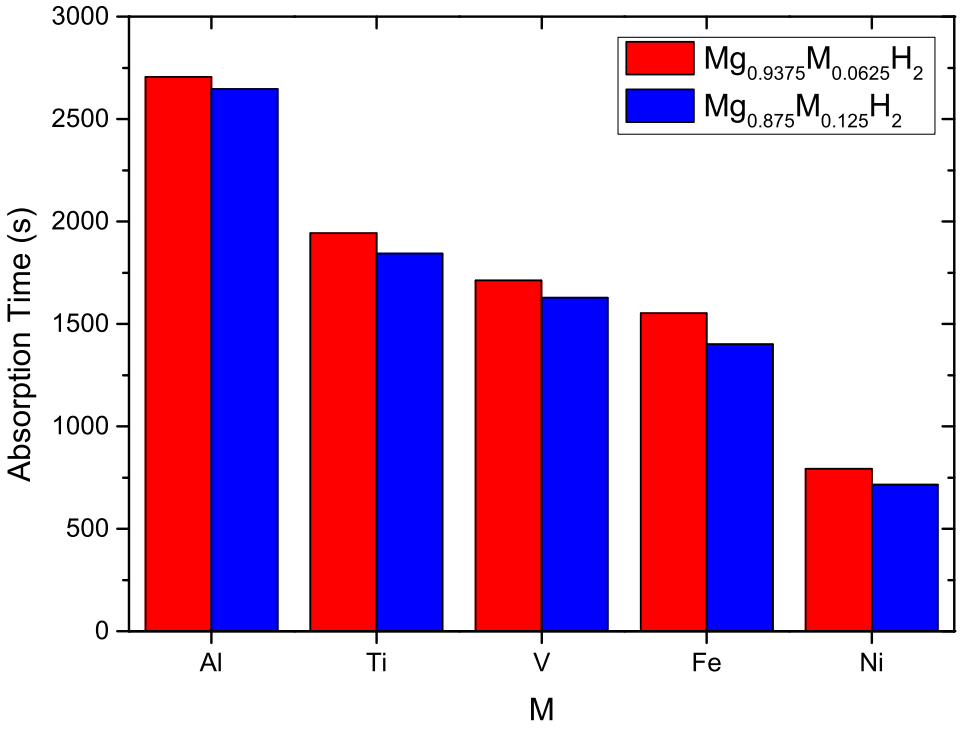

Figure 4.21: Absorption time of $Mg_{1-x}M_xH_2$ ($M = Al, Ti, V, Fe$ and Ni; $x = 0.0625$ and 0.125) at $400K$ and under $10bar$.

4.4 Conclusion

In this chapter, we have suggested a model to study the hydrogen ab/desorption kinetic properties for the pure MgH_2 and $Mg_{1-x}M_xH_2$ ($M = Al, Ti, V, Fe$ and Ni; $x =$ 6.25% and 12.5%) using Kinetic Monte Carlo (KMC) simulations.
Different process namely the absorption, desorption and diffusion have been taken into account and all corresponding activation energies have been calculated using ab-initio calculations. Incorporating all thermodynamical quantities of interest in our algorithm, we have investigated the hydrogen atom diffusion in magnesium hydride and studied the time of ab/desorption for different considered compounds. The effects of each elementary mechanism on the diffusion that we characterized through density distribution of hydrogen atoms, filling ratios, diffusion time, temperature and pressure have been studied.

We have shown, within KMC calculations, that the behavior of ab/desorption of the pur MgH_2 agree perfectly with the experimental results and the suggested material has slow kinetics at high temperature and pressure.
DFT calculations reveal that the energies corresponding to the hydrogen atom motions in the (001) plan are lower than the energies associated with the motion between two parallel (001) plans. Therefore, hydrogen atoms prefer to diffuse along X and Y directions instead of moving vertically which explain the slow kinetic of this material.

Combining the DFT method, which allows the computation of energy barriers, needed in the diffusion process, and the KMC method we have shown that the doped MgH_2 system improves considerably the thermodynamic properties and the ab/desorption kinetic of the material. The good performances exhibited in doped MgH_2 result from the fact that activation barriers for the dissociation of H_2, the barriers of diffusion and the diffusion time of H atoms in the pure MgH_2 are higher than those in MgH_2 doped with 6.25% of Al, Ti, V, Fe and Ni.
As a consequence, it can be concluded that alloying MgH_2 with small amounts of transition metals ($TM = Ti, V, Fe$ and Ni) and Al can drastically lower the stability of the systems, the decomposition temperature and accelerate the kinetic of ab/desorption without reducing much its high hydrogen capacity.
Following our study, we remark that the Ni presents the highest performances and is the most appropriate element for better hydrogen storage.

General Conclusion and Perspectives

In the present thesis, a theoretical investigation of the hydrogen storage properties of magnesium hydride (MgH_2) was presented. First-principles calculations have been used to investigate the structural properties, stability and temperature of desorption. Also, we have suggested a model to study the hydrogen storage ab/desorption kinetic properties using Kinetic Monte Carlo (KMC) simulations. The obtained results are in good agreement with the experimental ones. Furthermore, these studies show that the absorption/desorption properties of hydrogen can be improved by: (1) the addition of catalysts into the magnesium hydride, (2) application of the strain and/or (3) the nano-structuring.

As it is well known, the hydrogen storage technology was rapidly emerging as a fast alternative to fossil fuels and the storage of hydrogen in solid state compounds appears to be the most feasible solution since it is a safer and more convenient method compared to high-pressure compression and liquefaction technologies. In this regard, magnesium hydride is a potential compound for solid-state hydrogen storage due to its highly H storage capacities gravimetric as well as volumetric capacities, $7.66wt.\%$ and $110g/l.H_2$ respectively. However, it suffers from slow kinetics and a high decomposition temperature which limit its use as a material for on-board hydrogen storage systems. Several approaches have been adopted to improve its performance, among them catalysis and nano-structuring (nano-sizing) are considered as the most promising options for address these issues.

In order to give a deep insight of hydrogen storage in magnesium hydride like compounds, understand the underlying physical mechanisms and anticipate new materials that improve the hydrogen storage properties and meet the DoE criterions, we carried out a theoretical investigations of the thermodynamic properties by using ab initio calculations (DFT) and the sorption kinetic properties by developing a Kinetic Monte Carlo simulation method. Thus, we provide an examination of structural and thermodynamic properties of the pure MgH_2 by first principles. The calculation results show that MgH_2 has a high heat of formation and consequently a high stability and high desorption temperature which agree with the experimental findings in the literature. This is a good

agreement allowing the validation of our modeling approximations based on $FPLO$ using the GGA parameterizations.
By studying the electronic structure of MgH_2 we have shown that this high stability is due to the strong hybridization between magnesium and hydrogen atoms. So the addition of a small amount of $M = Al, Ti, V, Fe, Ni$, or a nano-structuring from bulk to thin films and/or by applying a strain, reduces this hybridization considerably, which improves the hydrogen storage properties of the magnesium hydride.

The investigation of the hydrogen diffusion in the pure magnesium hydride and MgH_2 doped with different metals M ($M = Al, Ti, V, Fe$ and Ni) was realized by developing, for the first time for this material, a model based on kinetic Monte Carlo method (KMC). In this numerical investigation, the activation energies calculated by DFT method for different elementary processes are implemented in our algorithm. Thus, by defining the relation between simulated time and Monte Carlo steps, we were able to simulate the hydrogen ab/desorption kinetics of the pure MgH_2 and the doped ones as function of temperature and pressure.
The obtained results show that the pure MgH_2 has slow kinetics even at high temperature, which is due on the one hand to the fact that magnesium hydride exhibits a high activation energies of H_2 molecular dissociation and slow H diffusion, on the other hand to the energy barriers of the hydrogen atom motions in the (001) plan, which are lower than those associated with the motion between two parallel plans. Therefore, hydrogen atoms prefer to diffuse along X and Y directions instead of moving vertically, which explains the slow kinetic of this material.
Furthermore, we have shown that the incorporation of small amounts of Al, Ti, V, Fe and Ni in MgH_2 system improves considerably the energy barriers needed for the dissociation of H_2 and hydrogen diffusion mechanisms and consequently leads to a great enhancement on the sorption kinetics of the material.
Following the obtained results, we may conclude that alloying MgH_2 with small amounts of transition metals ($TM = Ti, V, Fe$ and Ni) and Al can drastically lower the stability of the systems, the decomposition temperature and accelerate the kinetic of ab/desorption without reducing much its high hydrogen capacity.

Based on a combination of the first-principles calculations and kinetic Monte Carlo simulation, the different results obtained from the investigation of the thermodynamic and kinetic properties of MgH_2 hydride can be summarized in what follow:

- The pure MgH_2 has high gravimetric and volumetric storage capacities (7,660 $wt.\%$ and 109.619 $g.H_2/l$ respectively).

- The pure MgH_2 presents a high stability (-62,018 $kJ/mol.H_2$) and a high decomposition temperature (483,521 K).
- At high temperature and pressure, the results of simulations indicate that the hydride involves slow kinetics.
- The obtained behaviors are in agreement with those obtained experimentally and theoretically in other works.
- The high stability of the pure MgH_2 is due to the strong hybridization between Mg and H atoms.
- The slow kinetics of this compound result from the high activation barriers of the different elementary process that the system involves and to the fact that hydrogen atoms prefer to diffuse along X and Y directions instead of moving vertically.
- The stability, the decomposition temperature and the times of ab/desorption of hydrogen reduce considerably when doping MgH_2 with a small amount of TM ($TM = Ti, V, Fe$ and Ni) and Al.
- The addition of a small amount of $M = Al, Ti, V, Fe$ and Ni enhances the hybridization between $Mg-H$ and reduces the dissociation and diffusion activation energies, which improves the hydrogen sorption properties of the magnesium hydride.
- The nano-structuring from bulk to thin films improves considerably its thermodynamic properties. $\Delta H = -0.56eV/mol.H_2$ and $T_d = 414.75K$ for a thickness of $22nm$.
- Due to the contribution of strain energy, the stability and the decomposition temperature for strained MgH_2 thin film hydride are reduced relative to that of strain free system, which is beneficial for the improvement of the dehydrogenation properties of MgH_2.

Even though the work we present in this thesis shed light on the way thermodynamic and kinetic properties of magnesium hydride like compounds may be improve for better hydrogen storage, there are still other open questions that are put into perspective. The cycle life of tank is a relevant property for potential applications. Many experimental studies have addressed the subject but to the best of our knowledge, there are no theoretical investigation performed previously. It is therefore necessary to carry out a theoretical investigation of this property and its application in magnesium and other hydrides. We are also wondering how far the thermodynamic properties for hydrogen storage may be improved by considering nanoparticles of magnesium hydride-like.

Bibliography

[1] J.O. Abe , A.P.I. Popoola , E. Ajenifuja , O.M. Popoola. *Hydrogen energy, economy and storage: Review and recommendation.* Int J Hydrogen Energy, Available online 3 May 2019 In Press, Corrected Proof.

[2] J. Zhang , S. Yan, H. Qu. *Recent progress in magnesium hydride modified through catalysis and nanoconfinement.* Int J Hydrogen Energy 2018;43(3):1545-1565.

[3] Jose Bellosta von Colbe, Jose-Ramón Ares, Jussara Barale, Marcello Baricco, Craig Buckley, Giovanni Capurso, Noris Gallandat. *Application of hydrides in hydrogen storage and compression: Achievements, outlook and perspectives.* Int J Hydrogen Energy 2019;44(15):7780-7808.

[4] Demirbas A., *Storage and transportation opportunities of hydrogen.* Energy Sources Part B 2007;2(3):287-295.

[5] Timothy M. Ivancic, Son-Jong Hwang, Robert C. Bowman, Derek S. Birkmire, Craig M. Jensen, Terrence J. Udovic, Mark S. Conradi. *Discovery of a new Al species in hydrogen reactions of* $NaAlH_4$. The Journal of Physical Chemistry Letters 2010;1(15):2412-2416.

[6] Dalebrook AF, Gan W, Grasemann M, Moret S, Laurenczy G. *Hydrogen storage: beyond conventional methods.* Chem Commun 2013;49:8735–51.

[7] Pandey SK, Bhatnagar A, Shahi RR, Hudson M, Singh MK, Srivastava ON. *Effect of TiO2 nanoparticles on the hydrogen sorption characteristics of magnesium hydride.* J Nanosci Nanotechnol 2013;13:5493–9.

[8] Tozzini V, Pellegrini V. *Prospects for hydrogen storage in graphene.* Phys Chem Phys 2013;15:80–9.

[9] Durbin DJ, Malardier-Jugroot C. *Review of hydrogen storage techniques for on board vehicle applications.* Int J Hydrog Energy 2013;38:14595–617.

[10] Bhatnagar A, Pandey SK, Dixit V, Shukla V, Shahi RR, Shaz MA, Srivastava ON. *Catalytic effect of carbon nanostructures on the hydrogen storage properties of MgH_2–$NaAlH_4$ composite*. Int J Hydrog Energy 2014;39:14240–6.

[11] Eberle U, Felderhoff M, Schuth F. Chemical and physical solutions for hydrogen storage. Angew Chem Int Edit 2009;48:6608-30.

[12] George Crabtree, Mildred Dresselhaus, Michelle Buchanan. *The hydrogen economy*. Physics Today 2004;57(12):39-44.

[13] K.K. Gangu, S. Maddila, S.B. Mukkamala, S.B. Jonnalagadda. *Characteristics of MOF, MWCNT and graphene containing materials for hydrogen storage: A review*. Journal of Energy Chemistry 2018;000:1-13.

[14] Barthelemy H, Weber M, Barbier F. *Hydrogen storage: recent improvements and industrial perspectives*. Int J Hydrogen Energy 2017;42(11):7254-62.

[15] Brunner T, Kircher O. *Cryo-compressed hydrogen storage*. Hydrog Sci Eng Mater Process Syst Technol 2016;2:711–32.

[16] T. Sadhasivam , Hee-Tak Kim , Seunghun Jung , Sung-Hee Roh , Jeong-Hun Park , Ho-Young Junga. *Dimensional effcts of nanostructured Mg/MgH_2 for hydrogen storage applications: A review*. Renewable and Sustainable Energy Reviews 2017;72:523–534.

[17] Saba Niaz, Taniya Manzoor, Altaf Hussain Pandith. *Hydrogen storage: Materials, methods and perspectives*. Renewable and Sustainable Energy Reviews 2015;50:457–469.

[18] Rusman NAA, Dahari M. *A review on the current progress of metal hydrides material for solid-state hydrogen storage applications*. Int J Hydrogen Energy 2016;41:12108-26.

[19] Jia Y., Sun C., Shen S., Zou J., Mao S. S., and Yao X. *Combination of nanosizing and interfacial effect: future perspective for designing Mg-based nanomaterials for hydrogen storage*. Renew Sustain Energy Rev 2015;44:289-303.

[20] Zhang B, Wu Y. *Recent advances in improving performances of the lightweight complex hydrides Li-Mg-N-H system*. Prog Nat Sci: Mater Int 2017;27:21-33.

[21] Zhang F, Zhao P, Niu M, Maddy J. *The survey of key technologies in hydrogen energy storage*. Int J Hydrogen Energy 2016;41:14535-52.

[22] Grochala W. and Edwards P.P. *Thermal decomposition of the non-interstitial hydrides for the storage and production of hydrogen.* Chem Rev 2004;104:1238–1316.

[23] Jain IP, Lal C, Jain A. *Hydrogen storage in Mg: a most promising material.* Int J Hydrogen Energy 2010;35:5133–44.

[24] Shao H, Felderhoff M, Schüth F, Weidenthaler C. *Nanostructured Ti-catalyzed MgH2 for hydrogen storage.* Nanotechnology 2011;22:235401.

[25] Hanada N, Ichikawa T, Fujii H. *Catalytic effect of nanoparticle 3d-transition metals on hydrogen storage properties in magnesium hydride MgH2 prepared by mechanical milling.* J Phys Chem B 2005;109:7188–94.

[26] Agarwal S, Jain A, Jain P, Jangir M, Vyas D, Jain IP. *Effect of ZrCrCo alloy on hydrogen storage properties of Mg.* J Alloy Compd 2014;645:S518–S523.

[27] Liu G, Wang Y, Xu C, Qiu F, An C, Li L, Jiao L, Yuan H. *Excellent catalytic effects of highly crumpled graphene nanosheets on hydrogenation/dehydrogenation of magnesium hydride.* Nanoscale 2013;5:1074–81.

[28] Korablov D, Nielsen TK, Besenbacher F, Jensen TR. *Mechanism and kinetics of early transition metal hydrides, oxides, and chlorides to enhance hydrogen release and uptake properties of MgH2.* Powder Diffr 2015;30:S9–15.

[29] Barawi M, Granero C, Diaz-Chao P, Manzano CV, Martin-Gonzalez M, Jimenez-Rey D, Ferrer IJ, Ares JR, Fernández JF, Sanchez C. *Thermal decomposition of non-catalysed MgH2 films.* Int J Hydrog Energy 2014;39:9865–70.

[30] International energy agency technical report, 2013. Website: http://www.iea.org/publications/freepublications/publication/KeyWorld2013_FINAL_WEB.pdf (accessed 01.10.2013).

[31] Ibrahim Dincer, Canan Acar. *Review and evaluation of hydrogen production methods for better sustainability.* Int J Hydrogen Energy 2015;40(34):11094-11111.

[32] A. Zuttel, A. Borgschulte and L. Schlapbach (eds.). *Hydrogen as a Future Energy Carrier.* WILEY-VCH Verlag GmbH & Co. KGaA, Weinheim, GERMANY, ISBN: 978-3-527-30817-0, 2008, XIV+427 pages.

[33] Peter G. Bruce, Stefan A. Freunberger, Laurence J. Hardwick and Jean-Marie Tarascon. *Li–O_2 and Li–S batteries with high energy storage.* Nat Mater 2011;11:19–29.

[34] Trimm DL, Önsan ZI. *Onboard fuel conversion for hydrogen-fuel-cell-driven vehicles.* Catal Rev 2001;43:31–84.

[35] Singh S, Jain S, Venkateswaran PS, Tiwari AK, Nouni MR, Pandey JK, Goel S. *Hydrogen: a sustainable fuel for future of the transport sector*. Renew Sust Energy Rev 2015;51:623–33.

[36] Noris Gallandat, Krzysztof Romanowicz, Andreas Züttel. *An Analytical Model for the Electrolyser Performance Derived from Materials Parameters*. Journal of Power and Energy Engineering 2017;05:34-49.

[37] Muradov NZ, Veziroglu TN. *From hydrocarbon to hydrogen-carbon to hydrogen economy*. Int J Hydrogen Energy 2005;30:225-37.

[38] Levin DB, Chahine R. *Challenges for renewable hydrogen production from biomass. Int J Hydrogen Energy 2010;35:4962-9*.

[39] Awad AH, Veziroglu TN. *Hydrogen vs. synthetic fossil fuels*. Int J Hydrogen Energy 1984;9:355-66.

[40] Yilanci A, Dincer I, Ozturk HK. *A review on solar-hydrogen/fuel cell hybrid energy systems for stationary applications*. Prog Energy Combust Sci 2009;35:231-44.

[41] Walker G. (Ed.). *Solid state hydrogen storage materials and chemistry*. Woodhead Publishing, Cambridge 2008:3–15.

[42] Cleghorn S. J. C., Ren X., Springer T. E., Wilson M. S., Zawodzinski C., Zawodzinski T. A. and Gottes-feld, S. *PEM fuel cells for transportation and stationary power generation applications*. Int J Hydrog Energy 1997;22(12):1137–1144.

[43] Schlapbach L. and Züttel A. *Hydrogen storage materials for mobile applications*. Nature 2001;414:353–358.

[44] G. Waker (Ed.). *Solid state hydrogen storage materials and chemistry*. Woodhead Publishing, Cambridge 2008:18–47.

[45] W.R. Grove Esq. M.A. *On voltaic series and the combination of gases by platinum*. Philos Mag Ser 3 2009;14:127–130.

[46] Vipin Das, Sanjeevikumar Padmanabanb, Karthikeyan Venkitusamya, Rajasekar Selvamuthukumaranc, Frede Blaabjergd, Pierluigi Sianoe. *Recent advances and challenges of fuel cell based power system architectures and control – A review*. Renewable and Sustainable Energy Reviews 2017;73:10–18.

[47] Carrette L, Friedrich KA, Stimming U. *Fuel cells–fundamentals and applications*. Fuel Cells 2001;1(1):5–39.

[48] [19] M. A. Laughton. *Fuel cells*. Engineering Science and Education Journal 2002;11(1):7–16,.

[49] Cook Brian. *Introduction to fuel cells and hydrogen technology*. Eng Sci Educ J 2002;11(6):205–16.

[50] Prabhukhot PR,Wagh MM, Gangal AC. *A review on solid state hydrogen storage material*. Adv Energy Power 2016;4(2):11-22.

[51] Marban G, Valdes-Solis T. *Towards the hydrogen economy?*. Int J Hydrogen Energy 2007;32:1625-37.

[52] Edwards PP, Kuznetsov VL, David WI. *Hydrogen energy*. Philos Trans A Math Phys Eng Sci 2007;265(1853):1043-56.

[53] Ozturk T, Demirbas A. *Boron compounds as hydrogen storage materials*. Energy Sources Part A 2007;29(15):1415-23.

[54] Wang Y, Chen KS, Mishler J, Cho SC, Adroher XC. *A review of polymer electrolyte membrane fuel cells: technology, applications, and needs on fundamental research*. Appl Energy 2010;88:981-1007.

[55] Janot R, Latroche M, Percheron-Guegan A. *Development of a hydrogen absorbing layer in the outer shell of high pressure hydrogen tanks*. Mater Sci Eng B 2005;123:187-93.

[56] Yang-huan Zhang, Zhi-chao Jia, Ze-ming Yuan, Tai Yang, Yan Qi, Dong-liang Zhao; *Development and application of hydrogen storage*. J Iron Steel Res Int 2015;22(9):757-70.

[57] Sakintuna B, Lamari-Darkrim F, Hirscher M. *Metal hydride materials for solid hydrogen storage: a review*. Int J Hydrogen Energy 2007;32:1121-40.

[58] Mazzolai G. *Perspectives and challenges for solid state hydrogen storage in automotive applications*. Recent Pat Mater Sci 2012;5:1-12.

[59] T.Q. Hua, R.K. Ahluwalia, J.-K. Peng, M. Kromer, S. Lasher, K. McKenney, K. Law, J. Sinha. *Technical assessment of compressed hydrogen storage tank systems for automotive applications*. Int J Hydrogen Energy 2011;36:3037-49.

[60] Andreas Zuttel. *Materials for hydrogen storage*. Mater Today 2003;6(9):24-33.

[61] Sheriff SA, Yogi GD, Stefanakos E, Steinfield A. *Handbook of hydrogen energy*. Boca Raton, FL:CRC Press/Taylor & Francis Group, 2014.

[62] Abdalla M. Abdalla, Shahzad Hossain, Ozzan B. Nisfindy, Atia T. Azad, Mohamed Dawoodb , Abul K. Azada. *Hydrogen production, storage, transportation and key challenges with applications: A review.* Energy Conversion and Management 2018;165:602–627.

[63] Pesonen O, Alakunnas T. *Energy storage: a missing piece of the puzzle for the self-sufficient living.* Lapland: Lapland University of Applied Sciences; 2017. UAS publication series B: research reports and compilations URN:ISBN:978-952-316-186-3.

[64] von Helmolt R, Eberle U. *Fuel cell vehicles: status 2007.* J Power Sources 2007;165(2):833–43.

[65] Conte M, Iacobazzi A, Ronchetti M, Vellone R. *Hydrogen economy for a sustainable development: state-of-the-art and technological perspectives.* J Power Sources 2001;100:171–87.

[66] Godula-Jopek Agata (ed.). *Hydrogen production: by electrolysis.* John Wiley & Sons, 29 jui. 2015, 424 pages

[67] Jorgensen SW. *Hydrogen storage tanks for vehicles: Recent progress and current status.* Current Opinion in Solid State and Materials Science 2011;15(2):39-43.

[68] Midilli A, Ay M, Dincer I, Rosen M. *Hydrogen and hydrogen energy strategies I: current status and needs.* Renew Sustain Energy Rev 2005;9:255-71.

[69] Webb CJ. *A review of catalyst-enhanced magnesium hydride as a hydrogen storage material.* J Phys Chem Solids 2015;84:96-106.

[70] Jongh PE, Adelhelm P. *Nanosizing and nanoconfinement: new strategies towards meeting hydrogen storage goals.* Chem Sus Chem 2010;3:1332-48.

[71] Dorin Schitea, Muhammet Deveci, Mihaela Iordache, Kursad Bilgili, Ibrahim Zeki Akyurt, Ioan Iordache. *Hydrogen mobility roll-up site selection using intuitionistic fuzzy sets based WASPAS, COPRAS and EDAS.* Int J Hydrogen Energy 2019;44:8585-600.

[72] Mazloomi K, Gomes D. *Hydrogen as an energy carrier: prospects and challenges.* Renew Sustain Energy Rev 2012;16:3024-33.

[73] David E. *An overview of advanced materials for hydrogen storage.* J Mater Process Technol 2005;162-163:169-77.

[74] K. Edalati, R. Uehiro, Y. Ikeda, H.-W. Li, H. Emami, Y. Filinchuk, M. Arita, X. Sauvage, I. Tanaka, E. Akiba, Z. Horita. *Design and synthesis of a magnesium alloy for room temperature hydrogen storage*. Acta Mater 2018;149:88-96.

[75] Hwang HT, Varma A. *Hydrogen storage for fuel cell vehicles*. Curr Opin Chem Eng 2014;5:42-8.

[76] Ozarslan A. *Large-scale hydrogen energy storage in salt caverns*. Int J Hydrogen Energy 2012;37:14265-77.

[77] Zhang Y, Li J, Zhang T, Wu T, Kou H, Xue X. *Hydrogenation thermokinetics and activation behavior of non-stoichiometric Zr-based Laves alloys with enhanced hydrogen storage capacity*. J Alloy Comp 2017;694:300-8.

[78] Sleiman S, Huot J. *Microstructure and hydrogen storage properties of* $Ti_1V_{0.9}Cr_{1.1}$ *alloy with addition of x wt % Zr (x= 0, 2, 4, 8, and 12)*. Inorganics 2017;5(86):1-12.

[79] Mandal T. K., Gregory D. H. *Hydrogen: A future energy vector for sustainable development*. Proceedings of the Institution of Mechanical Engineers, Part C: Journal of Mechanical Engineering Science 2010;224(3):539-558.

[80] Eftekhari A, Fang B. *Electrochemical hydrogen storage: opportunities for fuel storage, batteries, fuel cells, and supercapacitors*. Int J Hydrogen Energy 2017;42:25143-65.

[81] Mazzolai G. *Perspectives and challenges for solid state hydrogen storage in automotive applications*. Recent Pat Mater Sci 2012;5:1-12.

[82] Chamoun R, Demirci UB, Miele P. *Cyclic dehydrogenatione(Re)hydrogenation with hydrogen-storage materials: an overview*. Energy Technol 2015;3:100-17.

[83] Lai H, Paskevicius M, Sheppard DA, Buckley CE, Thornton AW, Hill MR, Aguey-Zinsou K. *Hydrogen storage materials for mobile and stationary applications: current state of the art*. Chem Sus Chem 2015;8:2789-825.

[84] J. Zhu, L. Dai, Y. Yu, J. Cao, L. Wang. *A direct electrochemical route from oxides to TiMn2 hydrogen storage alloy*. Chinese J Chem Eng 2015;23:1865–1870.

[85] W. Chen, Y. Zhu, C. Yang, J. Zhang, M. Li, L. Li. *Significantly improved electrochemical hydrogen storage properties of magnesium nickel hydride modified with nano-nickel*. J. Power Sources 2015;280:132–140.

[86] Darkrim FL, Malbrunot P, Tartaglia GP. *Review of hydrogen storage by adsorption in carbon nanotubes*. Int J Hydrogen Energy 2002;27:193–202.

[87] Dillon AC, Jones KM, Bekkedahl TA, Kiang CH, Bethune DS, Heben MJ. *Storage of hydrogen in single-walled carbon nanotubes*. Nature 1997;386:377–9.

[88] A. Lueking, R.T. Yang. *Hydrogen spillover from a metal oxide catalyst onto carbon nanotubes implications for hydrogen storage*. J Catal 2002;206:165–168.

[89] A. Reyhani, S.Z. Mortazavi, A.Z. Moshfegh, A.N. Golikand, M. Amiri. *Enhanced electrochemical hydrogen storage by catalytic Fe-doped multi-walled carbon nanotubes synthesized by thermal chemical vapor deposition*. J. Power Sources 2009;188:404–410.

[90] R. Ravindra, B.R. Bhat. *Hydrogen Storage in Palladium Decorated Carbon Nanotubes Prepared by Solventless Method*. Int J Appl Phy Math 2012;2:63–66.

[91] Chen P, Wu X, Lin J, Tan KL. *High H2 uptake by alkali-doped carbon nanotubes under ambient pressure and moderate temperatures*. Science 1999;285:91–3.

[92] Rosi, N. L., Eckert, J., Eddaoudi,M., Vodak, D. T., Kim, J., O'Keeffe, M., and Yaghi, O. M. *Hydrogen storage in microporous metal-organic frameworks*. Science 2003;300:1127–1129.

[93] K.K. Gangu, S. Maddila, S.B. Mukkamala, S.B. Jonnalagadda. *A review on contemporary Metal–Organic Framework materials*. Inorg Chim Acta 2016;446:61–74.

[94] K.K. Gangu, S. Maddila, S.B. Jonnalagadda. *A review on synthesis, crystal structure and functionality of naphthalenedicarboxylate ligated metal-organic frameworks*. Inorg Chim Acta 2017;466:308–323.

[95] K.K. Gangu, S. Maddila, S.B. Mukkamala, S.B. Jonnalagadda. *Synthesis, characterisation and catalytic activity of 4, 5-imidazoledicarboxylate ligated Co (II) and Cd (II) metal-organic coordination complexes*. J Mol Struct 2017;1143:153–162.

[96] Wong-Foy A. G., Matzger A. J., andYaghi O.M. *Exceptional H_2 saturation uptake in microporous metal organic frameworks*. J Am Chem Soc 2006;128:3494–3495.

[97] Lin X., Jia J., Zhao X., Thomas K. M., Blake A. J., Walker G. S., Champness N. R., Hubberstey P. and Schröder M. *High H_2 adsorption by coordination-framework materials*. Angew Chem Int Ed 2006;45:7358–7364.

[98] Lee J. Y., Pan L., Kelly S. P., Jagiello J., Emge T. J. and Li J. *Achieving high density of adsorbed hydrogen inmicroporousmetal organic frameworks*. Adv Mater 2005;17:2703–2706.

[99] Henrietta W. Langmi, Jianwei Ren, Brian North, Mkhulu Mathe, Dmitri Bessarabov. *Hydrogen Storage in Metal-Organic Frameworks: A Review* Electrochimica Acta 2014;128:368–392.

[100] Côté A. P., Benin A. I., Ockwig N. W., O'Keeffe M., Matzger A. J. and Yaghi O. M. *Porous, crystalline, covalent organic frameworks*. Science 2005;310:1166–1170.

[101] Tilford R.W., Gemmil W. R.,zur Loye H. and Lavigne J. L. *Facile synthesis of a highly crystalline, covalently linked porous boronate network*. Chem Mater 2006;18:5296–5301.

[102] Côté A.P., El-Kaderi H.M., Furukawa H., Hunt J.R. and Yaghi O.M. *Reticular synthesis ofmicroporous and mesoporous 2D covalent organic frameworks*. J Am Chem Soc 2007;129:12914–12915.

[103] El-Kaderi H.M., Hunt J.R., Mendoza-Cortés J.L., Côté A.P., Taylor R.E., O'Keeffe M. and Yaghi O.M. *Designed synthesis of 3D covalent organic frameworks*. Science 2007;316:268–272.

[104] Han S.S., Furukawa H., Yaghi O.M. and Goddard W. A. *Covalent organic frameworks as exceptional hydrogen storage materials*. J Am Chem Soc 2008;130:11580–11581.

[105] Kaye S.S., Dailly A., Yaghi O.M. and Long J.R. *Impact of preparation and handling on the hydrogen storage properties of ZnO(1,4-benzenedicarboxylate) (MOF-5)*. J Am Chem Soc 2007;129:14176–14177.

[106] Li J, Cheng S, Zhao Q, Long P, Dong J. *Synthesis and hydrogen-storage behavior of metal–organic framework MOF-5*. Int J Hydrogen Energy 2009;34(3):1377–82.

[107] Xia L, Liu Q, Wang F, Lu J. *Improving the hydrogen storage properties of metal-organic framework by functionalization*. J Mol Model 2016;22(10):254.

[108] Bobbitt NS, Chen J, Snurr RQ. *High-throughput screening of metal-organic frameworks for hydrogen storage at cryogenic temperature*. J Phys Chem C 2016;120(48)27328-27341.

[109] Ozturk Z, Ali D, Sibel Z, Ozkan G. *Novel 2D micro-porous metal-organic framework for hydrogen storage*. Int J Hydrogen Energy 2016;41(28):12167-12174.

[110] Railey P, Song Y, Liu T, Li Y. *Metal organic frameworks with immobilized nanoparticles: Synthesis and applications in photocatalytic hydrogen generation and energy storage*. Mater Res Bull 2017;96:385–94.

[111] Rahali S, Belhocine Y, Seydou M. *Multiscale study of the structure and hydrogen storage capacity of an aluminum metal-organic framework.* Int J Hydrogen Energy 2017;42(22):15271-15282.

[112] M. Latroche, S. Surblé, C. Serre, C. Mellot-Draznieks, P.L. Llewellyn, J.-Lee, Chang J., Jhung S.H. and Férey G. *Hydrogen storage in the giant-pore metal-organic frameworks MIL-100 and MIL-101.* Angewandte Chemie International Edition 2006;45:8227-8231.

[113] J.Y. Lee, H. Wu, L. Jing. *An investigation of structural and hydrogen adsorption properties of microporous metal organic framework (MMOF) materials.* Int J Hydrogen Energy 2012;37:10473–10478.

[114] D. Denysenko, M. Grzywa, M. Tonigold, B. Streppel, I. Krkljus, M. Hirscher, Mugnaioli E., Kolb U., Hanss J. and Volkmer D. *Elucidating gating effects for hydrogen sorption in MFU-4-type triazolate-based metal-organic frameworks featuring different pore sizes.* Chem Eur J 2011;17:1837–1848.

[115] K. Lin, A.K. Adhikari, C. Ku, C. Chiang, H. Kuo. *Synthesis and characterization of porous HKUST-1 metal organic frameworks for hydrogen storage.* Int J Hydrogen Energy 2012;37:13865–13871.

[116] S.K. Bhatia, A.L. Myers. *Optimum Conditions for adsorptive storage.* Langmuir 2006;22:1688–1700.

[117] Lin X., Jia J., Hubberstey P., Schröder M. and Champness N.R. *Hydrogen storage in metal-organic frameworks.* Cryst Engng Commun 2007;9:438–448.

[118] Collins D.J and Zhou H.C. *Hydrogen storage in metal-organic frameworks.* J Mater Chem 2007;17:3154–3160.

[119] Sahaym U, Norton MG. *Advances in the application of nanotechnology in enabling a hydrogen economy.* J Mater Sci 2008;43:5395-429.

[120] Shan X, Payer JH, Jennings WD. *Mechanism of increased performance and durability of Pd-treated metal hydriding alloys.* Int J Hydrogen Energy 2009;34:363-9.

[121] Crivello JC, Denys RV, Dornheim M, Felderhoff M, Grant DM, Huot J, Yartys VA. *Mg-based compounds for hydrogen and energy storage.* Appl Phys A 2016;122(85):1-17.

[122] Blackburn JL, Parilla PA, Gennett T, Hurst KE, Dillon AC, Heben MJ. *Measurement of the reversible hydrogen storage capacity of milligram Ti-6Al-4V alloy*

samples with temperature programmed desorption and volumetric techniques. J Alloy Comp 2008;454(2008):483-90.

[123] Lim KL, Kazemain H, Yaakob Z, Daud WRW. *Solid-state materials and methods for hydrogen storage: a critical review.* Chem Eng Technol 2010;33(2):213-26.

[124] Lopez-Suarez A. *Influence of surface roughness on consecutively hydrogen absorption cycles in Ti-6Al-4V.* Int J Hydrogen Energy 2010;35:10404-11.

[125] Khafidz NZ, Zahira Y, Lim KL, Timmiati SN. *The kinetics of lightweight solid-state hydrogen storage materials: a review.* Int J Hydrogen Energy 2016;41:13131-51.

[126] Jain IP. *Hydrogen the fuel for 21st century.* Int J Hydrogen Energy 2009;34:7368-78.

[127] Ronnebro EC, Majzoub EH. *Recent advances in metal hydrides for clean energy applications.* Mater Res Soc 2013;38:452-8.

[128] Bullock RM. *Metal-hydrogen bond cleavage reactions of transition metal hydrides: hydrogen atom, hydride, and proton transfer reactions.* A J Crit Discussion Curr Lit 2006;12(1):1-33.

[129] Zaluski L, Zaluska A, Strom-Olsen JO. *Nanocrystalline metal hydrides.* J Alloy Comp 1997;253(254):70-9.

[130] Paskevicius M, Sheppard DA, Williamson K, Buckley CE. *Metal hydride thermal heat storage prototype for concentrating solar thermal power.* Energy 2015;88:469-77.

[131] Demirbas A. *Fuel properties of hydrogen, liquefied petroleum gas (LPG), and compressed natural gas (CNG) for transportation.* Energy Sources 2002;24:601-10.

[132] Jain RK, Jain A, Agarwal S, Lalla NP, Ganesan V, Phase DM, Jain IP. *Hydrogenation behaviour of Ce-based AB5 intermetallic compounds.* J Alloys Compd 2007;440(1-2):84-8.

[133] Jain IP, Lal C, Jain A. *Hydrogen storage in Mg: a most promising material.* Int J Hydrogen Energy 2010;35(10):5133-44.

[134] Ma L-J, Jia J, Wu H-S, Ren Y. *Ti-η2-(C2H2) and HCC-TiH as high capacity hydrogen storage media.* Int J Hydrogen Energy 2013;38(36):16185-92.

[135] N.A.A. Rusman, M. Dahari. *A review on the current progress of metal hydrides material for solid-state hydrogen storage applications.* Int J Hydrogen Energy 2016;41(28):Pages 12108-12126.

[136] Wu Z, Yang F, Bao Z, Nyamsi SN, Zhang Z. *Improvement in hydrogen storage characteristics of Mg-based metal hydrides by doping nonmetals with high electronegativity: a first-principle study.* Comput Mater Sci 2013;78(0):83-90.

[137] Varin RA, Czujko T, Wronski Z. *Particle size, grain size and $\gamma - MgH_2$ effects on the desorption properties of nanocrystalline commercial magnesium hydride processed by controlled mechanical milling.* Nanotechnology 2006;17(15):3856.

[138] Gasiorowski A, Iwasieczko W, Skoryna D, Drulis H, Jurczyk M. *Hydriding properties of nanocrystalline Mg2-xMxNi alloys synthesized by mechanical alloying (M=Mn, Al).* J Alloys Compd 2004;364(1-2):283-8.

[139] Falahati H, Barz DPJ. *Evaluation of hydrogen sorption models for AB5-type metal alloys by employing a gravimetric technique.* Int J Hydrogen Energy 2013;38(21):8838-51.

[140] Palewski T, Tristan NV, Drulis H, Cwik J. *Hydrogenation process of the Gd3M(M=Ni or Co) intermetallics compound.* J Alloys Compd 2005;404-406(0):584-7.

[141] Pan H, Liu Y, Gao M, Zhu Y, Lei Y. *The structural and electrochemical properties of La0.7Mg0.3(Ni0.85Co0.15)x (x=3.0-5.0) hydrogen storage alloys.* Int J Hydrogen Energy 2003;28(11):1219-28.

[142] Okada M, Kuriiwa T, Kamegawa A, Takamura H. *Role of intermetallics in hydrogen storage materials.* Mater Sci Eng A 2002;329-331(0):305-12.

[143] Wang L, Young K, Nei J, Pawlik D, Ng KYS. *Hydrogenation of AB5 and AB2 metal hydride alloys studied by in situ X-ray diffraction.* J Alloys Compd 2014;616(0):300-5.

[144] Jain RK, Jain A, Jain IP. *Effect of La-content on the hydrogenation properties of the Ce1-xLaxNi3Cr2 (x=0.2, 0.4, 0.6, 0.8, 1) alloys.* Int J Hydrogen Energy 2012;37(4):3683-8.

[145] Leng H, Ichikawa T, Fujii H. *Hydrogen storage properties of Li-Mg-N-H systems with different ratios of LiH/Mg(NH2)2.* J Phys Chem B 2006;110(26):12964-8.

[146] Srinivasan S, Escobar D, Goswami Y, Stefanakos E. *Effects of catalysts doping on the thermal decomposition behavior of Zn(BH4)2.* Int J Hydrogen Energy 2008;33(9):2268-72.

[147] Orimo S., Nakamori Y., Eliseo J.R., Züttel A. and Jensen C.M. *Complex hydrides for hydrogen storage*. Chem Rev 2007;107:4111–4132.

[148] Zuttel A, Wenger P, Rentsch S, Sudan P, Mauron P, Emmenegger C. *LiBH4 a new hydrogen storage material*. J Power Sources 2003;118(1-2):1-7.

[149] Ley MB, Jepsen LH, Lee Y-S, Cho YW, Bellosta von Colbe JM, Dornheim M, et al. *Complex hydrides for hydrogen storage - new perspectives*. Mater Today 2014;17(3):122-8.

[150] Huang ZG, Guo ZP, Calka A, Wexler D, Lukey C, Liu HK. *Effects of iron oxide (Fe2O3,Fe3O4) on hydrogen storage properties of Mg-based composites*. J Alloys Compd 2006;422(1-2):299-304.

[151] Albanese E, Kalantzopoulos GN, Vitillo JG, Pinatel E, Civalleri B, Deledda S, et al. *Theoretical and experimental study on Mg(BH4)2-Zn(BH4)2 mixed borohydrides*. J Alloys Compd 2013;580(Supplement 1(0)):S282-6.

[152] Smythe NC, Gordon JC. *Ammonia borane as a hydrogen carrier: dehydrogenation and regeneration*. Eur J Inorg Chem 2010;2010(4):509-21.

[153] Hwang HT, Al-Kukhun A, Varma A. *Hydrogen for vehicle applications from hydrothermolysis of ammonia borane: hydrogen yield, thermal characteristics, and ammonia formation*. Ind Eng Chem Res 2010;49(21):10994-1000.

[154] Yang J, Sudik A, Wolverton C, Siegel DJ. *High capacity hydrogen storage materials: attributes for automotive applications and techniques for materials discovery*. Chem Soc Rev 2010;39(2):656-75.

[155] Kang X-D, Luo J-H, Wang P.*Efficient and highly rapid hydrogen release from ball-milled 3NH3BH3/MMgH3 (M = Na, K, Rb) mixtures at low temperatures*. Int J Hydrogen Energy 2012;37(5):4259-66.

[156] Lee TB, McKee ML. *Mechanistic study of LiNH2BH3 formation from (LiH)4+NH3BH3 and subsequent dehydrogenation*. Inorg Chem 2009;48(16):7564-75.

[157] Wang K, Zhang J-G, He P. *Theoretical study on the structure and dehydrogenation mechanism of mixed metal amidoborane, NaLi(NH2BH3)2*. J Alloys Compd 2013;581(0):59-65.

[158] Wang P, Kang X-d. *Hydrogen-rich boron-containing materials for hydrogen storage*. Dalton Trans 2008;(40):5400-13.

[159] Zaluska A, Zaluski L, Ström-Olsen JO. *Nanocrystalline magnesium for hydrogen storage*. J Alloys Compd 1999;288(1–2):217–25.

[160] Barkhordarian G, Klassen T, Bormann RU. *Effect of Nb2O5 content on hydrogen reaction kinetics of Mg*. J Alloys Compd 2004;364(1–2):242–6.

[161] Hallenbeck PC, Abo-Hashesh M, Ghosh D. *Strategies for improving biological hydrogen production*. Bioresour Technol 2012;110:1–9.

[162] Reports of US DOE - The Fuel Cell Technologies Office (FCTO) - http://energy.gov/eere/fuelcells/materials-based-hydrogen-storage

[163] Saita I, Li L, Saito K, Akiyama T. *Hydriding combustion synthesis of Mg2NiH4*. J Alloy Compd 2003;356:490–3.

[164] Pang Y, Liu Y, Zhang X, Gao M, Pan H. *TiF4-doped Mg(AlH4)2 with significantly improved dehydrogenation properties*. Int J Hydrog Energy 2013;38:13343–51.

[165] Mao J, Guo Z, Yu X, Liu H, Wu Z, Ni J. *Enhanced hydrogen sorption properties of Ni and Co-catalyzed MgH2*. Int J Hydrog Energy 2010;35:4569–75.

[166] Ma T, Isobe S, Wang Y, Hashimoto N, Ohnuki S. *Nb-gateway for hydrogen desorption in Nb2O5 catalyzed MgH2 nanocomposite*. J Phys Chem C 2013;117:10302–7.

[167] Wang Y, Wu SW, Yu H, Gong NN, Cao ZQ, Zhang K. *Hydrogen desorption/absorption kinetics of MgH2 catalyzed with TiO2*. Adv Mat Res 2014;986:88–91.

[168] Isobe S, Umeda A, Wakasugi T, Ma T, Yamagami R, Hino S, Wang Y, Hashimoto N, Ohnuki S. *Microscopic study on hydrogenation mechanism of MgH2 catalyzed by Nb2O5*. Mater Trans 2014;55:1175–8.

[169] Singh RK, Sadhasivam T, Sheeja GI, Singh P, Srivastava ON. *Effect of different sized CeO2 nano particles on decomposition and hydrogen absorption kinetics of magnesium hydride*. Int J Hydrog Energy 2013;38:6221–5.

[170] Yu XB, Guo YH, Yang H, Wu Z, Grant DM, Walker GS. *Improved hydrogen storage in magnesium hydride catalyzed by nanosized Ti0.4Cr0.15Mn0.15V0.3 alloy*. J Phys Chem C 2009;113:5324–8.

[171] Pitt MP, Paskevicius M, Webb CJ, Sheppard DA, Buckley CE, Gray EM. *The synthesis of nanoscopic Ti based alloys and their effects on the MgH2 system compared with the MgH2+0.01Nb2O5 benchmark*. Int J Hydrog Energy 2012;37:4227–37.

[172] Shahi RR, Bhatanagar A, Pandey SK, Shukla V, Yadav TP, Shaz MA, Srivastava ON. *MgH2–ZrFe2Hx nanocomposites for improved hydrogen storage characteristics of MgH2.* Int J Hydrog Energy 2015;40:11506–13.

[173] Ismail M, Juahir N, Mustafa NS. *Improved hydrogen storage properties of MgH2 co-doped with FeCl3 and carbon nanotubes.* J Phys Chem C 2014;118:18878–83.

[174] Chaise A, Rango PD, Marty P, Fruchart D, Miraglia S, Olives R, Garrier S. *Enhancement of hydrogen sorption in magnesium hydride using expanded natural graphite.* Int J Hydrog Energy 2009;34:8589–96.

[175] Singh RK, Raghubanshi H, Pandey SK, Srivastava ON. *Effect of admixing different carbon structural variants on the decomposition and hydrogen sorption kinetics of magnesium hydride.* Int J Hydrogen Energy 2010;35:4131–7.

[176] Niaz NA, Hussain ST, Nasir S, Ahmad I. *Improved hydrogen desorption kinetics of MgH2 nanoparticles by using TiC nanocatalyst.* Key Eng Mater 2012;510:371–7.

[177] Liu G, Wang Y, Jiao L, Yuan H. *Solid-state synthesis of amorphous TiB2 nanoparticles on graphene nanosheets with enhanced catalytic dehydrogenation of MgH2.* Int J Hydrog Energy 2014;39:3822–9.

[178] Li X, Qin Y, Fu J, Zhao J. *A Gupta potential for magnesium in hcp phase.* Comp Mater Sci 2015;98:328–32.

[179] . P. Vajeeston, P. Ravindran, B.C. Hauback, H. Fjellvag, A. Kjekshus, S. Furuseth, M. Hanfland. *Structural stability and pressure-induced phase transitions in MgH2.* Phys Rev B 2006;73(22):224102.

[180] J.C. Crivello, B. Dam, R.V. Denys, M. Dornheim, D.M. Grant, J. Huot, T.R. Jensen, P. Jongh, M. Latroche, C. Milanese, D. Milcius, G.S. Walker, C.J. Webb, C. Zlotea, V.A. Yartys. *Review of magnesium hydride-based materials: development and optimisation.* Appl Phys A 2016;122:97.

[181] M. Dornheim, T. Klassen. *High Temperature Hydrides.* Encyclopedia of Electrochemical Power Sources, Elsevier, Amsterdam 2009:459–472.

[182] Liu T, Wang C, Wu Y. *Mg-based nanocomposites with improved hydrogen storage performances.* Int J Hydrogen Energy 2014;39(26):14262-74.

[183] Yermakov AY, Mushnikov NV, Uimin MA, Gaviko VS, Tankeev AP, Skripov AV, et al. *Hydrogen reaction kinetics of Mg-based alloys synthesized by mechanical milling.* J Alloys Compd 2006;425(1-2):367-72.

[184] Prigent J, Gupta M. *Ab initio study of the hydrogenation properties of Mg-based binary and ternary compounds Mg2X(X = Ni, Si) and YMgNi4.* J Alloys Compd 2007;446-447(0):90-5.

[185] Ouyang LZ, Cao ZJ, Yao L, Wang H, Liu JW, Zhu M. *Comparative investigation on the hydrogenation/dehydrogenation characteristics and hydrogen storage properties of Mg3Ag and Mg3Y.* Int J Hydrogen Energy 2014;39(25):13616-21.

[186] He G, Jiao L-F, Yuan H-T, Zhang Y-Y, Wang Y-J. *Preparation and electrochemical properties of MgNieMB (M =Co, Ti) composite alloys.* J Alloys Compd 2008;450(1-2):375-9.

[187] Holtz RL. *Basic user's guide for NRL 6323 hydrogen storage system.* Naval Research Laboratory: Washingon, DC, 1996.

[188] Friedlmeier G, Groll M. *Experimental analysis and modeling of the hydriding kinetics of Ni-doped and pure Mg.* J Alloys Compds 1997;253–254:550–5.

[189] Andreasen A, Vegge T, Pedersen AS. *Compensation effect in the hydrogenation/dehydrogenation kinetics of metal hydrides.* J Phys Chem B 2005;109:3340–4.

[190] Guoxian L, Erde W, Shoushi F. *Hydrogen absorption and desorption characteristics of mechanically milled Mg–35wt% FeTi1.2 powders.* J Alloys Compds 1995;223:111–4.

[191] Huot J, Liang G, Boily S, Neste AV, Schulz R. *Structural study and hydrogen sorption kinetics of ball-milled magnesium hydride.* J Alloys Compds 1999;293–295:495–500.

[192] Billur Sakintuna, Farida Lamari-Darkrim , Michael Hirscher. *Metal hydridematerials for solid hydrogen storage: A review.* Int J Hydrogen Energy 2007;32:1121-1140.

[193] Zaluski L, Zaluska A, Tessier P, Ström-Olsen JO, Schulz R. *Catalyti effect of Pd on hydrogen absorption in mechanically alloyed Mg2Ni LaNi5 and FeTi.* J Alloys Compds 1995;217:295–300.

[194] Zaluski L, Zaluska A, Ström-Olsen JO. *Hydrogen absorption in nanocrystalline Mg2Ni formed by mechanical alloying.* J Alloys Compds 1995;217:245–9.

[195] Baer R, Zeiri Y, Kosloff R. *Hydrogen transport in nickel (1 1 1).* Phys Rev B 1997;55(16):952–74.

[196] Bloch J, Mintz MH. *Kinetics and mechanisms of metal hydride formation - a review.* J Alloys Compds 1997;253–254:529–41.

[197] Holtz RL, Imam MA. *Hydrogen storage characteristics of ball milled magnesium–nickel and magnesium–iron alloys.* J Mater Sci 1999;34:2655–63.

[198] Gennari FC, Castra FJ, Urretavizcaya G, Meyer G. Catalytic effect of Ge on hydrogen desorption from MgH2. J Alloys Compds 2002;334:277–84.

[199] Liang G, Huot J, Boily S, Neste AV, Schulz R. *Hydrogen storage properties of the mechanically milled MgH2–V nanocomposite.* J Alloys Compds 1999;291:295–9.

[200] Iwakura C, Nohara S, Zhang SG, Inoue H. *Hydriding and dehydriding characteristics of an amorphous Mg2Ni–Ni composite.* J Alloys Compds 1999;285:246–9.

[201] Liang G, Huot J, Boily S, Neste AV, Schulz R. *Hydrogen storage properties of nanocrystalline Mg1.9Ti0.1Ni made by mechanical alloying.* J Alloys Compds 1999;282:286–90.

[202] Chen H, Yu H, Zhang Q, Liu B, Liu P, Zhou X, et al. *Enhancement in dehydrating performance of magnesium hydride by iron incorporation: a combined experimental and theoretical investigation.* J Power Sources 2016;322:179-86.

[203] El-Eskandarany MS, Shaban E, Ali N, Aldakheel F, Alkandary A. *In-situ catalyzation approach for enhancing the hydrogenation/dehydrogenation kinetics of MgH2 powders with Ni particles.* Sci Rep 2016;6:37335.

[204] Chen J, Xia G, Guo Z, Huang Z, Liu H, Yu X. *Porous Ni nanofibers with enhanced catalytic effect on the hydrogen storage performance of MgH2.* J Mater Chem A 2015;3(31):15843-8.

[205] Jung KS, Lee EY, Lee KS. *Catalytic effects of metal oxide on hydrogen absorption of magnesium metal hydride.* J Alloys Compds 2005;421(1–2):179–84.

[206] Song MY, Bobet J-L, Darriet B. *Improvement in hydrogen sorption properties of Mg by reactive mechanical grinding with Cr2O3,Al2O3 and CeO2.* J Alloys Compds 2002;340:256–62.

[207] Dehouche Z, Klassen T, Oelerich W, Goyette J, Bose TK, Schulz R. *Cycling and thermal stability of nanostructured MgH2–Cr2O3 composite for hydrogen storage.* J Alloys Compds 2002;347:319–23.

[208] Chen BH, Chuang YS. *Improving the hydrogenation properties of MgH2 at room temperature by doping with nano-size ZrO2 catalyst.* J Alloys Compd 2016;655:21-7.

[209] Chen P, Zhu M. *Recent progress in hydrogen storage.* Mater Today 2008;11(12):36-43.

[210] Yu X, Tang Z, Sun D, Ouyang L, Zhu M. *Recent advances and remaining challenges of nanostructured materials for hydrogen storage applications*. Prog Mater Sci 2017;88:1-48.

[211] Zhao-Kargera Z, Witter R, Bardajı EG, Wang D, Cossement D, Fichtner M. *Influence of nanoconfinement on reaction pathways of complex metal hydrides*. Energy Procedia 2012;29:731-7.

[212] H Shao, G Xin, J Zheng, X Li, E Akiba. *Nanotechnology in Mg-based materials for hydrogenstorage*. Nano Energy 2012;1:590-601.

[213] Sadhasivam T, Hudson MSL, Pandey SK, Bhatnagar A, Singh MK, Gurunathan K, Srivastava ON. *Effects of nano size mischmetal and its oxide on improving the hydrogen sorption behaviour of MgH2*. Int J Hydrogen Energy 2013;38:7353–62.

[214] Hanada N, Ichikawa T, Hino S, Fujii H. *Remarkable improvement of hydrogen sorption kinetics in magnesium catalyzed with Nb2O5*. J Alloy Compd 2006;420:46–9.

[215] Lu H-B, Poh C-K, Zhang LC, Guo ZP, Yu XB, Liu HK. *Dehydrogenation characteristics of Ti-and Ni/Ti-catalyzed Mg hydrides*. J Alloy Compd 2009;481:152–5.

[216] Pighin SA, Capurso G, Russo SL, Peretti HA. *Hydrogen sorption kinetics of magnesium hydride enhanced by the addition of Zr8Ni21 alloy*. J Alloy Compd 2012;530:111–5.

[217] Polanski M, Bystrzycki J, Plocinski T. *The effect of milling conditions on microstructure and hydrogen absorption/desorption properties of magnesium hydride (MgH2) without and with Cr2O3 nanoparticles*. Int J Hydrog Energy 2008;33:1859–67.

[218] Tian M, Shang C. *Nano-structured MgH2 catalyzed by TiC nanoparticles for hydrogen storage*. J Chem Technol Biotechnol 2011;86:69–74.

[219] Pourabdoli M, Raygan S, Abdizadeh H, Uner D. *Determination of kinetic parameters and hydrogen desorption characteristics of MgH2-10wt%(9Ni–2Mg–Y) nanocomposite*. Int J Hydrog Energy 2013;38:11910–9.

[220] Borsa DM, Gremaud R, Baldi A, Schreuders H, Rector JH, Kooi B, Vermeulen P, Notten PHL, Dam B, Griessen R. *Structural, optical, and electrical properties of MgyTi1-yHx thin films*. Phys Rev B 2007;75:205408.

[221] Singh S, Eijt SWH, Zandbergen MW, Legerstee WJ, Svetchnikov VL. *Nanoscale structure and the hydrogenation of Pd-capped magnesium thin films prepared by plasma sputter and pulsed laser deposition*. J Alloy Compd 2007;441:344–51.

[222] Tan Z, Chiu C, Heilweil EJ, Bendersky LA. *Thermodynamics, kinetics and microstructural evolution during hydrogenation of iron-doped magnesium thin films.* Int J Hydrog Energy 2011;36:9702–13.

[223] Dura JA, Kelly ST, Kienzle PA, Her J-H, Udovic TJ, Majkrzak CF, Chung C-J, Clemens BM. *Porous Mg formation upon dehydrogenation of MgH2 thin films.* J Appl Phys 2011;109:093501.

[224] Jain IP. *Hydrogen the fuel for 21st century.* Int J Hydrog Energy 2009;34:7368–78.

[225] R. K. Pathria. *Statistical Mechanics, second edition.* Butterworth-Heinemann, 1996.

[226] D. A. McQuarrie. *Statistical Thermodynamics.* University Science Books, 1973.

[227] D. de Fontaine. *Solid State Physics.* Edited by H. Ehrenreich, Academic Press, NY, 1994, p.33.

[228] A. Van der Ven, M. K. Aydinol, G. Ceder, G. Kresse, J. Hafner. *First-principles investigation of phase stability in LixCoO2.* Phys Rev B 1998;58:2975.

[229] A. Van de Walle, G. Ceder. *Automating first-principles phase diagram calculations.* J. Phase Equilibria 2002;23:348.

[230] C. Wolverton, V. Ozolins, A. Zunger. *First-principles theory of short-range order in size-mismatched metal alloys: Cu-Au, Cu-Ag, and Ni-Au.* Phys Rev B 1998;57:4332.

[231] M. E. Arroyo y de Dompablo, A. Van der Ven, and G. Ceder. *First-principles calculations of lithium ordering and phase stability on LixNiO2.* Phys Rev B 2002;66:064112.

[232] V. Ozolins, C. Wolverton, and A. Zunger. *Cu-Au, Ag-Au, Cu-Ag, and Ni-Au intermetallics: First-principles study of temperature-composition phase diagrams and structures.* Phys. Rev. B 1998;57:6427.

[233] A. Seko, K. Yuge, F. Oba, A. Kuwabara, I. Tanaka, and T. Yamamoto. *First-principles study of cation disordering in MgAl2O4 spinel with cluster expansion and Monte Carlo simulation.* Phys Rev B 2006;73:094116.

[234] A. Van der Ven and G. Cedar. *First-principles calculation of the electronic structure and EELS spectra at the graphene/Ni(111) interface.* Phys Rev B 2005;71:054102.

[235] H. R. Tang, A. Van der Ven, and B. L. Trout. Phys Rev B 2004;70:045420.

[236] M. Born and J.R. Oppenheimer. *Zur Quantentheorie der Molekeln.* Ann der Physik 1927;389:457-484.

[237] D. R. Hartree. *The Wave Mechanics of an Atom with a Non-Coulomb Central Field. Part I. Theory and Methods* Proc. Cambridge Phil. Soc. 1928;24(1):89.

[238] V. Fock. *Näherungsmethode zur Lösung des quantenmechanischen Mehrkörperproblems*. Z. Physik 1930;61:126-148.

[239] J.C. Slater. *The Theory of Complex Spectra*. Phys Rev 1929;34:1293.

[240] C.D. Sherrill and H.F. Schaefer III. *The Configuration Interaction Method: Advances in Highly Correlated Approaches*. Advances in quantum chemistry 1999;34:143-269.

[241] H. Kümmel. *Origins of the Coupled Cluster Method*. Theoretica chimica acta 1991;80(2-3):81–89.

[242] Chr. Møller and M. S. Plesset. *Note on an Approximation Treatment for Many-Electron Systems*. Phys Rev 1934;46:618.

[243] J.A. Pople, M. Head-Gordon, K. Raghavachari. *Quadratic configuration interaction. A general technique for determining electron correlation energies*. J Chem Phys 1987;87:5968.

[244] C. Angeli1, R. Cimiraglia, S. Evangelisti, T. Leininger, J.-P. Malrieu. *Introduction of n-electron valence states for multireference perturbation theory*. J Chem Phys 2001;114:10252.

[245] C. Trindle and D. Shillady. *Electronic Structure Modeling: Connections Between Theory and Software*. NW: CRC Press, 2008.

[246] L.H. Thomas. *The calculation of atomic fields*. Mathematical Proceedings of the Cambridge Philosophical Society 1927;23:542.

[247] E. Ferm. *Un metodo statistico per la determinazione di alcune priorietà dell'atome*. Rend Accad Naz Lincei 1927;6:602.

[248] P.A.M. Dirac. *Note on Exchange Phenomena in the Thomas Atom*. Proc Cambridge Phil Roy Soc 1930;26:376.

[249] C.F. von Weizsacker. *Zur Theorie der Kernmassen*.Z Phys 1935;96:431.

[250] E. Wigner, Trans. *Effects of the electron interaction on the energy levels of electrons in metals*. Faraday Soc 1938;34:67.

[251] R.P. Feynman, N. Metropolis, and E. Teller. *Equations of State of Elements Based on the Generalized Fermi-Thomas Theory*. Phys Rev 1949;75:1561.

[252] P. Hohenberg and W. Kohn. *Inhomogeneous Electron Gas*. Phys Rev 1964;136:B864.

[253] N.C. Handy. *Lecture Notes in Quantum Chemistry II*. European Summer School in Quantum Chemistry, Editors: Roos, Björn O.(Ed.) 1994.

[254] N. D. Mermin. *Thermal Properties of the Inhomogeneous Electron Gas*. Phys Rev 1965;137:A1441.

[255] W. Kohn and L. J. Sham. *Self-Consistent Equations Including Exchange and Correlation Effects*. Phys. Rev 1965;140:A1133.

[256] J.P. Perdew. *Density functional theory and the band gap problem*. Int J Quantum Chem 1985;28:497.

[257] J.P. Perdew and K. Burke. *Comparison shopping for a gradient-corrected density functional*. Int J Quant Chem 1996;57:309.

[258] F. Herman, J. P. Van Dyke, and I. P. Ortenburger. *Improved Statistical Exchange Approximation for Inhomogeneous Many-Electron Systems*. Phys Rev Lett 1969;22:807.

[259] P.S. Svendsen and U. von Barth. *Gradient expansion of the exchange energy from second-order density response theory*. Phys Rev B 1996;54:17402.

[260] J.P. Perdew and Y. Wang. *Accurate and simple analytic representation of the electron-gas correlation energy*. Phys Rev B 1992;45:13244.

[261] J.P. Perdew, K. Burke, and M. Ernzerhof. *Generalized Gradient Approximation Made Simple*. Phys Rev Lett 1996;77:3865.

[262] H.J. Monkhorst and J. D. Pack. *Special points for Brillouin-zone integrations*. Phys Rev B 1976;13:5188.

[263] H. Hellmann. *Einfuhrung in die Quantumchemie*. Leipzig : Franz Deuticke, 1937.

[264] R.P. Feynman. *Forces in Molecules*. Phys Rev 1939;56:340.

[265] K. Koepernik et H. Eschrig. *Full-potential nonorthogonal local-orbital minimum-basis band-structure scheme*. Phys Rev B 1999;59(3):1743-1757.

[266] *FPLO Homepage*, http://www.fplo.de/.

[267] H. Eschrig. *Optimized LCAO Method and the Electronic Structure of Extended Systems*. Springer-Verlag Berlin Heidelberg, 1989.

[268] Frenkel, D. and Smit, B. *Understanding Molecular Simulation: From Algorithms to Application* Computational Science Series 2001 (book).

[269] P. Boyle. *Options: A monte carlo approach.* Journal of Financial Economics 1977;4(3):323-338.

[270] I. Lymperopoulos and J. Lygeros. *Sequential monte carlo methods for multi-aircraft trajectory prediction in air traffic management.* Int J Adaptive Control and Signal Processing 2010;24(10): pp. 830-849.

[271] A. Kim, A. Rosen, V. Brander, and T. Buchanan. *Selective muscle activation following electrical stimulation of the collateral ligaments of the human knee joint.* Archives of Physical Medicine and Rehabilitation 1995;76(8):750-757.

[272] Q. Dong, X. Wang, L. Su, and Q. Liu. *Modeling on growth of pseudomonas aeruginosa with diferent inoculum sizes.* Nongye Jixie Xuebao/Transactions of the Chinese Society for Agricultural Machinery 2015;46(12):246-252.

[273] E. Standish and A. Fienga. *Accuracy limit of modern ephemerides imposed by the uncertainties in asteroid masses.* Astronomy and Astrophysics 2002;384(1)322-328.

[274] M. Enciso, C. Schutte, and L. Delle Site. *Influence of ph and sequence in peptide aggregation via molecular simulation.* Journal of Chemical Physics 2015;143(24).

[275] D.P. Kroese, T. Brereton, T. Taimre, and Z. I. Botev. *Why the monte carlo method is so important today* Wiley Interdisciplinary Reviews: Computational Statistics 2014;6(6):386-392.

[276] N. Metropolis, A. W. Rosenbluth, M. N. Rosenbluth, A. H. Teller, and E. Teller. *Equation of state calculations by fast computing machines.* The Journal of Chemical Physics 1953;21(6):1087-1092.

[277] W.K. Hastings. *Monte carlo sampling methods using markov chains and their applications.* Biometrika 1970;57(1):97-109.

[278] Landau D., Binder K. *A guide to Monte Carlo simulations in statistical physics (2nd ed.).* Cambridge; New York: Cambridge University Press 2005.

[279] R. Durrett. *Essentials of Stochastic Processes.* New York, Heidelberg, Dordrecht, London: Springer, 2012.

[280] R. Durrett. *Probability: theory and examples.* Cambridge series in statistical and probabilistic mathematics, Cambridge; New York : Cambridge University Press, 2010.

[281] K.P. Murphy. *Machine learning: a probabilistic perspective*. Adaptive computation and machine learning series, Cambridge, MA: MIT Press, 1 edition cop. 2012.

[282] N. Metropolis and S. Ulam. *The Monte Carlo Method*. Journal of the American Statistical Association 1949;44:335.

[283] Andersen M, Panosetti C and Reuter K. *A Practical Guide to Surface Kinetic Monte Carlo Simulations*. Front Chem 2019;7:202.

[284] A.F. Voter. *Introduction to the kinetic monte carlo method*. In: Sickafus K.E., Kotomin E.A., Uberuaga B.P. (eds) Radiation Effects in Solids. NATO Science Series, vol 235. Springer, Dordrecht 2007.

[285] F.M. Bulnes, V. D. Pereyra, and J. L. Riccardo. *Collective surface diffusion: n-fold way kinetic Monte Carlo simulation*. Phys Rev E 1998;58:86.

[286] G.H. Vineyard. *Frequency factors and isotope effects in solid-state rate processes*. J Phys Chem Solids 1957;3:121.

[287] M. Kotrla, J. Krug, and P. Smilauer. *Submonolayer growth with decorated island edges*. Surface Science 2000;454-456:681-685.

[288] Y. Li, X. Chen, and J. Su. *Study on formation of step bunching on 6h-sic (0001) surface by kinetic monte carlo method*. Applied Surface Science 2016;371:242-247.

[289] P. Stout. *Modeling surface kinetics and morphology during 3c, 2h, 4h, and 6h-sic (111) step-flow growth*. Journal of Vacuum Science and Technology A: Vacuum, Surfaces and Films 1998;16(6):3314-3327.

[290] L. Zhou. *Progress and problems in hydrogen storage methods*. Renewable and Sustainable Energy Reviews 2005;9(4):395-408.

[291] M.Y. Song, S.N. Kwon, H.R. Park, et S.H. Hong. *Improvement in the hydrogen storage properties of Mg by mechanical grinding with Ni, Fe and V under H2 atmosphere*. Int J Hydrogen Energy 2011;36(21):13587-13594.

[292] M. Cabo, S. Garroni, E. Pellicer, C. Milanese, A. Girella, A. Marini, E. Rossinyol, S. Suriñach, et M. D. Baró. *Hydrogen sorption performance of MgH2 doped with mesoporous nickel- and cobalt-based oxides*. Int J Hydrogen Energy 2011;36(9):5400-5410.

[293] S. Kurko, L. Matović, N. Novaković, B. Matović, Z. Jovanović, B. P. Mamula, et J. Grbović Novaković. *Changes of hydrogen storage properties of MgH2 induced by boron ion irradiation*. Int J Hydrogen Energy 2011;36(1):1184-1189.

[294] H. Gasan, O.N. Celik, N. Aydinbeyli, et Y.M. Yaman. *Effect of V, Nb, Ti and graphite additions on the hydrogen desorption temperature of magnesium hydride.* Int J Hydrogen Energy 2012;37(2):1912-1918.

[295] G. Barkhordarian, T. Klassen, et R. Bormann. *Catalytic Mechanism of Transition-Metal Compounds on Mg Hydrogen Sorption Reaction.* J Phys Chem B 2006;110(22):11020-11024.

[296] D. Zhou, P. Peng, et J. Liu. *First-principles calculation of dehydrogenating properties of MgH2-V systems.* Science in China Series E 2006;49(2);129-136.

[297] C.X. Shang, M. Bououdina, Y. Song, and Z.X. Guo. *Mechanical alloying and electronic simulations of (MgH2+ M) systems (M= Al, Ti, Fe, Ni, Cu and Nb) for hydrogen storage.* Int J Hydrogen Energy 2004;29(1):73-80.

[298] M. Bhihi, M. Lkham et al. *First Principle Calculations for improving Desorption Temperature in $Mg_{16}H_{32}$ Doped with Ca, Sr and Ba Elements.* Bulletin of Materials Science 2014;37(7):1731-1736.

[299] N. Novaković, J. Grbović Novaković, L. Matović, M. Manasijević, I. Radisavljević, B. Paskaš Mamula and N. Ivanović. *Ab initio calculations of MgH2, MgH2:Ti and MgH2:Co compounds.* Int J Hydrogen Energy 2010;35(2):598-608.

[300] Xiao X.B, Zhang W.B, Yu W.Y, Wang N and Tang B.Y. *Energetics and electronic properties of Mg7TMH16 (TM=Sc, Ti, V, Y, Zr, Nb): An ab initio study.* Physica B 2009;404:2234.

[301] Gremaud R, Broedersz C.P, Borsa D.M, Schreuders H, Rector J.H, B Dam B and Griessen R. *Hydrogenography: An Optical Combinatorial Method To Find New Light-Weight Hydrogen-Storage Materials.* Adv. Mater. 2007;19:2813.

[302] Araujo C.M and Ahuja R. *Electronic and optical properties of pressure induced phases of MgH2.* J Alloys Comp 2005;404:220.

[303] Hou Z.F. *First-principles investigation of Mg(AlH4)2 complex hydride.* Journal of Power Sources 2006;159:111.

[304] Bouhadda Y, Rabehi A and Bezzari-Tahar-Chaouche S. *First-principle calculation of MgH2 and LiH for hydrogen storage.* Revue des Energies Renouvelables 2007;10:545.

[305] Alapati S.V, Johnson J.K and Sholl D.S. *First principles screening of destabilized metal hydrides for high capacity H2 storage using scandium.* J. Alloys Comp 2007;446-447:23.

[306] Velikokhatnyi O.I. and Kumta P.N. *Energetics of the lithium-magnesium imide–magnesium amide and lithium hydride reaction for hydrogen storage: An ab initio study*. Materials Science and Engineering B 2007;140:114.

[307] M. Bortz, B. Bertheville, G. Böttger, et K. Yvon. *Structure of the high pressure phase $\gamma - MgH2$ by neutron powder diffraction*. Journal of Alloys and Compounds, 1999;287(1-2):L4-L6.

[308] M. Bhihi, M. Lakhal, H. Labrim, A. Benyoussef, A. El kenz, O. Mounkachi et E. K. Hlil. *Prediction of hydrogen storage in Mg1-xMxH2 (M= Ti, V, Fe, $0 \leq x \leq 0.1$) by first principle calculations*. Chinese Physics B 2012;21(9):097501.

[309] H. Nakamura, D. Nguyen-Manh, et D. G. Pettifor. *Electronic structure and energetics of LaNi5, $\alpha - La2Ni10H$ and $\beta - La2Ni10H14$*. Journal of Alloys and Compounds 1998;281(2):81-91.

[310] Kittel C. *Introduction to Solid State Physics*. New York: Wiley, 1986.

[311] Pozzo M, Alfe D. *Structural properties and enthalpy of formation of magnesium hydride from quantum Monte Carlo calculations*. Phys Rev B 2008;77:104103.

[312] Yamagychi M, Akiba E. In: Cahn RW, Haasen P, Kramer EJ, editors. *Materials science and technology*. vol. 3B. New York: VCH; 1994, p.333.

[313] Togo A, Tanaka I. *First principles phonon calculations in materials science*. Scr Mater 2015;108:1–5.

[314] Yu R, Lam P.K. *Electronic and structural properties of MgH2*. Phys Rev B 1988;37:8730.

[315] R.Westerwaal,C.Broedersz, R.Gremaud, M.Slaman, A.Borgschulte, W.Lohstroh, K.Tschersich, H. Fleischhauer, B. Dam, R. Griessen. *Study of the hydride forming process of in-situ grown MgH2 thin films by activated reactive evaporation*. Thin Solid Films 2008;516:4351.

[316] Department of Energy. *Technical System Targets: Onboard Hydrogen Storage*. US DRIVE, Washington, 2014.

[317] Klebanoff L.E, Keller J.O. *5 Years of hydrogen storage research in the U.S. DOE Metal Hydride Center of Excellence (MHCoE)*. Int J Hydrogen Energy 2013;38:4533.

[318] Baldi A, Palmisano V, Gonzalez-Silveira M, Pivak Y, Slaman M, Schreuders H, Dam B, Griessen R. *Quasifree Mg–H thin films*. Appl Phys Lett 2009;95:071903.

[319] Mooij LPA, Baldi A, Boelsma C, Shen K, Wagemaker M, Pivak Y, Schreuders H, Griessen R, Dam B. *Interface Energy Controlled Thermodynamics of Nanoscale Metal Hydrides*. Adv Energy Mater 2011;1:754-8.

[320] Tao S.X, Notten P.H.L, van Santen R.A, Jasen A.P. *Dehydrogenation properties of epitaxial (1 0 0) MgH2/TiH2 multilayers – A DFT study*. J Comput Mater Sci 2011;50:2960-6.

[321] Yoshimura K, Yamada Y, Okada M. *Hydrogenation of Pd capped Mg thin films at room temperature*. Surf. Sci. 2004;566–568:751–752.

[322] Oguchi H, Tan Z, Heilweil E.J, Bendersky L.A. *In-situ infrared imaging methodology for measuring heterogeneous growth process of a hydride phase*. Int J Hydrogen Energy 2010;35:1296-99.

[323] Ye S.Y, Chan S.L.I, Ouyang L.Z, Zhu M. *Hydrogen storage and structure variation in Mg/Pd multi-layer film*. J Alloys Compd 2010;504:493-7.

[324] Pereira V.M, Castro Neto A.H. *Strain Engineering of Graphene's Electronic Structure*. Phys Rev Lett 2009;103:046801-4.

[325] Mandal Taraknath. *Strain induced phase transition in CdSe nanowires: Effect of size and temperature*. Appl Phys Lett 2012;101:021906-9.

[326] Hao S.Q, Sholl D.S. *Effect of TiH2–Induced Strain on Thermodynamics of Hydrogen Release from MgH2*. J Phys Chem C 2012;116:2045-50.

[327] Lu J, Choi Y.J, Fang Z.Z, Sohn H.Y, Ronnebro E. *Hydrogen Storage Properties of Nanosized MgH2-0.1TiH2 Prepared by Ultrahigh-Energy-High-Pressure Milling*. J Am Chem Soc 2009;131:15843-52.

[328] Ham B, Junkaew A, Arroyave R, Park J, Zhou H-C, Foley D, Rios S, Wang H, Zhang X. *Size and stress dependent hydrogen desorption in metastable Mg hydride films*. Int J Hydrogen Energy 2014;39:2597-2607.

[329] Krozer A, Kasemo B. *Hydrogen uptake by Pd-coated Mg: absorptione decomposition isotherms and uptake kinetics*. J Less-Common Met 1990;160(2):323-342.

[330] Zhang J, Zhou Y.C, Ma Z.S, Sun L.Q, Peng P. *Strain effect on structural and dehydrogenation properties of MgH2 hydride from first-principles calculations*. Int J Hydrogen Energy 2013;38:3661-6.

[331] Tang J.L, Zhu J, Qin W.F, Xiong J, Li Y.R. *Structure and dielectric characteristics of epitaxially strained BaTiO3 thin films.* J Mater Sci Mater Electron 2008;19:466-70.

[332] Benzidi H, Lakhal M, Benyoussef A, Hamedoun M, Loulidi M, Mounkachi O. *First principle study of strain effect on structural and dehydrogenation properties of complex hydride LiBH4.* Int J Hydrogen Energy 2017;42:19481-86.

[333] Kratzer P. *Monte Carlo and kinetic Monte Carlo methods.* ArXiv:0904.2556; 2009.

[334] Broom D.P. *Hydrogen Storage Materials: The Characterisation of Their Storage Properties.* Publisher: Springer-Verlag London, eBook ISBN:978-0-85729-221-6; 2011.

[335] Vegge T. *Locating the rate-limiting step for the interaction of hydrogen with Mg(0001) using density-functional theory calculations and rate theory.* Phys Rev B 2004;70:035412.

[336] Du A.J, Smith S.C, Yao X.D and Lu G.Q. *First-Principle Study of Adsorption of Hydrogen on Ti-Doped Mg(0001) Surface.* J. Phys. Chem B 2006;110:21747.

[337] Patah A, Takasaki A, Szmyd J S. *Influence of multiple oxide (Cr2O3/Nb2O5) addition on the sorption kinetics of MgH2.* Int J Hydrogen Energy 2009;34:3032-303.

[338] Rango P, Chaise A, Charbonnier J, Fruchart D, Jehan M, Marty Ph, et al. *Nanostructured magnesium hydride for pilot tank development.* J Alloy Comp 2007;445-447:52.

[339] Klyukin K, Shelyapina MG, Fruchart D. *Hydrogen induced phase transition in magnesium: An Ab initio study.* J Alloy Comp 2013;580:S10.

[340] Tan XH, Wang L, Holt CMB, Zahiri B, Eikerling MH, Mitlin D. *Body centered cubic magnesium niobium hydride with facile room temperature absorption and four weight percent reversible capacity.* Phys Chem Chem Phys 2012;14:10904.

[341] Wang H, Lin HJ, Cai WT, Ouyang LZ, Zhu M. *Tuning kinetics and thermodynamics of hydrogen storage in light metal element based systems-a review of recent progress.* J Alloys Compd 2016;658:280-300.

[342] Yu H, Bennici S, Auroux A. *Hydrogen storage and release: kinetic and thermodynamic studies of MgH2 activated by transition metal nanoparticles.* Int J Hydrogen Energy 2014;39(22):11633-41.

[343] Barkhordarian G, Klassen T, Bormann R. *Effect of Nb2O5 content on hydrogen reaction kinetics of Mg.* J Alloys Compd 2004;364(1):242-6.

[344] Idris NH, Mustafa NS, Ismail M. *MnFe2O4 nanopowder synthesised via a simple hydrothermal method for promoting hydrogen sorption from MgH2.* Int J Hydrogen Energy 2017;42(33):21114-20.

[345] Ping Li, Qi Wan, Ziliang Li, Fuqiang Zhai, Yunlong Li, Liqun Cui, Xuanhui Qu, Alex A. Volinsky. *MgH_2 dehydrogenation properties improved by $MnFe_2O_4$ nanoparticles.* J Power Sources 2013;239: 201-206.

[346] Ismail M, Mustafa NS, Juahir N, Yap FAH. Catalytic effect of CeCl3 on the hydrogen storage properties of MgH2. Mater Chem Phys 2016;170:77-82.

[347] Zhang W, Cheng Y, Han D, Han S. *The hydrogen storage properties of MgH2-Fe3S4 composites.* Energy 2015;93:625-30.

Appendix A

List of publications

1. G Tiouitchi, **M Lakhal**, M Abdelaoui, M Loulidi, E Salmani, M Hamedoun, A Benyoussef, A Kara, A El Kenz, H Ez-Zahraouy and O Mounkachi1. *Stability, Electronic Structure and thermodynamic properties of MgH_2 thin films: A first-principle study.* **International Journal of Hydrogen Energy** 2019, submitted.

2. M Garara, H Benzidi, **M Lakhal**, M Loulidi, H Ez-Zahraouy, A El Kenz, M Hamedoun, A Benyoussef, A Kara and O Mounkachi1. *Phosphorene: A promising candidate for H_2 storage at room temperature.* **International Journal of Hydrogen Energy** 2019, submitted.

3. H Benzidi, **M Lakhal**, M Abdellaoui, M Garara, A Benyoussef, M Loulidi, M Hamedoun, O Mounkachi. *Improved thermodynamic properties of doped $LiBH_4$ for hydrogen storage: First-principal calculation.* **International Journal of Hydrogen Energy** 2019, accepted.

4. M El Khatabi, M Bhihi, **M Lakhal**, M Abdellaoui, A Benyoussef, A El Kenz, M Loulidi. *Enhanced hydrogen sorption kinetics of co-doped MgH_2 hydrides.* **Computational Materials Science** 2018;152:192-195.

5. A Al-Shami, **M Lakhal**, M Hamedoun, A El Kenz, A Benyoussef, M Loulidi, A Ennaoui, O Mounkachi. *Tuning the optical and electrical properties of orthorhombic hybrid perovskite $CH_3NH_3PbI_3$ by first-principles simulations: Strain-engineering.* **Solar Energy Materials and Solar Cells** 2018;180:266-270.

6. A Sibari, A Marjaoui, **M Lakhal**, Z Kerrami, A Kara, M Benaissa, A Ennaoui, M Hamedoun, A Benyoussef, O Mounkachi. *Phosphorene as a promising anode material for $(Li/Na/Mg)$-ion batteries: a first-principle study.* **Solar Energy Materials and Solar Cells** 2018;180:253-257.

7. M Abdellaoui, **M Lakhal**, H Benzidi, O Mounkachi, A Benyoussef, A El Kenz, M Loulidi. *The hydrogen storage properties of Mg-intermetallic-hydrides by ab initio calculations and kinetic Monte Carlo simulations.* **International Journal of Hydrogen Energy** 2018, in press.

8. H Benzidi, M Garara, **M Lakhal**, M Abdalaoui, A Benyoussef, M Louilidi, M Hamedoun, O Mounkachi. *Vibrational and thermodynamic properties of $LiBH_4$ polymorphs from first-principles calculations.* **International Journal of Hydrogen Energy** 2018;43(13):6625-6631

9. H Benzidi, **M Lakhal**, A Benyoussef, M Hamedoun, M Loulidi, O Mounkachi. *First principle study of strain effect on structural and dehydrogenation properties of complex hydride $LiBH_4$.* **International Journal of Hydrogen Energy** 2017;42(30):19481-19486.

10. M Abdellaoui, **M Lakhal**, M Bhihi, M El Khatabi, A Benyoussef, A El Kenz, M Loulidi. *First principle study of hydrogen storage in doubly substituted Mg based hydrides Mg_5MH_{12} ($M = B, Li$) and Mg_4BLiH_{12}.* **International Journal of Hydrogen Energy** 2016;41(45):20908-20913.

11. H Benzidi, O Mounkachi, **M Lakhal**, A Benyoussef, A El Kenz. *Compression effect on electronic properties and hydrogen desroption of $LiBH_4$: First principal study.* **Renewable and Sustainable Energy Conference** (IRSEC), 2016:568-570.

12. Z Kerrami, A Sibari, **M Lakhal**, A Benyoussef, M Benaissa, O Mounkachi, , M. Hamedoun. *Effect of biaxial strain on SnO_2 bandgap: First-principles calculations.* **Renewable and Sustainable Energy Conference** (IRSEC), 2016:853-856.

13. A Sibari, Z Kerrami, A Marjaoui, **M Lakhal**, A Benyoussef, M Benaissa, O Mounkachi, A Kara. *Phosphorene as a promising anode material for lithium-ion batteries: A first-principle study.* **Renewable and Sustainable Energy Conference** (IRSEC), 2016:931-934.

14. O Mounkachi, E Salmani, **M Lakhal**, H Ez-Zahraouy, M Hamedoun, M Benaissa, A Kara, A Ennaoui, A Benyoussef. *Band-gap engineering of SnO_2.* **Solar Energy Materials and Solar Cells** 2016;148,34-38.

15. M Bhihi, M El Khatabi, **M Lakhal**, S Naji, H Labrim, A Benyoussef, A El Kenz, M Loulidi. *First principle study of hydrogen storage in doubly substituted Mg based hydrides.* **International Journal of Hydrogen Energy** 2015;40(26):8356-8361.

16. **M Lakhal**, M Bhihi, A Benyoussef, A El Kenz, M Loulidi, S Naji. *The hydrogen ab/desorption kinetic properties of doped magnesium hydrid MgH_2 systems by first principles calculations and kinetic Monte Carlo simulations.* **International Journal of Hydrogen Energy** 2015;40(18):6137-6144.

17. **M Lakhal**, M Bhihi, S Naji, O Mounkachi, A Benyoussef, M Loulidi, A El Kenz. *Half-metallic Ferromagnetism in TM-doped MgH_2 hydride.* **Applied Physics A** 2015;119(4):1587-1593.

18. B Khalil, S Naji, A Benyoussef, H Labrim, M Bhihi, **M Lakhal**, A Belhaj, A El Kenz. *Effects of Oxygen Vacancy Defect on Magnetic Properties of $(Ca, Mn)O$ Doped System.* **Moroccan Journal of Condensed Matter** 2015;17(2).

19. M Bhihi, **M Lakhal**, S Naji, H Labrim, A Belhaj, A Benyoussef, A El Kenz, M Loulidi, B Khalil, O Mounkachi, M Abdellaoui, EK Hlil. *First Principle Calculations for improving Desorption Temperature in $Mg_{16}H_{32}$ Doped with Ca, Sr and Ba Elements.* **Bulletin of Materials Science** 2014;37(7):1731-1736.

20. S Naji, B Khalil, H Labrim, M Bhihi, A Belhaj, A Benyoussef, **M Lakhal**, A El Kenz. *Interdistance Effects on Flat and Buckled Silicene Like-bilayers.* **Journal of Physics: Conference Series**, 2014;491(1):012006.

21. B Khalil, S Naji, H Labrim, M Bhihi, AG El Hachimi, **M Lakhal**, A Belhaj, A Benyoussef, A El Kenz. *Magnetic Properties of SrO Doped with 3d Transition Metals.* **Journal of superconductivity and novel magnetism** 2014;27(1):203-208.

22. **M Lakhal**, M Bhihi, H Labrim, A Benyoussef, S Naji, A Belhaj, B Khalil, M Abdellaoui, O Mounkachi, M Loulidi. *Kinetic Monte Carlo and density functional study of hydrogen diffusion in magnesium hydride MgH_2.* **International Journal of Hydrogen Energy** 2013;38(20):8350-8356.

23. M Bhihi, **M Lakhal**, H Labrim, A Benyoussef, A El Kenz, O Mounkachi, EK Hlil. *Hydrogen storage of $Mg1-xM_xH_2$ $(M = Ti, V, Fe)$ studied using first-principles calculations.* **Chinese Physics B** 2012;21(9):097501

24. O Mounkachi, **M Lakhal**, H Labrim, M Hamedoun, A Benyoussef, A El Kenz, M Loulidi, M Bhihi. *Magnetic Properties of $Zn_{0.9}(Mn_{0.05}Ni_{0.05})O$ Nanoparticule: Experimental and Theoretical Investigation.* **Journal of Magnetism and Magnetic Materials** 2012;324(12):1945-1947.

Appendix B

List of conferences and workshops

1. 1st International Materials Science and Engineering for Green Energy Conference, Ifrane, Morocco, May 10-12, 2017,
   Oral: Ultra-thin MgH_2 layer, a promising new nano-material for hydrogen storage.

2. 3rd Euro-Mediterranean Conference on Materials and Renewable Energies, Marrakech, Morroco, November 2-6, 2015,
   Poster: The hydrogen ab/desorption kinetic properties of doped magnesium hydride systems by first principles calculations and kinetic Monte Carlo simulation.

3. 3rd Euro-Mediterranean Conference on Materials and Renewable Energies, Satellite Workshops, Rabat, Morocco, October 9-11, 2015,
   Local Organizing Committee.

4. 7th African Laser Center Annual Workshop and 3rd Moroccan Days on Nanoscience and Nanotechnology, Rabat, Morocco, 3-5 November, 2014,
   Poster: Electronic and thermodynamic properties of MgH_2 and MgH_2 doped from first principles and kinetic Monte Carlo.

5. 1er Séminaire sous le thème: Le stockage d'hydrogène et méthodes de calcul de la structure électronique et les properties magnétiques, Rabat, Maroc, 22-26 septembre 2014.

6. 12th International Conference on Condensed Matter and Statistical Physics (ICCMPS), Errachidia, Morocco, October 30-November 01, 2013,
   Oral: Kinetic Monte Carlo and Density Functional study of hydrogen diffusion in Magnesium Hydride MgH_2

7. Euro-Mediterranean Conference on Materials and Renewable Energies; From Nanoscience to Renewable Energies and to biology, Istres, France, June 10-14, 2013,

Poster: Electronic and thermodynamic properties of MgH_2 from first principles and kinetic Monte Carlo

8. US-MORROCO Workshop on Nano-Materials and Renewable Energies, Al Akhawayn University in Ifrane, Morocco, November 17-19, 2011,
   Poster1 : Prediction of Hydrogen Storage in $Mg_{1-x}M_xH_2$ ($M = Ti, V, Fe$, $0 \leq x \leq 0.1$) by First Principle Calculations.
   Poster2 : Magnetic Properties of $Zn_{0.9}(Mn_{0.05}Ni_{0.05})O$ Nano-particule: Experimental and Theoretical Investigation.

9. 11th International Conference on Condensed Matter and Statistical Physics, Agadir, Morocco, October 19-21, 2011,
   Poster: Stability Study of Doped MgH_2 Hydride with Defects by ab-initio Calculations.

Appendix C

Published papers on hydrogen storage

ARTICLE IN PRESS

INTERNATIONAL JOURNAL OF HYDROGEN ENERGY XXX (XXXX) XXX

Available online at www.sciencedirect.com

ScienceDirect

journal homepage: www.elsevier.com/locate/he

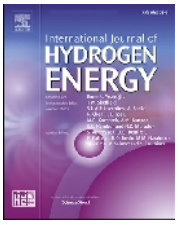

Improved thermodynamic properties of doped $LiBH_4$ for hydrogen storage: First-principal calculation

H. Benzidi [a,*], *M. Lakhal* [a], *M. Abdellaoui* [a], *M. Garara* [a], *A. Benyoussef* [b], *A. El kenz* [a], *M. Loulidi* [a], *M. Hamedoun* [b], *O. Mounkachi* [a,**]

[a] *Laboratory of Condensed Matter and Interdisciplinary Sciences (LaMCScI), Associated to CNRST (URAC 12), Physics Department, Faculty of Sciences, Mohammed V University, Rabat, Morocco*

[b] *Materials and Nanomaterials Center, MAScIR Foundation, Rabat Design Center Rue, Mohamed Al Jazouli Madinat Al Irfane, Rabat 10 100, Morocco*

ARTICLE INFO

Article history:
Received 27 February 2019
Received in revised form
6 April 2019
Accepted 23 April 2019
Available online xxx

Keywords:
First-principal calculations
Electronic properties
Complex hydride
Hydrogen-storage
Enthalpy
Kinetics

ABSTRACT

First-principles calculations have been performed on lithium borohydride $LiBH_4$ using the ultrasoft pseudopotential method, which is a potential candidate for hydrogen-storage materials due to its extremely large gravimetric capacity of 18 mass % hydrogen. We focus on an orthorhombic phase observed at ambient conditions and predict its fundamental properties; De-hydrogenation and electronic properties of doped $Li_{1+x}B_{1-x}H_4$ by Li (with $0 < x < 0.75$); to be used as a material for hydrogen-storage; are studied from density-functional theory based first-principles calculations. The results suggest that the substitution of B by Li decrease the desorption enthalpy of hydrogen from 75 kJ/mol.l to 40. Our calculation results show the function of Li in improving thermodynamics, which provides a favorable thermodynamic modification.

Introduction

As a new energy vector, hydrogen presents an attractive alternative fuel that can be produced from the electrolysis of water [1–3]. It is considered as a clean and renewable source of energy since it does not release greenhouse gas emissions [4,5]. In addition, hydrogen is considered as a good energy carrier, thanks to its combustion which generates about three times more energy than other fossil fuels [6]. All these qualities make hydrogen the key to the global energy revolution. However, the difficulties encountered in the storage and transportation of hydrogen without risk, efficiently and safely prevent its wide use and commercialization [7].

Among the available techniques for the storage of hydrogen, two forms are the most known: storage of gas under high pressure and storage of hydrogen in liquid form at low-temperature. Each of these methods has disadvantages

* *Corresponding author.*
** *Corresponding author.*
E-mail addresses: hind.benzidi@gmail.com (H. Benzidi), o.mounkachi@gmail.com (O. Mounkachi).
https://doi.org/10.1016/j.ijhydene.2019.04.241

which hinder their use, such as the safety problem that occurs when using high pressures (compression storage) and the energy cost necessary to cool the hydrogen (cryogenic storage). In recent decades, a new method of storing hydrogen in solid materials has emerged, enabling hydrogen atoms to be absorbed and stored in metallic matrixes such as metal hydrides, complex hydrides, intermetallic, Organic compounds and porous materials (activated carbons, carbon nanotubes and nanofibers and zeolites) [8–17].

The hydrogen-storage in complex and intermetallic hydrides are attracting considerable interest due to their high gravimetric capacities. However, the release of hydrogen in these materials requires a high temperature due to the chemical bonding of hydrogen in the interstitial sites of the host material for intermetallic compounds or covalent and ionic into the crystal structure of complex hydride. The magnesium hydride (MgH_2) one of the most studied intermetallic hydride. It presents 7.66% wt of H_2. It should be mentioned that dual-tuning effects of the thermodynamics and kinetics is one of the keys for hydrogen economy and hydrogen-storage materials issues. Thus, can be partially achieved by doping [18–21] or by reducing the particle size using a ball milling process [22–26].

The complex hydrides $LiBH_4$ has the highest capacities (18.3%wt of H_2) among other solid storing materials, the structure of lithium borohydride is a combination of the stable hydride LiH and a relatively unstable boron hydride which forms the complex hydride. Where, the hydrogenated complexes $[BH_4]^-$ ionically bind to the alkali-metal Li, this complex nature (ionic and covalent binding) of lithium borohydride is the reason for its complicated decomposition. Therefore, the release of hydrogen involves a several steps process under pressures of the order of 10 MPa and a very high desorption temperature [27–29].

$LiBH_4 \rightarrow LiH + B + 3/2H_2$ Reaction 1

$LiBH_4 \rightarrow Li + B + 2H_2$ Reaction 2

To avoid these difficulties, different techniques are adopted including, doping additives (metal halide [30], oxides [31], amides [32,33], reactive hydride composites [34,35], Nanoporous [36,37] are mixtures, by ball mill. For realizing a storage system of hydrogen several objectives are targeted: (i) increasing storage mass capacities, (ii) improving reversibility, (iii) carrying out cycling, (iv) improving kinetics of reaction, (vi) stabilizing the systems.

For that, various studies have been done to minimize the temperature desorption of $LiBH_4$, for example, Gennari et al. examined the composite mixtures of $6LiBH_4$ and RECl with RE = Ce, Gd and observed an amelioration in the decomposition temperature of $LiBH_4$ [38] Other researchers have worked on a mixture of $LiBH_4$ by Re=Er may decrease the decomposition temperature of about 373 K [39,40]. Widely of experimental work based on the enhance the sorption properties of $LiBH_4$ by nanoconfinement in porous materials [12,36,41–50]. Inside Nanoporous carbon or Nanoporous silica, faster dehydrogenation kinetics is reported for $LiBH_4$, accompanied by a decrease of the de-hydrogenation temperature by at least 100 °C [49]. It is relatively difficult to remove hydrogen from the surface of bulk crystals than from the surface of the clusters and nanowhiskers. This result is reported by Vajeeston P. et al. [51]. Since a chemical interaction between the products and an intermediate compound of the $LiBH_4$ reaction steps gives an improvement of the hydrogenation effect of the nanoconfined $LiBH_4$ [52]. AU et al. [53] recorded that metal halides $TiCl_3$, TiF_3, and ZnF_2 strongly ameliorate the desorption temperature via cation exchange interaction, a part of the halide doped $LiBH_4$. FANG et al. [54] remarked that TiF_3 indicate the predominant effect of $TiCl_3$ on the reversible de-hydrogenation of $LiBH_4$. In addition, metal oxides have been reported to be an effective method to reduce the hydrogen-storage performance of $LiBH_4$. In 2008, Yu et al. studied the effect of TiO_2 on $LiBH_4$ finding a clear influence on the thermodynamic properties of $LiBH_4$ especially the temperature, which decreases from 220 °C to 150 °C, due to the transfer of charge between B and Ti [55]. And also, Zuttel et al. noticed that TiO_2 have a decorative role in destabilizing LiBH4 with desorption of 9 %wt $LiBH_4$ [27]. The same effect is achieved with other oxidation, but with different variations or the stabilization changes as follows: $F_2O_3 > V_2O_5 > Nb_2O_5 > TiO_2 > SiO_2$ [56]. According to the study by Han et al. [57], the de-hydrogenation temperature was reduced to 230 °C, after grinding with MoS_2, which decreased by 80 °C relative to pure $LiBH_4$.

$LiBH_4$ is well known by the strong ionic bond between Li^+ cation and anion (BH_4^-). The removal of the charge transfer between the anion and the cation could considerably weaken the interactions of the ionic bonds in the complex BH_4, thus making the hydrogen more labile [58]. The B–H bond between H and B is easy to dissociate. To disrupt the B–H bond many efforts have been reported:

- Orimo et al. have proposed the substitution of the Li^+ cations by more electronegative elements, such as Mg, or Cu, Nb [59–61] and Al [62–64] is an effective mean of lowering the de-hydrogenation temperature of $LiBH_4$.
- Another decisive strategy is the anion substitution, which can stabilize the too unstable borohydrides or destabilize the too stable borohydrides [65,66]. It is reported that a significant improvement in the anion of $LiBH_4$ is an important result of the substitution of BH_4^- with Cl^-, F^-, Br^- and I^- anions in $LiBH_4$ [63,66–74].

By first-principles calculation methods, Gong XJ et. Al [66] proved that the migration barrier energy declines from 4.03 eV to 3.09 eV by calculating the diffusion pathway of H atom from one [BH_4] to the nearby [BH_4] on the clean and Mg-doped $LiBH_4$ (010) surfaces, respectively. This result shows that the H atoms easily diffuse on the Mg-doped $LiBH_4$ (010) surface rather than on the pure surface. In addition, the calculated average hydrogen desorption energies of Nb-doped LiBH4 (010) surface are found to be smaller than the pure $LiBH_4$ (010) [66]. All of this proves that enhancing the desorption properties of $LiBH_4$ can be effectively achieved through the doping strategy. However, even with the aid of these technologies, the dehydriding/rehydrating properties of $LiBH_4$ are still far below those required for practical application. This necessitates the development of a new method/technology to assess the potential of $LiBH_4$ for the hydrogen-storage application. From our previous work [75], the high stability of the

Please cite this article as: Benzidi H et al., Improved thermodynamic properties of doped $LiBH_4$ for hydrogen storage: First-principal calculation, International Journal of Hydrogen Energy, https://doi.org/10.1016/j.ijhydene.2019.04.241

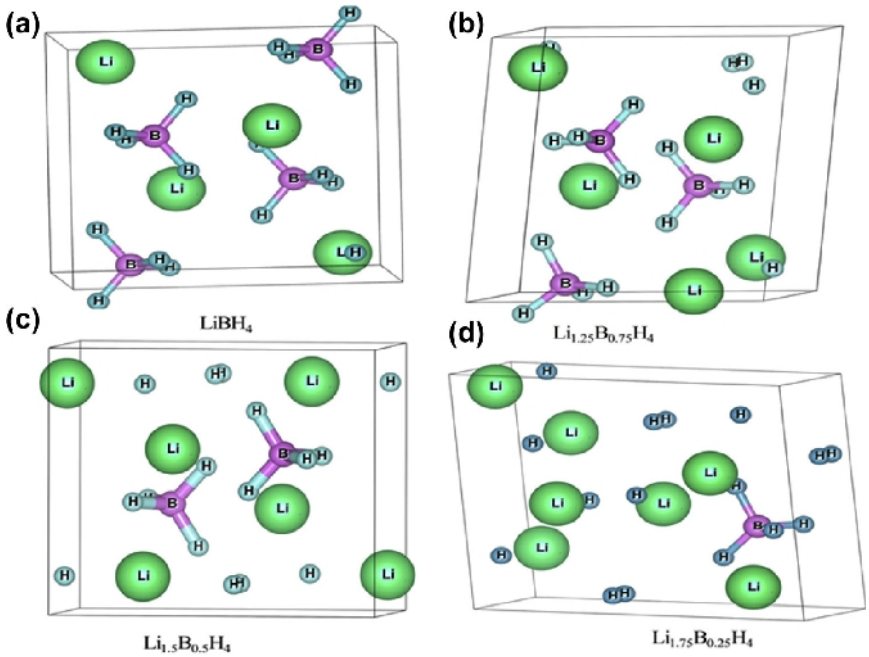

Fig. 1 – Crystal structures of (a) pure, (b) $Li_{1.25}B_{0.75}H_4$ (c) $Li_{1.5}B_{0.5}H_4$ (d) $Li_{1.75}B_{0.25}H_4$. Green, pink and blue balls represent respectively Li, B and H atoms. (For interpretation of the references to colour in this figure legend, the reader is referred to the Web version of this article)

system $LiBH_4$ is mainly due to the high hybridization between B and H atoms. For this reason, it was thought to have substituted the B by the light elements such as Lithium to reduce this hybridization and consequently reduce the energy of formation of the system.

In this study, we present a novel substitution approach to tune the problematic thermodynamic of $LiBH_4$. According to the first-principles calculation results, were used to investigate the effect of the substitution of boron by lithium inside $LiBH_4$ lattice. In addition, the vibrational and thermodynamic properties were investigated to explore the possibility of lowering the hydrogen desorption temperature and reversibility of substituted lithium borohydride structure.

Models and computational details

To study the decomposition reaction of doped $LiBH_4$, the cell of $Li_{1+x}B_{1-x}H_4$ (x = 0, 0.25, 0.5, 0.75) (see Fig. 1) was used to model the substitution of Li at B site in $LiBH_4$ bulk. The present calculations have been performed using the first-principles calculations based on a density-functional theory approach [76] the exchange and correlation energy corrections included through a generalized gradient approximation (PBE-GGA) [77], with plane wave pseudopotential method (PWSCF); as implemented in the Quantum Espresso code [78]. All pseudopotentials are constructed using the ultrasoft pseudopotential method [79], with a cutoff kinetic energy of 680 eV and the k-point grids for the Brillouin zone integration are sited to be 6 × 8 × 6, these values give good convergence of the total energy within 1 meV/atom. The atomic positions and the cell parameters, including the cell volume, are fully optimized by minimizing the Hellmann-Feynman forces and stresses without any symmetry constraint. All structures are considered to be fully relaxed when the Hellmann-Feynman forces on the atoms are smaller than 0.01 eV/Å.

The vibrational density of states (VDOS) was calculated using the software PHONOPY [80]. The phonon Eigenmodes are obtained by solving the eigenvalue problem for the

Table 1 – Lattice parameter, volume, formation enthalpy, gravimetric and volumetric capacity of $Li_{1+x}B_{1-x}H_4$ (x = 0, 0.25, 0.5, 0.75).

System	Parameters (Å)			Volume	Formation enthalpy (kJ/mol)	Gravimetric capacity (wt%)	Volumetric capacity (g H_2/l)
	a	b	c				
$LiBH_4$	7,05	4,33	6,74	205,75	−192.12	18,5	146,37
$Li_{1.25}B_{0.75}H_4$	6,50	4,32	7,18	200.88	−174.44	18,88	132,3
$Li_{1.5}B_{0.5}H_4$	7,54	4,03	6,67	203.1	−141.87	19,36	130,86
$Li_{1.75}B_{0.25}H_4$	7,93	3,93	6.65	206.59	−119.95	20,31	128,65

Please cite this article as: Benzidi H et al., Improved thermodynamic properties of doped $LiBH_4$ for hydrogen storage: First-principal calculation, International Journal of Hydrogen Energy, https://doi.org/10.1016/j.ijhydene.2019.04.241

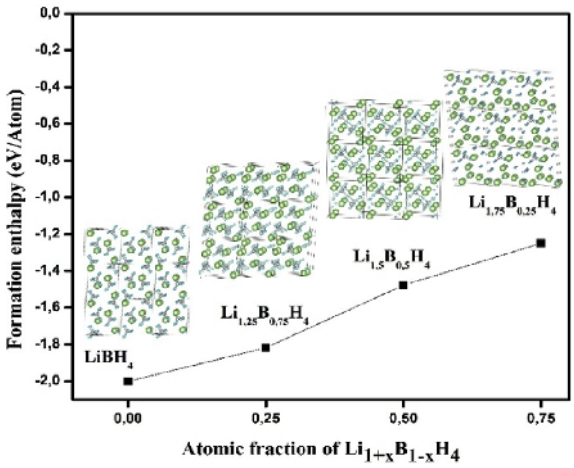

Fig. 2 – Formation enthalpies from the calculated static density-functional theory as function of atomic fraction of Li in $Li_{1+x}B_{1-x}H_4$.

dynamical matrix which is calculated by the force-constant using a finite displacement method based on the Parlinski-Li-Kawazoe method. The atomic displacement is set to be 0.02 Å. Several research groups have synthesized and characterized LiBH4, the reported X-ray diffraction data show that at the ambient condition the LiBH4 crystallizes in orthorhombic space group *Pnma* (62), and lattice parameters are a = 7.178 Å, b = 4.436 Å, and c = 6.803 Å [81]. At the first step, the experimental crystal structure was fully relaxed without any symmetry constraint of LiBH4 unit cell. Once the phonon spectrum is obtained, we can easily compute the temperature dependence of the vibrational specific, heat capacity Cv and the entropy S at constant-volume, as described below.

For calculations of lattice properties, the Helmholtz free energy is given by the equation below:

$$F = E + H_{vib} + TS_{vib} \quad (1)$$

Where E, H_{vib}, and S_{vib} are the internal energy of the crystal, harmonic phonon energy and entropy contributing to the lattice vibration.

The harmonic phonon energy is given by the equation below:

$$H_{vib}(T) = \sum_i \frac{1}{2}\hbar\omega_i + \hbar\omega_i\left[\exp\left(\frac{\hbar\omega_i}{K_\beta T}\right) - 1\right]^{-1} \quad (2)$$

Table 2 – Desorption enthalpy and temperature of $Li_{1+x}B_{1-x}H_4$ (x = 0, 0.25, 0.5, 0.75).

System	First reaction $LiBH_4 \rightarrow LiH + B + 3/2H_2$		Second reaction $LiBH_4 \rightarrow Li + B + 2H_2$	
	E_{des} (kJ/mol)	T_{des}(K)	E_{des} (kJ/mol)	T_{des}(K)
$LiBH_4$	75.75	658.75	96.06	835.31
$Li_{1.25}B_{0.75}H_4$	62.38	542.49	87.22	758.44
$Li_{1.5}B_{0.5}H_4$	61.46	534.48	70.93	616.81
$Li_{1.75}B_{0.25}H_4$	46.854	407.42	59.97	521.52

The entropy S and the heat capacity C_v at constant volume are given by the equations below:

$$S_{vib}(T) = k_\beta \sum_i \frac{\frac{\hbar\omega_i}{K_\beta T}}{\exp\left(\frac{\hbar\omega_i}{k_\beta T}\right) - 1} - \ln\left[1 - \exp\left(-\frac{\hbar\omega_i}{k_\beta T}\right)\right] \quad (3)$$

$$C_v = \left(\frac{\partial E}{\partial T}\right)_v = \sum_i k_\beta \left(\frac{\hbar\omega_i}{k_\beta T}\right)^2 \frac{\exp\left(\frac{\hbar\omega_i}{k_\beta T}\right)}{\left[\exp\left(\frac{\hbar\omega_i}{k_\beta T}\right) - 1\right]^2} \quad (4)$$

where ω is the phonon frequency and T is the temperature. k_B and $\hbar$ are the Boltzmann constant and the reduced Planck constant, respectively.

Results and discussion

Structural properties and formation enthalpies

In order to investigate the substitution of boron by lithium, the geometries of $Li_{1+x}B_{1-x}H_4$ (with x = 0.25, 0.5, 0.75) were fully relaxed. This substitution breaks the symmetry of $LiBH_4$ because of the different atomic radii of Li (1.52 Å), B (0.85 Å), which causes different lattice parameters and cell volumes for pure $LiBH_4$ and $LiBH_4$ substituted. Consequently, create changes on the periodicity of the crystal. As shown in Fig. 1. The relaxed lattice parameters and volume of all the systems are listed in Table 1. The possibility of the structure of $LiBH_4$ substituted by Li was evaluated by calculating the formation enthalpy of $LiBH_4$ and the related $Li_{1+x}B_{1-x}H_4$ (with x = 0.25, 0.5, 0.75). The formation enthalpies are calculated based on the equation:

$$Li_{1+x}B_{1-x}H_4 \rightarrow (1+x)Li + (1-x)B + 2H_2 \ (x = 0,\ 0.25,\ 0.5,\ 0.75)$$

Reaction 3

The formation enthalpy for each structure is determined with respect to the most stable structure of the pure elements. The calculated enthalpies are presented in Fig. 2, and reported in (kJ/mol) unit in Table 2. In all cases, the substitution of B by Li in the $LiBH_4$ lattice is an exothermic process. By virtue of,

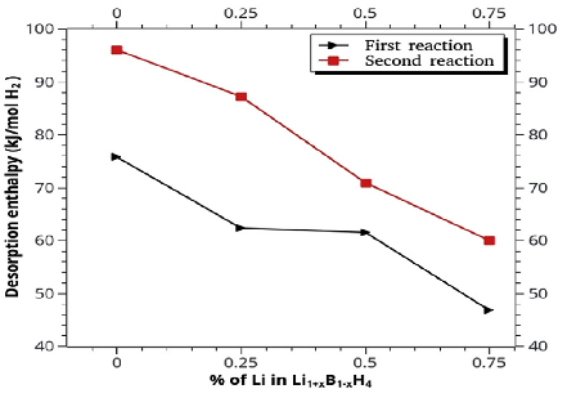

Fig. 3 – Desorption enthalpy and temperature as function of Li-substitution rate of $Li_{1+x}B_{1-x}H_4$ (x = 0, 0.25, 0.5, 0.75).

Please cite this article as: Benzidi H et al., Improved thermodynamic properties of doped $LiBH_4$ for hydrogen storage: First-principal calculation, International Journal of Hydrogen Energy, https://doi.org/10.1016/j.ijhydene.2019.04.241

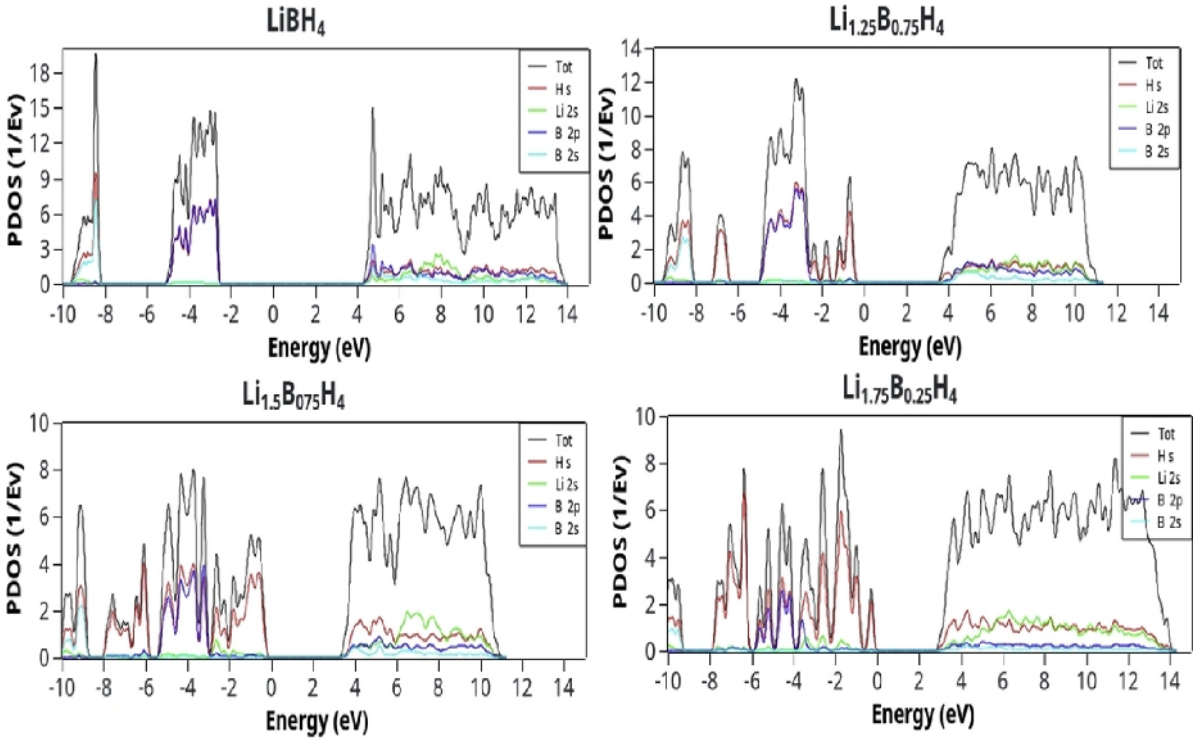

Fig. 4 – The calculated Total and partial DOS of $Li_{1+x}B_{1-x}H_4$ (x = 0, 0.25, 0.5, 0.75).

negative heats of formation, the complex hydride is thermodynamically stable with respect to the complete decomposition into its basic constituents (B, Li, and H_2).

De-hydrogenation properties

To further investigate the effects of the substitution on the de-hydrogenation behavior of $LiBH_4$. The desorption enthalpy E_{des}, which is the most important thermodynamic parameter, has been calculated and used to predict de-hydrogenation proprieties. As seen in Table 2. For pure $LiBH_4$, the computed desorption enthalpies for the first reaction (partial decomposition) is 75.7 kJ/mol H_2, which agrees well with the reported DFT calculation results [71,82,83]. Considering reversible hydrogen-storage as finding systems for which $30 \leq \Delta H \leq 60$ kJ/mol H_2 and that yield significant gravimetric quantities of H_2. In view of, the de-hydrogenation enthalpy ΔH is significantly less than 30 kJ/mol H_2, the material will not be easily reversible. However, for an ideal material for hydrogen-storage, the heat of formation ΔH should be around 40 kJ/mol (H_2) [84].

The temperature of de-hydrogenation can be reliably estimated by $\Delta H = T\Delta S$, where ΔH and ΔS are the enthalpy and entropy change of the de-hydrogenation reaction. The entropy changes estimate that $95 \leq \Delta S \leq 140$ JK-1 mol^{-1}. For almost all the intermetallic hydride the variation entropy reaction is $\Delta S = 130\,JK{-}1\ mol^{-1}$. H_2 corresponding to the change entropy of hydrogen gas to solid hydrogen. The stability of the hydride can be described and compared with the enthalpy of reaction only. For complex hydrides, the situation is a bit more complicated and entropy of the reaction appears to be lower and variable for different complex hydrides. Based on the theoretical calculation, it has estimated the value of ΔS about 115 J/K. mol H_2 [85]. The predicted decomposition temperature is 658.75 K for the first reaction (see Fig. 3) . This temperature is still too high for practical applications. According to the calculated desorption enthalpies listed in Table 2, The modified crystal structures after Li doping for the first equation is nearly reduced to 62.38, 61.46 and 46.85 kJ/mol H_2 with increasing the substitution level from x = 0.25 to 0.75.

Likewise, the de-hydrogenation temperature is reduced by 150 K of with about 20.31 wt% of hydrogen released at about 407.42 for $Li_{1.75}B_{0.25}H_4$. Therefore, the decomposition reaction following Eq. (1) is thermodynamically favorable than the process following Eq. (2). From a thermodynamic point of view. Generally, the stabilities of the reaction products are dramatically reduced with increasing the percentage of Li, our calculations show that substitution of B by Li in $LiBH_4$ structure result in a favorable modification of the thermodynamics that essentially constraints the potential of $LiBH_4$ for hydrogen-storage application.

Electronic structure

To understand and explain the improved performance of de-hydrogenation process during application of substitution

Please cite this article as: Benzidi H et al., Improved thermodynamic properties of doped $LiBH_4$ for hydrogen storage: First-principal calculation, International Journal of Hydrogen Energy, https://doi.org/10.1016/j.ijhydene.2019.04.241

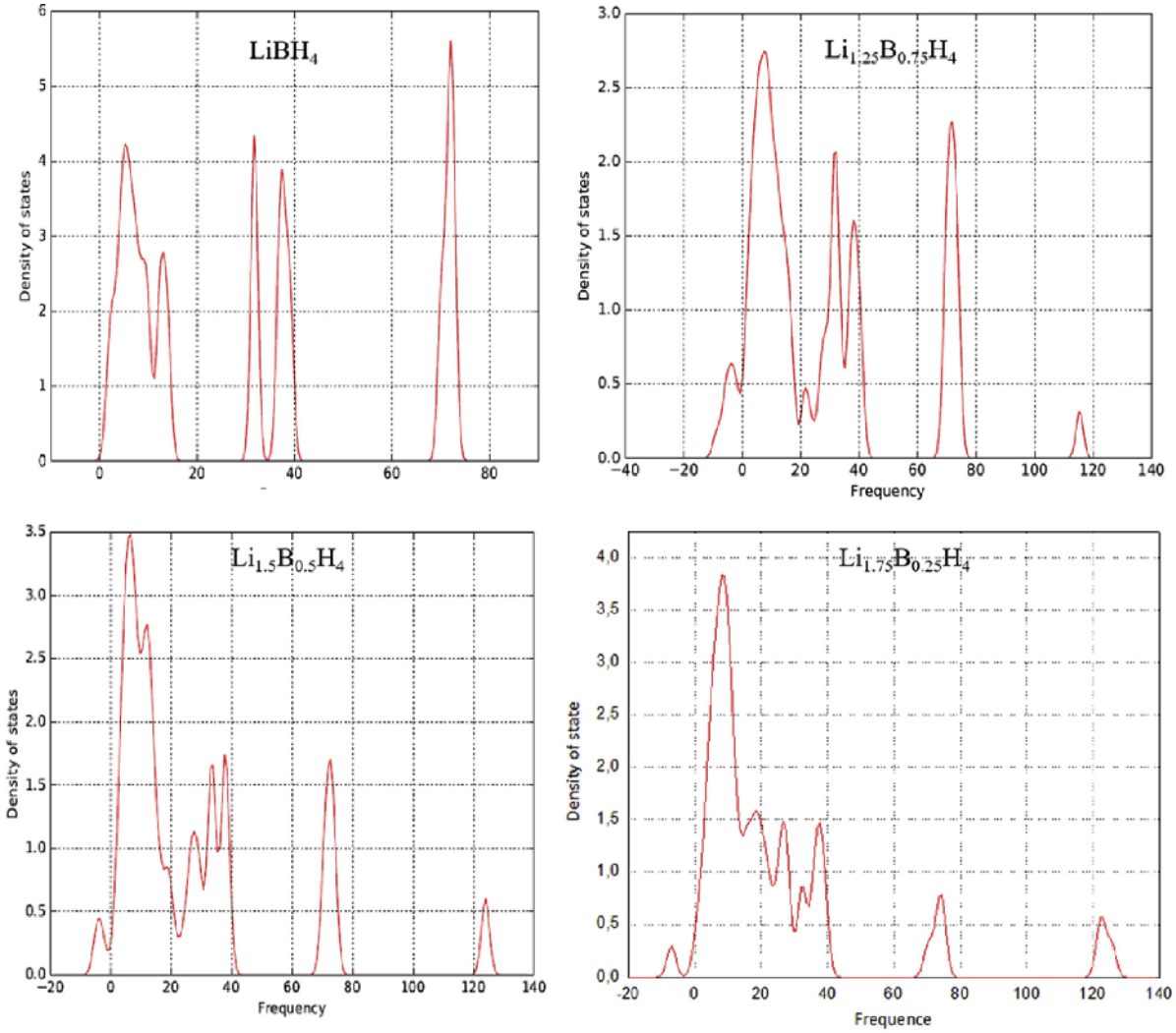

Fig. 5 – Phonon density of states of $Li_{1+x}B_{1-x}H_4$ (x = 0, 0.25, 0.5, 0.75).

with lithium, the density of states of pure and modified of $LiBH_4$ structure. This study will clarify the effect of the substitution with Lithium on the hydrogenation performance of this system.

Fig. 4 presents the total and partial densities of states for $Li_{1+x}B_{1-x}H_4$ with x varied from 0 to 0.75. In these figures, the Fermi level (E_F) is set to zero and used as a reference. The total density of state of pure shows an insulator behavior with the calculated energy gap of 6.79 eV. The gap energy value is a good agreement with the experimental and theoretical values [75,86–88]. The Valence band split into two regions: The region I (low-energy states) which composed of B-2s and H-1s orbitals and the region II (high-energy states) consist of B-2p and H-1s orbitals, which show a high hybridization. Boron atoms form covalent bonds with surrounding four H atoms. Because there is a little contribution of Li orbitals to the occupied states, Li atoms are thought to be ionized as Li^+ cations. As expected, after the substitution of boron by Li, the strong hybridization between BH begins to weaken by increasing the rate of substitution, and other states of individual hydrogen begin to appear, it can be explained that the covalent band between B and H has broken and other binding begins to appear to form hydrogen molecules in interstitial sites. This translates the release of the desorption enthalpy by adding the percentage of Li in the $LiBH_4$ structure. We should note also that the energy band gap decreases with increasing the percent of Li inside the $LiBH_4$ framework.

Lattice dynamic stability

To further study the lattice stability of $Li_{1+x}B_{1-x}H_4$ (x = 0, 0.25, 0.5, 0.75) compounds first-principles phonon calculations are carried out.

Please cite this article as: Benzidi H et al., Improved thermodynamic properties of doped $LiBH_4$ for hydrogen storage: First-principal calculation, International Journal of Hydrogen Energy, https://doi.org/10.1016/j.ijhydene.2019.04.241

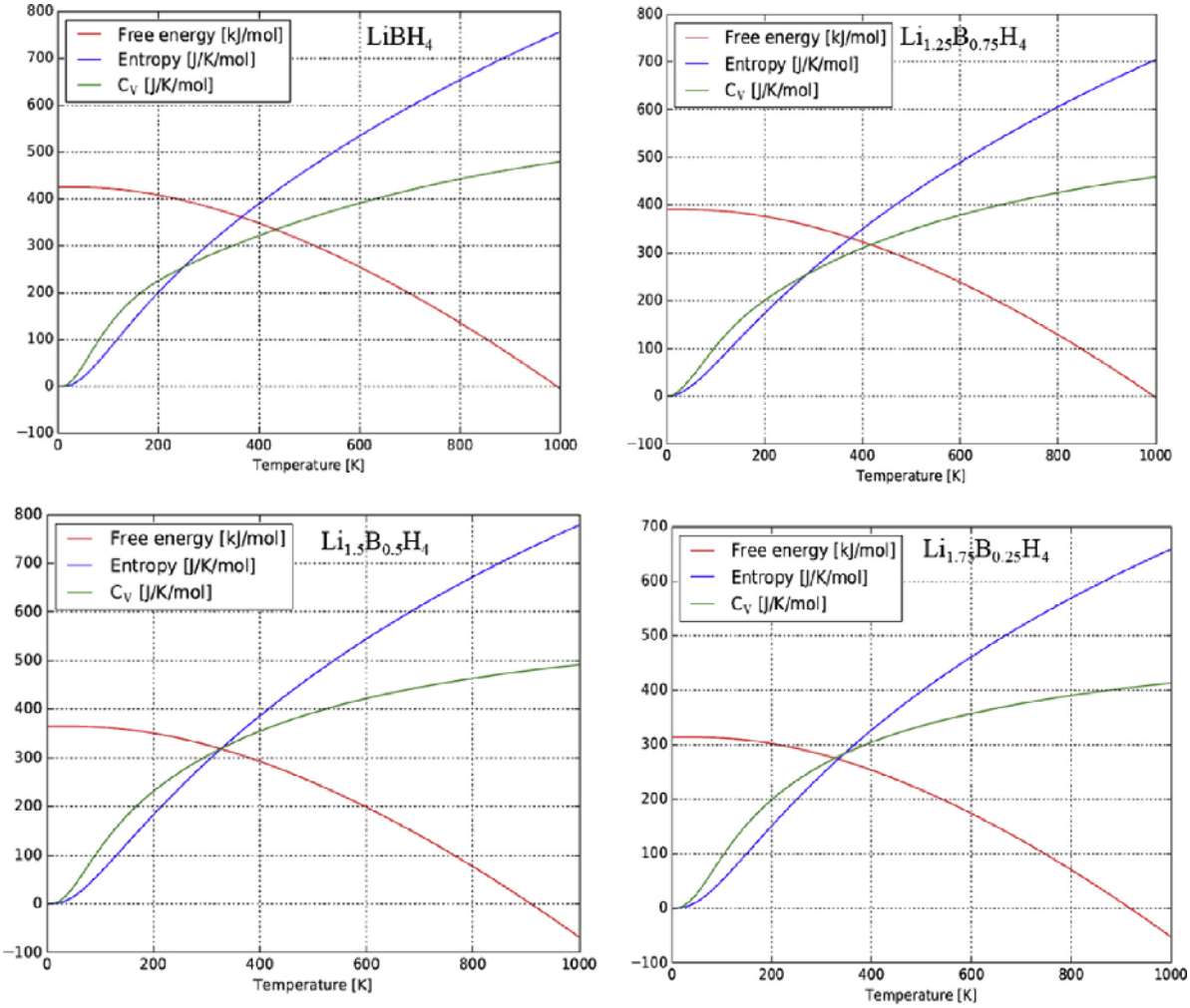

Fig. 6 – Temperature Helmholtz free energy F (V, T), vibrational entropy S, and heat capacity C_v of $Li_{1+x}B_{1-x}H_4$ (x = 0, 0.25, 0.5, 0.75).

According to harmonic approximation, this is possible when all the phonons have real and positive frequencies. Negative or imaginary frequencies of phonons indicate that crystal is dynamically unstable [80]. In our present study, from Fig. 5(a) any negative frequencies are not observed for the pure $LiBH_4$ compound. This means the compound is mechanically stable [89]. The phonon density of state shows three branches of optical phonons separated from the phonon branches of lower frequencies. The reason for the separation of these branches is from the lower mass H present in the compound. The peak in the lower energy region corresponds to the acoustic branches in the dispersion plot. The next separated higher energy peaks represent the coupled optical phonon branches. In the case of the modified $LiBH_4$ structure Fig. 5(b, c, d) a small phonon branches in the negative frequency range of −15 THz (negative frequencies are representative of imaginary frequencies. The vibration of the hydrogen is more independent than that of the complex bond of BH_4. Which explains the reduction of desorption enthalpies for modified $LiBH_4$ lattice. We believe applying external pressure can eliminate these imaginary phonons.

Lattice thermodynamic properties

Thermal properties such as Helmholtz free energy, entropy and constant-volume specific heat (C_V) as a function of temperature are computed using phonopy. It can be seen from Fig. 6 that the lattice heat capacity increases slowly with the temperature in the initial stage. The lattice heat capacity approaches almost linear when the temperature exceeds 400 K. Besides, with the increasing of Li-substitution concentration, the lattice heat capacities of the modified systems have small increases. Although Li-substitution has slight effects on the lattice heat capacity of $LiBH_4$, and the current framework can be useful to characterize complicated crystal structures of complex hydrides materials. Finally, the present framework is

Please cite this article as: Benzidi H et al., Improved thermodynamic properties of doped $LiBH_4$ for hydrogen storage: First-principal calculation, International Journal of Hydrogen Energy, https://doi.org/10.1016/j.ijhydene.2019.04.241

beneficial to optimize the material composition or to design a new modified crystal of $LiBH_4$, which could be applicable as solid-state hydrogen-storage materials.

Conclusions

To sum up, this study points towards the idea of the substitution of boron by lithium atom in the lithium borohydride $Li_{1+x}B_{1-x}H_4$ (x = 0, 0.25, 0.5, 0.75) framework. Firstly, the possibility of the fabrication of these systems was confirmed by the negative value of formation enthalpies and the weak soft modes in phonon dispersion of all the systems. Furthermore, the de-hydrogenation temperature is reduced to 521.52 K for fully released hydrogen for $Li_{1.75}B_{0.25}H_4$ system. The significantly enhanced hydrogen-storage properties of the $Li_{1+x}B_{1-x}H_4$ (x = 0, 0.25, 0.5, 0.75) systems are attributed to the decrease of the boron atoms in the lithium borohydride framework, which lead to a weaker hybridization between Boron and Hydrogen atoms, and subsequently high gravimetric capacities. Our theoretical calculations provide a novel approach for effectively tuning thermodynamics of $LiBH_4$, a leading candidate for high-capacity hydrogen-storage. Experimentally evidencing these theoretical predictions may pave a new way to pursue improved hydrogen-storage properties of $LiBH_4$ and other related complex hydrides.

REFERENCES

[1] de Valladares M-R. Mary-Rose de Valladares GMIHTCP (TCP). Global trends and outlook for hydrogen, ISBN 978-1-945951-07-7.
[2] Sprake D, Vagapov Y, Lupin S, Anuchin A. Housing estate energy storage feasibility for a 2050 scenario. In: Internet Technol Appl ITA 2017 – Proc 7th Int Conf 2017; 2017. p. 137–42. https://doi.org/10.1109/ITECHA.2017.8101925.
[3] Sørensen B, Spazzafumo G, Sørensen B, Spazzafumo G. Hydrogen. Hydrog Fuel Cells 2018:5–105. https://doi.org/10.1016/B978-0-08-100708-2.00002-3.
[4] Züttel A, Remhof A, Borgschulte A, Friedrichs O. Hydrogen: the future energy carrier. Philos Trans R Soc A Math Phys Eng Sci 2010;368:3329–42. https://doi.org/10.1098/rsta.2010.0113.
[5] IEA. Global energy & CO2 statuts report. ©OECD/IEA; 2017.
[6] Schlapbach L, Züttel A. Hydrogen-storage materials for mobile applications. Nature 2001;414:353–8. https://doi.org/10.1038/35104634.
[7] Dagdougui H, Sacile R, Bersani C, Ouammi A, Dagdougui H, Sacile R, et al. Hydrogen storage and distribution: implementation scenarios. Hydrog Infrastruct Energy Appl 2018:37–52. https://doi.org/10.1016/B978-0-12-812036-1.00004-4.
[8] Schlapbach L, Züttel A. Hydrogen-storage materials for mobile applications. Nature 2001;414:353–8. https://doi.org/10.1038/35104634. Co-Published with Macmillan Publishers Ltd, UK.
[9] Liu Y, Pan H. Hydrogen storage materials. New futur Dev Catal 2013:377–405. https://doi.org/10.1016/B978-0-444-53880-2.00018-1. Elsevier.
[10] Bellosta von Colbe J, Ares J-R, Barale J, Baricco M, Buckley C, Capurso G, et al. Application of hydrides in hydrogen storage and compression: achievements, outlook and perspectives. Int J Hydrogen Energy 2019:1–29. https://doi.org/10.1016/j.ijhydene.2019.01.104.
[11] Zhang L, Zheng J, Xiao X, Wang X, Huang X, Liu M, et al. A new strategy to remarkably improve the low-temperature reversible hydrogen desorption performances of LiBH4 by compositing with fluorographene. Int J Hydrogen Energy 2017;42:20046–55. https://doi.org/10.1016/J.IJHYDENE.2017.05.060.
[12] Gross Adam F, Vajo * John J, Van Atta Sky L, Olson GL. Enhanced hydrogen storage kinetics of LiBH4 in nanoporous carbon scaffolds. 2008. https://doi.org/10.1021/JP711066T.
[13] Hartman MR, Rush JJ, Udovic TJ, Bowman RC, Hwang SJ. Structure and vibrational dynamics of isotopically labeled lithium borohydride using neutron diffraction and spectroscopy. J Solid State Chem 2007;180:1298–305. https://doi.org/10.1016/j.jssc.2007.01.031.
[14] Shao J, Xiao X, Fan X, Zhang L, Li S, Ge H, et al. Low-temperature reversible hydrogen storage properties of LiBH $_4$: a synergetic effect of nanoconfinement and nanocatalysis. J Phys Chem C 2014;118:11252–60. https://doi.org/10.1021/jp503127m.
[15] Shao J, Xiao X, Fan X, Huang X, Zhai B, Li S, et al. Enhanced hydrogen storage capacity and reversibility of LiBH4 nanoconfined in the densified zeolite-templated carbon with high mechanical stability. Nanomater Energy 2015;15:244–55. https://doi.org/10.1016/J.NANOEN.2015.04.023.
[16] Suib SL, Liu Y, Pan H. Hydrogen storage materials. New Futur. Dev. Catal.; 2013. p. 377–405. https://doi.org/10.1016/B978-0-444-53880-2.00018-1. Chapter 13.
[17] Chen P. Hydrogen storage: liquid and chemical. Compr Renew Energy 2012:157–77. https://doi.org/10.1016/B978-0-08-087872-0.00414-5.
[18] Abdellaoui M, Lakhal M, Benzidi H, Mounkachi O, Benyoussef A, El Kenz A, et al. The hydrogen storage properties of Mg-intermetallic-hydrides by ab initio calculations and kinetic Monte Carlo simulations. Int J Hydrogen Energy 2018. https://doi.org/10.1016/J.IJHYDENE.2018.04.225.
[19] Abdellaoui M, Lakhal M, Bhihi M, El Khatabi M, Benyoussef A, El Kenz A, et al. First principle study of hydrogen storage in doubly substituted Mg based hydrides Mg5MH12 (M = B, Li) and Mg4BLiH12. Int J Hydrogen Energy 2016;41:20908–13. https://doi.org/10.1016/J.IJHYDENE.2016.04.122.
[20] Lakhal M, Bhihi M, Labrim H, Benyoussef A, Naji S, Belhaj A, et al. Kinetic Monte Carlo and density functional study of hydrogen diffusion in magnesium hydride MgH2. Int J Hydrogen Energy 2013;38:8350–6. https://doi.org/10.1016/J.IJHYDENE.2013.04.157.
[21] Lakhal M, Bhihi M, Benyoussef A, El Kenz A, Loulidi M, Naji S. The hydrogen ab/desorption kinetic properties of doped magnesium hydride MgH2 systems by first principles calculations and kinetic Monte Carlo simulations. Int J Hydrogen Energy 2015;40:6137–44. https://doi.org/10.1016/J.IJHYDENE.2015.02.137.
[22] Ouyang L, Cao Z, Wang H, Hu R, Zhu M. Application of dielectric barrier discharge plasma-assisted milling in energy storage materials – a review. J Alloy Comp 2017;691:422–35. https://doi.org/10.1016/J.JALLCOM.2016.08.179.
[23] Ouyang LZ, Cao ZJ, Wang H, Liu JW, Sun DL, Zhang QA, et al. Enhanced dehydriding thermodynamics and kinetics in Mg(In)–MgF2 composite directly synthesized by plasma milling. J Alloy Comp 2014;586:113–7. https://doi.org/10.1016/J.JALLCOM.2013.10.029.
[24] Ouyang LZ, Cao ZJ, Wang H, Liu JW, Sun DL, Zhang QA, et al. Dual-tuning effect of in on the thermodynamic and kinetic

Please cite this article as: Benzidi H et al., Improved thermodynamic properties of doped $LiBH_4$ for hydrogen storage: First-principal calculation, International Journal of Hydrogen Energy, https://doi.org/10.1016/j.ijhydene.2019.04.241

ARTICLE IN PRESS

INTERNATIONAL JOURNAL OF HYDROGEN ENERGY XXX (2018) 1–9

Available online at www.sciencedirect.com

ScienceDirect

journal homepage: www.elsevier.com/locate/he

The hydrogen storage properties of Mg-intermetallic-hydrides by ab initio calculations and kinetic Monte Carlo simulations

M. Abdellaoui [a,*], M. Lakhal [a], H. Benzidi [a], O. Mounkachi [b], A. Benyoussef [b,c], A. El Kenz [a], M. Loulidi [a]

[a] Laboratory of Condensed Matter and Interdisciplinary Sciences (LaMCScI), Associated to CNRST (URAC 12), Physics Department, Faculty of Sciences, Mohammed V University, Rabat, Morocco

[b] Institute of Nanomaterials and Nanotechnologies, MASciR, Rabat, Morocco

[c] Hassan II Academy of Science and Technology, Rabat, Morocco

ARTICLE INFO

Article history:
Received 15 February 2018
Received in revised form
5 April 2018
Accepted 27 April 2018
Available online xxx

Keywords:
Hydrogen storage
Intermetallic hydrides
Kinetic Monte Carlo
Ab initio calculations
Thermodynamic properties
Kinetic of absorption

ABSTRACT

First-principle calculations and kinetic Monte-Carlo simulations were performed to study the hydrogen storage properties of the intermetallic hydrides $MgNiH_3$, $MgCoH_3$ and thier mixture namely $MgCo_{0.5}Ni_{0.5}H_3$.

Based on the heat of formation, desoprtion temperature, activation energies computed from DFT calculations and KMC simulations, we show that the $MgNiH_3$ involves a fast kinetic while it is thermodynamically unstable (−9.96 kJ/mol.H_2; 76.61 K) whereas $MgCoH_3$ has a high thermodynamic stability (−73.32 kJ/mol.H_2; 560.97 K) which prevents their application for mobile hydrogen storage.

On the other hand, the electronic structures show that the Ni weakens the strong Co−H bonding of the mixture $MgCo_{0.5}Ni_{0.5}H_3$, which enhances significantly its stability and its desorption temperature (−45.92 kJ/mol.H_2 and 351.33 K) without reducing its high volumetric capacity 133.73 g.H_2/l. Kinetic Monte-Carlo simulations show that $MgCo_{0.5}Ni_{0.5}H_3$ exhibits a fast charging time (only 4.6 min at 400 K and 10 bar).

Thermodynamic properties including entropy S, Gibbs free energy G and thermal expansion coefficient are predicted within the quasi-harmonic approximation. It is verified that crystal structure of $MgCo_{0.5}Ni_{0.5}H_3$ is stable.

Introduction

Magnesium hydride is a potentiel material for hydrogen storage, due on the one hand to its high gravimetric and volumetric storage capacities (7.6%.wt and 110 g.H_2/l respectively) and on the other hand to its light weight [1–6]. However, on the practical level, Magnesium exhibits a very slow absorption/desorption kinetics, excessive thermodynamic stability ($\Delta H = -75$ kJ/mol.H_2) involving high desorption temperature of 350 °C and exothermic absorption reaction [7–11].

* Corresponding author.
E-mail address: bdellaoui@gmail.com (M. Abdellaoui).

https://doi.org/10.1016/j.ijhydene.2018.04.225
0360-3199/

Please cite this article in press as: Abdellaoui M, et al., The hydrogen storage properties of Mg-intermetallic-hydrides by ab initio calculations and kinetic Monte Carlo simulations, International Journal of Hydrogen Energy (2018), https://doi.org/10.1016/j.ijhydene.2018.04.225

The magnesium-based intermetallics currently available do not allow high capacities (1–4%.wt) [12,13], but they are known by their moderate stability and therefore offer reversibility of hydriding at lower temperatures compared to the MgH_2 compound.

Currently, experimental as well theoretical investigations are moving towards the exploration of new intermetallic compounds such as MgNi, MgCo, MgCu and their hydrides [14–19]. Several objectives are targeted: (i) increasing storage mass capacities, (ii) improving reversibility, (iii) carrying out cycling, (iv) improving kinetics of reaction [20–26].

In order to improve the properties of the intermetallic based Magnesium MgNi, different substitutions of the Ni element were considered [27–32]. Such substitutions modify the properties of the intermetallics [33,34] as the metallic rays of the different elements change. By this way, the substitution will leads to a modification of the mesh parameters of the compound and therefore the size of the interstitial sites where the hydrogen is located. Particularly, the substitution may cause variations in the volumetric storage capacity of the compound and therefore a variation in the massic capacity. After all, the existence of several different atoms may lead to the dissociation of the H_2 molecule and then, improve the hydration kinetic.

Recently, it has been shown that Mg–Fe/Mg_2FeH_6 and Mg–Co/Mg_2CoH_5 [35] are stable thermodynamically, while MgNi/$MgNi_{1.02}H_{2.2}$ and Mg_2Ni/Mg_2NiH_4 couple faster kinetics with a reduced hydride formation enthalpy [36–38]. Especially, it was shown that Mg–Co based hydrides are more stable [39,40] than Mg–Ni based hydride [28]. Thus, in this paper the combination between those hydrides is expected to result in a moderate stability and high kinetics without much loss to the storage capacity of the compound.

Mg alloys crystallize in several types of structures BCC, FCC and HCP. The body-centred cubic (BCC) has more interstitial space than the face-centred cubic (FCC) or the hexagonal close-packed (HCP) structures [41–44]. Thus, BCC alloys absorb more hydrogen and are more attractive candidates to be explored as materials for hydrogen storage than the conventional intermetallic compounds. In recent years, Ti-based BCC phase alloys are studied intensively because of their remarkable hydrogen capacities. However, the high cost is one of the critical drawbacks limiting their successful practical applications [45–47].

More recently, Mg–Co and Mg–Ni BCC alloys are successfully synthesized by the mechanical alloying (MA) method [48–51]. In addition, Their hydride formation energies are calculated using a BCC lattice and a perovskite structure of $MgCoH_3$ and $MgNiH_3$ hydrides [37,38]. Vegge and his coworkers [52] studied the properties of the perovskite structure $MgTMH_3$ (TM = 3d transition metals). They found that the stability of these alloys hydrides tend to decrease from MgSc to MgFe [52]. These observed trends were explained by a model developed in Refs. [38,52].

The aim of this work is to study the hydrogen storage properties of the intermetallics materials $MgCoH_3$, $MgNiH_3$ in their mixture. Thus, we will present their thermodynamical properties and their ab/desorption kinetics by using first principale calculations and Kinetic Monte Carlo simulations.

To perform such computations, the activation energies for different elementary processes are needed and computed by ab initio calculations. Taking into account these calculations, the hydrogen diffusion in intermetallics based magnesium hydrides ($MgCoH_3$, $MgNiH_3$) and their mixture are studied using KMC simulations. The stability of the studied compounds is estimated by computing the heats of formation and desorption temperature. The obtained results are supported by an analysis of the density of states (DOS). So, in section Model and computational methods the model and methods to perform our calculation are presented. Section Results and discussion is devoted to the discussion of our numerical results. The conclusion is given in the last section.

Model and computational methods

Kinetic Monte Carlo calculation

In this subsection, model based on kinetic Monte Carlo method (KMC) [53,54] and its application to the investigation of hydrogen diffusion in Mg-based intermetallic hydride are shortly described. The activation energies, for different elementary processes are needed and calculated by DFT calculations then implemented in a KMC algorithm. Depending on temperature and pressure, the hydrogen diffusion time in $MgMTH_3$ (MT = Co,Ni), $MgCo_{0.5}Ni_{0.5}H_3$ systems can be predicted by using the relation between simulated time and Monte Carlo steps (equation (1)). Detailed model have been reported previously in Refs. [54,55].

$$\Delta t = -\frac{\ln(u)}{\sum_{i=1}^{N} \nu_0 \exp\left(-\frac{E_i^a}{K_\beta T}\right)} \quad (1)$$

where ν_0 is the jump frequency (usually set to 10^{-13} Hz), E_i^a the activation energy of ith diffusion process (dissociation of H_2, adsorption and diffusion) taken from first-principles calculations (see section Density functional theory calculations), N is the total possible events in the system, K_β the Boltzmann constant and u is a uniformly distributed random variable $0 < u \leq 1$.

To study the absorption of H, a $2 \times 2 \times 2$ supercell is considered containing initially only the host matrice MgCo, MgNi and $MgCo_{0.5}Ni_{05}$. Hydrogen is adsorbed on the (001) surface, then the interstitial sites will be occupied progressively by H atoms at each time step. Periodic boundary conditions are considered along X- and Y-directions to simulate an infinite system.

Each hydrogen atom has eight nearest available H vacancy sites: 4 in the same plane, two in the upper adjacent plane and two are located at the lower adjacent plane, as shown in Fig. 1. The H atoms can move from an interstitial site to another one depending on the corresponding activation energies (see section Thermodynamic properties).

Density functional theory calculations

In order to study the hydrogen properties of our systems and determine the activation energies necessary for KMC

Please cite this article in press as: Abdellaoui M, et al., The hydrogen storage properties of Mg-intermetallic-hydrides by ab initio calculations and kinetic Monte Carlo simulations, International Journal of Hydrogen Energy (2018), https://doi.org/10.1016/j.ijhydene.2018.04.225

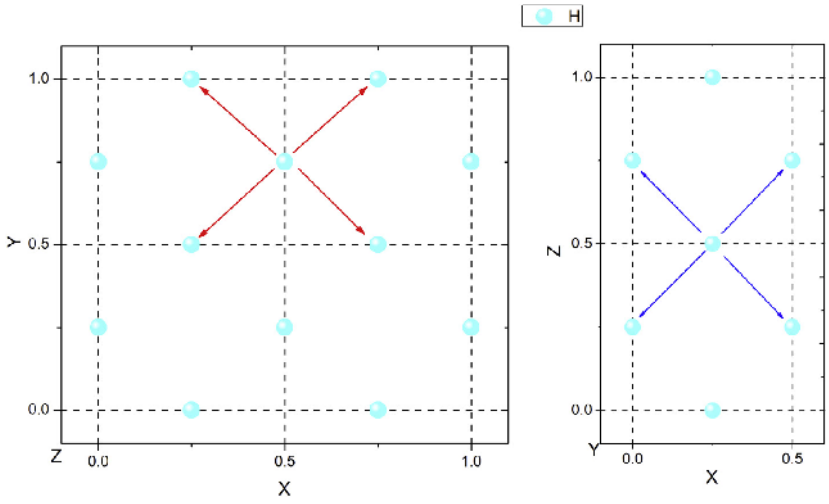

Fig. 1 – Representative scheme of nearest available H vacancy sites.

simulations, ab-intio calculations based on the all-electron full-potential local-orbital minimum-basis scheme FPLO9.00-34 [46–48,56] were used. They are performed to solve the Kohn-Sham equations using the scalar-relativistic scheme. The parameterization of the exchange-correlation energy is done within the generalized gradient approximation GGA [57]. To ensure that the calculations have a high accuracy, self-consistent criteria of the both energy and the density are used with a precision of 10^{-8} Ha and 10^{-6} $Ha^{-1}A^{\circ -3}$ respectively.

MgCo crystallize in the B2-CsCl structure (Pm-3m space group N°221) and MgNi crystallize in two structures B2-CsCl and the tetragonal CuTi type (P4/mmm, N° 123) [38,52]. Those structures contain two atoms, i.e. a magnesium atom placed at the corner (0,0,0) and a Co or Ni atom at the centre (0.5, 0.5, 0.5). For hydride systems, three additional hydrogen atoms are placed at octahedral sites at (0.5, 0.5, 0.0), (0.5, 0.0, 0.5) and (0.0, 0.5, 0.5) (perovskite structure [52]).

All calculations were conducted using a 2 × 2 × 2 supercell, see Fig. 2 (which allows us to reach the desired mixture system $MgCo_{0.5}Ni_{0.5}$) and 6 × 6 × 6 k-point mesh to accurate Brillouin zone integrations. The lattice parameters are optimized using the relaxation method for all systems and their hydrides (see Table 1). The calculated equilibrium values agree with results obtained in previous works [38,52].

In order to access the stability of $MgCo_{0.5}Ni_{0.5}H_3$, the thermodynamic properties such as internal energy, entropy and Gibbs free energy were calculated using the software PHONOPY [58].

Results and discussion

Crystal structure

The lattice parameters are optimized using the relaxation method for all systems (intermetallics and their hydrides) (see Table 1). The calculated equilibrium values and cells volume are consistent with the results obtained in previous studies [38,52].

The introduction of the hydrogen induces an expansion in the cell volume which increases following the order $MgCoH_3 < MgCo_{0.5}Ni_{0.5}H_3 < MgNiH_3$.

Formation enthalpy of binary intermetallics

Before discussing the properties of the intermetallic hydrides, firstly the stability of the intermetallic hosts without hydrogen are discussed. The reaction related to the formation of binary intermetallics is as follows:

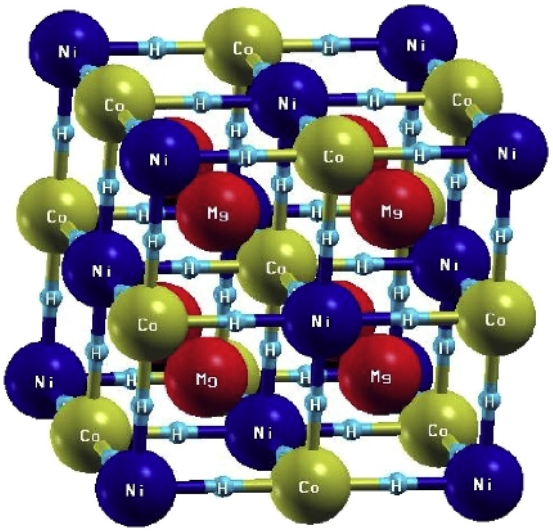

Fig. 2 – Supercell presented $MgCo_{0.5}Ni_{0.5}H_3$; Magnesium atoms are in red, Cobalt atom in yellow, Nickel atom in blue dark and hydrogen atoms in blue. (For interpretation of the references to color/colour in this figure legend, the reader is referred to the Web version of this article.)

Please cite this article in press as: Abdellaoui M, et al., The hydrogen storage properties of Mg-intermetallic-hydrides by ab initio calculations and kinetic Monte Carlo simulations, International Journal of Hydrogen Energy (2018), https://doi.org/10.1016/j.ijhydene.2018.04.225

Table 1 – Relaxed lattice parameters, space group and equilibrium volumes (V); a_{eq}: our calculation.

Systems	Parameters	Space-group	Volume V (Å^3)
MgNi	a_{eq} = 3.050	221-Pm-3m	28.37 (exp. 28.44 [38])
MgNi	a = 2.987; c = 3.127 [38]	123-P4/mmm	27.90 [38]
MgCo	a_{eq} = 3.026 (3.07 [52])	221-Pm-3m	27.70
$MgCo_{0.5}Ni_{0.5}$	a_{eq} = 3.035	221-Pm-3m	27.95
$MgCoH_3$	a_{eq} = 3.310 (3.33 [52])	221-Pm-3m	36.26
$MgNiH_3$	a_{eq} = 3.370 (3.39 [52])	221-Pm-3m	38.27; 37.01 [38]
$MgCo_{0.5}Ni_{0.5}H_3$	a_{eq} = 3.340	P1	37.25

$$Mg + TM \rightarrow MgTM\ (TM = Co, Ni) \quad (2)$$

To calculate the heat of formation of the reaction (equation (2)), the total energy of the pure element Mg and the transition metals Co or Ni are subtracted from intermetallics binary energy:

$$\Delta H\ (MgTM) = E_{tot}\ (MgTM) - E_{tot}\ (Mg) - E_{tot}\ (TM) \quad (3)$$

Where, E_{total}(Mg) and E_{total}(TM) are respectively the total energy of magnesium and simple elements Co or Ni. E_{total}(MgTM) is the binary intermetallic energy. The different energies are listed in Table 2 and compared with other results obtained in previous works.

Several models have been developed to predict the stability of a metal compound. Miedema proposed a mathematical model to calculate the effect on the thermodynamic stability of an additional element(s) to the metallic compound [59,60]. Bouten and Miedema relied on this theory to calculate the enthalpy formation of pure metal hydrides and deduced from there the formation enthalpy of an intermetallic hydride knowing only the enthalpy of formation of the intermetallic compound. They observed that more unstable intermetallic compound more its hydride is stable and vice versa [18].

As shown in Table 2, the binary intermetallic MgCo is unstable while MgNi is stable. Following the empirical model of Miedema et al. [18], the stability of their hydrides can be predicted from the heat of formation of intermetallic compounds without any calculations. So, the MgCo hydride ($MgCoH_3$) will be stable while $MgNiH_3$ will be unstable, which is in agreement with our results (see Table 2). This fact will be confirmed later by our calculations in section Stability of intermetallic hydrides: formation energy.

Stability of intermetallic hydrides: formation energy

Formation energies are an excellent way to determine if the predicted phases are likely to be stable. The formation energies of binary intermetallic hydrides were calculated from the difference of the total energies between the products and reagents involved in the following reaction:

$$MgTM + 3/2H_2 \rightarrow MgTMH_3 \text{ avec TM is Co or Ni} \quad (4)$$

$$\Delta H\ (MgTMH_3) = Etot(MgTMH_3) - Etot(MgTM) - 3/2Etot(H_2) \quad (5)$$

The calculated energy of the molecule H_2 is Etot (H_2) = −2.320 Ry [61].

The heat of formation obtained for $MgNiH_3$, ΔH = −9.96 kJ/mol.H_2, is in good agreement with the value obtained in previous works [38,52]. This value indicates that this system is thermodynamically unstable whereas $MgCoH_3$ has a high thermodynamic stability due to its high formation enthalpy ΔH = −73.32 kJ/mol.H_2 (see Table 2), which is in agreement with the measured values −79.00 kJ/mol.H_2<ΔH < −70.00 kJ/mol.H_2 of some Mg–Co–H systems [36,40]. It can be seen that the hydride formation energy is strongly related to the stability of the intermetallic compound, which is a confirmation of the Miedema model criteria (Table 2).

To enhance the stability of $MgCoH_3$ and $MgNiH_3$ we suggest preparing a mixture of $MgCoH_3$ and $MgNiH_3$ that reaches a desirable heat of formation value comprised between the ones of the two systems. For this purpose, we study the mixture $MgCo_{0.5}Ni_{0.5}H_3$.

The formation energy of $MgCo_{0.5}Ni_{0.5}$ H_3 is given in Table 2. This energy is required to form the hydride phase following the reaction:

$$MgCo_{0.5}Ni_{0.5} + 3/2H_2 \rightarrow MgCo_{0.5}Ni_{0.5}H_3 \quad (6)$$

The enthalpy of formation of $MgCo_{0.5}Ni_{0.5}H_3$ is calculated according to the following expression:

$$\Delta H = E_{tot}(MgCo_{0.5}Ni_{0.5}H_3) - E_{tot}(MgCo_{0.5}Ni_{0.5}) - 3/2E_{tot}t(H_2) \quad (7)$$

It follows that the mixture of $MgCoH_3$ and $MgNiH_3$ enhances the heat of formation from −9.96 kJ/mol.H_2 for $MgNiH_3$

Table 2 – Total energies and formation energies of binary intermetallics and their hydrides.

Intermetallics systems	Total energy (Ry/f.u)	ΔH (KJ/mol)	Intermetallics hydrides	Total energy (Ry/f.u)	ΔH (KJ/mol.H_2)
MgCo (Pm-3m)	−3187.59359812	−4.740	$MgCoH_3$	−3191.15717351	−73.32; −62.72 [52]
MgNi (Pm-3m)	−3442.36916607	−40.19; −41.97 [38]	$MgNiH_3$	−3445.86055489	−9.96; −8.68 [52]
MgNi (P4/mmm)	−3442.36878846	−38.61; −42.16 [38]	_	_	_
$MgCo_{0.5}Ni_{0.5}$ (P1)	−3314.98032812	−21.08	$MgCo_{0.5}Ni_{0.5}H_3$	−3318.51283574	−45.92

Please cite this article in press as: Abdellaoui M, et al., The hydrogen storage properties of Mg-intermetallic-hydrides by ab initio calculations and kinetic Monte Carlo simulations, International Journal of Hydrogen Energy (2018), https://doi.org/10.1016/j.ijhydene.2018.04.225

and from −73.32 kJ/mol.H_2 for $MgCoH_3$ to reaches the value −45.92 kJ/mol.H_2 for $MgCo_{0.5}Ni_{0.5}H_3$ (see Table 2) which is close to the optimum value −40 kJ/mol H_2 proposed in Ref. [62]. Thus, the stability of the compound is enhanced.

Desorption temperatures

In this section, the formation energies obtained in section Stability of intermetallic hydrides: formation energy are used to estimate the desorption temperature of the studied compounds according to the following equation (8):

$$\Delta H = T\Delta S \tag{8}$$

Where, the variation of the entropy is taken at standard pressure and temperature to be equal to $\Delta S \approx \Delta S(H_2) = 130.7$ J/mol.K [63–65].

The results listed in Table 3 show that $MgNiH_3$ has a very low decomposition temperature equal to 76.61 K while $MgCoH_3$ has a high desorption temperature of order 560.97 K. This prevents their application for mobile hydrogen storage.

A mixture of $MgCoH_3$ and $MgNiH_3$ can have a great effect in enhancing the stability of the compounds, leading to a decomposition temperature of 351.33 K without a drastic reduction to their high volumetric capacity 133.73 g.H_2/l (see Table 3).

Willems et al. [66] suggest that more the hydride is stable more its volume variation relative to its intermetallic volume compound is low. The same principle can be applied here to the desorption temperature which decreases as a function of volume variation of the compounds ΔV/V (%) (see Fig. 3).

It can be concluded that the intermetallic hydride ($MgCo_{0.5}Ni_{0.5}H_3$) satisfies several hydrogen storage criteria (stability −40 kJ/mol.H_2 [62], decomposition temperature 289–393 K for a PEMFC [67] and volumetric capacity 70 g.H_2/l [68,69]) and therefore very advantageous as a material for hydrogen storage, except for the gravimetric capacity which remains limited 3.49 wt%. This compound is therefore well suited for applications where the gravimetric of the system is not a priority constraint, such as stationary applications in accordance with Sandia National Laboratories [70].

Thermodynamic properties

Knowledge of the thermodynamic properties is essential for studying crystal, for that the thermodynamic parameters of $MgCo_{0.5}Ni_{0.5}H_3$ such entropy (S), internal Energy (E) and the thermal expansion coefficient were determined through quasi-harmonic approximation (QHA) using the phonopy package [58] then Gibbs free energy G is computed through the obtained internal energy E and entropy S. The calculated values at temperature from 0 K to 1000 K are illustrated in Fig. 4 and Fig. 5.

Table 3 – Desorption temperatures and storage capacities for $MgCoH_3$, $MgNiH_3$ and $MgCo_{0.5}Ni_{0.5}H_3$.

Systems	Desorption temperatures (K)	Cv (g.H_2/l)	Cg (wt %)
$MgCoH_3$	560.97 this work; 482.42 [52]	137.38	3.483
$MgNiH_3$	76.61 this work; 66.80 [52]	130.01	3.478
$MgCo_{0.5}Ni_{0.5}H_3$	351.33 this work	133.73	3.488

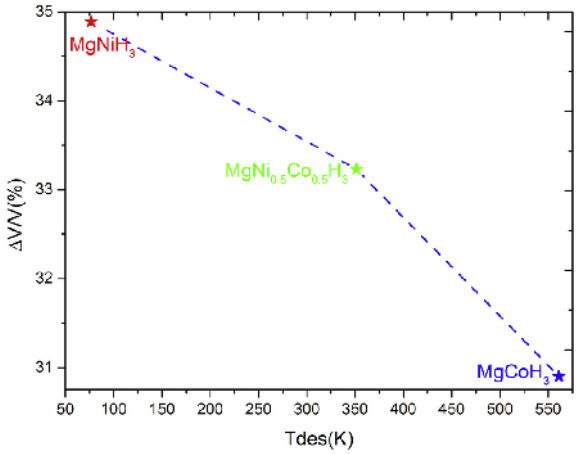

Fig. 3 – ΔV/V (%) percentages of the volume variation as function of desorption temperature for $MgCoH_3$, $MgNiH_3$ and $MgCo_{0.5}Ni_{0.5}H_3$.

The thermodynamic stability of a crystal structure depends on the Gibbs free energy. This is the minimum free energy of a crystal structure where the unit cell is allowed to change in response to temperature. The smaller the values of Gibbs free energy, the better the thermal stability of material will be.

In our case, the free energy is found to be negative and decreases with increasing temperature while the entropy increases in same temperature range, see Fig. 4.

The coefficient of thermal expansion (CTE) is another important thermodynamic quantity. It relates the change in volume of a material to change in temperature and it is given by:

$$\alpha_V = \frac{1}{V}\left(\frac{\partial V}{\partial T}\right)_p \tag{9}$$

A negative value for CTE indicates a contraction on negative thermal expansion (NTE) while a positive value indicates

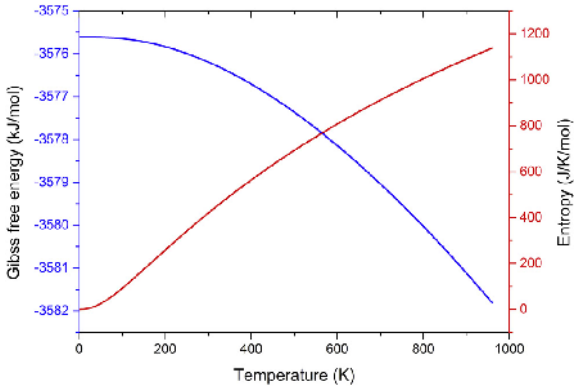

Fig. 4 – Gibss free energy and entropy for $MgCo_{0.5}Ni_{0.5}H_3$ as function of temperature.

Please cite this article in press as: Abdellaoui M, et al., The hydrogen storage properties of Mg-intermetallic-hydrides by ab initio calculations and kinetic Monte Carlo simulations, International Journal of Hydrogen Energy (2018), https://doi.org/10.1016/j.ijhydene.2018.04.225

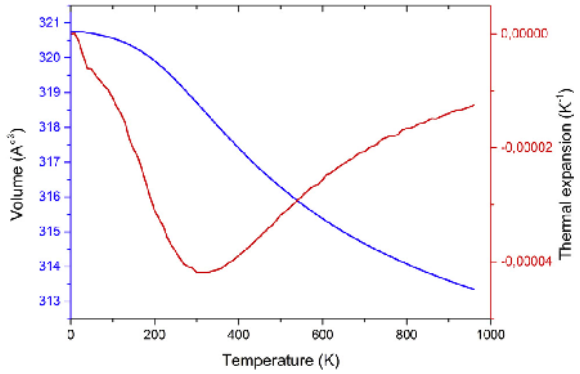

Fig. 5 – Volume variation and thermal expansion for $MgCo_{0.5}Ni_{0.5}H_3$ as function of temperature.

a positive thermal expansion (PTE). From Fig. 5, it is found to be dependent on temperature and remains negative in the whole range of temperature. This results is confirmed by the volume decrease as function of temperature which indicates a contraction of cell parameters.

Absorption time by kinetic Monte Carlo simulation

As is well known, the first principles calculations are limited to T = 0 K. It can inform us about the structural parameters, the total energies of the systems then the energy of formation and desorption temperature are computed through the obtained energies. But the kinetic absorption properties could be derived by using Kinetic Monte Carlo simulation at temperature different to 0 K.

To study the absorption kinetic of ours hydride systems by KMC simulation, a large number of energy barriers are computed in a 2 × 2 × 2 supercell for each studied systems and regrouped by range in Table 4.

Our calculations show that energies depend on the surrounding H and host atoms. When the number of hydrogen atoms increases in the system, the barriers get enlarged. For the same ath of diffusion, the H diffusion barrier energies decrease in the following order: $MgCoH_3$, $MgCo_{0.5}Ni_{0.5}H_3$ and $MgNiH_3$. This means that H atoms can move more easily inside MgNiH3 than $MgCo_{0.5}Ni_{0.5}H_3$ and $MgCoH_3$. In other words, the interaction between interstitial H atoms and Mg–Ni host is less strong than the interaction in $MgCoH_3$. Moreover, incorporation of Ni with Mg–Co–H weakens the interaction between interstitial H atoms and Mg–Co and thus enhances the stability of the systems, which is in agreement with the results reported in sections Stability of intermetallic hydrides: formation energy and Desorption temperatures. This will be confirmed later by the analysis of electronic structures in sections Electronic structure.

Table 4 – Activation energies intervals for H diffusion process in $MgCoH_3$, $MgNiH_3$, and $MgCo_{0.5}Ni_{0.5}H_3$.

Systems	Activation range energies
$MgCoH_3$	0.065_0.67
$MgCo_{0.5}Ni_{0.5}H_3$	0.064_0.66
$MgNiH_3$	0.056_0.65

Having determined the activation energies, the KMC method can be applied to study the kinetic properties of $MgNiH_3$, $MgCoH_3$ and $MgCo_{0.5}Ni_{0.5}H_3$. The absorption times at 400 K and 10 bar are represented for each system cited above in Fig. 6.

It can be noticed from Fig. 6 that the $MgNiH_3$ has a fast charging kinetic even at a temperature of 400 k. This can be explained on one hand by the low stability of the system (see sections Stability of intermetallic hydrides: formation energy) and on another hand by the fact that the calculated diffusion barriers for $MgNiH_3$ are very small compared to those of $MgCoH_3$ and $MgCo_{0.5}Ni_{0.5}H_3$. The fast absorption time could have a great advantage for hydrogen storage but the low stability (−9.96 kJ/mol.H_2) and the low desorption temperature (76.61 K) which exhibits $MgNiH_3$ hinders its application.

However, in previous sections we have shown that the mixture between $MgNiH_3$ and $MgCoH_3$ has great effect in enhancing its hydrogen storage properties. Thus, that increases the charging time but the absorption kinetic is still fast enough to fill the tank in only 4.6 min at 400 K and 10bar (see Fig. 6). This finding is pretty much similar to results of L. Xie et al. [71]. They show that the nanostructured $Mg_2Ni_{1-x}Co_x$ compounds present superior sorption kinetics then Mg2Ni.

The effect of the temperature on the charging kinetic is represented in Fig. 7 for $MgCoH_3$ for 10 bar and a temperatures ranging from 410 K to 450 K with a step of 10 K. It showed clearly that the reaction speed increases significantly by increasing the temperature.

For a temperature of 430 K the system already reaches the rate of saturation in only a period equivalent to 4.5 min.

In order to emphasize the fact that the $MgCo_{0.5}Ni_{0.5}H_3$ is one of the potential candidates for mobile application, we summarize in Table 5 [26] the absorption times for Mg based alloys obtained in our previous works.

We observe from Table 5 that the studied system in this paper $MgCo_{0.5}Ni_{0.5}H_3$ presents the shortest charging kinetic time compared to our previous work results.

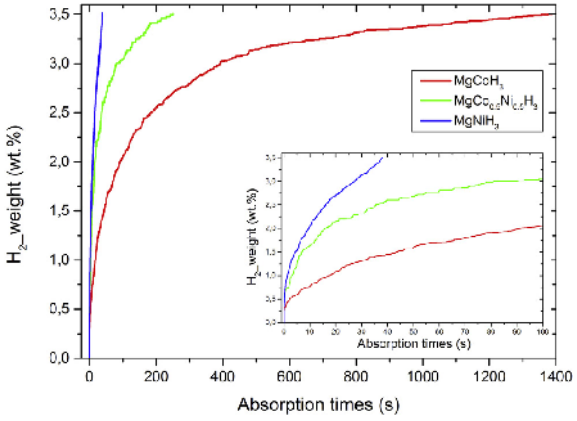

Fig. 6 – Charging kinetic for $MgNiH_3$, $MgCo_{0.5}Ni_{0.5}H_3$ and $MgCoH_3$ at 400 K and 10 bar.

Please cite this article in press as: Abdellaoui M, et al., The hydrogen storage properties of Mg-intermetallic-hydrides by ab initio calculations and kinetic Monte Carlo simulations, International Journal of Hydrogen Energy (2018), https://doi.org/10.1016/j.ijhydene.2018.04.225

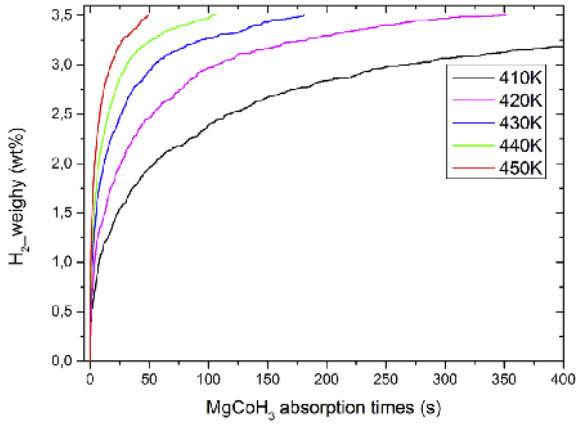

Fig. 7 – Charging kinetic for $MgCo_{0.5}Ni_{0.5}H_3$ at different temperatures and 10bar.

Table 5 – The charging kinetic times at 400 K and 10bar of our previous work results.

System at 400 K and 10bar	Absorption times (s)
MgH_2 ($Mg_{16}H_{32}$) at 633 K	4175.54004
$Mg_{15}AlH_{32}$	2532.40894
$Mg_{15}TiH_{32}$	1948.09314
$Mg_{15}VH_{32}$	1695.13867
$Mg_{15}FeH_{32}$	1461.11255
$Mg_{15}NiH_{32}$	740.96338
$Mg_8Co_4Ni_4H_{24}$ This work	276.52100

Electronic structure

The electronic structure calculations are performed to obtain density of states (DOS) which is the main tool used to elucidate the chemical bonding characteristics of the studied systems. For this purpose, it is interesting to study the effects of doping $MgCoH_3$ by Ni on the stability of this hydride.

The total DOS and the partial density of states (PDOS) of $MgCoH_3$ and $MgCo_{0.5}Ni_{0.5}H_3$ are plotted in Fig. 8 and Fig. 9, respectively.

It follows from Fig. 8 that there are two parts in the valence band (VB). The first part covers the band energy range from −10.00 to −5.00 eV, which is called the "lower VB" and is composed of a strong hybridization between H-s, Mg (s,p) and Co-3d states. The second part, with an energy ranging from −4.00 to 0.00 eV, is called the "high VB", originating almost exclusively from Mg (s,p) and Co-3d states.

However, the DOS of $MgCo_{0.5}Ni_{0.5}H_3$ exhibits a VB divided into the following three distinct regions (see Fig. 9): a lower VB with a band energy ranging from −10.00 to −5.00 eV composed of H (1,2,3)-s, Mg (s,p) and the 3d states of Co(1,2) and Ni(1,2); the second part with an energy range from −4.0 to −2.5eV is called the "middle VB" and presents a weak hybridization between Mg(s,p), Co1-3d, Co2-3d and the N_i1-3d, N_i2-3d states; and the last part is the "high VB" (from −2.50 eV to 0.00 eV), which exhibits strong hybridization between the Co-3d and Ni-3d states. Beyond the Fermi level, the DOS is dominated by the Mg(s,p) states. Moreover, the analysis of the $MgCoH_3$ DOS reveals the occurrence of the following three bonds: a weak bond between Mg–Co, another very weak bonding between Mg–H, and a strong bond between H–Co that reinforces the stability of this system. In addition to the above mentioned bonds, the DOS of $MgCo_{0.5}Ni_{0.5}H_3$ exhibits a new very strong bond between Co–Ni, whereas the Co–H form a very weak bond because the hybridization between the orbital of Co and H atoms is not relevant.

Thus, the H atoms are trapped more stably inside $MgCoH_3$ than $MgCo_{0.5}Ni_{0.5}H_3$ alloys because the strong hybridization between Co and Ni weakens the H–Co bond. In other words, incorporation of 50% of Ni into intermetallic hydride can efficiently reduce the interactions between interstitial H atoms and the Mg–Co host, which leads to a reduction in the system stability; this observation may explain the results reported in previous sections.

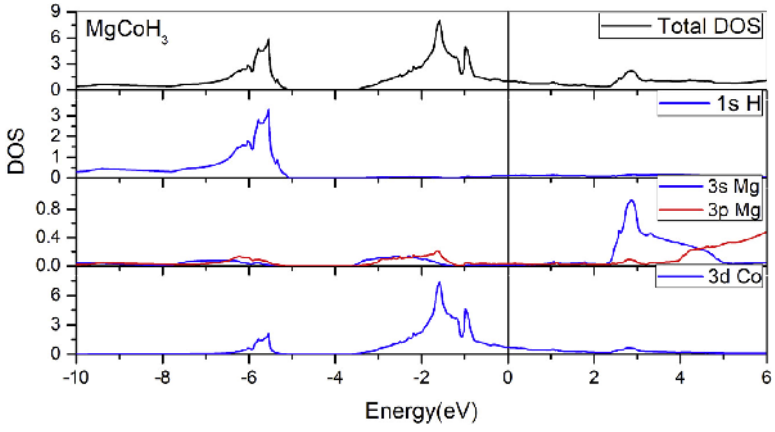

Fig. 8 – Total and partial DOS of $MgCoH_3$ compound.

Please cite this article in press as: Abdellaoui M, et al., The hydrogen storage properties of Mg-intermetallic-hydrides by ab initio calculations and kinetic Monte Carlo simulations, International Journal of Hydrogen Energy (2018), https://doi.org/10.1016/j.ijhydene.2018.04.225

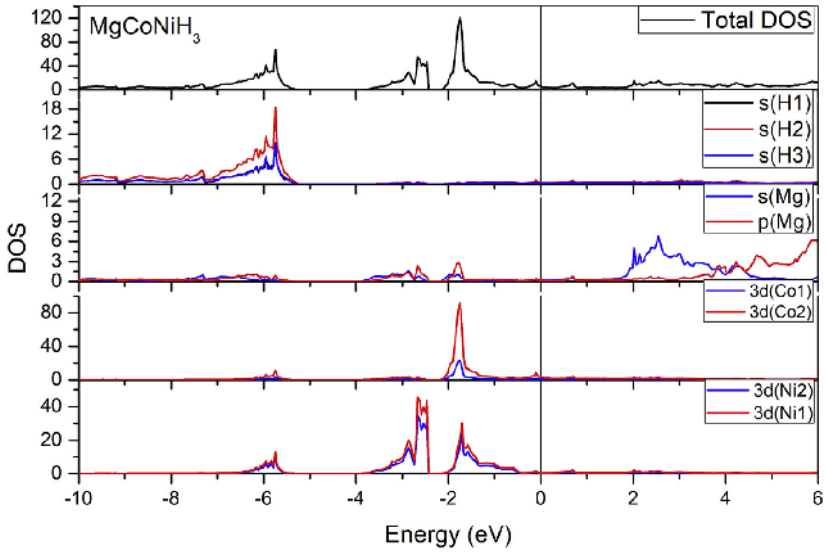

Fig. 9 – Total and partial DOS of the $MgCo_{0.50}Ni_{0.50}H_3$ compound.

Conclusion

First-principle calculations and kinetic Monte-Carlo simulations are performed to study the hydrogen storage properties of the intermetallic hydrides $MgNiH_3$, $MgCoH_3$ and $MgCo_{0.5}Ni_{0.5}H_3$. Based on KMC simulations, heat of formation and desortion temperature, we have shown that the fast absorption kinetic of $MgNiH_3$ could have been a great advantage for hydrogen storage but its low stability (−9.96 kJ/mol.H_2) and its low temperature (76.61 K) hinders its use. However, preparing a mixture between $MgNiH_3$ and $MgCoH_3$ has great effect in enhancing its hydrogen storage properties. Thus, we have shown that mixture enhances the stability ($\Delta H = -45.92$ kJ/mol.H_2) and desorption temperature ($T = 351.33$ K) of $MgCo_{0.5}Ni_{0.5}H_3$ without decreasing its high volumetric capacity 133.73 g.H_2/l and the absorption kinetic that exhibites is still fast enough to fill the tank in only 4.6 min at 400 K and 10 bar. Finally, thermodynamic properties including entropy S, Gibbs free energy G and thermal expansion coefficient are obtained and analyzed.

REFERENCES

[1] Cabo M, Garroni S, Pellicer E, Milanese C, Girella A, Marini A, et al. Int J Hydrogen Energy 2011;36(9):5400–10.
[2] Liu C, Li F, Ma LP, Cheng HM. Adv Mater 2010;22:E28–62.
[3] Aguey-Zinsou K, Ares-Fernández J. Energy Environ Sci 2010;3:526–43.
[4] Jain I, Lal C, Jain A. Int J Hydrogen Energy 2010;35:5133–44.
[5] Zhang F, Zhao P, Niu M, Maddy J. Int J Hydrogen Energy 2016;41:14535–52.
[6] Wu Z, Zhu L, Yang F, Jiang Z, Zhang Z. Int J Hydrogen Energy 2016;41:18550–61.
[7] Belkbir L, Joly E, Gerard N. Int J Hydrogen Energy 1981;6:2145–56.
[8] Zheng J, Li X, Akiba E. Nano Energy 2012;1:590.
[9] Kurko S, Matovic L, Novakovic N, Matovic B, Jovanovic Z, Paskas Mamula B, et al. Int J Hydrogen Energy 2011;36:1184–9.
[10] Bogdanovic B, Bohmhammel K, Christ B, Reiser A, Schlichte K, Vehlen R, et al. J Alloy Compd 1999;84:282.
[11] Wu Z, Yang F, Zhu L, Feng P, Zhang Z, Wang Y, et al. Int J Hydrogen Energy 2016;41:16108–21.
[12] Boncour VP. J Adv Sci 2007;9:16–21.
[13] Rusman NAA, Dahari M. Int J Hydrogen Energy 2016;41:12108–26.
[14] Hyunjeong K, Nakamur J, Huaiyu S, Yumiko N, Akiba E, Chapman KW, et al. J Phys Chem C 2011;115:20335–41.
[15] Chubin W, Antonov VE, Denys RV, Kulakov VI, Yartys VA. J Prog Nat Sci Mater Int 2017;27:74–80.
[16] Takamura H, Kakuta H, Goto Y, Watanabe H, Kamegawa A, Okada M, et al. J. Alloys Compd 2005;404–406:372–6.
[17] Chou HS, Huang JC, Lai YH, Chang LW, Du XH, Chu JP, et al. J Alloys Compd 2009;483:341–5.
[18] Van Mal H, Buschow K, Miedema A. J Less-Common Met 1974;35:65–76.
[19] Mezbahul-Islam M, Kevorkov D, Meradj M. J Chem Thermodynamics 2008;40:1064–76.
[20] Bhihi M, Lakhal M, Labrim H, Benyoussef A, El Kenz A, Mounkachi O, et al. J Chin Phys B 2012;21:097501.
[21] Bhihi M, El Khatabi M, Lakhal M, Naji S, Labrim H, Benyoussef A, et al. Int J Hydrogen Energy 2015;40:8356–61.
[22] El Khatabi M, Bhihi M, Naji S, Labrim H, Benyoussef A, El Kenz A, et al. Int J Hydrogen Energy 2016;41:4712–8.
[23] Bhihi M, Lakhal M, Naji S, Labrim H, Belhaj A, Benyoussef A, et al. Bull Mater Sci 2014;37:731–6.
[24] Abdellaoui M, Lakhal M, Bhihi M, El Khatabi M, Benyoussef A, El Kenz A, et al. Int J Hydrogen Energy 2016;41(45):20908–13.
[25] Reule H, Hirscher M, Weißhardt A, Krönmuller H. J Alloys Compd 2000;305:246–52.
[26] Lakhal M, Bhihi M, Benyoussef A, El Kenz A, Loulidi M, Naj S. Int J Hydrogen Energy 2015;40(18):6137–44.
[27] Kamata Y, Kuriiwa T, Kamegawa A, Okada M. Mater Trans 2009;50(8):2064–8.
[28] Orimo S, Ikeda K, Fujii H, Saruki S, Fukunaga T, Zuttel A. J Acta Mater 1998;46:4519.

Please cite this article in press as: Abdellaoui M, et al., The hydrogen storage properties of Mg-intermetallic-hydrides by ab initio calculations and kinetic Monte Carlo simulations, International Journal of Hydrogen Energy (2018), https://doi.org/10.1016/j.ijhydene.2018.04.225

ARTICLE IN PRESS

INTERNATIONAL JOURNAL OF HYDROGEN ENERGY XXX (2018) 1–7

Available online at www.sciencedirect.com

ScienceDirect

journal homepage: www.elsevier.com/locate/he

Vibrational and thermodynamic properties of $LiBH_4$ polymorphs from first-principles calculations

H. Benzidi [a], *M. Garara* [a], *M. Lakhal* [a], *M. Abdalaoui* [a], *A. Benyoussef* [b], *A. El kenz* [a], *M. Louilidi* [a], *M. Hamedoun* [b], *O. Mounkachi* [a,b,*]

[a] *Laboratoire de Matière Condensée et Sciences Interdisciplinaires (LaMCScI), B.P. 1014, Faculty of Science, Mohammed V University, Rabat, Morocco*

[b] *Materials and Nanomaterials Centre, Moroccan Foundation for Advanced Science, Innovation and Research, MAScIR, Rabat, Morocco*

ARTICLE INFO

Article history:
Received 17 July 2017
Received in revised form
6 February 2018
Accepted 7 February 2018
Available online xxx

Keywords:
First principles calculations
Hydrogen storage
$LiBH_4$
Enthalpy
Hydride
Phonon

ABSTRACT

The study of phonons describes the thermodynamic properties behavior of compounds with small atoms because phonons have an important influence on its properties. Lithium borohydride, $LiBH_4$, is one of the suitable materials for hydrogen storage solid state. Although the transformations of Lithium borohydride $LiBH_4$ were repeatedly studied by experiments and fundamental side, these transformations are still under discussion. In the present work, the mode vibrational analysis of orthorhombic and hexagonal $LiBH_4$ structures were considered with ab initio lattice-dynamics based on the quasi-harmonic approximation approach as implemented in Phonopy code. The results show that the orthorhombic structure is thermodynamically stable, while the hexagonal structure is unstable owing to the presence of negative mode frequency. The thermal expansion behavior and various thermodynamic properties stability like heat capacity, entropy and Helmholtz energy were also studied and the obtained results are in good agreement with experiments. This shows a deep connection between stability and strength and helps researchers to estimate accurately the thermodynamic performance of $LiBH_4$ materials.

Introduction

Lithium borohydride is known as a considerable potential candidate for solid hydrogen storage state, owing to its competence to store 18 wt% of hydrogen, which is substantially larger than the DOE roadmap value for 2015 [1]. Nevertheless, the phase transition mechanisms of $LiBH_4$ have not fully understood. Consequently, it is important to explain in detail the thermodynamic properties behavior of $LiBH_4$ according to temperature. Therefore, basic research studied the crystal structure of $LiBH_4$ at several temperatures and pressures and the complex phase transition scheme was analyzed [2,3]. At ambient conditions, lithium borohydride crystallized in the orthorhombic structure (Pnma, 62) and go through a first-order phase transition on heating at 381 K to a hexagonal high-temperature phase ($P6_3mc$, 186). At ambient temperature, a phase transition into a high-pressure phase (Ama2) is observed around 0.6 GPa and a second transition at

* *Corresponding author*. Laboratoire de Matière Condensée et Sciences Interdisciplinaires (LaMCScI), B.P. 1014, Faculty of Science, Mohammed V University, Rabat, Morocco.
E-mail addresses: o.mounkachi@mascir.com, o.mounkachi@gmail.com (O. Mounkachi).

https://doi.org/10.1016/j.ijhydene.2018.02.042
0360-3199/

Please cite this article in press as: Benzidi H, et al., Vibrational and thermodynamic properties of $LiBH_4$ polymorphs from first-principles calculations, International Journal of Hydrogen Energy (2018), https://doi.org/10.1016/j.ijhydene.2018.02.042

18 GPainduce to a cubic phase (Fm-3m) [4]. The melting of the compound appears at around 550 K. All reported experimental structural studies of $LiBH_4$ have mentioned a tragic increase in hydrogen thermal displacements by almost 2 orders of degree from 4 to 400 K. This was attributed to dynamical disorder in the hexagonal high-temperature phase [5,6]. Buchter et al. [7] reported that for the energies smaller than ~ 15 meV, the phonon density of states of $LiBH_4$ in the low-temperature phase depends quadratically on the phonon energy although for the high temperature phase a continuous dependency is examined, affirming a high lattice anharmonicity in the high-temperature phase. First-principles calculations were very acknowledged to augur structures properties of $LiBH_4$ polymorphs. Despite the fact that, most calculations were realized for the ground state at the zero temperature, a recent advance in computational technique enables us to determine the entire phonon dispersion of solids. Thus, can compute specific heats, vibrational entropy, furthermore many thermodynamic quantities according of temperature. The present study purpose of clarifying the origin of phase transition in $LiBH_4$ by first principles lattice dynamics calculations. Also, the thermodynamics properties of the $LiBH_4$ were be calculated in order to compare the phase transition temperature between orthorhombic and hexagonal structure. In section computational method, the details and methods to perform our calculation are given. Section result and discussion is devoted to the presentation, the discussion and the comparison of numerical results. In the last section, the conclusion is given.

Computational method

The first-principles calculations within the density functional theory (DFT) [8] were performed using the Quantum Espresso program [9]. The generalized gradient approximation (GGA) [11] in the form of the Perdew-Burke-Ernzerhof (PBE) functional [10] was used to solve the Kohn-Shame equation. The structures were optimized by a full relaxation of the ion positions as well as the volume of the unit cell, the electronic ground-state steps were allowed to converge to an accuracy of 10^{-8} Ry. During each of the electronic steps, a plane-wave energy cutoff of 50 Ry was used for all calculations. The Brillouin zones of the unit cells are represented by Monkhorst-Pack special k-point scheme with 8 x 10 x 8 for orthorhombic LiBH4 (o-$LiBH_4$) and 10 x 10 x 8 for hexagonal $LiBH_4$ (h-$LiBH_4$) grid meshes. Computational settings such as plane wave cutoff energy, the number of k-points, and convergence criteria were carefully chosen for high numerical accuracy. Once the converged structures for the both orthorhombic and hexagonal structure were obtained, in order to access the stability of materials, the vibrational density of states (VDOS) was calculated using the software PHONOPY [12]. The VDOS is evaluated using a finite displacement method based on the Parlinski-Li-Kawazoe method. Displacements of 0.02 Å were used for the calculation of the force constants in the displacement method [13]. A larger displacement was used to avoid possible numerical inaccuracies in the system. A complete force constant matrix was obtained, and the phonon frequencies (ω) were then calculated by diagonalization of the dynamical matrix, over the electronic density of states. The Helmholtz energy was thus obtained by combining them with the 0 K total energy calculated within (Plane-Wave Self-Consistent Field method).

Result and discussion

Crystalline structures and optimizations

Using first principles calculations, two $LiBH_4$ phases (o-$LiBH_4$ and h-$LiBH_4$) were built by using crystallographic data in Ref. [14], then, their cell parameters and atomic positions were optimized. As a result, the corresponding total energies as function of the unit cell volume are obtained and plotted in Fig. 1. The relaxed lattice constants and atom positions of $LiBH_4$ phases along with the experimental data are summarized in Table 1. The optimized lattice parameters of both structures are in good agreement with previous theoretical and experimental results [14–16].

Furthermore, the bond length between two different atoms is also calculated and the results are listed in Table 2. This

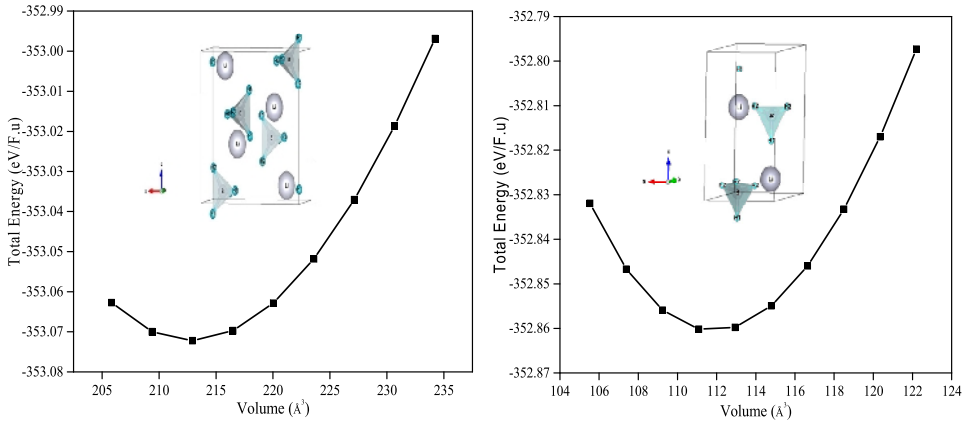

Fig. 1 – Total energy versus primitive unit cell volume of o-$LiBH_4$ (left) and h-$LiBH_4$ (right).

Please cite this article in press as: Benzidi H, et al., Vibrational and thermodynamic properties of $LiBH_4$ polymorphs from first-principles calculations, International Journal of Hydrogen Energy (2018), https://doi.org/10.1016/j.ijhydene.2018.02.042

Table 1 – Lattice parameters and positions for hexagonal and orthorhombic symmetries. Experimental results are included for comparison.

	Parameters			Positions						
		Calculated	Experimented [14]		Calculated			Experimented [14]		
o-$LiBH_4$				Li	0.1567	0.250	0.1015	0.157	0.250	0.1015
	a	7.2145	7.1785	B	0.3092	0.250	0.4275	0.304	0.250	0.4305
	b	4.3652	4.4368	H	0.8090	0.250	0.9275	0.900	0.250	0.9560
	c	6.6180	6.8032	H	0.4102	0.250	0.2719	0.404	0.250	0.2800
				H	0.2085	0.024	0.4270	0.172	0.054	0.4280
h-$LiBH_4$	a	4.1898	4.2763	Li	1/3	2/3	0.1107	1/3	2/3	0
	b	4.1898	4.2763	B	1/3	2/3	0.5362	1/3	2/3	0.5530
	c	7.3072	6.9484	H	1/3	2/3	0.3697	1/3	2/3	0.3700
				H	0.174	0.349	0.5927	0.172	0.344	0.6240

Table 2 – Interatomic distances (Å) of hydrogen and other neighboring atoms. Experimental results are included for comparison.

System	Interatomic distances (Å)							
	Calculated (at 0 K)				Experimented [7,17]			
	Li-H	B-H	H-H	Li-B	Li-H	B-H	H-H	Li-B
o-$LiBH_4$	1.9831	1.2234	1.9691	2.3408	1.980	1.25	1.80	2.475
	2.0516	1.2273	1.9934	2.5229	2.090	1.28	1.73	2.521
	2.0516	1.2289	2.0167	2.5237	2.150	1.04	2.13	2.542
	2.2499				2.289			
	2.3162				2.380			
h-$LiBH_4$	1.8924	1.2164	1.9919	2.4796	2.300	1.27	2.13	2.496
	2.0999	1.2219	2.1978	–	2.570	1.29	2.74	3.106
	2.0999		2.9138		2.629			
	2.9922				2.870			

result is in good agreement with recent theoretical results obtained by ab initio calculations [17] where the relative differences between the theoretical and experimental of the interatomic distances are essentially due to the larger difference of the temperature factors.

Phonon dispersion

Once the converged structures for each phase were obtained, the vibrational density of state (VDOS) are evaluated with a method utilizes a phonon calculation at 0 K to see if there are imaginary phonon modes, also called soft mode. The unit cell of orthorhombic (o-$LiBH_4$) structure holding four formula units have 72 modes, while the hexagonal (h-$LiBH_4$) structure holding two formula units have 36 modes. The Fig. 2 shows the density of states of phonons in both structures of $LiBH_4$ which is divided into three regions for o-LiBH4 (Fig. 2a) and four regions for h-LiBH4 hexagonal phase (Fig. 2b). Similar to the previous works [18,19], the present study shows that h-$LiBH_4$ ($P6_3mc$) phase (Fig. 2b) has a phonon with an imaginary frequency which indicates that the hexagonal structure is unstable. Or, the absence of any imaginary phonon frequencies in the entire Brillion zone of Fig. 2a confirms that o-LiBH4 (Pnma) structure is dynamically stable.

In the phonon PDOS (Fig. 3) for o- and h-$LiBH_4$, the region at low frequencies are composed of Li, B and H atoms states, by reason of the heavy weight of B and Li which is greater than hydrogen atoms and the vibration frequency of these atoms is visibly below than that of the hydrogen atom. While between 30 and 40 THz, two peaks are observed and composed of H atoms and a small fraction of states of B atoms. The apparent peaks at high frequencies are mostly composed of H states since its atomic mass is much lighter than those of the other atoms. The only noticeable difference between the orthorhombic phase (Fig. 3a) and hexagonal (Fig. 3b) is that the peak composed of H atoms appear at negative frequencies for h-$LiBH_4$.

In the phonon PDOS (Fig. 3) for o- and h-$LiBH_4$, the region at low frequencies are composed of Li, B and H atoms states, while between 30 and 40 THz, two peaks are observed and composed of H atoms and a small fraction of states of B atoms. The apparent peaks at high frequencies are mostly composed of H states since its atomic mass is much lighter than those of the other atoms. The only noticeable difference between the orthorhombic phase and hexagonal is that the peak composed of H atoms appear at negative frequencies for h-$LiBH_4$.

Thermodynamic properties

Based on the phonon frequencies, the thermodynamic functions of $LiBH_4$ phases can be obtained. The Helmholtz free energy could be written as:

$$F = E + H_{vib} + TS_{vib} \quad (1)$$

where, E, H_{vib} and $S_{vib\ are}$ the static electronic energy of the crystal, internal energy and entropy contributing to the lattice

Please cite this article in press as: Benzidi H, et al., Vibrational and thermodynamic properties of $LiBH_4$ polymorphs from first-principles calculations, International Journal of Hydrogen Energy (2018), https://doi.org/10.1016/j.ijhydene.2018.02.042

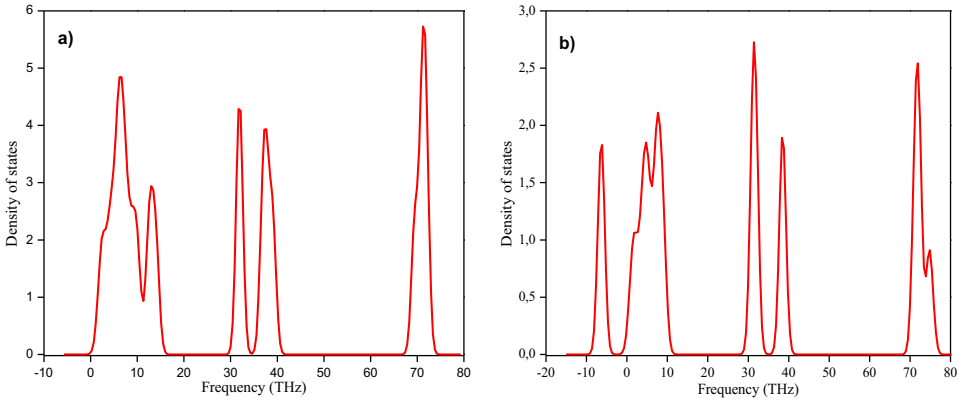

Fig. 2 – Phonon density of states of o-$LiBH_4$ (a) and h-$LiBH_4$ (b).

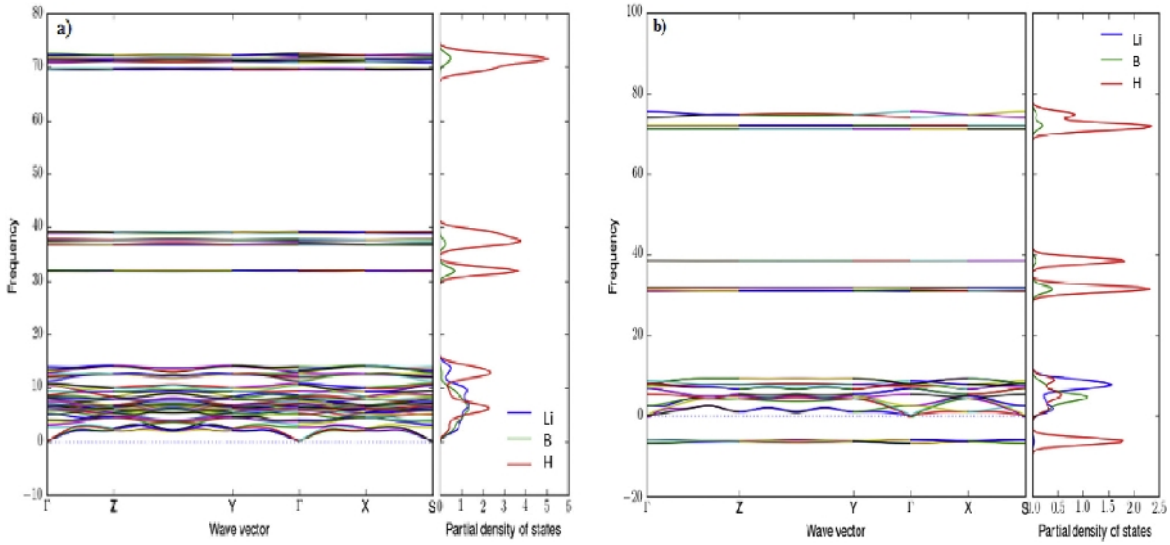

Fig. 3 – Phonon band structure and PDOS of o-$LiBH_4$ (a) and h-$LiBH_4$(b).

vibration. Within the harmonic approximation these contributions are given by:

$$H_{vib}(T) = \sum_i \frac{1}{2}\hbar\omega_i + \hbar\omega_i\left[\exp\left(\frac{\hbar\omega_i}{K_\beta T}\right) - 1\right]^{-1} \quad (2)$$

$$S_{vib}(T) = k_\beta \sum_i \frac{\frac{\hbar\omega_i}{K_\beta T}}{\exp\left(\frac{\hbar\omega_i}{k_\beta T}\right) - 1} - \ln\left[1 - \exp\left(-\frac{\hbar\omega_i}{k_\beta T}\right)\right] \quad (3)$$

where the sums run over vibrational frequencies, k_B is the Boltzmann factor and T is the absolute temperature. The zero-point energy ZPE can be recovered from equation (2) in the limit H_{vib} (T = 0); the Fig. 4 plots the calculated H_{vib} and S_{vib} of $LiBH_4$ phases as a function of temperature. Although having different structures, the H_{vib} and S_{vib} exhibit similar temperature dependencies for both structures. From Fig. 4a, it is noticed that the ZPE of h-$LiBH_4$ is about 7 kJ mol^{-1} lower than that of o-$LiBH_4$. Above 300 K, the internal energies H_{vib} increase almost linearly with temperature, tending to display k_BT behavior. Even more, at low temperature, the entropy S_{vib} of h-$LiBH_4$ is higher than that of o-$LiBH_4$, while increasing the temperature the o-$LiBH_4$ entropy becomes superior (see Fig. 4b).

The zero-point, enthalpy and entropic contributions to the free energy of the different phases are summarized in Table 3. As a further test of our computational methodology, there, our calculations results are compared to other values reported in the literature [20,22] and find good agreement.

The molar heat capacity has an importance in terms of energy, time and costs involved in changing temperatures of objects. Hence it is important as it will present a notion of how much energy will be appropriate to heat or cool an object of a given mass by a given supply. This will give information as to how long the heating or cooling process will take under a

Please cite this article in press as: Benzidi H, et al., Vibrational and thermodynamic properties of $LiBH_4$ polymorphs from first-principles calculations, International Journal of Hydrogen Energy (2018), https://doi.org/10.1016/j.ijhydene.2018.02.042

Table 3 – Comparison of vibrational enthalpy and entropy results with experimental data.

System	ZPE = H_{vib} (T = 0) (kJ mol^{-1})	ZPE other works [20,22]	$E_{vib} = H_{vib}-ZPE$	E_{vib} [20]	S_{vib} (T = 300K) (J mol^{-1} K^{-1})	S_{vib} [20]
o-$LiBH_4$	106.03	107.1106.5, 108.1	10.8 (300 K)	10.8	73.97	63.6
h-$LiBH_4$	99.9	–	21.2 (450 K)	–	75.57	–

given supply. The molar heat capacity at constant volume C_v and at constant pressure C_p are given by equations (4) and (5) and the results are presented in Fig. 5 and Table 4:

$$C_v = \left(\frac{\partial E}{\partial T}\right)_v = \sum_i k_\beta \left(\frac{\hbar\omega_i}{k_\beta T}\right)^2 \frac{\exp\left(\frac{\hbar\omega_i}{k_\beta T}\right)}{\left[\exp\left(\frac{\hbar\omega_i}{k_\beta T}\right)-1\right]^2} \quad (4)$$

$$C_p(T,p) = -T\frac{\partial^2 G(T,p)}{\partial T^2} = C_v(T,V(T,p)) + T\frac{\partial V(T,p)}{\partial T}\frac{\partial S(T,V)}{\partial V}\Big|_{V=V(T,p)} \quad (5)$$

At constant pressure, some of the heat goes into expanding the system, which does external work, and therefore leaves less energy available for raising the temperature. The heat capacity depends on the temperature, it increases with increasing temperature and this translates an accumulation of energy in the vibrational movement. Beyond room temperature, experimental values for the molar heat capacity of orthorhombic and hexagonal phases of $LiBH_4$ were realized by many authors. El Kharbachi et al. [23] deliberate the heat capacity from ambient temperature to approaching the melting point of the compound at 553 K using calorimetric measurements and found the following value C_p (285.6 K) = 76.6 ± 0.9 J K^{-1} mol^{-1}. At lower temperatures (i.e. 15–303 K), Hallett and Johnston [24] found the heat capacity of $LiBH_4$ by adiabatic calorimetry and proposed, for the standard molar heat capacity and entropy at 298.15 K, values of C_p (298.15 K) = 82.563 J K^{-1} mol^{-1} and S (298.15 K) = 75.860 ± 0.125 J K^{-1} mol^{-1}. Kim et al. [25] calculated by ab-initio methods the molar heat capacity for the hexagonal and orthorhombic phases from 0 to 1000 K. The agreement with the experimental data is limited, mainly at high temperatures. In fact, at room temperature, the value of Cp for the orthorhombic phase is around 10 J K^{-1} mol^{-1} lower than that obtained experimentally, while for the hexagonal phase at 450 K there is a difference about 23 J K^{-1} mol^{-1}. At constant volume, all the heat that goes into the system increases the temperature of the system and no external work is done. According to the phase diagram for $LiBH_4$ composition [3], at high temperature a coexistence of different phase (H_2 gas, LiH solid, B solid) can be observed between 450K and 850 K then the LiH decomposes and transforms to Li-liquid. A regular theory of heat capacity for liquids has not been accomplished and is still a rich area of research [27]. Thus, we find that we need more heat to raise the temperature of unit mass of the system over 1 K under constant pressure conditions, compared to the heat required to increment the temperature of the same unit mass of the system through 1K and under constant volume conditions.

The coefficient of thermal expansion (CTE) relates the change in volume of a material as a function of temperature change under constant pressure, and it is given by:

$$\alpha_v = \frac{1}{V}\left(\frac{\partial V}{\partial T}\right)_p \quad (6)$$

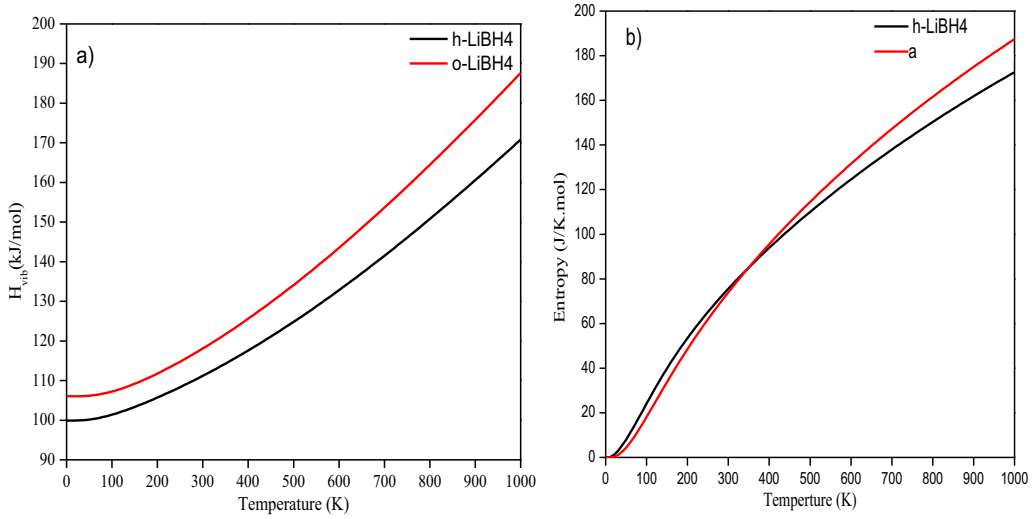

Fig. 4 – Vibrational enthalpy (a) and entropy (b) as function of temperature of both $LiBH_4$ structures.

Please cite this article in press as: Benzidi H, et al., Vibrational and thermodynamic properties of $LiBH_4$ polymorphs from first-principles calculations, International Journal of Hydrogen Energy (2018), https://doi.org/10.1016/j.ijhydene.2018.02.042

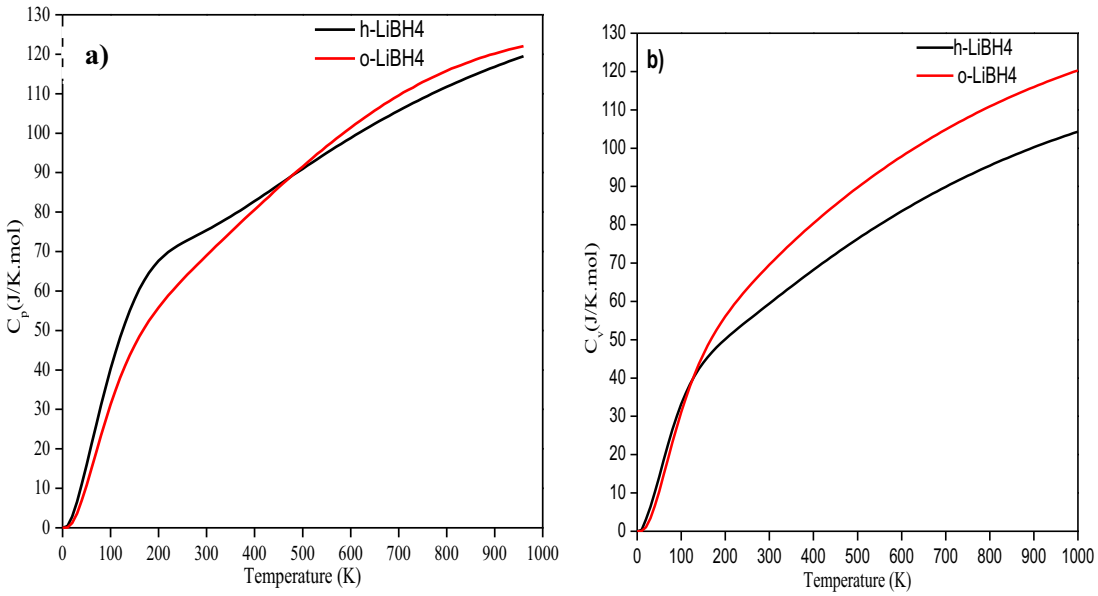

Fig. 5 – Calculated heat capacity as function of temperature of o-$LiBH_4$ and h-$LiBH_4$ at constant pressure (a) and constant volume (b).

Table 4 – Calculated heat capacity of o-$LiBH_4$ and h-$LiBH_4$ at constant pressure and constant volume compared with other calculated and experimental data.

System	C_p(J K^{-1} mol^{-1})	C_p other works	C_v(J K^{-1} mol^{-1})	C_v other works
o-$LiBH_4$	69.03 (300 K)	76.6 ± 0.9 (285.6 K) [23] 81.51 (298 K) [26]	59.45 (300 K)	–
h-$LiBH_4$	86.87 (450 K)	95.43 (450 K) [26]	85.23 (450 K)	–

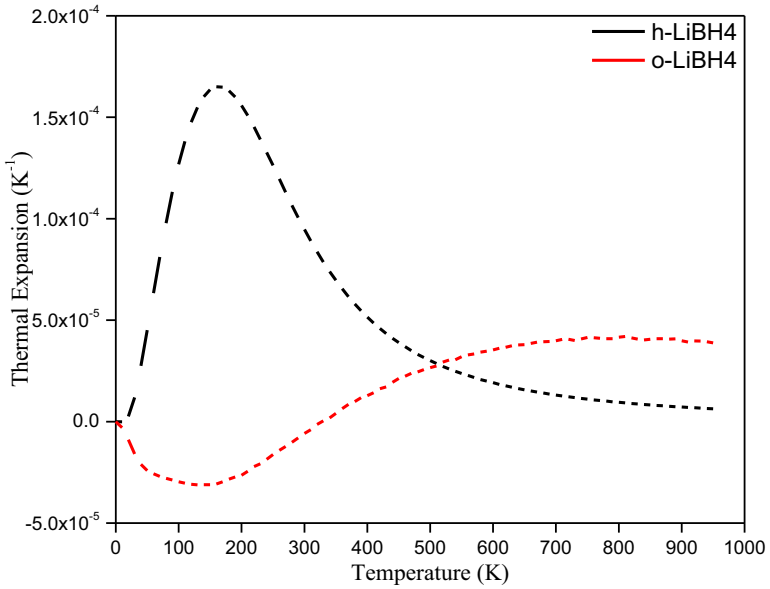

Fig. 6 – The coefficient of thermal expansion as function of temperature of o-$LiBH_4$ and h-$LiBH_4$.

Please cite this article in press as: Benzidi H, et al., Vibrational and thermodynamic properties of $LiBH_4$ polymorphs from first-principles calculations, International Journal of Hydrogen Energy (2018), https://doi.org/10.1016/j.ijhydene.2018.02.042

A negative value for CTE indicates a contraction on negative thermal expansion (NTE) while a positive value indicates a positive thermal expansion (PTE). From Fig. 6, it is found to be strongly dependent on temperature but remains negative for o-$LiBH_4$ (-2.5×10^{-5}) and positive for h-$LiBH_4$ ($1{,}6 \times 10^{-4}$) until to 500 K. Above 500 K for both phases are near ZTE.

Conclusion

First-principles DFT calculations combined with a quasi-harmonic approximation method were used to investigate phonon contribution of $LiBH_4$ polymorphs. The obtained optimized structural parameters of Pnma and P63mc structures are in good agreement with other results. Computed vibrational properties were used to illustrate thermodynamic properties of $LiBH_4$ phases (orthorhombic and hexagonal) like the vibrational enthalpy, entropy and the molar heat capacity etc. these properties are collected in order to compare other theoretical and experimental finding to our ab-initio calculation. Our obtained results are in good agreement with existing data. Thus, allowed us to understand some properties of a small atom like hydrogen which are not observable experimentally.

REFERENCES

[1] Satyapal S, Petrovic J, Read C, Thomas G, Ordaz G. The U.S. Department of Energy's National Hydrogen Storage Project: progress towards meeting hydrogen-powered vehicle requirements. Catal Today 2007. https://doi.org/10.1016/j.cattod.2006.09.022.
[2] Meisner GP, Scullin ML, Balogh MP, Pinkerton FE, Meyer MS. Hydrogen release from mixtures of lithium borohydride and lithium amide: a phase diagram study. J Phys Chem B 2006. https://doi.org/10.1021/jp056019b.
[3] Yan Y, Remhof A, Hwang S-J, Li H-W, Mauron P, Orimo S, et al. Pressure and temperature dependence of the decomposition pathway of LiBH4. Phys ChemChem Phys 2012. https://doi.org/10.1039/c2cp40131b.
[4] Dmitriev V, Filinchuk Y, Chernyshov D, Talyzin A, Ilewski A, Andersson O, et al. Pressure-temperature phase diagram of LiBH4: synchrotron X-ray diffraction experiments and theoretical analysis. Phys Rev B 2008. https://doi.org/10.1103/PhysRevB.77.174112.
[5] Gomes S, Hagemann H, Yvon K. Lithium boro-hydride LiBH4: II. Raman spectroscopy. J Alloys Compd 2002. https://doi.org/10.1016/S0925-8388(02)00668-0.
[6] Hagemann H, Gomes S, Renaudin G, Yvon K. Raman studies of reorientation motions of [BH4]- anionsin alkali borohydrides. J Alloys Compd 2004. https://doi.org/10.1016/S0925-8388(03)004687.
[7] Buchter F, Łodziana Z, Mauron P, Remhof A, Friedrichs O, Borgschulte A, et al. Dynamical properties and temperature induced molecular disordering of LiBH4 and LiBD4. Phys Rev B Condens Matter Mater Phys 2008. https://doi.org/10.1103/PhysRevB.78.094302.
[8] Kresse G, Furthmüller J, Efficient iterativeKresse G, Furthmüller J. Efficient iterative schemes for ab initio total-energy calculations using a plane-wave basis set. Phys Rev B 1996;54(16):11169–86. Retrieved from: http://link.aps.org/doi/10.1103/PhysRevB.54.1. Phys Rev B 1996.
[9] Giannozzi P, Baroni S, Bonini N, Calandra M, Car R, Cavazzoni C, et al. Quantum espresso: a modular and opensource software project for quantum simulations of materials. J Phys Condens Matter 2009;21:395502. https://doi.org/10.1088/0953-8984/21/39/395502.
[10] Perdew JP, Chevary JA, Vosko SH, Jackson KA, Pederson MR, Singh DJ, et al. Atoms, molecules, solids, and surfaces applications of the generalized gradient approximation for exchange and correlation (vol. 46, Pg 6671, 1992). Phys Rev B 1992. https://doi.org/10.1103/Physrevb.48.4978.2.
[11] Perdew JP, Burke K, Ernzerhof M. Generalized gradient approximation made simple. Phys Rev Lett 1996;77:3865e8. https://doi.org/10.1103/PhysRevLett.77.3865.
[12] Togo A, Tanaka I. First principles phonon calculations in materials science. Scr Mater 2015. https://doi.org/10.1016/j.scriptamat.2015.07.021.
[13] Parlinski K, Li Z, Kawazoe Y. First-principles determination of the soft mode in cubic ZrO2. Phys Rev Lett 1997. https://doi.org/10.1103/PhysRevLett.78.4063.
[14] Soulié JP, Renaudin G, Erný R, Yvon K. Lithium boro-hydride LiBH4: I. Crystal structure. J Alloys Compd 2002. https://doi.org/10.1016/S0925-8388(02)00521-2.
[15] Miwa K, Ohba N, Towata SI, Nakamori Y, Orimo SI. First-principles study on lithium borohydride LiBH4. Phys Rev B Condens Matter Mater Phys 2004. https://doi.org/10.1103/PhysRevB.69.245120.
[16] Zuttel A, Rentsch S, Fischer P, Wenger P, Sudan P, Mauron P, et al. Hydrogen storage properties of LiBH4. J Alloys Compd 2003:515–20. https://doi.org/10.1016/S0925-8388(02)01253–01257.
[17] Tekin A, Caputo R, Züttel A. First-principles determination of the ground-state structure of LiBH4. Phys Rev Lett 2010. https://doi.org/10.1103/PhysRevLett.104.215501.
[18] Miwa K, Ohba N, Towata S, Nakamori Y, Orimo S. First-principles study on copper substituted lithium borohydride, (Li 1-xCux)BH4. J Alloys Compd 2005. https://doi.org/10.1016/j.jallcom.2004.09.090.
[19] Gremaud R, Zttel A, Borgschulte A, Ramirez-Cuesta AJ, Refson K, Colognesi D. Origin of the large anharmonicity in the phonon modes of LiBH4. Chem Phys 2013. https://doi.org/10.1016/j.chemphys.2013.10.001.
[20] Siegel DJ, Wolverton C, Ozolins V. Reaction energetics and crystal structure of Li4BN3H10 from first principles. Phys Rev B 2007. https://doi.org/10.1103/Physrevb.75.014101. Artn 014101\nDoi.
[22] Łodziana Z, Vegge T. Structural stability of complex hydrides: LiBH_{4} revisited. Phys Rev Lett 2004;93:1–4. https://doi.org/10.1103/PhysRevLett.93.145501.
[23] El Kharbachi A, Pinatel E, Nuta I, Baricco M. A thermodynamic assessment of LiBH 4. Calphad Comput Coupling Phase Diagrams Thermochem 2012. https://doi.org/10.1016/j.calphad.2012.08.005.
[24] Zhang LJ, Di YY, Dou JM. Low-temperature heat capacities and thermodynamic properties of n-undecylammonium bromide monohydrate C11H28BrNO(s). Phase Transitions 2012. https://doi.org/10.1080/01411594.2012.660638.
[25] Kim KC, Allendorf MD, Stavila V, Sholl DS. Predicting impurity gases and phases during hydrogen evolution from complex metal hydrides using free energy minimization enabled by first-principles calculations. Phys ChemChem Phys 2010. https://doi.org/10.1039/c001657h.
[26] El Kharbachi A, Nuta I, Hodaj F, Baricco M. Above room temperature heat capacity and phase transition of lithiféum tetrahydroborate. Thermochim Acta 2011. https://doi.org/10.1016/j.tca.2011.02.043.
[27] Dehimi L, Benguerba Y, Virginie M, Hijazi H. Microkinetic modelling of methane dry reforming over Ni/Al2O3 catalyst. Int J Hydrogen Energy 2017. https://doi.org/10.1016/j.ijhydene.2017.05.231.

Please cite this article in press as: Benzidi H, et al., Vibrational and thermodynamic properties of $LiBH_4$ polymorphs from first-principles calculations, International Journal of Hydrogen Energy (2018), https://doi.org/10.1016/j.ijhydene.2018.02.042

Computational Materials Science 152 (2018) 192–195

Contents lists available at ScienceDirect

Computational Materials Science

journal homepage: www.elsevier.com/locate/commatsci

Enhanced hydrogen sorption kinetics of co-doped MgH_2 hydrides

M. El Khatabi[a,*], M. Bhihi[a], M. Lakhal[a], M. Abdellaoui[a], A. Benyoussef[b,c], A. El Kenz[a], M. Loulidi[a]

[a] Laboratoire de Matière Condensée et Sciences Interdisciplinaires (LaMCScI), Faculty of Sciences, University Mohammed V-Agdal, Rabat, Morocco
[b] Institute of Nanomaterials and Nanotechnology, MAScIR, Rabat, Morocco
[c] Hassan II Academy of Science and Technology, Rabat, Morocco

ARTICLE INFO

Keywords:
MgH_2
Double substitution
Density functional theory calculations
Kinetic Monte Carlo simulations
Activation energy
Hydrogen ab/desorption kinetic

ABSTRACT

Double substituted MgH_2 sorption kinetic is studied by combining density functional theory (DFT) and Kinetic Monte Carlo (KMC) simulations. The DFT calculations were performed to compute the energy barriers of the relevant elementary processes, which will be used as a database for the KMC simulations. The study provides a discussion of the mechanism behind the hydrogen reaction path on magnesium hydride (adsorption, dissociation, surface migration, penetration, and diffusion) as we took into account the density distribution of hydrogen atoms as well as the filling ratios, the diffusion time and finally the temperature. Based on the obtained results, the double substitution not only improves MgH_2 stability and desorption temperature but also its adsorption and desorption kinetics. Among the studied systems $Mg_{14}ZnLiH_{32}$ exhibits the best results with the fastest ab/desorption kinetic, in addition to its ideal heat of formation ΔH = -38.27 kJ/mol and high gravimetric capacity 7.25 wt%.

1. Introduction

The need for an alternative, -sustainable and clean- energy, source is becoming more pressing, as the world faces serious challenges such as global warming, depleted energy sources (i.e. fossil fuels) and overpopulation. Hydrogen, as an energy carrier, has attracted researchers' attention for its exceptional characteristics, like its high energy density, abundance and environmental friendliness. Although hydrogen appears as the most versatile and viable alternative; its storage remains the biggest hurdle to its practical applications.

Magnesium hydride (MgH_2) is one of the promising candidates for on-board hydrogen storage, due mainly to its high gravimetric capacity 7.65 wt% [1]. However its industrial application is hindered by its high stability, desorption temperature as well as slow hydrogenation/dehydrogenation kinetics [2]. Many experimental and theoretical researches, have been carried out to assess MgH_2 hydrogen, storage properties improvement, through different approaches like "Mechanical alloying [3,4]; alloying with transition metals oxides [5,6]; simple substitution [7–11]; double substitution with transition metals [12,13]. In addition to these works, other studies investigated hydrogen sorption kinetic improvement [14,15].

In our previous studies [9–12] we investigated the influence of single and double substitution, with different elements from the periodic table, on MgH_2 hydrogen storage properties. The improvement of MgH_2 thermodynamic properties was very apparent, in all the studied cases. However, it was shown that the stability is improved at the expense of the gravimetric capacity or vice versa. Yet in the case of double substitution, the stability was reduced and the gravimetric capacity was maintained around that of MgH_2. For $Mg_{14}ZnLiH_{32}$ and $Mg_{14}TiAlH_{32}$ their heats of formation were $\Delta H = -38.27$ kJ/mol and $\Delta H = -37.26$ kJ/mol respectively [12], far below MgH_2 heat of formation $\Delta H = -62.57$ and close to the heat of formation required for hydrogen storage materials $\Delta H = -40$ kJ/mol (H2) [16], and their gravimetric capacities were 7.25 wt% and 7.21 wt% respectively, indeed below MgH_2 gravimetric capacity of 7.65 wt%,as the doping elements are heavier (Transition metals), however above the DOE target for 2017 (5.5 wt%) and around the DOE optimum target (7.5 wt%) [17]. Since the effect of double substitution, on MgH_2 thermodynamics, was displayed via the decrease of the stability and desorption temperature, its effect on MgH_2 kinetics remains to be identified.

The objective of this paper is assess the effect of double substitution on the sorption kinetics of MgH_2.This is through an investigation of the absorption/desorption kinetic of $Mg_{14}ZnLiH_{32}$ and $Mg_{14}TiAlH_{32}$ by combining density functional theory (DFT) and Kinetic Monte Carlo (KMC) simulations. Throughout the DFT calculations, the energy barriers, of the elementary processes, were computed so to be later used as a database for the KMC simulations.

* Corresponding author.
E-mail address: elkhatabi.maryem@gmail.com (M. El Khatabi).

https://doi.org/10.1016/j.commatsci.2018.05.051
Received 5 December 2017; Received in revised form 27 May 2018; Accepted 28 May 2018

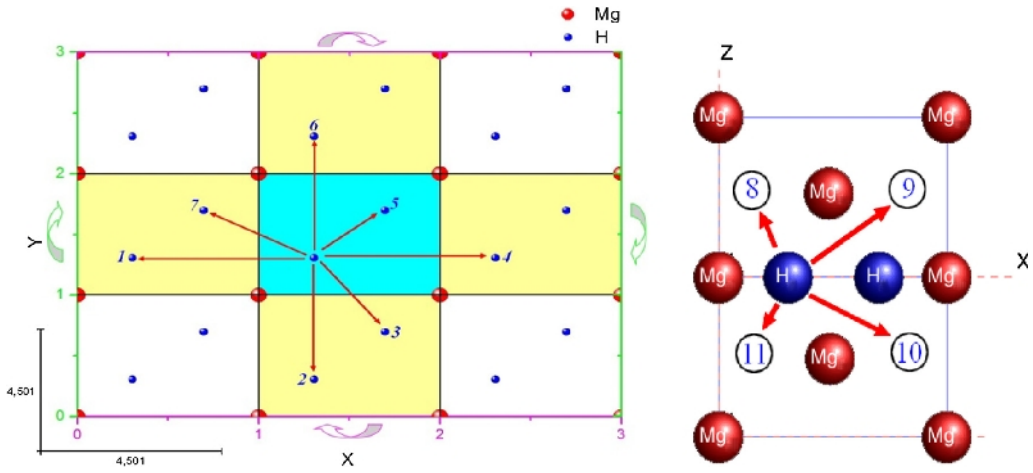

Fig. 1. Representative scheme of neighbor's sites. Left denotes the seven neighbors in the same plane; Right denotes the four neighbors in the upper and lower adjacent plane.

2. Computational method and model

MgH_2 crystallizes in a rutile structure. Its space group is (P42/mnm, N°136), and lattice parameters are: a = b = 4.501 Å and c = 3.01 Å [18]. Mg and H wyckoff positions are 2a (0, 0, 0) and 4f (0.304, 0.304, 0) respectively. In this study, a 2 × 2 × 2 supercell consisting of 16 Mg atoms and 32H atoms has been used. In this atomic representation, two Mg atoms are substituted by Li and Zn in the first system whereas in the second system they are substituted by Al and Ti, which correspond to a concentration of 12.6%. All lattices parameters are relaxed.

2.1. Kinetic Monte Carlo simulations

To investigate the hydrogen diffusion in our systems, we apply KMC method [19] to our model described in detail in the reference [14]. We consider a large super cell and periodic boundary conditions along X and Y-directions to simulate an infinite system. Each hydrogen atom has eleven nearest neighbors, seven in the same plane and four in the upper and lower adjacent plane Fig. 1.

Various possible events including processes of dissociation, adsorption, diffusion to the free neighbors and desorption are considered. At each KMC step one of the above processes is randomly selected with a probability:

$$P_i = \frac{R_i}{R} \tag{1}$$

The rate transition R_i associated to the i^{th} process and the total rate transition R are given respectively by:

$$R_i = \upsilon_0 \exp\left(\frac{E_i^a}{K_\beta T}\right) \tag{2}$$

$$R = \sum_{i=1}^{N} R_i \tag{3}$$

where υ_0 describes the jump frequency (usually set to 10^{13} Hz), E_i^a the activation energy of i^{th} process taken from first principles calculations (see Section 3.1) and K_β the Boltzmann constant. The time of hydrogen atoms displacement is incremented by t, which is defined as the inverse of the total rate transition:

$$\Delta t = -\frac{\ln(u)}{R} \tag{4}$$

where u is a uniformly distributed random variable between $0 < u < 1$.

The adsorption of the hydrogen molecule, which is located at the surface (0 0 1) of a super-cell, containing initially only magnesium and (Li, Zn) for the first system and (Al, Ti) for the second, start by its decomposition into two H atoms that diffuse from an interstitial site to another according to the corresponding activation energies. These energies are obtained from the DFT calculations and implemented in the KMC algorithm.

2.2. Density functional theory calculations

For each material more than 300 configurations are required to determine the different energy barriers for the hydrogen diffusion. In order to compute such barriers, we have used ab initio calculations based on the all-electron full-potential local-orbital minimum-basis scheme FPLO9.00-34 [20,21] to solve the Kohn-Sham equations using the scalar-relativistic. The parameterization of the exchange–correlation energy has been done within the generalized gradient approximation GGA [22]. To ensure a high accuracy in our calculation, we used self-consistent criteria for both the energy and the density with precision of 10^{-8} Ha and 10^{-6}, respectively. A mesh of (6 × 6 × 6) k-points in the Brillouin zone was used in our calculation. The total energy is calculated using the scalar-relativistic scheme, for all configurations.

3. Results and discussion

The DFT calculations are performed to compute the heat of formation as well as the energy barriers of the relevant elementary processes, so to be used as a database for the KMC simulations.

As previously mentioned this study is a follow up study. Based on our previous founding [12], double substituted MgH_2 systems exposed excellent thermodynamic improvement, as well as great gravimetric capacities, compared to pure and single substitution MgH_2 (Table 1). The aim of this study is to assess the effect of double substitution, as

Table 1
Calculated heat of formation (kj/mol H_2) and gravimetric capacities (wt%).

System	Gravimetry (wt%)	Heat of formation (kJ/mol H_2)
MgH_2	7.65	−62.57
$Mg_{15}TiH_{32}$	7.25	−51.24
$Mg_{14}TiAlH_{32}$	7.21	−37.26
$Mg_{15}ZnH_{32}$	6.97	−53.04
$Mg_{14}ZnLiH_{32}$	7.25	−38.27

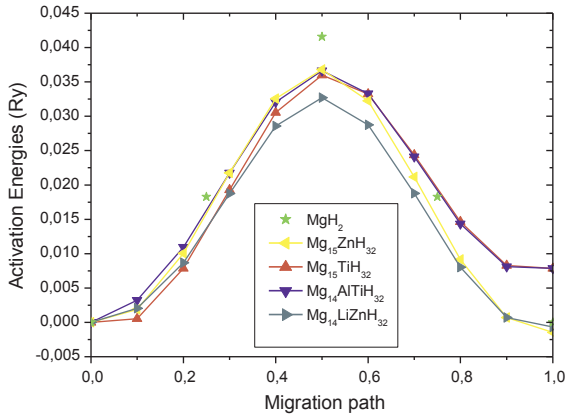

Fig. 2. Activation energy curves of hydrogen atom migration between two interstitial sites.

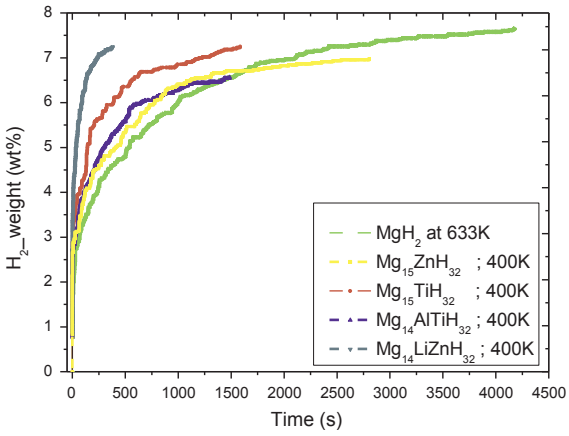

Fig. 3. Hydrogen absorption curves of pure MgH_2 at 633 k and single/double substituted MgH_2 at 400 k.

well, on the sorption kinetics of MgH_2.

3.1. Activation energy

According to our proposed model [14], each hydrogen atom has eleven nearest potential H vacancy sites: seven in the same plane, two in the upper adjacent plane whereas the remaining two are located at the lower adjacent plane. The migration of H atoms between interstitial sites, after dissociation, is done within the restraints of the activation energies. These energies vary according to the surrounding atoms and the target-interstitial sites.

From Fig. 2 we notice that, for the same hydrogen migration path, MgH_2 exposes the highest activation energy compared to single and double substituted MgH_2 systems. The material that exposes the lowest activation energy is $Mg_{14}ZnLiH_{32}$. Since MgH_2 exposes the highest activation energy as well as the highest stability among the studied systems, while $Mg_{14}ZnLiH_{32}$, the closest system to the optimum heat of formation, features the lowest activation energy. We may conclude, from the obtained results (Table 1 and Fig. 2), that the activation energy is strongly linked to the stability of the system. In other words the existence of the doping elements in the system influence the bond's strength between Mg and H, the weakening of Mg-H bond gives more freedom to the hydrogen atoms and thereby reduces the activation energy.

For the present study the activation barrier for the pure MgH_2 is 0.57 eV which is higher than the theoretical values (0.37 eV, 0.38 eV and 0.39 eV) listed in [23–25] respectively. As for the difference, between our activation barrier values, we assume that it may be mostly due to the difference in the used methods for the calculations; in our case we used the FPLO code based on "Full-potential", whereas for the referenced articles, the code used is the VASP code based on "pseudo-potential".

3.2. The sorption time by kinetic Monte Carlo simulation

Following the computation of the different heat of formations and activation barriers, we implement the obtained result in our KMC model, in order to plot the sorption kinetic curves of the studied systems. The kinetic curves are performed at 633 K and 400 K for the pure MgH_2 and for the doped/co-doped systems respectively. The difference in the simulating temperatures is mainly due to the fact that the doped/co-doped systems release/uptake hydrogen at lower temperatures compared to the pure MgH_2.

Fig. 3 gives the different curves of the hydrogen absorption kinetic for the studied systems. As mentioned in the figure the KMC simulations were performed under a pressure of 10 bar for all the systems and a temperature of 400 K except for MgH_2 pure where the temperature equals 633 K. The curves can be divided into two distinct parts. The first part, in which starts the filing process of the system, exposes a fast rate of hydrogen absorption in function of time. This is mainly due the high availability of potential hydrogen vacancy sites in addition to the temperature and pressure applied on the adsorption surface. For the second part and as the gravimetric capacity of the systems increase, the number of hydrogen vacancy sites decrease causing an increase of the activation energies and therefore resulting in a slowdown of hydrogen absorption in function of time. As shown in the figure MgH_2 pure exhibit the slowest absorption kinetic among the studied systems whereas $Mg_{14}ZnLiH_{32}$ exposed the best absorption kinetic.

To assess the improvement in the absorption kinetic of MgH_2, we plotted in Fig. 4 the average filling time for the single and double substituted systems. For comparison, we included results from previous studies where MgH_2-Ni exhibited the best average filling time [15]. As shown in the Fig. 4, $Mg_{14}ZnLiH_{32}$ exposed the fastest absorption kinetics with an average filling time under 500 s. It can also be seen that the double substituted system "$Mg_{14}ZnLiH_{32}$" exposed an average filling time about 9 times faster than the single substituted system "$Mg_{15}ZnH_{32}$". From the obtained results, it can be concluded that double substitution with Li-Zn does greatly improve the absorption kinetics of MgH_2.

The curves of the hydrogen desorption kinetic for the different

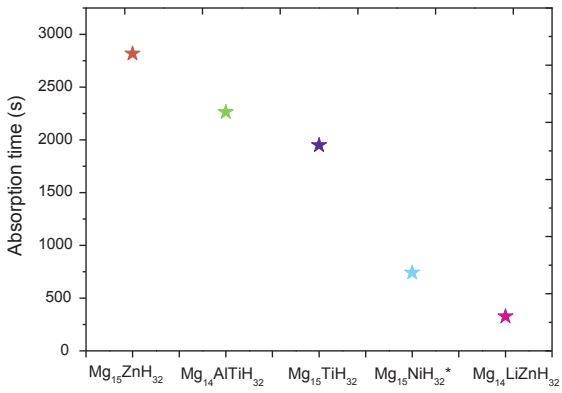

Fig. 4. The Average filling time of single and double substituted MgH_2 at 400 k and 10 bar. Result from previous theoretical study is included for comparison. *Reference [15].

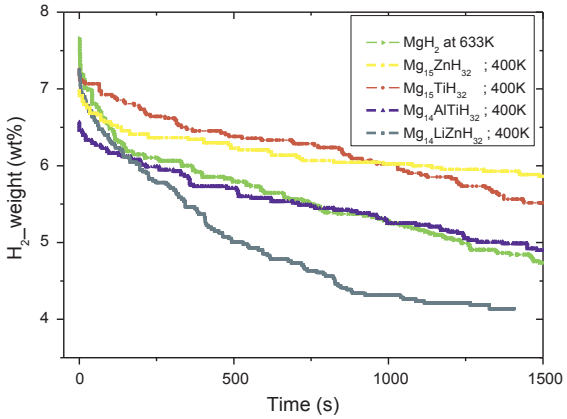

Fig. 5. Hydrogen desorption curves of pure MgH_2 at 633 k and single/double substituted MgH_2 at 400 k.

systems is plotted in the Fig. 5, the KMC simulations were performed under the same condition- pressure and temperature- as for the case of absorption kinetic. At the beginning of the desorption process, and as seen in the figure, we observe, a fast release of the hydrogen atoms in function of time. As time goes by the rate of hydrogen released decreases in function of time. We note that a certain amount of hydrogen remained in the materials. The unreleased hydrogen atoms move inside, by occupying the newly vacant sites, instead of leaving the materials. For a complete desorption of hydrogen, the systems should be put under high vacuum, the preformed KMC simulation could not meet with such extreme condition. Based on these results single and double substitution of MgH_2 not only improved MgH_2 thermodynamics but also its sorption kinetics.

Compared to single substituted systems, the double substituted systems exposed generally the best results taken into account the improvement of all properties: the thermodynamics, the sorption kinetic and also the gravimetric capacities.

The hydrogen absorption/desorption kinetic curves, in pure MgH_2, exhibits a behavior similar to the ones observed in experimental findings with a quantitative difference. The difference is due to Various factors, such as the difference in the operating pressures and temperatures and also to some specific conditions like (measurement in vacuum, under He flow, …etc) [26,27].

4. Conclusion

Combining density functional theory (DFT) and Kinetic Monte Carlo (KMC) simulations, the effect of double substitution on MgH_2 sorption kinetic was investigated. Throughout this study it was confirmed that, double substitution improves MgH_2 thermodynamic properties as well as its sorption kinetic, in addition to preserve high gravimetric capacities. Among the studied system $Mg_{14}ZnLiH_{32}$ exposed the best ab/desorption kinetic in addition to exposing the heat of formation, $\Delta H = -38.27$ kJ/mol, and the gravimetric capacity 7.25 wt%.

Acknowledgments

This work was supported by the CNRST (RS/04) in the framework of the national program Dev-RS/04. The authors acknowledge its financial support.

Data availability

The raw/processed data required to reproduce these findings cannot be shared at this time as the data also forms part of an ongoing study.

References

[1] M. Hirscher, Handbook of hydrogen storage: new materials for future energy storage, March;2010.
[2] G. Liang, J. Huot, S. Boily, A. Van Neste, R. Schulz, Catalytic effect of transition metals on hydrogen sorption in nanocrystalline ball milled MgH_2-Tm (Tm = Ti, V, Mn, Fe and Ni) systems, J. Alloys Compd. 292 (1999) 247.
[3] J. Charbonnier, P. De Rango, D. Fruchart, S. Miraglia, L. Pontonnier, S. Rivoirard, N. Skryabina, P. Vulliet, Hydrogenation of transition element additives (Ti, V) during ball milling of magnesium hydride, J. Alloys Compd. 383 (2004) 205.
[4] X. Shang, M. Bououdina, Y. Song, Z.X. Guo, Mechanical alloying and electronic simulations of (MgH_2 + M) systems (M = Al, Ti, Fe, Ni, Cu and Nb) for hydrogen storage, Int. J. Hydrogen Energy 29 (2004) 73.
[5] M.Y. Song, J.-L. Bobet, B. Darriet, Improvement in hydrogen sorption properties of Mg by reactive mechanical grinding with Cr_2O_3, Al_2O_3 and CeO_2, J. Alloys Compd. 340 (2002) 256.
[6] M. Cabo, S. Garroni, E. Pellicer, C. Milanese, A. Girella, A. Marini, et al., Hydrogen sorption performance of MgH_2 doped with mesoporous nickel- and cobalt-based oxides, Int. J. Hydrogen Energy 36 (2011) 5400.
[7] X.-B. Xiao, W.-B. Zhang, W.-Y. Yu, Na Wang and B-Y Tang, Energetics and electronic properties of Mg_7TMH_{16} (TM = Cs, Ti, V, Y, Zr, Nb): An ab initio study, Phys. B 404 (2009) 2234.
[8] M.G. Shelyapina, D. Fruchart, P. Wolfers, Electronic structure and stability of new FCC magnesium hydrides Mg7MH16 and Mg6MH16 (M [Ti, V, Nb): An ab initio study, Int. J. Hydrogen Energy 35 (2010) 2025.
[9] M. Bhihi, M. Lakhal, H. Labrim, A. Benyoussef, A. El Kenz, O. Mounkachi, E.K. Hlil, Hydrogen storage of $Mg_{1-x}H_xH_2$ (M = Ti, V, Fe) studied using first-principles calculations, Chin. Phys. B 21 (2012) 097501.
[10] M. Bhihi, M. Lakhal, S. Naji, H. Labrim, A. Belhaj, A. Benyoussef, A. EL Kenz, M. Loulidi, B. Khalil, O. Mounkachi, M. Abdellaoui, E.K. Hlil, First principle calculations for improving desorption temperature in $Mg_{16}H_{32}$ doped with Ca, Sr and Ba elements, Bull. Mater. Sci. 37 (2014) 1731.
[11] M. El Khatabi, M. Bhihi, S. Naji, H. Labrim, A. Benyoussef, A. El Kenz, M. Loulidi, Study of doping effects with 3d and 4d-transition metals on the hydrogen storage properties of MgH_2, Int. J. Hydrogen Energy 41 (2016) 4712.
[12] M. Bhihi, M. El Khatabi, M. Lakhal, S. Naji, H. Labrim, A. Benyoussef, A. El Kenz, M. Loulidi, First principal study of hydrogen storage in doubly substituted Mg based hydrides, Int. J. Hydrogen Energy 40 (2015) 8356.
[13] M. Abdellaoui, M. Lakhal, M. Bhihi, M. El Khatabi, A. Benyoussef, A. El Kenz, M. Loulidi, First principle study of hydrogen storage in doubly substituted Mg based hydrides Mg_5MH_{12} (M = B, Li) and Mg_4BLiH_{12}, Int. J. Hydrogen Energy (2016).
[14] M. Lakhal, M. Bhihi, H. Labrim, A. Benyoussef, S. Naji, A. Belhaj, B. Khalil, M. Abdellaoui, O. Mounkachi, M. Loulidi, A. El Kenz, Kinetic monte carlo and density functional study of hydrogen diffusion in magnesium hydride MgH_2, Int. J. Hydrogen Energy 38 (2013) 8350.
[15] M. Lakhal, M. Bhihi, A. Benyoussef, A. El Kenz, M. Loulidi, S. Naji, The hydrogen ab/desorption kinetic properties of doped magnesium hydride MgH_2 systems by first principles calculations and kinetic Monte Carlo simulations, Int. J. Hydrogen Energy 40 (2015) 6137.
[16] M. Ramzan, S. Lebegue, R. Ahuja, Transition metal doped MgH_2: A material to potentially combine fuel-cell and battery technologies, Int. J. Hydrogen Energy 35 (2010) 10373.
[17] L.E. Klebanoff, J.O. Keller, 5 Years of hydrogen storage research in the U.S. DOE Metal Hydride Center of Excellence (MHCoE), Int. J. Hydrogen Energy 38 (2013) 4533.
[18] M. Bortz, B. Bertheville, G. Bottger, K. Yvon, Structure of the high pressure phase –MgH_2 by neutron powder diffraction, J. Alloys Compd. 287 (1999) L4.
[19] Kratzer P. Monte Carlo and kinetic Monte Carlo methods, 2009. arXiv:0904.2556.
[20] http://www.fplo.de.
[21] K. Koepernik, H. Eschrig, Full-potential nonorthogonal local-orbital minimum-basis band-structure scheme, Phys. Rev. B 59 (1999) 1743.
[22] J.P. Perdew, K. Burke, M. Ernzerhof, Generalized gradient approximation made simple, Phys. Rev. Lett. 77 (1996) 3865–3868.
[23] S. Hao, D.S. Sholl, Hydrogen diffusion in Mg H 2 and Na Mg H 3 via concerted motions of charged defects, Appl. Phys. Lett. 93 (2008) 251901.
[24] M.S. Park, A. Janotti, C.G. Van de Walle, Formation and migration of charged native point defects in MgH2: First-principles calculations, Phys. Rev. B 80 (2009) 064102.
[25] V. Koteski, J. Belosevic-Cavor, K. Batalovic, J. Radakovic, A. Umicevic, Hydrogen diffusion in MgH2 doped with Ti, Mn and Fe, RSC Adv. 5 (2015) 34894–34899.
[26] C.X. Shang, M. Bououdina, Y. Song, Z.X. Guo, Mechanical alloying and electronic simulations of (MgH2 + M) systems (M = Al,Ti,Fe,Ni,Cu and Nb) for hydrogen storage, Int. J. Hydrogen Energy 29 (1) (2004) 73e80..
[27] N. Hanada, T. Ichikawa, H. Fujii, Catalytic effect of nanoparticle 3d-transition metals on hydrogen storage properties in magnesium hydride MgH2 prepared by mechanical milling, J. Phys. Chem. B 109 (2005) 7188.

INTERNATIONAL JOURNAL OF HYDROGEN ENERGY XXX (2017) 1–6

Available online at www.sciencedirect.com

ScienceDirect

journal homepage: www.elsevier.com/locate/he

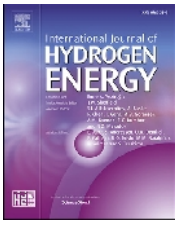

First principle study of strain effect on structural and dehydrogenation properties of complex hydride $LiBH_4$

H. Benzidi [a], *M. Lakhal* [a], *A. Benyoussef* [b], *M. Hamedoun* [b], *M. Loulidi* [a], *A. El kenz* [a], *O. Mounkachi* [b,*]

[a] *LMPHE (URAC 12), Physics Department, Faculty of Sciences, Mohammed V University, Rabat, Morocco*
[b] *Materials and Nanomaterials Center, MAScIR Foundation, Rabat Design Center Rue Mohamed Al Jazouli Madinat Al Irfane Rabat 10 100 Morocco*

ARTICLE INFO

Article history:
Received 20 February 2017
Received in revised form
6 June 2017
Accepted 7 June 2017
Available online xxx

Keywords:
Lithium borohydride
Hydrogen storage properties
First-principles calculation
Strain effect
Desorption enthalpy
Activation energies

ABSTRACT

Using the first-principles calculations based on density functional theory (DFT), the structure, stability, thermodynamic and kinetic properties of complex hydride $LiBH_4$ under different biaxial strains have been investigated. The results show that the free strain $LiBH_4$ involves a high stability and the biaxial tensile or compressive strain lowers the hydrogen desorption enthalpy of this system. Further, the diffusion activation energy of hydrogen atom in $LiBH_4$ is also decreased which can accelerate the hydrogenation kinetic of $LiBH_4$.

Introduction

Newly, it has been more focus on sustainable and renewable sources of energy as alternatives to the actual use of fossil fuels [1]. In many ways, hydrogen is the perfect fuel, it is abundant, the most efficient and produces no emissions when used in a fuel cell or combustion engine [2]. However, hydrogen potential has not been realized even partially mainly because up of storage and commercial production difficulties [3–5]. A complex hydride $LiBH_4$ is a favorable prospect for solid-state hydrogen storage material capable of releasing the DOE target, because of the attractive volumetric capacity 121 $kg.H_2/m^3$, and the highest gravimetric capacity at room temperature exists 18.3 wt% [3,6]. $LiBH_4$ liberates hydrogen in different reaction step, a partial decomposition of $LiBH_4$ yields 13.5 wt% [7] of hydrogen through reaction:

$$LiBH_4 \rightarrow LiH + B + 3/2H_2 \quad (1)$$

The low-temperature desorption for orthorhombic phase liberates only a 0.3 wt% of hydrogen, and $LiBH_4$ can liberate 13.5 wt% of hydrogen only at high-temperature phase above

* *Corresponding author.*
E-mail addresses: o.mounkachi@mascir.com, o.mounkachi@gmail.com (O. Mounkachi).
http://dx.doi.org/10.1016/j.ijhydene.2017.06.068

Please cite this article in press as: Benzidi H, et al., First principle study of strain effect on structural and dehydrogenation properties of complex hydride $LiBH_4$, International Journal of Hydrogen Energy (2017), http://dx.doi.org/10.1016/j.ijhydene.2017.06.068

674 K. Further, the rehydrogenation is achieved at 350 bar H_2 and 873 K [8]. High desorption conditions, kinetics, and irreversibility limit his application for hydrogen storage. The formation enthalpy of reaction (equation (1)) is 74 kJ/mol.H_2 and the corresponding entropy of reaction is 115 J/mol.K based on the pressure-concentration temperature (PCT) isotherm measurement [9]. To reduce hydrogen desorption enthalpy several approaches have been performed. The most used approach is the addition of catalysts metal, metal halides [10], oxides [11,12], amides [13] or metal hydride to complex hydride $LiBH_4$ [14,15]. The addition of oxide SiO_2 to the pure $LiBH_4$ could reduce hydrogen desorption temperature to 473 K with 10 wt% of hydrogen desorbed [16]. Haizhen Liu et al. [17] assume that hydrogen desorption properties of $LiBH_4$ can be improved by the addition of Al and AlH_3, and the $2LiBH_4 + AlH_3$ composite achieved 11.2 wt% of Hydrogen and the desorption temperature is reduced by more than 303 K. Moreover, mixing the metal hydride MgH_2 with complex hydride $LiBH_4$ with $TiCl_3$ catalyst leads to a reversible system which could store 8.1 wt% and reduce relatively hydrogen desorption enthalpy about 25 kJ/mol [18]. The recent approach used is nanoengineering to confine $LiBH_4$ in Nanoporous [19,20] or mix $LiBH_4$ with nanotubes [21]. For example, Vajeeston P. et al. [22] reported that is relatively easier to remove hydrogen from the surface of the clusters and nanowhiskers than from bulk crystals and (010) surface is the most stable. Another study of confined $LiBH_4$ nanoparticles revealed that the reason for the improved (de)hydrogenation effect of nanoconfined $LiBH_4$ is a chemical interaction between the products and an intermediate compound of $LiBH_4$ reaction steps [23]. Gross et al. [24] declared that $LiBH_4$ incorporated within Nanoporous carbon induce to 6.4 wt% of hydrogen desorbed between 573 and 800 K and $LiBH_4$ rehydrated at 600 K under 100 bar of hydrogen. In order to use Lithium borohydride as an energy carrier in mobile applications, it is necessary to ameliorate the thermodynamics properties of hydrogen storage in $LiBH_4$ without reducing its high gravimetric capacity (18.3 wt%). In this study, the role of biaxial strain on the particles of $LiBH_4$ and their effect on the stability, thermodynamic properties, and hydrogenation kinetics was investigated. In section computational methods, the details and methods to perform our calculation are given. Section Results and discussion is devoted to the presentation, the discussion and the comparison of our numerical results with those obtained experimentally. In the last section, the conclusion is given.

Computational methods

At ambient conditions, $LiBH_4$ crystallizes in the orthorhombic structure with space group *Pnma* (No. 62) [25], see Fig. 1. The lattice constants are a = 7.178 Å, b = 4.437 Å, c = 6.803 Å. Li, B, H1, H2 and H3 atoms occupy the 4c (0.1568, 0.25, 0.1015), 4c (0.3040, 0.25, 0.4305), 4c (0.900, 0.25, 0.956), 4c (0.404, 0.25, 0.280) and 8d (0.172,0.054, 0.428) sites respectively [25]. In this structure, each anion $[BH4]^+$ is surrounded by four lithium Li^+ and each Li^+ cations surrounded by four anions $[BH4]^+$ in both tetrahedral configurations.

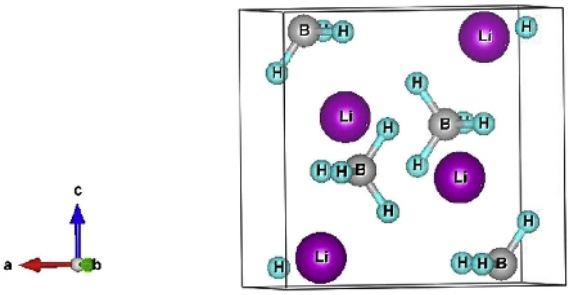

Fig. 1 – Orthorhombic structure (a) and density of state (b) of $LiBH_4$.

Once the crystalline structure of the unstrained unit cell of $LiBH_4$ was fully relaxed, the mechanical biaxial strain is imposed on the relaxed $LiBH_4$ unit cell along x[100] and y[010] directions according to equation (2); [26]:

$$\varepsilon_{xx}(\%) = \varepsilon_{yy}(\%) = \frac{a(b) - a_0(b_0)}{(a_0(b_0))} \quad (2)$$

where the lattice constants a(b) of $LiBH_4$ unit cell are constrained to several different values, differing from the equilibrium lattice constants $a_0(b_0)$ by fractions ranging from −6% to 6% by step of 1%. The lattice constant c is obtained by allowing all atomic positions to relax to a minimum energy state under each strain. All atomic positions in each strained $LiBH_4$ unit cell with constrained lattice constants 'a' and 'b' were fully optimized to obtain the lattice constant c using the Broyden–Fletcher–Goldfarb–Shanno (BFGS) method [27]. In general, the negative value of $\varepsilon_{xx}(\varepsilon_{yy})$ represents the compression strain state in the x and y-axes, although the positive value of $\varepsilon_{xx}(\varepsilon_{yy})$ indicates that the model under a tensile strain [28].

All calculations were carried out in the context of density functional theory (DFT). The generalized gradient approximation (GGA) in the form of the Perdew–Burke–Ernzerhof (PBE) functional [29] and plane wave pseudopotential method (PWSCF) implemented in the Quantum Expresso code are used to solve the Kohn–Shame equation [30]. Energy cutoff of 50 Ry and k-point samplings of 6 × 8 × 6 were used for all the calculations. To ensure a high accuracy in our performed computations, both self-consistent criterions of the energy and the density together with a precision of 10^{-8} Ry and 10^{-6} Ry respectively were used. Atomic and parameters relaxation was performed with an energy convergence of 10^{-7} Ry and a force convergence of 10^{-4} Ry per Bohr.

The energies of (un)strained $LiBH_4$ unit cell are calculated then the desorption enthalpies are deduced from Equation (3):

$$\Delta H_{des} = E_{tot}(B) + E_{tot}(LiH) + \frac{3}{2}E_{tot}(H_2) - E_{tot}(LiBH_4) \quad (3)$$

where $E_{tot}(LiBH_4)$ presents the total energy of strain-free and strained $LiBH_4$ and $E_{tot}(B)$, $E_{tot}(LiH)$, $E_{tot}(H_2)$ are the total energy of boron, lithium hydride, and hydrogen molecule respectively. The used lattice parameters and the calculated energies are given in Table 1.

The molecule Hydrogen energy $E_{tot}(H_2) = -2.330$ Ry are in good agreement with that obtained by FLOP in Refs. [31,32].

Please cite this article in press as: Benzidi H, et al., First principle study of strain effect on structural and dehydrogenation properties of complex hydride $LiBH_4$, International Journal of Hydrogen Energy (2017), http://dx.doi.org/10.1016/j.ijhydene.2017.06.068

Table 1 – Lattice parameters, total energy of each component.

Component	LiH	B	H_2	$LiBH_4$
Crystalline structure	Cc	Rhomo	hcp	Ortho
Parameter a(Å)	4.01	4.90	3.64	7.15
Parameter b(Å)	4.01	4.90	3.64	4.36
Parameter c(Å)	4.01	12.55	3.43	6.61
Total energy (Ry/f.u)	−16.06	−6.288	−2.330	−25.93
Desorption Enthalpy (kJ/mol.H_2)				75.73

Results and discussion

Structural and thermodynamics properties of (un)strained $LiBH_4$

Before studying the thermodynamic properties of $LiBH_4$ under deferent biaxial strains, first, the results of the structural optimization and desorption enthalpy of the free strain $LiBH_4$ are presented. The cell parameters of the relaxed structure are a = 7.151 Å, b = 4.361 Å, c = 6.610 Å, the difference between the experimental and calculated unit cell parameters a, b and c are around 0.38% using PWSCF method. This difference is in good agreement with previous first principles studies [25,33–37]. Then the desorption enthalpy of reaction (1) was calculated from equation (3).

The calculated enthalpy of the strain-free $LiBH_4$ is 75.73 kJ/mol.H_2, which is close to other value obtained experimentally and theoretical [34–38]. The relaxed $LiBH_4$ presents a high desorption enthalpy and to explain that result the electronic density was calculated and illustrated in Fig. 2.

The electronic structure of the $LiBH_4$ exhibits a non-metallic character with a large energy band gap of 6.8 eV, which is closer to the theoretical and experimental values [23,25,34]. Total DOS of free-strain $LiBH_4$ is divided into three distinct regions, two regions in the valence band, region I from −7.15 to −5.76 eV, region II from −2.67 eV to fermi level and the third one is the conduction band (region III: from 7 to 16.2 eV). Region I is mainly contributed by B-s and H-s states while the region II is contributed by H-s and B-p states. Partial Dos in region III show a high hybridization of the orbitals by B-p, B-s and Li-s with orbital H-s, which contributes to covalent mixed ionic interactions between $[BH4]^-$ and Li^+. The B-p and H-s states are energetically degenerate in region II, which clearly facilitates the formation of the hybridization condition for the appearance of the complex covalent bonds of the hydride structure.

To reduce the high stability of the compound, a biaxial tensile/compressive strain was applied along the [100] and [010] directions (equation (2)). The effects of the strains in the lattice parameter c and volume of $LiBH_4$ are represented in Fig. 3a. This figure shows that for the maximum biaxial compressive strain of −6% the lattice parameter c of complex hydride $LiBH_4$ takes the highest values then decreases by increasing strain rate applied by 1%. On the other side, the volume increases in the opposite direction by increasing the strain applied to $LiBH_4$, the same behavior is seen for MgH_2 under strain [26]. So, it can be concluded that the biaxial tensile or compressive strain is likely to cause deformation of the crystal structure of $LiBH_4$ and its lattice distortion becomes severe with increasing the biaxial strain.

As well, Figs. 3b and 4 show the total energy and desorption enthalpy as a function of biaxial strain in $LiBH_4$ unit cell respectively. Generally, the structural stability of crystal is associated with its total energy, and the minimum total energy indicates the most stable crystal structure [25]. It can notice that the total energy of strained $LiBH_4$ increased compared to the total energy of pure-strain $LiBH_4$. Therefore, either compression or biaxial tensile cause destabilization of the $LiBH_4$ structure. According to Fig. 4 it is noted that the desorption enthalpy decreases during the application of biaxial strain on the $LiBH_4$ structure relative to that of strain-free of $LiBH_4$. This suggests that either the tensile or

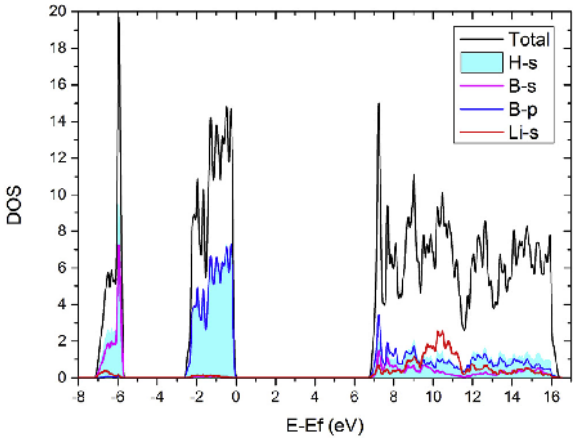

Fig. 2 – Total and partial DOS of free-strain $LiBH_4$.

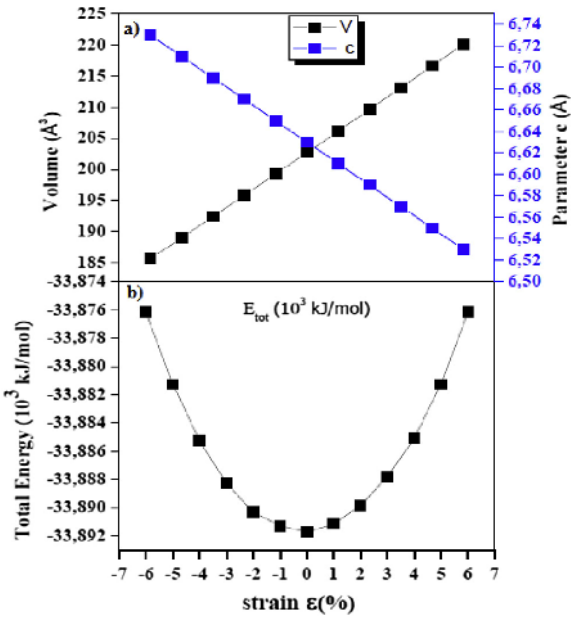

Fig. 3 – Representation of (a) c parameter and volume; (b) energy as a function of biaxial strain on $LiBH_4$.

Please cite this article in press as: Benzidi H, et al., First principle study of strain effect on structural and dehydrogenation properties of complex hydride $LiBH_4$, International Journal of Hydrogen Energy (2017), http://dx.doi.org/10.1016/j.ijhydene.2017.06.068

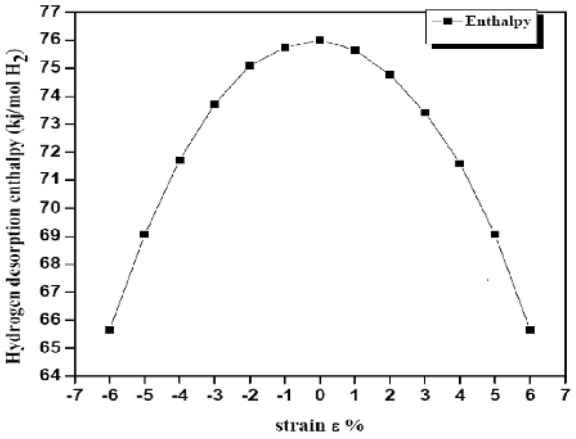

Fig. 4 – The hydrogen desorption enthalpy according to biaxial strain ε (%) in the structure on $LiBH_4$.

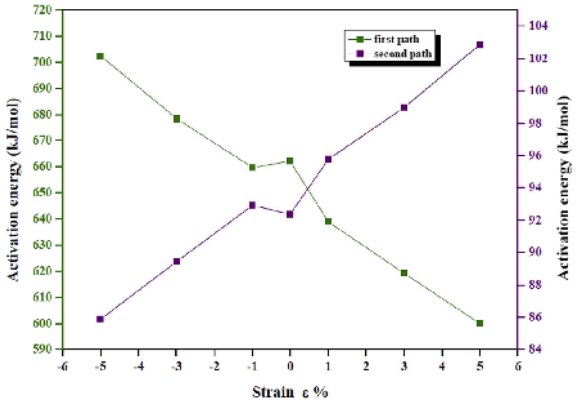

Fig. 6 – Activation energies for hydrogen diffusion.

compressive strain is applied improve the thermodynamic dehydrogenation because of the contribution of strain energy. The results show that hydrogen desorption enthalpy reduced from 75.73 kJ/mol.H_2 for the free-strain $LiBH_4$ structure to 65 kJ/mol.H_2 for the $LiBH_4$ structure under the compression of 6% strain. Therefore, a gain of 20.73 kJ/mol.H_2 was obtained by application of biaxial strain on the $LiBH_4$ structure.

Activation energies for hydrogen diffusion in $LiBH_4$

After dissociation, the hydrogen atoms can move from one site to interstitial site according to the corresponding activation energies. based on our model, each hydrogen atom has four nearest neighbors available sites in the same distance, which is represented by the first path and the second path is the hydrogen atom displacement anion $[BH4]^+$ to another anion $[BH4]^+$ neighbors. Fig. 5a and b shows the diffusion of energy barriers of H corresponding to the first path and second one respectively in the (un)strain structure of $LiBH_4$. The free-strain diffusion activation energy of hydrogen atom for the first path is 665.702 kJ/mol but for the second path, the energy diffusion activation of a hydrogen atom is 92.873 kJ/mol which is lower. It can be concluded that the hydrogen atom easily moves along the second path relative to the first path. Particularly Fig. 6 shows that the diffusion activation energy of hydrogen atom along the first path decrease under tensile strain from 665.702 kJ/mol to 603.241 kJ/mol. Otherwise, for the second path, the diffusion activation energy of hydrogen atom decreases by increasing the compression, from 92.873 kJ/mol value to 86.361 kJ/mol. This increases favorably the kinetics of hydrogen desorption in complex hydride $LiBH_4$.

Electronic charge density of (un)strained $LiBH_4$

The calculation of the electronic charge density which is usually presented in a plane or in a direction, informs us about the charge transfer and therefore on the ionic or covalent nature of the liaisons. Therefore, to see the nature of the character of bonds considered hydrides, the charge density was calculated in the (001), (100) and (010) planes. Fig. 7 shows a contour map of the charge distribution for the most stable state (0%) and strained state (5%, −5%). The amount of electronic charge at every point in space is determined and all points having the same value for the electron density in the plane is joined by a line, a contour line. In the first hand for the free-strained state, an equal sharing of density was observed between bore and hydrogen atoms which are interpreted by covalent binding. In anion $[BH4]^+$ the electronic charge is heavily concentrated in the internuclear region where it forms a bridge of high density between the three nuclei. In the other hand, the anion $[BH4]^+$ and Li^+ cations form an ionic bonding because the bond formed between the anion and cations have

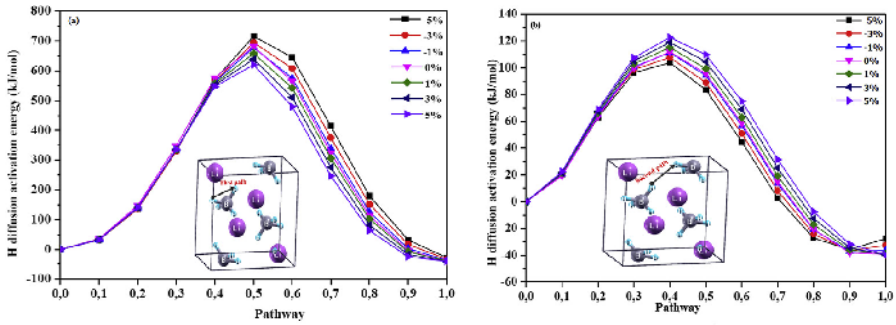

Fig. 5 – Energy curves for diffusing hydrogen between two interstitial sites along the first path (a) and second path (b).

Please cite this article in press as: Benzidi H, et al., First principle study of strain effect on structural and dehydrogenation properties of complex hydride $LiBH_4$, International Journal of Hydrogen Energy (2017), http://dx.doi.org/10.1016/j.ijhydene.2017.06.068

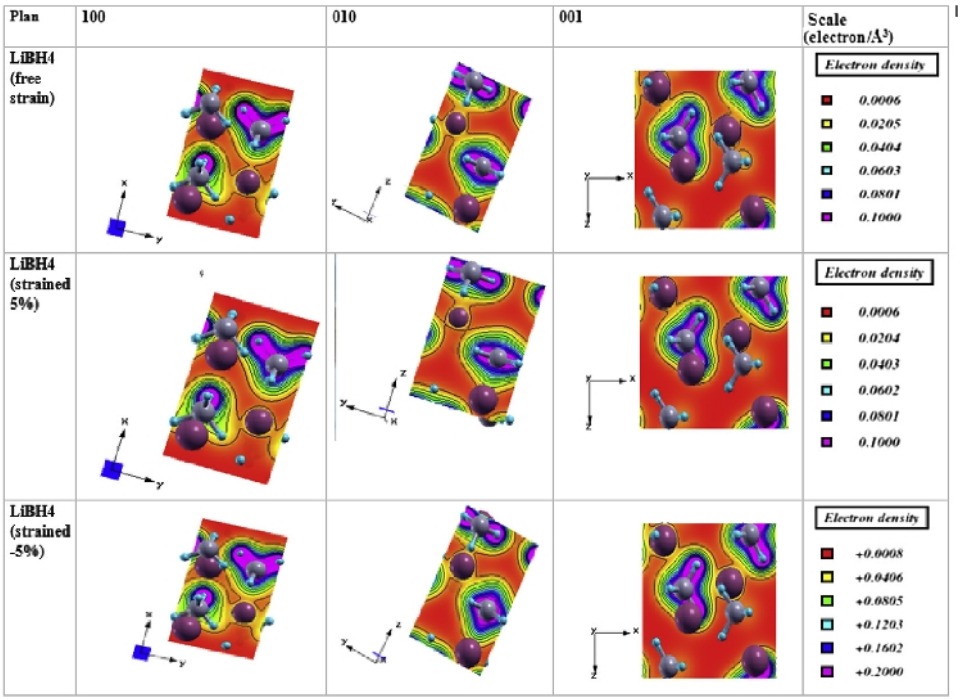

Fig. 7 – The three-dimensional (3D) electron density contour maps for (100), (010), (001) planes according to rate strain.

very different affinities for the electronic charge density. The calculation shows that there is a continuous distortion of the original atomic density distributions, a distortion which increases as the internuclear distance decreases. The contours maps demonstrate that the compressive strain (−5%) cause the greatest decrease in electron density of $[BH4]^+$ and Li^+ bonds of complex hydride $LiBH_4$. Due to these effects, the transfer of charge density from lithium cation to anion is very evident, in this case, the system becomes unstable and it's easy to remove hydrogen atoms which could explain the decrease of desorption enthalpy under compressive strain.

Conclusions

The first-principles plane-wave pseudopotential method based on density functional theory was used to study strain effect on complex hydride $LiBH_4$. Improving thermodynamic properties and kinetics hydrogenation in the hydride $LiBH_4$ are summarized in the following:

- Biaxial tensile or compressive strain tends to result in the deformation of the crystal structure of $LiBH_4$, and the destabilization of the structure becomes severe with increasing biaxial strain.
- When the compressive or tensile strain applied on the $LiBH_4$ structure the enthalpies desorbing Hydrogen of hydride $LiBH_4$ are reduced relative to that of free-strain $LiBH_4$, which is beneficial to improve the thermodynamic properties of $LiBH_4$.
- The DFT calculations show that the energy barriers for different paths decrease according to the hydrogenation kinetics of $LiBH_4$.

Acknowledgements

1- We would like to thank Mr. Ari.p.Seitsonen from Department of Chemistry at Ecole NormalSuperieureFrance, which provided us with the necessary On the QuantumEspresso code.

2- This work was supported by the MESRSFC (Ministre de l'Enseignement Superieur, de la. Recherche Scientifique et de la Formation des Cadres) in the Framework of the national program PPR Under contract no. PPR/2015/71.

REFERENCES

[1] Schlapbach L, Züttel A. Hydrogen-storage materials for mobile applications. Nature 2001;414:353–8. http://dx.doi.org/10.1038/35104634.
[2] Dodds PE, Staffell I, Hawkes AD, Li F, Grünewald P, McDowall W, et al. Hydrogen and fuel cell technologies for heating: a review. Int J Hydrogen Energy 2015;40:2065–83. http://dx.doi.org/10.1016/j.ijhydene.2014.11.059.
[3] Chen P, Zhu M. Recent progress in hydrogen storage. Mater Today 2008;11:36–43. http://dx.doi.org/10.1016/S1369-7021(08)70251-7.
[4] Zuttel A. Materials for hydrogen storage. Mater Today 2003;6:24–33. http://dx.doi.org/10.1016/S1369-7021(03)00922-2.

Please cite this article in press as: Benzidi H, et al., First principle study of strain effect on structural and dehydrogenation properties of complex hydride $LiBH_4$, International Journal of Hydrogen Energy (2017), http://dx.doi.org/10.1016/j.ijhydene.2017.06.068

INTERNATIONAL JOURNAL OF HYDROGEN ENERGY XXX (2016) 1–6

Available online at www.sciencedirect.com

ScienceDirect

journal homepage: www.elsevier.com/locate/he

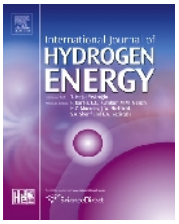

First principle study of hydrogen storage in doubly substituted Mg based hydrides Mg_5MH_{12} (M = B, Li) and Mg_4BLiH_{12}

M. Abdellaoui [a], M. Lakhal [a], M. Bhihi [a], M. El Khatabi [a], A. Benyoussef [a,b,c,*], A. El Kenz [a], M. Loulidi [a]

[a] LMPHE, (URAC), Faculté des Sciences, Université Mohammed V-Rabat, Morocco
[b] Institute of Nanomaterials and Nanotechnology, MAScIR, Rabat, Morocco
[c] Hassan II Academy of Science and Technology, Rabat, Morocco

ARTICLE INFO

Article history:
Received 13 March 2016
Received in revised form
10 April 2016
Accepted 10 April 2016
Available online xxx

Keywords:
Magnesium hydride
Formation energy
Hydrogen storage capacity
First principal calculation
Desorption temperature

ABSTRACT

The effect of single and double substitution with lightweight elements Boron (B) and Lithium (Li) on the thermodynamic properties of MgH_2 are investigated by using first principles calculations. Our results show an improvement of hydrogen storage properties of double substituted MgH_2, in contrast to the case of single substitution, along with a remarkable increase of its gravimetric and volumetric capacities which exceed those of pure MgH_2. Given that Mg_4LiBH_{12} exposes a heat of formation around −32.03 kj/mol as well as a gravimetric and volumetric capacity of 9.45 wt% and 123.08 gH_2/l respectively, it may be considered as a potential candidate for hydrogen storage transportation applications. A detailed analysis of the density of states and charge transfer, of the studied systems, is presented to understand the underlying mechanisms behind MgH_2 thermodynamics improvements.

Introduction

Nowadays, Hydrogen is one of the most promising renewable energies that has emerged as a solution to overcome the rarity of fossil fuels and to protect the environment. It is the most abundant element on earth and its energy density is three times that of diesel. Moreover the outcome of its combustion is water. These qualities make hydrogen the ideal energy of tomorrow.

Hydrogen storage method should involve high volumetric, gravimetric capacity, a fast sorption rate at relatively low temperatures, and a recycling high tolerance. Alternative methods have been proposed including high pressure gas cylinders, liquid hydrogen, physisorption of hydrogen on materials with a high specific surface area, and hydrogen storage through hydrides. Among the different methods for hydrogen storage, the solid storage proves to be the best.

The magnesium based hydride (MgH_2) is one of the most promising materials for hydrogen storage applications due to its high gravimetric and volumetric capacities (7.65 wt% and 110 gH_2/l, respectively) [1]. However, the rather slow hydrogen sorption proprieties, as well as the high desorption

* Corresponding author.
E-mail address: benyous.a@gmail.com (A. Benyoussef).
http://dx.doi.org/10.1016/j.ijhydene.2016.04.122

Please cite this article in press as: Abdellaoui M, et al., First principle study of hydrogen storage in doubly substituted Mg based hydrides Mg_5MH_{12} (M = B, Li) and Mg_4BLiH_{12}, International Journal of Hydrogen Energy (2016), http://dx.doi.org/10.1016/j.ijhydene.2016.04.122

temperature (573–673 K) hinder its commercial applications [2]. That is why various attempts have been made in order improve MgH_2 hydrogen absorbing and desorbing characteristics.

Experimentally, Nobuko Hanada et al. (2003) clarified the correlation between hydrogen storage and crystallographic properties in nanostructural magnesium hydride MgH_2 prepared by mechanical milling under hydrogen gaseous atmosphere. At the early stage of milling process, the rapid decrease in powder size leads to lowering the hydrogen desorption temperature (by 70 K), while the reduction of crystallite size of MgH_2 during milling dominates and controls the decrease in hydrogen storage capacity from 7.3 to 6.1 wt% [3].

Recently, it has been reported that adding additives or catalysts is considered as one of the most effective strategy to decrease the metal-hydrogen bonds energy and reduce the stability and desorption temperature of MgH_2 [4–19] by facilitating the Mg–H dissociation. Especially, the transition metals additive including their oxides.

Various theoretical calculations have been performed to understand the relevant mechanism dealing with the thermodynamic properties on magnesium hydride [20–22]. Combining the density functional theory (DFT) and Kinetic Monte Carlo simulation we have shown, in a previous work, that the pure MgH_2 presents a high stability and a high decomposition temperature [23,24]. At high temperature and pressure, the results of simulations indicate that the hydride involves slow kinetics [24].

On the other hand alloying MgH_2 with small amounts of transition metals mixture TM (TM = Ti, V and Fe, Sc, Zn) [23,25–27] or alkaline metal AM (AM = Ca, Sr and Ba) [28] or Al [25] improve the stability and the desorption temperature of hydrogen in Mg with decrease in the storage capacity from 7.65 wt% for the pure MgH_2 to 6.97 wt% for $Mg_{15}ZnH_2$ [26]. Also we have proposed a double substitution, with Al and Li as a second element due to their small weight, firstly to decrease the heat of formation and also the desorption temperature, and secondly to preserve the gravimetric storage capacity of MgH_2 [26].

The aim of this paper is to improve the thermodynamic properties of MgH_2 while increasing its storage capacities by studying the effect of substitution by lightweight metals like Li and B. This approach was proposed to overcome the drop of the gravimetric and volumetric capacities, which occurs in the large case cited above.

In the first part of the calculations we initiate a single substitution, where the system is doped by either Li or B (Mg_5LiH_{12}, Mg_5BH_{12}). The results show a decrease of MgH_2 stability and desorption temperature, however the results were not sufficient to reach the optimum values of heat of formation [29] and desorption temperature for a PEMFC (Proton Exchange Membrane Fuel Cells or Polymer Electrolyte Membrane Fuel Cells) [30]. In the second part we study the effect of double substitution with Li and B (Mg_4LiBH_{12}) as an approach to improve the results already obtained. Indeed, such approach leads to an important improvement of the thermodynamic properties accompanied by an increase of the gravimetric and volumetric capacities from 7.65 to 9.45 wt% and from 110 to 123.08 g H_2/l respectively.

Computational details

In this paper, we used ab initio calculations based on the all-electron full-potential local-orbital minimum-basis scheme FPLO9.00-34 [31,32]. This has been performed to solve the Kohn–Sham equations using the scalar-relativistic scheme. The parameterization of the exchange-correlation energy has been done within the generalized gradient approximations [33]. To ensure a high accuracy in our performed computations, we used both self-consistent criterions of the energy and the density together with a precision of 10^{-8} Ha and 10^{-6} Ha^{-1} $Å^{-3}$ respectively. For an accurate Brillouin zone integration, we considered a 12 × 12 × 4 K-point mesh.

MgH_2 has a tetragonal symmetry ($P4_2/mnm$, Group No.136). Mg and H atoms occupy the Wyckoff positions (0, 0, 0) and (0.304, 0.304, 0) respectively. MgH_2 lattice parameters are a = b = 4.501 Å and c = 3.010 Å [34]. A supercell of 1 × 1 × 3 of MgH_2 unit cell has been used for this study. For the case of single substitution 1 Mg atom was substituted by either B or Li (Mg_5LiH_{12}, Mg_5BH_{12}), whereas for double substitution two Mg atoms were substituted by B and Li respectively (Mg_4BLiH_{12}). The different systems are presented in Fig. 1.

Results and discussion

First of all, we relax the lattice parameters using the relaxation method, then we calculate the total energies and deduce the heat of formation and desorption temperature for each system. Finally, based on the charge exchange values and the density of states, we discuss the effect of doping on the stability of the systems.

Equilibrium structure and storage capacities

The systems relaxed lattice parameters are listed in Table 1, our calculated values are in fair agreement with other works results [23,35].

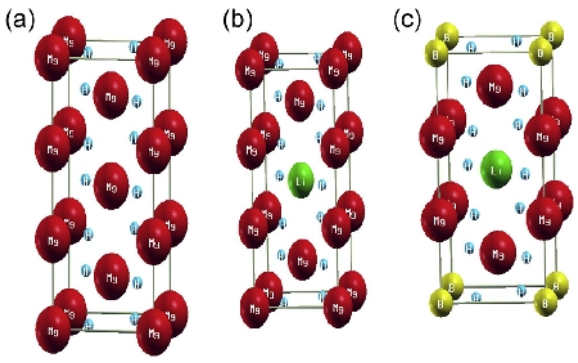

Fig. 1 – Crystal structures of (a) pure, (b) M-doped MgH_2 where M = B or Li; (c) Co-doped MgH_2. Red, blue, green and yellow balls represent respectively Mg, H, Li and B atoms. (For interpretation of the references to colour in this figure legend, the reader is referred to the web version of this article.)

Please cite this article in press as: Abdellaoui M, et al., First principle study of hydrogen storage in doubly substituted Mg based hydrides Mg_5MH_{12} (M = B, Li) and Mg_4BLiH_{12}, International Journal of Hydrogen Energy (2016), http://dx.doi.org/10.1016/j.ijhydene.2016.04.122

Table 1 – Relaxed lattice parameters, equilibrium volumes (V) and gravimetric and volumetric capacities.

System	a = b(Å)	c (Å)	Volume V (Å^3)	Gravimetric capacity (wt%)	Volumetric capacity (g H_2/l)
Mg_6H_{12}	4.545	9.006	186.037	7.65	107.11 (110.00)
	4.585 [23]				
	4.465 [35]				
Mg_5BH_{12}	4.435	8.78	172.696	8.31	115.38
Mg_5LiH_{12}	4.462	9.112	181.415	8.54	109.84
Mg_4BLiH_{12}	4.373	8.466	161.896	9.45	123.08

As the atomic radius of atoms decreases in this order Mg (159.9 pm) > Li (152 pm) > B (79.5 pm), the lattice parameters decrease in the same order when we replace one or two Mg by Li, B and Li–B. As a consequence, a reduction in the cell volume leads to an increase in the volumetric capacity from 110 g H_2/l for MgH_2 (pure MgH_2) to 123.08 g H_2/l for the co-doped system.

Along the increase of the volumetric capacity, a remarkable increase of the gravimetric capacity from 7.65 to 9.45 wt% is noticed, which is mainly due the lightweight nature of the doping elements B and Li.

Thermodynamic properties

The heat of formation ΔH is the most important thermodynamic parameter used to identify and classify materials for hydrogen storage. This is due to the fact that it allows both determining the heat of the hydrogenation reaction (if ΔH < 0 the hydride is stable and vice versa), and deducing the desorption temperature of hydrogen. This quantity ΔH could be defined as the difference between the sum of total energy of products and reactants [36]. However for an ideal material, for hydrogen storage transportation applications, the heat of formation ΔH should be in the range 20–40 kj/mol (H_2) [37].

The reactions related to the formation of hydrides in our study are:

$$6Mg + 6H_2 \rightarrow Mg_6H_{12} \quad (1)$$

$$5Mg + M + 6H_2 \rightarrow Mg_5MH_{12}\ (M = B \text{ or } Li) \quad (2)$$

$$4Mg + B + Li + 6H_2 \rightarrow Mg_4BLiH_{12} \quad (3)$$

Based on these reactions, we have calculated the heat of formation of pure, single doped and co-doped MgH_2 according to the following formulas:

$$\Delta H = E_{tot}(Mg_6H_{12}) - 6E_{tot}(Mg) - 6E_{tot}(H_2) \quad (4)$$

$$\Delta H = E_{tot}(Mg_5MH_{12}) - 5E_{tot}(Mg) - E_{tot}(M) - 6E_{tot}(H_2) \quad (5)$$

$$\Delta H = E_{tot}(Mg_4BLiH_{12}) - 4E_{tot}(Mg) - E_{tot}(B) - E_{tot}(Li) - 6E_{tot}(H_2) \quad (6)$$

The value of the total energy of the H_2 molecule is $E_{tot}(H_2) = -2.320$ Ry, was taken from Refs. [38,39]. The total energies of pure elements have been calculated using their lattice parameters given in Ref. [40]. And the temperature of dehydrogenation can be estimated by Refs. [23–28,44]:

$$T_d = \Delta H/\Delta S \quad (7)$$

The heats of formation and desorption temperatures of the studied systems are listed in Table 2.

The calculated heat of formation and decomposition temperature of MgH_2 are comparable to those obtained in previous works [23–28]. MgH_2 exhibits high stability and also high decomposition temperature. The single substitution of Mg by Li and B increases the heat of formation for Mg_5LiH_{12} and Mg_5BH_{12} (Table 2), which reduces the stability and the decomposition temperature of the hydride. The obtained value for the substitution of Mg by Li is in good agreement with the measured value −48.3449 kJ/mol H_2 given in Ref. [43]. Unfortunately, such performances are not satisfying according to the optimum values of heat of formation and desorption temperature advised by the department of energy DOE (ΔH = 20–40 kJ/mol H_2, T ≈ 300 K). We remark that the substitution with Li element doesn't lead to a significant decreasing of the desorption temperature since the heat of formation doesn't get a significant decreasing (Table 1) and then the system keeps a relatively high stability.

Thus, as an approach to improve these results, we propose to study the effect of double substitution with Li and B (Mg_4LiBH_{12}). It can be stated that the system exhibits a significant improvement of the dehydrogenation thermodynamics, for a co-doping by B, Li as compared to the single doping (Table 1), accompanied by a remarkable increase of the gravimetric capacity due the lightweight nature of the doping elements (Table 2) (Table 3).

In order to assert the approach used in this work, some of the best results obtained in different studies on hydrogen

Table 2 – Heat of formation and desorption temperature for pure, single and double substituted MgH_2.

System	Heat formation (kJ/mol H_2)	Desorption temperature (k)
Mg_6H_{12}	−62.95	475.83
	−79.577 [23]	482.52 [24,25]
	−63.018 [24,25]	460.12 [26–28]
	−62.57 [26–28]	
Mg_5BH_{12}	−15.95	122.03
Mg_5LiH_{12}	−56.17	429.83
Mg_4BLiH_{12}	−32.03	271.64

Please cite this article in press as: Abdellaoui M, et al., First principle study of hydrogen storage in doubly substituted Mg based hydrides Mg_5MH_{12} (M = B, Li) and Mg_4BLiH_{12}, International Journal of Hydrogen Energy (2016), http://dx.doi.org/10.1016/j.ijhydene.2016.04.122

Table 3 – Summary of our previous work results.

System		Gravimetric capacity (wt%)	Heat of formation (kJ/mol H_2)
$Mg_{16}H_{32}$	This work	7.65	−62.95
$Mg_{14}AlZnH_{32}$	[26]	6.94	−38.87
$Mg_{14}AlTiH_{32}$	[26]	7.21	−37.26
$Mg_{14}LiZnH_{32}$	[26]	7.25	−38.27
$Mg_{14}Sr_2H_{32}$	[28]	7.07	−33.85
$Mg_{15}VH_{32}$	[25]	7.20	−43,601
$Mg_{15}NiH_{32}$	[25]	7.08	−42,625
$Mg_{15}CrH_{32}$	[27]	7.19	−38.79
$Mg_{15}NbH_{32}$	[27]	6.59	−40.96
Mg_5BH_{12}	This work	8.31	−15.95
Mg_5LiH_{12}	This work	8.54	−56.17
Mg_4BLiH_{12}	This work	9.45	−32.03

storage in MgH_2 are collected, for comparison, in Table 4. Throughout these different studies [25–28], MgH_2 was either doped or co-doped by a variety of elements of the periodic table. It was proved that single substitution as well as double substitution improved MgH_2 thermodynamics properties. However the nature of the doping atoms, which mostly are heavy elements, affects negatively the system gravimetric capacities which may increase considerably if the MgH_2 is co-doped by lightweight elements B and Li without losing the performances of the thermodynamic properties of the hydride. Thus, we show that Mg_4BLiH_{12} exhibits the best hydrogen storage properties.

Density of states

To understand the co-doping effect on the hydrogenation performances, we calculated the density of states of MgH_2 and Mg_4BLiH_{12}. The total and partial density of state (TDOS and PDOS) of both pure and double substituted MgH_2 are shown in Fig. 2 and Fig. 3 respectively.

From the total and partial DOS of the pure MgH_2 (Fig. 2), we can see that the hydride exhibits a strong orbital hybridization between Mg(3s-3p) and H(1s) orbitals which explains its high heat formation obtained in Section Thermodynamic properties and consequently its high stability. On the other hand, the PDOS and TDOS of Mg_4BLiH_{12} (Fig. 3) show the creation of a new orbital hybridization between Li(2p)-Mg(3p), B(2s,2p)-Mg(3s,3p) and Li(2p)-H(1s) in addition to a weak orbital hybridization between B(2p)-Li(2p). The apparition of new bonding between the different elements weakens the strong bonding between Mg and H which may explain the destabilization of the system and as a result the decrease of heat of formation and desorption temperature previously mentioned.

Charge analysis

Given that, the bonding nature between elements is defined from their charge density. Hence, MgH_2 exhibits a mixture of an ionic-covalent bond [26], which is in agreement with our results, $Mg^{1.509+}$ and $H^{0.754-}$ (Table 4). In the present study MgH_2 is either doped or co-doped with Boron and Lithium, thus we observe a decrease of the charge density of both Mg and H (Table 4). This result may be explained by the charge transfer between the elements forming the systems. Especially, between Hydrogen and Magnesium (Mg–H), Hydrogen and Boron or Lithium (B–H or H–Li).

We note that the stability and also the desorption temperature of the systems depend on the charge quantity received by the hydrogen [41]. When the charge received by H decreases, the stability and decomposition temperature decrease. As shown clearly from Table 4, the charge decreases as follows: $Mg_6H_{12} \rightarrow Mg_5LiH_{12} \rightarrow Mg_4BLiH_{12} \rightarrow Mg_5BH_{12}$ which is the same order of the system's destabilisation. The charge decreases, particularly for Hydrogen atoms located near Boron and Lithium atoms, indicating that MgH_2 ionic bonding becomes weaker, which therefore explains the improvement of its dehydrogenation performances [42].

Conclusion

First-principles calculations have been performed to investigate the heat of formation, temperature of desorption of the pure MgH_2, Mg_5MH_{12} (M = B and Li) and Mg_4BLiH_{12} systems. We have shown that the co-doping improves considerably the thermodynamic properties and the storage capacities of the material since the co-doping with B and Li weakens the Mg–H bonds due to the strong hybridization between Mg and M p orbitals. The analysis of the charge transfer between different elements shows that the charge received by H decreases leading to a decrease of stability and desorption temperature. The study we performed shows that the double substitution with Li and B (Mg_4LiBH_{12}) leads to an important improvement in the thermodynamic properties accompanied by an increase of the gravimetric and volumetric capacities from 7.65 to 9.45 wt% and from 110 to 122.65 gH_2/l respectively. In addition, the obtained values of heat of formation (−32.03 kJ/mol H_2) and desorption temperature (271.64 K) are in concordance with those advised by the department of energy DOE (ΔH = 20–40 kJ/

Table 4 – Heat of formation and the charge density of the different elements in the studied systems. The +(−) sign indicates that charge is transferred (received).

System	Mg_6H_{12}		Mg_5LiH_{12}		Mg_4BLiH_{12}		Mg_5BH_{12}	
ΔH (kJ/mol H_2)	−62.95		−56.17		−32.03		−15.95	
Charge	*Mg*	1.509^+	*Mg*	1.478^+	*Mg*	1.486^+	*Mg*	1.449^+
			Li	0.852^+	**Li**	0.872^+		
					B	0.717^+	**B**	0.717^+
			$H_{closest}$**Li**	0.607^-	$H_{closest}$-**B**	0.549^-	$H_{closest}$-**B**	0.535^-
	H	0.754^-	H	0.736^-	*H*	0.715^-	H	0.757^-

Please cite this article in press as: Abdellaoui M, et al., First principle study of hydrogen storage in doubly substituted Mg based hydrides Mg_5MH_{12} (M = B, Li) and Mg_4BLiH_{12}, International Journal of Hydrogen Energy (2016), http://dx.doi.org/10.1016/j.ijhydene.2016.04.122

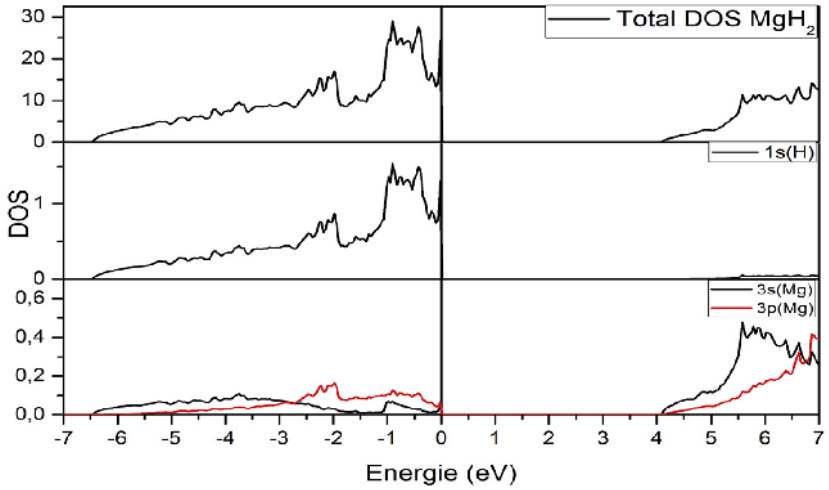

Fig. 2 – Total and partial density of states for MgH_2.

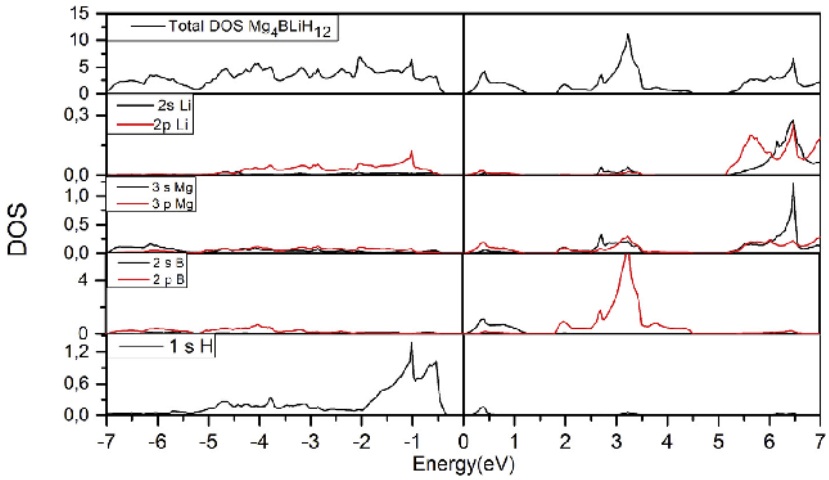

Fig. 3 – Total and partial density of states for Mg_4BLiH_{12}.

mol H_2, T ≈ 300 K). Thus, it appears that Mg_4LiBH_{12} stands as one of the best material for hydrogen storage due to its outstanding characteristics. To the best of our knowledge, such compound haven't yet implemented and synthesized. It is worth to achieve an experimental analysis of its thermodynamics properties and test its potential applications.

REFERENCES

[1] Shang CX, Bououdina M, Guo ZX. Structural stability of mechanically alloyed (Mg+10Nb) and (MgH_2+10Nb) powder mixtures. J Alloys Compd 2003;349:217.
[2] Liang G, Huot J, Boily S, Van Neste A, Schulz R. Catalytic effect of transition metals on hydrogen sorption in nanocrystalline ball milled MgH_2–Tm (Tm=Ti, V, Mn, Fe and Ni) systems. J Alloys Comp 1999;292:247.
[3] Hanada Nobuko, Ichikawa Takayuki, Orimo Shin-Ichi, Fujii Hironobu. Correlation between hydrogen storage properties and structural characteristics in mechanically milled magnesium hydride MgH_2. J Alloys Comp 2004;366:269–73.
[4] Tanniru Mahesh, Slattery Darlene K, Ebrahimi Fereshteh. A study of stability of MgH_2 in Mg–8at%Al alloy powder. Int J Hydrogen Energy 2010;35:3555–64.
[5] Chourashiya MG, Yang Dong-Cheol, Kim Sae-Youn, Park Choong-Nyeon, Park Chan-Jin. Comparison of commercial and hydriding-combustion-synthesized Mg-hydride. Mater Lett 2012;66:42–5.
[6] Wei Lingjun, Zhu Yunfeng, Li Liquan. Effect of SiC on hydrogen storage properties of $Mg_{95}Ni_5$ prepared by hydriding combustion synthesis and mechanical milling. J Alloys Compd 2012;539:215–20.
[7] Gasan H, Celik ON, Aydinbeyli N, Yaman YM. Effect of V, Nb, Ti and graphite additions on the hydrogen desorption temperature of magnesium hydride. Int J Hydrogen Energy 2012;37:1912–8.
[8] Song Myoung Youp, Kwak Young Jun, Lee Seong Ho, Song Jiyoung, Mumm Daniel R. Enhancement of hydrogen-storage performance of MgH_2 by Mg_2Ni formation and

Please cite this article in press as: Abdellaoui M, et al., First principle study of hydrogen storage in doubly substituted Mg based hydrides Mg_5MH_{12} (M = B, Li) and Mg_4BLiH_{12}, International Journal of Hydrogen Energy (2016), http://dx.doi.org/10.1016/j.ijhydene.2016.04.122

INTERNATIONAL JOURNAL OF HYDROGEN ENERGY 40 (2015) 6137–6144

Available online at www.sciencedirect.com

ScienceDirect

journal homepage: www.elsevier.com/locate/he

The hydrogen ab/desorption kinetic properties of doped magnesium hydride MgH_2 systems by first principles calculations and kinetic Monte Carlo simulations

M. Lakhal [a], M. Bhihi [a], A. Benyoussef [a,b,c], A. El Kenz [a], M. Loulidi [a,*], S. Naji [a,d]

[a] Laboratoire de Magnétisme et Physique des Hautes Energies(L.M.P.H.E.), URAC 12, Université Mohammed-V, Faculté des Sciences, B.P. 1014, Rabat, Morocco
[b] Institute of Nanomaterials and Nanotechnologies, MASciR, Rabat, Morocco
[c] Hassan II Academy of Science and Technology, Rabat, Morocco
[d] Department of Physics, Faculty of Science, IbbUniversity, Ibb, Yemen

ARTICLE INFO

Article history:
Received 4 November 2014
Received in revised form
13 February 2015
Accepted 28 February 2015
Available online 2 April 2015

Keywords:
Hydrogen storage
Magnesium hydride
Kinetic Monte Carlo
Ab-initio calculations
Diffusion mechanisms
Activation energies

ABSTRACT

Hydrogen storage ab/desorption kinetic properties of MgH_2 and MgH_2 doped with different metal M (M = Al,Ti,V,Fe and Ni) are investigated by using both DFT method and kinetic Monte-Carlo simulations. The first principles calculations show that the energy barriers decrease considerably when doping with a small amount of M element leading to a decreasing of both the stability and the decomposition temperature of the material. Based on the activation energies computed from DFT calculations, we show within the kinetic Monte-Carlo method that the ab/desorption time is reduced considerably without reducing much the hydrogen storage capacity of the material. From our analysis, we observed that the Ni element exhibits the most appropriate thermodynamical properties for hydrogen storage and the best kinetic of hydrogen absorption/desorption.

Introduction

Nowadays, hydrogen is considered as one of the most promising energy carriers alternatively to the fossil fuels including coal, oil and natural gas. The energetic sources will be depleting and also they are involved in the global warming. However, the development of hydrogen faces a significant problem concerning its storage. Indeed, hydrogen storage method should involve high volumetric, gravimetric capacity, a fast sorption rate at relatively low temperatures, and a recycling high tolerance. Alternative methods have been proposed including high pressure gas cylinders, liquid hydrogen, physisorption of hydrogen on materials with a high

* Corresponding author. Tel.: +212 661299306.
E-mail address: loulidi@fsr.ac.ma (M. Loulidi).
http://dx.doi.org/10.1016/j.ijhydene.2015.02.137

specific surface area, and hydrogen storage through hydrides (e.g. Boron and Magnesium hydrides). The latter is very promising due to its high hydrogen storage capacities [1–5].

More recently, it has been shown that magnesium hydride is one of the most attractive materials for hydrogen storage applications due to its high gravimetric and volumetric capacities (7.65 wt.% and 110 gH_2/l, respectively) [5]. However, this material shows slow hydrogen absorption and desorption kinetics as well as high dissociation temperature 573–673 K. These characteristics reduce its application concerning the hydrogen storage [4,6].

In a previous work, we have studied the hydrogen storage ab/desorption kinetic properties for the pure MgH_2 using Kinetic Monte Carlo simulation, then we have characterized it through density distribution of Hydrogen, filling ratios, diffusion time, temperature and pressure. The behavior of ab/desorption agree with the experimental results. The simulated computations show that the material has slow kinetics at high temperature and pressure [7]. Various attempts have been made in order to improve magnesium hydrogen absorbing-desorbing characteristics. Experimentally, it has been shown that the ball-milling with a small amount of transition metals (*TM*) or their oxides drastically accelerate the hydrogen kinetics. Moreover, they reduce the decomposition temperature of the hydride [4,5,8,9]. In recent experiment, it was shown that adding $MnFe_2O_4$ nanoparticles improve considerably the thermodynamic dehydrogenation properties of ball-milled MgH_2 doped with 7 mol% $MnFe_2O_4$ [10].

Various theoretical calculations have been performed to understand the relevant mechanism dealing with the alloying effects on the thermodynamic properties on magnesium hydride [11–13]. Based on density functional theory (DFT), we have shown, in a previous work, that alloying MgH_2 with small amounts of transition metals mixture TM (*TM* = *Ti*,*V* and *Fe*) or alkaline metal *AM* (*AM* = *Ca*,*Sr* and *Ba*) improve the stability and the desorption temperature of hydrogen in *Mg* [14,15].

The aim of this work is to study, using Kinetic Monte Carlo simulation (KMC) based on first principles calculations, the hydrogen storage ab/desorption kinetic properties of MgH_2 doped with different metal *M* (*M* = *Al*,*Ti*,*V*,*Fe* and *Ni*). To perform such computations, the activation energies that are needed for different elementary processes are estimated by performing ab-initio calculation. The hydrogen diffusion in magnesium hydride (such as dissociation of H_2, adsorption and diffusion of hydrogen) is then studied using KMC simulation. The paper is organized as follows: in sec. 2, we briefly review our calculation method while sec. 3 is devoted to the presentation and discussion of our numerical results which are compared with those obtained experimentally. The conclusion is given in the last section.

Model and computational methods

Kinetic Monte Carlo simulation

The application of the kinetic Monte Carlo (KMC) method [16] to our system is shortly described in this subsection since the detailed model based on has been reported previously in Ref. [7]. The filling of the *H* atoms is based on adsorption/desorption dissociation and diffusion processes. The adsorption of H_2, which is located at the surface (001) of a super-cell containing initially only magnesium and *M* atoms (*M* = *Al*, *Ti*, *V*, *Fe* and *Ni*), is followed by its decomposition into two *H* atoms that diffuse from an interstitial site to another one depending on the corresponding activated energies. Such activated energies are obtained from DFT calculation and implemented in the KMC method. Periodic boundary conditions have been considered along *X* and *Y*-directions to simulate an infinite system.

Defining the relation between simulated time and Monte Carlo steps (eq (1)), we can predict the hydrogen diffusion time in $Mg_{0.9375}M_{0.0625}H_2$ (*M* = *Al*,*Ti*,*V*,*Fe* and *Ni*) systems as function of temperature and pressure such that:

$$\Delta t = -\frac{ln(u)}{\sum_{i=1}^{N} \nu_0 exp\left(-\frac{E_i^a}{K_\beta T}\right)} \quad (1)$$

where ν_0 is the jump frequency (usually set to 10^{13} Hz), E_i^a the activation energy of i^{th} diffusion process (dissociation of H_2, adsorption and diffusion) taken from first-principles calculations (see sec. 2.2), *N* is the total possible events in the system, K_β the Boltzmann constant and *u* ($0 < u \leq 1$) is a uniformly distributed random variable.

Density functional theory calculations

For each material more than 300 configurations are needed to determine the different energy barriers required for hydrogen diffusion. In order to compute such barriers, we have used ab-initio calculations based on the all-electron full-potential local-orbital minimum-basis scheme FPLO9.00-34 [17,18] to solve the Kohn–Sham equations using the scalar-relativistic. The parameterization of the exchange-correlation energy has been done within the generalized gradient approximation GGA of the Perdew, Burke, Ernzerhof [19]. To ensure a high accuracy in our calculation, we used self-consistent criteria for both the energy and the density with precision of $10^{-8}Ha$ and $10^{-6}Ha^{-1}Å^{-3}$,respectively. A mesh of ($6 \times 6 \times 6$) k-points in the Brillouin zone was used in our calculation. The total energy is calculated using the scalar-relativistic scheme, for all configurations.

The hydride MgH_2 is crystallized in the rutile-type structure ($P4_2/mnm$, space group N°136) at ambient conditions [20]. All our calculations are carried out using a super-cell containing 15 *Mg* atoms, 1 *M* atom (*M* = *Al*,*Ti*,*V*,*Fe* and *Ni*) and 32 *H* atoms, denoted henceforth as *Mg*15*MH*32 as shown in Fig. 1. This choice corresponds to an *M* doped concentration of 6.25%.

The lattice parameters used in all calculation are the relaxed parameters (see Table 1) and the activation energies have been obtained from the maximal energy appearing in the possible paths between the initial *H* position and the final empty one.

Results and discussion

To apply Monte Carlo calculations in modeling *H* diffusion, we should implement some parameters including

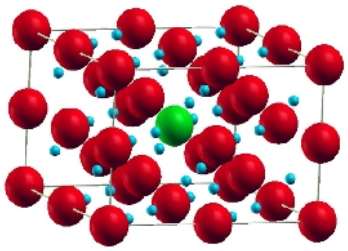

Fig. 1 – Super-cell presenting *Mg*15*MH*32; red spheres are *Mg* atoms, *H* atoms are the blue spheres and the green sphere is the *M* atom. (For interpretation of the references to colour in this figure caption, the reader is referred to the web version of this article.)

thermodynamical ones. A priory, there are many ways to get such parameters. However, we follow DFT method based on ab-initio calculations.

Thermodynamic properties from DFT method

In order to study the thermodynamic properties of $Mg_{0.9375}M_{0.0625}H_2$ ($M = Al,Ti,V,Fe$ and Ni) systems including heat of formation and desorption temperature, we first determine the equilibrium lattice parameters using the relaxation method. Indeed, we optimize the $Mg_{0.9375}M_{0.0625}H_2$ structures by evaluating the total energy as function of super cell volume. Our results are listed in Table 1, which indicates that the equilibrium parameters for the pure MgH_2 system are $a = b = 4.5094$ Å and $c = 3.0163$ Å being in good agreement with those obtained in the literature [14,20]. The addition of *M* atoms generates a small variation of the lattice parameters.To get desorption temperature, we need also to consider the following reaction related to the formation of the hydride $Mg_{0.9375}M_{0.0625}H_2$ ($M = Al,Ti,V,Fe$ and Ni), which reads as:

$$0.9375Mg + 0.0625M + H_2 \rightarrow Mg_{0.9375}M_{0.0625}H_2 \quad (2)$$

To calculate the heat formation of the reaction (eq (2)) we subtract the total energies of the pure element *Mg*, the atom *M* ($M = Al,Ti,V,Fe$ and Ni) and the hydrogen molecule from its hydride $Mg_{0.9375}M_{0.0625}H_2$ obtained from relaxation method:

$$\Delta H = E_{tot}(Mg_{0.9375}M_{0.0625}H_2) - 0.9375E_{tot}(Mg) - 0.0625E_{tot}(M) - E_{tot}(H_2) \quad (3)$$

Using the value of hydrogen total energy $E_{tot}(H_2) = -2.330Ry$ reported in Refs. [7], the resulting heats of formation of the studied systems are listed in Table 1. It is shown, on the one hand, that $\Delta H = -63.018kJ/mol.H_2$ for MgH_2 structure is close to the theoretical values obtained using different methods: $-63.18kJ/mol.H_2$ [11], -75.99 kJ/mol.H_2 [12], -69.51 kJ/mol.H_2 [13], -82 kJ/mol.H_2 [21], -54.4 KJ/mol.H_2 [22], -71.98 KJ/mol.H_2 [23] and also close to the experimental value $-76.15 \pm 9.2kJ/mol.H_2$ obtained in Ref. [24]. The difference between these values is due to the different methods used in the different calculations (FP-LAPW, PAW and FPLO). On the other hand, the addition of the *M* atom ($M = Al,Ti,V,Fe$ and Ni) to MgH_2 reduces the stability of MgH_2, which can lead to an improvement of the dehydrogenation kinetics. Such results well agree with the trend observed theoretically [11–14,22,23]. Moreover, our results show that the destabilization effect is enhanced in the following order *Ti*,*Al*,*Fe*,*V*,*Ni* and without unduly influenced the storage capacities (see Table 1).

The temperature of dehydrogenation can be estimated from the thermodynamical relation $\Delta H = T\Delta S$. During heating, the entropy change of the solid is very small compared to that of the gas, so the entropy change during the decomposition reaction is primarily due to the H_2 evolution. At the standard pressure and temperature, for most simple metal hydrides, the entropy is taken to be $\Delta S \approx \Delta S(H2) = 130.7$ J/mol.K, corresponding to the entropy change due to a mole of gas transforming into the solid [25]. For most of the dehydrogenation reactions, it is estimated that ΔS is in the range of 95J/molK $< \Delta S <$ 140J/molK [26]. If one approximates the entropy ΔS of the system at the standard pressure and temperature by $\Delta S(H_2) = 130.7$ J/mol.K as mentioned above, the obtained decompostion temperatures are underestimated. Indeed, the obtained decomposition temperature of the pure MgH_2 is $T_{des} = 482.52$ K and it decreases significantly with a small amount of *Al*,*Ti*,*V*,*Fe* and Ni. It is worthwhile to note that for $\Delta S = 95$J/molK we obtained $T_{des} = 663.35$ K for MgH_2, which is in good agreement with other values reported in Refs. [4,6,12,14] and it reaches a significant decreasing for the hydride magnesium doped with 6.25% of Ni($T_{des} = 448.95$ K).

Electronic structure

The density of state has been used to analyze and explain the effect of the addition of *M* elements ($M = Al,Ti,V,Fe$ and Ni) on both the stability and desorption temperature in $Mg_{1-x}M_xH_2$. For this purpose, the total (DOS) and the partial (PDOS) densities of electronic states of MgH_2 with and without *M* metals have been calculated and plotted in Figs. 2–4.

The electronic structure of the pure MgH_2 exhibits a non-metallic character with energy gap of 3.745 *eV* (Fig. 2a), which is smaller than the experimental value 5.16 *eV* [27] or 5.6 eV [28] while it is closer to the theoretical value 3.6 *eV* reported in Ref. [29]. We believe that this difference between the

Table 1 – The lattice parameters and the thermodynamical quantities of $Mg_{0.9375}M_{0.0625}H_2$ ($M = Al,Ti,V,Fe$)

Systems	Relaxed parameters (Å)	Cg (wt %)	ΔH(KJ/mol.H_2)	H_2 dissociation (eV)
MgH_2 super cell	$a = b = 9.0188$; $c = 6.0272$	7.660	−63.018	0.8
$Mg_{0.9375}Al_{0.0625}H_2$	$a = b = 9.0616$;$c = 6.0599$	7.611	−47.947	0.31
$Mg_{0.9375}Ti_{0.0625}H_2$	$a = b = 8.9416$;$c = 5.9796$	7.253	−51.417	0.37
$Mg_{0.9375}V_{0.0625}H_2$	$a = b = 9.0020$;$c = 6.0200$	7.203	−43.601	0.34
$Mg_{0.9375}Fe_{0.0625}H_2$	$a = b = 8.9416$;$c = 5.9796$	7.127	−44.972	0.36
$Mg_{0.9375}Ni_{0.0625}H_2$	$a = b = 8.9719$;$c = 5.9999$	7.081	−42.625	0.32

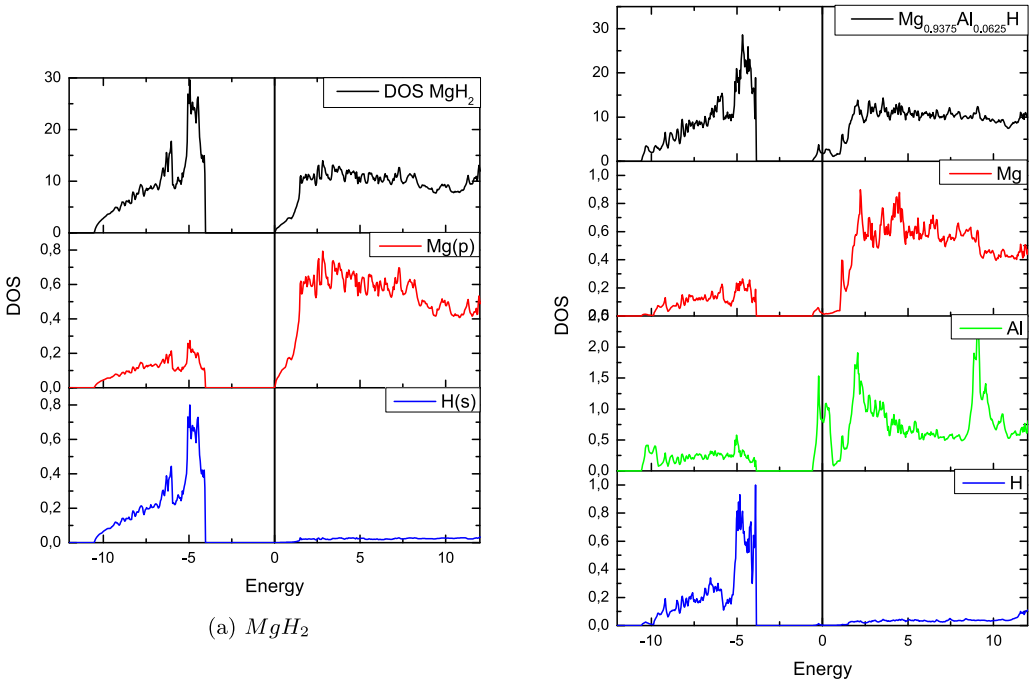

(a) MgH_2 (b) $Mg_{0.9375}Al_{0.0625}H_2$

Fig. 2 – Total and partial DOS for the pure MgH_2 and $Mg_{0.9375}Al_{0.0625}H_2$.

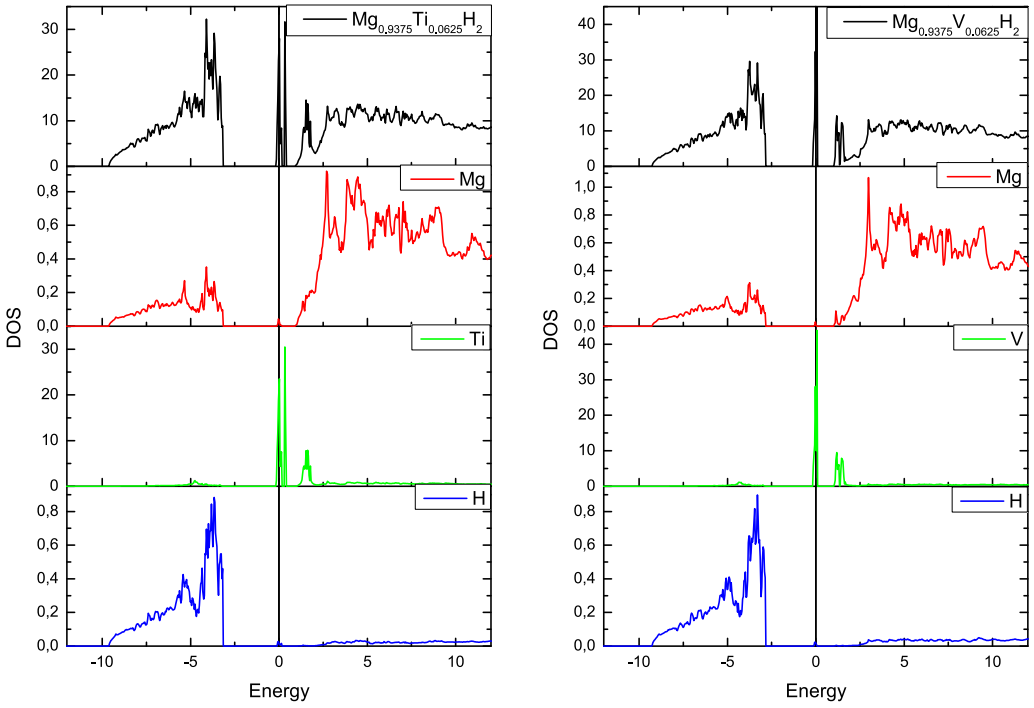

(a) $Mg_{0.9375}Ti_{0.0625}H_2$ (b) $Mg_{0.9375}V_{0.0625}H_2$

Fig. 3 – Total and partial DOS for $Mg_{0.9375}Ti_{0.0625}H_2$ and $Mg_{0.9375}V_{0.0625}H_2$.

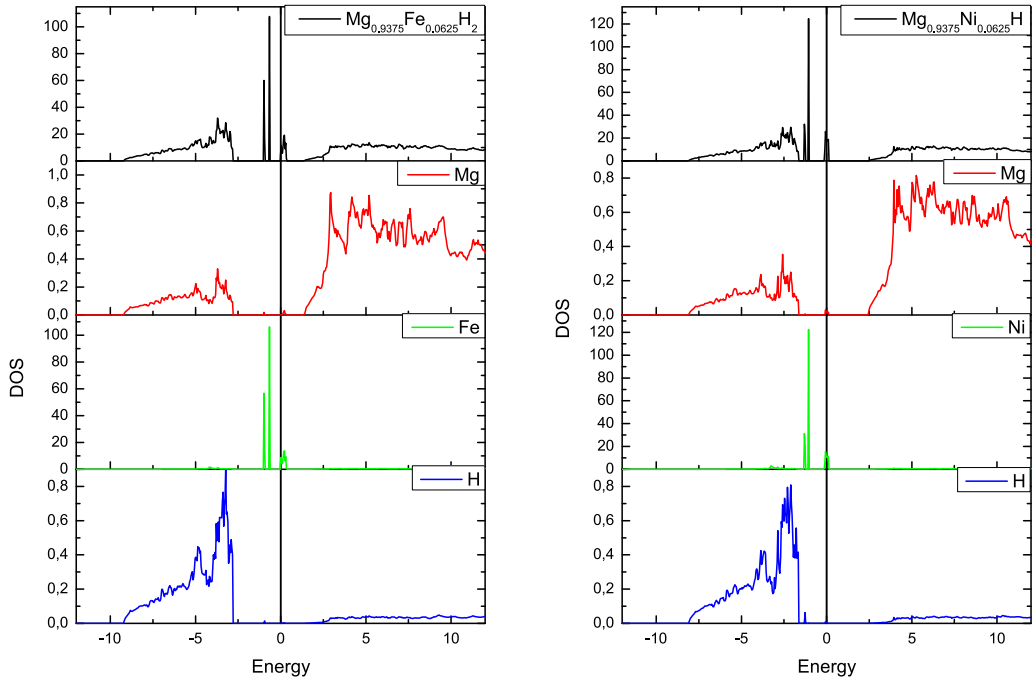

(a) $Mg_{0.9375}Fe_{0.0625}H_2$ (b) $Mg_{0.9375}Ni_{0.0625}H_2$

Fig. 4 – Total and partial DOS for $Mg_{0.9375}Fe_{0.0625}H_2$ and $Mg_{0.9375}Ni_{0.0625}H_2$.

experimental results and our calculation is due to the first principles calculations based on the density functional theory which usually suffers from the errors in the estimation of the band-gap.

The electronic structure of $Mg_{0.9375}M_{0.0625}H_2$ ($M = Al,Ti,V,Fe$ and Ni) shows that the states of "d-orbitals" of transition metal TM (Ti,V,Fe and Ni) and "p-states" of Al are localized in the band gap. The main contribution to the total DOS comes form the M elements. This indicates that there is a weak hybridization on the one hand between $TM-d$ and $H-s$ on the other hand between $Al-p$ and $H-s$ orbitals unlike the pure MgH_2 where a strong hybridization between the H and Mg atoms occurs. Moreover, no hybridization between TM and Mg atoms has been observed, while a weak hybridization between $Al-p$ and Mg occurs. This ascertainment is in agreement with the results of sec. 3.1, where the addition of Al and TM (Ti,V,Fe and Ni) in MgH_2 decreases the stability and the desorption temperature of the mixtures. We note that the MgH_2 doped Ni material exhibits the highest density of state near the Fermi level.

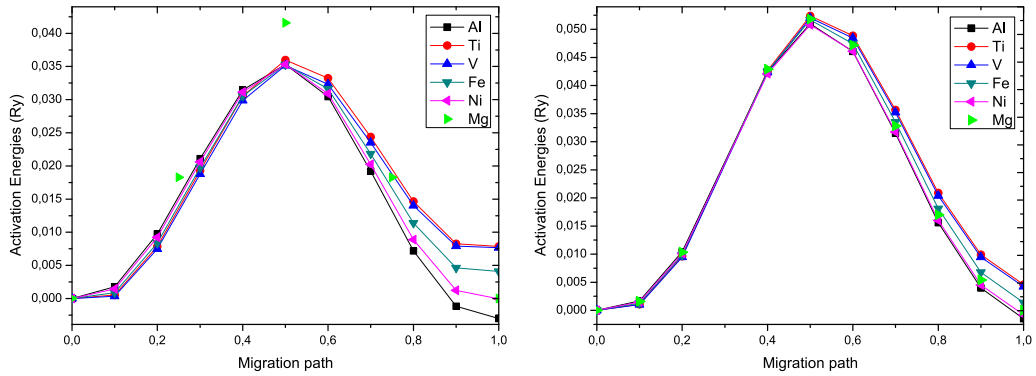

(a) Planar motion (b) inter-planar motion

Fig. 5 – Energy curves for an H atom diffusing between two interstitial sites along different paths in different mixture of $Mg_{0.9375}M_{0.0625}H_2$ ($M = Al,Ti,V,Fe$ and Ni).

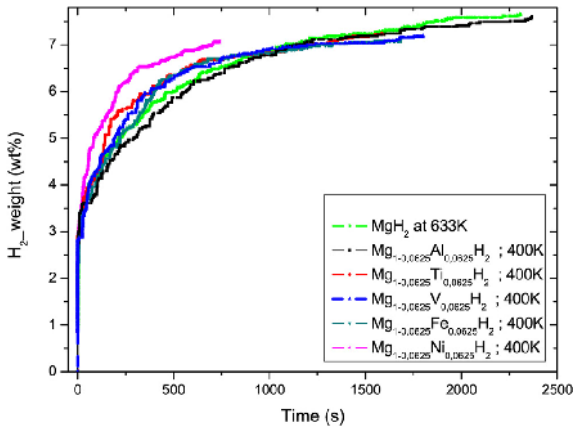

Fig. 6 – Simulation charging kinetic for the pure MgH_2 at 633 K and $Mg_{0.9375}M_{0.0625}H_2$ (M = Al,Ti,V,Fe and Ni), under 10 bar.

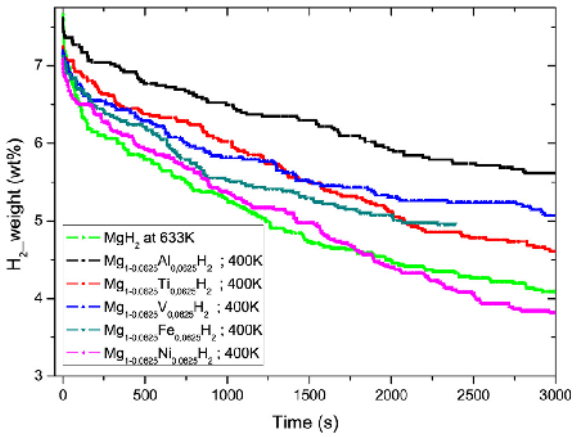

Fig. 8 – Simulation discharging kinetic for the pure MgH_2 at 633 K and $Mg_{0.9375}M_{0.0625}H_2$ (M = Al,Ti,V,Fe and Ni), under 1 bar.

Activation energies

Based on our model [7], each hydrogen atom has eleven nearest available H vacancy sites: seven in the same plane, two in the upper adjacent plane and the remaining two ones are located at the lower adjacent plane. After dissociation, the *H* atoms can move from an interstitial site to another one depending on the corresponding activated energies.

For later use, a large number of energy barriers has been computed. Among them two situations are illustrated in Fig. 5. In particular, we have found that the energies depend on the surrounding atoms and the target-interstitial sites. Increasing hydrogen atom number in the system, the barriers get enlarged. Indeed, DFT calculations reveals that the energies of planar motion of Hydrogen atoms (in plans (001)) are lower than the energies associated with the motion between two parallel plans for all cases. Therefore, hydrogen atom prefer to diffuse along *X* and *Y* direction instead of moving vertically. For the same path of diffusion, we find that the *H* barrier energies with the *M* atoms (M = *Al*,*Ti*,*V*,*Fe* and *Ni*) are generally less than that inside the pure MgH_2. This finding suggests that the *H* atoms are trapped more stably inside MgH_2 than $Mg_{0.9375}M_{0.0625}H_2$ alloys. In other words, incorporation of small quantity of *Al*,*Ti*,*V*,*Fe* or *Ni* into magnesium hydride can efficiently reduce the interaction between interstitial *H* atoms and *Mg* host and thus reduce the stability of the systems, which is in agreement with the results reported in Thermodynamic properties from DFT method section.

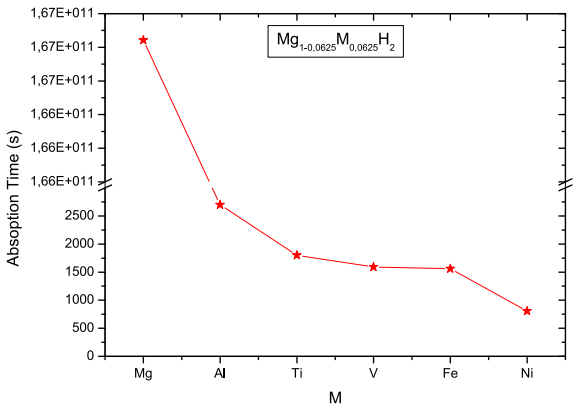

Fig. 7 – The average of filling time at 400 K and 10 bar for the pure MgH_2 and $Mg_{0.9375}M_{0.0625}H_2$ (M = Al,Ti,V,Fe and Ni).

Having determined the thermodynamic properties of MgH_2 structure using DFT method, the KMC method may be applied to study the kinetic properties of metal doped MgH_2 as described below.

The ab/desorption time by kinetic Monte Carlo simulation

The amount of absorbed hydrogen as a function of reaction time calculated (in wt. %) for MgH_2 and $Mg_{0.9375}M_{0.0625}H_2$ (M = *Al*,*Ti*,*V*,*Fe* and *Ni*) is shown in Fig. 6. Starting from an empty cell, the rate of hydrogen filled in our material exhibits a fast increasing with respect to time of absorption. Such behavior is due to the initial conditions and the initial pressure applied on the adsorption surface. Once the number of hydrogen atoms increases in the system, the activation energies increase and then the *H* atoms move with difficulties to the empty sites. For this reason, after a while from the beginning the amount of hydrogen augments slowly as function of time until reaching a maximal value for each system, which is the gravimetric capacity of the material (see Table 1).

As a result, our KMC simulations show that the absorption kinetic of different doped materials $Mg_{0.9375}M_{0.0625}H_2$ at temperature 400 K and pressure 10 bar is very fast compared to the absorption in MgH_2 at high temperature and pressure (633 K,10 bar). This is due to the fact that *H* barrier energies with the *M* atoms (M = *Al*,*Ti*,*V*,*Fe* and *Ni*) are lower than that inside the pure MgH_2. The average filling time for the pure and

Table 2 – The dehydrogenation thermodynamical quantities of $MgH_2 + 7mol\%\ MnFe_2O_4$ [10] and MgH_2 doped Ni

Systems	Hydrogen released (wt %) at 1 bar	Activation energy (KJ/mol.H_2)	T_{des}(K)
$MgH_2 + 7mol\%\ MnFe_2O_4$ [10]	5.05 in 1 h and 573 K	64.55	573.15
$Mg_{0.9375}Ni_{0.0625}H_2$	3.33 in 1/2 h and 400 K	42.625	$326.13 < T_{des} < 448.95$

doped MgH_2 materials, which is computed by using random Monte-Carlo sampling, is represented in Fig. 7. It follows clearly from this figure that the additive *M* element leads to significantly improved hydrogenation kinetics even at low temperature. For the desorption process, the addition of *M* atoms in MgH_2 improve the kinetic of desorption at low temperature but the system does not completely desorbs all hydrogen atoms which prefer to move inside rather leaving the system (see Fig. 8). In order to discharge all hydrogen atoms, one needs a high vacuum that we cannot realize within our KMC simulations. Both absorption and desorption kinetics exhibit a behavior quite similar to that observed in experiments with a quantitative difference, which is due to the used pressure and temperatures values being smaller or higher than the experimental ones and to the specific conditions of various experiments (if desorption was measured in vacuum, under He flow, … etc) [5,12,30]. In addition, upon hydrogenation of magnesium a number of phase transitions, which we are not able to simulate within our approach, occur [31–33]. The simulation of such structural phase transitions needs more appropriate model and some sophisticated and laborious methods, which we hope develop later.

However, alloying MgH_2 with small amounts of transition metals ($TM = Ti,V,Fe$ and Ni) and Al may accelerate the kinetic of absorption/desorption without reducing much its high hydrogen capacity (Table 1). We point out that the MgH_2 doped Ni presents the fastest ab/desorption kinetic since it exhibits the lowest energy barriers.

Conclusion

First-principles calculations have been used to investigate the heat of formation, temperature of desorption, diffusion barrier and time of diffusion of interstitial hydrogen atoms in the pure MgH_2 and $Mg_{0.9375}M_{0.0625}H_2$ ($M = Al,Ti,V,Fe$ and Ni) systems. Combining the DFT method, which allows the computation of energy barriers, needed in the diffusion process, and the KMC method we have shown that the doped MgH_2 system improves the thermodynamic properties and the ab/desorption kinetic of the material as summarized in what follow:

- The pure MgH_2 presents a high stability and a high decomposition temperature. At high temperature and pressure, the results of simulations indicate that the hydride involves slow kinetics.
- The stability and the decomposition temperature reduce considerably when doping MgH_2 with a small amount of $TM(TM = Ti,V,Fe$ and $Ni)$ and Al.
- DFT calculations reveal that the energies corresponding to the hydrogen atom motions in the (001) plan are lower than the energies associated with the motion between two parallel (001) plans. Therefore, hydrogen atoms prefer to diffuse along *X* and *Y* directions instead of moving vertically.
- The activation barrier for the dissociation of H_2, the barrier of diffusion and the diffusion time of *H* atoms in the pure MgH_2 are higher than those in MgH_2 doped with 6.25% of Al,Ti,V,Fe and Ni.

As a consequence, it can be concluded that alloying MgH_2 with small amounts of transition metals ($TM = Ti,V,Fe$ and Ni) and Al can drastically lower the stability of the systems, the decomposition temperature and accelerate the kinetic of ab/desorption without reducing much its high hydrogen capacity. Following our study, we remark that the Ni presents the highest performances and is the most appropriate element for better hydrogen storage. It is worthwhile to note that our theoretical study predicts that the MgH_2 doped Ni gives better dehydrogenation thermodynamical quantities compared to those obtained experimentally for MgH_2 doped $MnFe_2O_2$ nanoparticles [10](For comparison see Table 2).

Acknowledgement

This work was supported by CNRST in the framework of the national program Dev-RS/04. The authors acknowledge its financial support.

REFERENCES

[1] Zuttel A. Materials for hydrogen storage. Mater Today 2003;6(9):24–33.
[2] Zhou L. Progress and problems in hydrogen storage methods. Renew Sustain Energy Rev 2005;9(4):395–408.
[3] Chen P, Zhu M. Recent progress in hydrogen storage. Mater Today 2008;11(12):36–43.
[4] Song MY, Kwon SN, Park HR, Hong SH. Improvement in the hydrogen storage properties of Mg by mechanical grinding with Ni, Fe and V under H_2 atmosphere. Int J Hydrogen Energy 2011;36(21):13587–94.
[5] Cabo M, Garroni S, Pellicer E, Milanese C, Girella A, Marini A, Rossinyol E, Suriach S, Bar MD. Hydrogen sorption performance of MgH_2 doped with mesoporous nickel- and cobalt-based oxides. Int J Hydrogen Energy 2011;36(9):5400–10.
[6] Kurko S, Matovi L, Novakovi N, Matovi B, Jovanovi Z, Mamula BP, Grbovi Novakovi J. Changes of hydrogen storage properties of MgH_2 induced by boron ion irradiation. Int J Hydrogen Energy 2011;36(1):1184–9.
[7] Lakhal M, Bhihi M, Labrimb H, Benyoussef A, Naji S, Belhaj A, et al. Kinetic Monte Carlo and density functional study of hydrogen diffusion in magnesium hydride MgH_2. Int J Hydrogen Energy 2013;38(2):8350–6.

ARTICLE IN PRESS

INTERNATIONAL JOURNAL OF HYDROGEN ENERGY XXX (2015) 1–6

Available online at www.sciencedirect.com

ScienceDirect

journal homepage: www.elsevier.com/locate/he

First principle study of hydrogen storage in doubly substituted Mg based hydrides

M. Bhihi [a], M. El Khatabi [a], M. Lakhal [a], S. Naji [a,b], H. Labrim [c], A. Benyoussef [a,d,e], A. El Kenz [a], M. Loulidi [a,*]

[a] LMPHE, (URAC), Faculté des Sciences, Université Mohammed V, Morocco
[b] Department of Physics, Faculty of Science, Ibb University, Ibb, Yemen
[c] Centre National de l'Energie, des Sciences et des Techniques Nucléaires, Rabat, Morocco
[d] Institute of Nanomaterials and Nanotechnology, MAScIR, Rabat, Morocco
[e] Hassan II Academy of Science and Technology, Rabat, Morocco

ARTICLE INFO

Article history:
Received 26 December 2014
Received in revised form
27 March 2015
Accepted 10 April 2015
Available online xxx

Keywords:
Hydrogen storage capacity
First principle calculations
Formation energy
Mg based hydrides
Desorption temperature
FPLO

ABSTRACT

Ab-initio calculations are carried out to analyze the improvement of hydrogen storage properties, in Mg-based hydrides, through a double substitution ($Mg_{14}TMAlH_{32}$ and $Mg_{14}TMLiH_{32}$ TM = Ti, Sc, Zn). The calculations are performed using the all-electron full-potential local-orbital minimum-basis scheme (FPLO9.00-34). Our results indicate a decrease of the heat of formation and desorption temperature, while preserving the gravimetric storage capacity around 7.6 wt%, these outcomes are probably due to the second substitution, Al or Li, which are characterized by their light weights. Discussions of the charge exchange and the density of states are done, to offer more possible explanations of our results.

Introduction

With the raising worldwide awareness of the environment and rarity of fossil fuels, new generation of energies, particularly clean and renewable energies, has emerged as a solution. Hydrogen is one of these energies, accurately as an energy carrier. It is the most abundant element on earth. Its energy density is three times that of diesel and the outcome of its combustion is water. These qualities make hydrogen the ideal energy of tomorrow. Among the different methods for hydrogen storage, the solid storage has proven to be the best.

The magnesium based hydride (MgH_2) is one of the most promising materials for hydrogen "solid" storage applications due to its high gravimetric and volumetric capacities (7.65 wt.% and 110gH_2/l, respectively) [1]. However, the rather slow hydrogen sorption proprieties, as well as the high desorption temperature (573–673 K) hinder its commercial applications [2]. That is why various attempts have been made in order to improve MgH_2 hydrogen absorbing and desorbing characteristics. Experimentally, it has been reported that

* Corresponding author.
E-mail addresses: loulidi@fsr.ac.ma, loulidim60@gmail.com (M. Loulidi).
http://dx.doi.org/10.1016/j.ijhydene.2015.04.061

mixing magnesium or magnesium hydride with small amounts of transition metals (TM), including their oxides, radically accelerate the hydrogen kinetics along a considerable decrease of desorption temperatures [3–10]. Also several theoretical studies have been carried out to predict effects of substitution on the thermodynamic properties of the magnesium-based hydrides [11–21]. The obtained results are in a good agreement with experimental investigations.

The aim of this paper is to contribute to these works by studying the effect of substitution on the hydrogen sorption proprieties of MgH_2. In the first step of the calculations we initiate a single substitution, where the system was doped with 6.25% of transition metals ($Mg_{15}MH_{32}$ where M = Ti, Sc and Zn). The results were satisfying but were not sufficient to reach the optimum values of heat of formation −40 kJ/mol H_2 [11] and desorption temperature 289–393 K for a PEMFC (*Proton Exchange Membrane Fuel Cells Or Polymer Electrolyte Membrane Fuel Cells*) [22]. In the second step we increased the amount of TM in the system, 12.5%, as an approach to improve the results already obtained. However, this has led to an important decrease of the gravimetry. For example in the case of $Mg_{14}Ti_2H_{32}$ the gravimetry dropped to 6.88wt% instead of 7.25 wt% and 7.6 wt% for $Mg_{15}TiH_{32}$ and MgH_2 respectively. To prevent this decrease of the gravimetry, we proceeded by a double substitution, TM and either Li or Al. Our approach was based on the proprieties that characterize Al and Li, particularly their small weight. The systems studied in this paper are ($Mg_{14}TMAlBH_{32}$ and $Mg_{14}TMLiBH_{32}$, TM = Ti, Sc and Zn). The heat of formation and desorption temperature are calculated, and also the orbital hybridization and the exchange of charge between elements. These calculations are carried out to explain the effect of double substitution on the dehydrogenation proprieties of these systems. In Sec. 2 we present the computational detail carried using ab-initio calculations, while Sec. 3 is devoted to the obtained results and their discussion. Our conclusion is given in Sec. 4.

Computational details

In this paper, we used ab initio calculations based on the all-electron full-potential local-orbital minimum-basis scheme FPLO9.00-34 [23,24]. This has been performed to solve the Kohn–Sham equations using the scalar-relativistic scheme. The parameterization of the exchange-correlation energy has been done within the generalized gradient approximations [25]. To ensure a high accuracy in our performed computations, we used both self-consistent criterions of the energy and the density together with a precision of 10^{-8} Ha and 10^{-6} respectively. For an accurate Brillouin zone integration, we considered a $12 \times 12 \times 12$ K-point mesh. The valence basis state sets are (3s,3p) and (1s) for the Mg and the H respectively. Lattice parameters "a = b and c" have been optimized, for each Mg based hydride ($Mg_{14}TMAlH_{32}$ and $Mg_{14}TMLiH_{32}$), using the relaxation method.

Results and discussion

First of all, we relaxed the lattice parameters using the relaxation method, then we calculated the energies of formation, and deduced the desorption temperature. Finally we discussed, based on the charge exchange values and the density of states, the effect of doping on the stability of the systems.

Structural parameters and relaxation

MgH_2 exhibits a rutile structure. Its space group is (P42/mnm, N°136), and lattice parameters are: a = b = 4.501 Å and c = 3.01 Å [26]. The Wyckoff position of Mg and H are 2a (0, 0, 0) and 4f (0.304, 0.304, 0) respectively.

The relaxed lattice parameters are listed in Table 1, our calculated values are in fair agreement with other works results [14,17].

In order to reach small concentrations, we use a large primitive supercell, $2 \times 2 \times 2$ of MgH_2 unit cells. In this atomic representation, one Mg atom, is replaced by transition metals TM (TM = Ti, Sc or Zn) and another one is replaced by either Al or Li atoms. These replacements create changes on the periodicity of the crystal. The new system symmetry structure is (Cmmm space group N°65) with 17 non-equivalents site.

Hydrides stability: heat of formation

The heat of formation ΔH, which is the most important thermodynamic parameter, has been calculated and used to predict the stability of the studied systems. For $\Delta H < 0$ kJ/mol(H_2) the system is stable, and for $\Delta H > 0$ kJ/mol(H_2) the system is unstable. However, for an ideal material for hydrogen storage, the heat of formation ΔH should be around −40 kJ/mol (H_2) [11].

This quantity ΔH can be defined as the difference between the total energy of products and reactants [9]:

$$\Delta H_{HF} = \sum E_{tot}(\text{products}) - \sum E_{tot}(\text{reactants}) \quad (1)$$

The reactions related to the formation of the hydrides MgH_2 and $Mg_{14}TMAH_{32}$ are:

$$Mg + H_2 \rightarrow MgH_2 \quad (2)$$

Table 1 – Wyckoff positions of no equivalent atoms.

No.	Element	X	Y	Z
1	Ti	0	0.5	0
2	Li	0	0	0.5
3	Mg	0	0.75	0.25
4	Mg	0.25	0.5	0.25
5	Mg	0.75	0.25	0
6	Mg	0	0	0
7	Mg	0	0.5	0.5
8	Mg	0.75	0.25	0.5
9	H	0	0.65215	0
10	H	0	0.84785	0
11	H	0.34785	0.25	0.25
12	H	0.75	0.40215	0
13	H	0.09785	0	0.25
14	H	0.40215	0	0.25
15	H	0	0.65215	0.5
16	H	0	0.84785	0.5
17	H	0.75	0.40215	0.5

Please cite this article in press as: Bhihi M, et al., First principle study of hydrogen storage in doubly substituted Mg based hydrides, International Journal of Hydrogen Energy (2015), http://dx.doi.org/10.1016/j.ijhydene.2015.04.061

Table 2 – Theoretical and Experimental heat of formation for MgH_2.

Theoretical works	Experimental work
−79,577 [17]	−74,3 ± 0,5 [29]
−55.648 to −65.196 [33]	−81,2 [30]
−71.1 [32]	−76.15 ± 9.2 [14,31]
−62.57 This work	−68.00 ± 9.2 [32]

Table 3 – Gravimetry and heat of formation for single and double substituted MgH_2.

Systems	Gravimetry (wt %)	Heat of formation (kJ/mol de H_2)
$Mg_{16}H_{32}$	7.65	−62.57
$Mg_{14}AlScH_{32}$	7.26	−44.25
$Mg_{14}AlZnH_{32}$	6.94	−38.87
$Mg_{14}AlTiH_{32}$	7.21	−37.26
$Mg_{14}LiScH_{32}$	7.6	−57.99
$Mg_{14}LiTiH_{32}$	7.55	−47.06
$Mg_{14}LiZnH_{32}$	7.25	−38.27
$Mg_{15}TiH_{32}$	7.25	−51.24
$Mg_{15}ZnH_{32}$	6.97	−53.04
$Mg_{15}ScH_{32}$	7.30	−58.63

$$14\ Mg + TM + A + 16\ H_2 \rightarrow Mg_{14}TMAH_{32}\ (A = Al \text{ or } Li \text{ and } TM = Ti, Sc, Zn) \quad (3)$$

Based on these reactions, we have calculated the heat of formation of MgH_2 and $Mg_{14}TMAH_{32}$ according to the following formulas:

$$\Delta H = E_{tot}(MgH_2) - E_{tot}(Mg) - E_{tot}(H_2) \quad (4)$$

$$\Delta E_{HF} = E_{tot}(Mg_{14}TMAH_{32}) - 14E_{tot}(Mg) + E_{tot}(TM) + E_{tot}(A) - 16E_{tot}(H_2) \quad (5)$$

The value of the total energy of the H_2 molecule is $E_{tot}(H_2) = -2.320$ Ry, was taken from Refs. [5,27]. The total energies of pure elements have been calculated using their lattice parameters given in Ref. [28].

Based on the all-electron full-potential local-orbital minimum-basis scheme method, implemented in FPLO9.00-34 version, we calculated the total energy and the heat of formation of MgH_2 using the optimized lattices parameters. The obtained results are listed in Table 2.

As previously mentioned single substitution, with different elements, was one of the various methods suggested to destabilize MgH_2 [2–8,17,19,20]. In this study, and through single substitution, we found that the heat of formation of $Mg_{15}TMH_{32}$ (TM = Sc, Zn and Ti) are −58.63, −53.04, −51.24 kJ/mol H_2 respectively, which indicate the destabilization of the parent system MgH_2 (−62.57 kJ/mol H_2). However increasing the percentage of TM, known for their heavy weight, in the system can affect negatively the gravimetry and the volumetry. That is why, In order to meet the ideal heat of formation −40 kJ/mol H_2, without decreasing the gravimetry, we proceeded by a double substitution. The first element is one of the transition metals and the second is either Li or Al. Our choice "Li and Al" was based on their proprieties especially small weight.

The heat of formation calculated for these systems confirm our choice of double substitution, since for the systems $Mg_{14}AlTMH_{32}$ ΔH values are between −37.26 and −44.25 kJ/mol H_2, also for $Mg_{14}LiTMH_{32}$ the values are between −38.27 and −57.99 kJ/mol H_2. As it has been expected, the heat of formation decreased, while the gravimetry remained almost unchanged, around 7.6 wt%. See Table 3.

The substitution with small amounts of alloying, TM and Al or TM and Li, within MgH_2 reduces its stability leading to an improvement in term of the heat of formation and the desorption temperature which will be discussed below.

Desorption temperature

The thermodynamic properties of the hydrides are described by the standard Gibbs energy [34]:

$$\Delta G = \Delta H - T\Delta S,\ (\Delta S \approx \Delta S\ (H_2) = 130.7\ J/mol\ K) \quad (6)$$

where ΔH and ΔS are the heat of formation and the entropy change of the dehydrogenation reaction respectively. At the decomposition temperature T_d and the constant pressure, the standard Gibbs energy ΔG becomes zero. Therefore, the temperature of dehydrogenation can be estimated by:

$$T_d = \Delta H/\Delta S \quad (7)$$

Table 4 – Desorption temperature and the charge of the different elements in the studied systems.

Systèmes	MgH_2		$Mg_{14}AlScH_{32}$		$Mg_{14}AlZnH_{32}$		$Mg_{14}AlTiH_{32}$	
Temperature (°k)	460.12		325.39		285.86		274.03	
Charges	*Mg*	1.509^+	*Mg*	1.453^+	*Mg*	1.465^+	*Mg*	1.454^+
			Al	1.405^+	*Al*	1.419^+	*Al*	1.439^+
	H	0.754^-	*Sc*	1.687^+	*Zn*	1.111^+	*Ti*	1.568^+
			H	0.688^-	*H*	0.686^-	*H*	0.685^-
Systems	**MgH_2**		**$Mg_{14}LiScH_{32}$**		**$Mg_{14}LiZnH_{32}$**		**$Mg_{14}LiTiH_{32}$**	
Temperature (°k)	460.12		426.42		281.44		346.06	
Charges	*Mg*	1.509^+	*Mg*	1.480^+	*Mg*	1.482^+	*Mg*	1.476^+
			Li	0.862^+	*Li*	0.848^+	*Li*	0.860^+
	H	0.754^-	*Sc*	1.954^+	*Zn*	1.144^+	*Ti*	1.818^+
			H	0.743^-	*H*	0.699^-	*H*	0.739^-

Please cite this article in press as: Bhihi M, et al., First principle study of hydrogen storage in doubly substituted Mg based hydrides, International Journal of Hydrogen Energy (2015), http://dx.doi.org/10.1016/j.ijhydene.2015.04.061

According to the Equation (7) the decomposition temperature of pure MgH_2 is 460.12 K, which is in agreement with other works values 573–673 K [1,5,17]. This temperature is still high for practical use since the optimum ranges are 289–393 K for a PEMFC [22].

As mentioned earlier, the double substitution has a great impact on the heat of formation. The same behavior is insight at the desorption temperature, as the decrease of T_d is around 15–30% see Table 4.

The result may be explained by the charge transfer between the elements forming the systems. Specially, between the Hydrogen and the Magnesium Mg–H, the Hydrogen and the transition metals H-TM (TM = Ti, Sc or Zn) and between the hydrogen and Lithium or Aluminum H–Li, H–Al. We note that the stability and also the desorption temperature of the systems depends on the charge quantity received by the hydrogen. When the charge, received by H, decreases the stability decreases and also desorption temperature decreases.

Generally the charge transfer between two elements defines the type of the binding between them. For MgH_2 crystal, it is reported that the nature of binding Mg–H is a mixture of covalent and ionic bonds. However the binding is more ionic than covalent. As shown clearly from Table 4, the charge transfer decrease as follows: Sc→Ti→Zn for $Mg_{14}LiTMH_{32}$, and Sc→Zn→Ti for $Mg_{14}AlTMH_{32}$. The decrease of this charge transfer, particularly between Mg–H, indicate that the ionic bonding becomes weaker, which therefore help improve the dehydrogenation performance of MgH_2.

MgH_2 $(H^{0.754-})$ → $Mg_{14}LiScH_{32}$ $(H^{0.743-})$ → $Mg_{14}LiTiH_{32}$ $(H^{0.739-})$ → $Mg_{14}LiZnH_{32}$ $(H^{0.699-})$

MgH_2 $(H^{0.754-})$ → $Mg_{14}AlScH_{32}$ $(H^{0.688-})$ → $Mg_{14}AlZnH_{32}$ $(H^{0.686-})$ → $Mg_{14}AlTiH_{32}$ $(H^{0.685-})$

State density analysis

To understand and explain the improvement of the hydrogenation performances, during the double substitution, we calculated the density of states of MgH_2, $Mg_{14}TMAlH_{32}$ and $Mg_{14}TMLiH_{32}$. This study will help to clarify the effect of the co-doping on the hydrogenation performances of these systems.

Through the study of the total and partial density of state (DOS and P-DOS) of pure (Fig. 1) and double substituted MgH_2 (Figs. 2–3), we conclude that the pure MgH_2 (Fig. 1) has an insulator feature, with a wide band gap Eg = 4.06 eV. This value is better than our previous results Eg = 2.74 eV [17], where the study was carried out by the KKR-CPA code, and still in fair agreement with other theoretical [33,32,35] and experimental works Eg = 5.16 eV [36] or 5.6 eV [37]. In the valence band for MgH_2 (see Fig. 1), we observed two parts: the first one is characterized by a high hybridization between 3p and 1s orbital of Mg and H respectively, and the second one is characterized by a small hybridization between 3s and 1s orbital of Mg and H respectively.

To predict the nature of the bonding created, after substitution in MgH_2 parent, we analyzed the location of the element's orbital. The partial and total density of states of $Mg_{15}TM–LiH_{32}$ (TM = Ti, Sc and Zn) (Fig. 2) show the creation of a very weak hybridization between Li–Mg and Li–H. However noticeable hybridizations appear between TM-Mg and TM-H, but are still weaker than the ones between Mg–H. This reflects the creation of the bonding between TM and both Mg and H, at the expense of the current bonding between Mg and H.

In the case of $Mg_{15}TMAlH_{32}$ (TM = Ti, Sc and Zn) (Fig. 3) the partial and total density of states show a better hybridization between Al and both Mg and H than the ones between Li–Mg and Li–H. Also hybridizations between TM and all elements except hydrogen were observed.

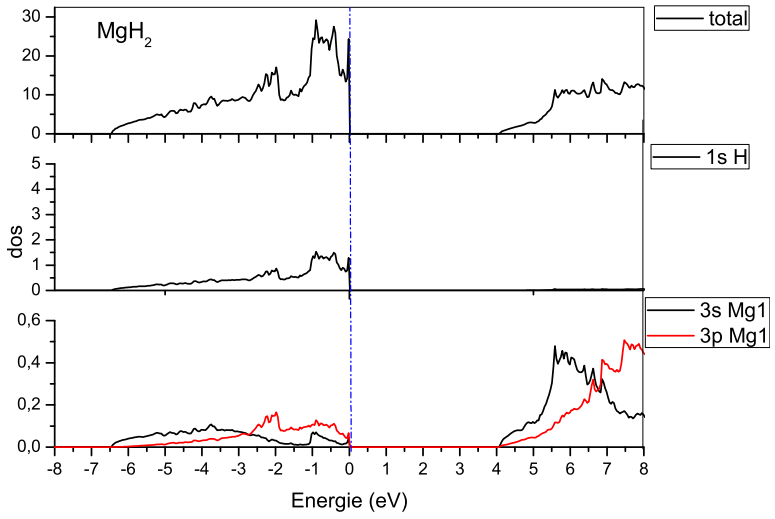

Fig. 1 – Total and partial density of states for MgH_2.

Please cite this article in press as: Bhihi M, et al., First principle study of hydrogen storage in doubly substituted Mg based hydrides, International Journal of Hydrogen Energy (2015), http://dx.doi.org/10.1016/j.ijhydene.2015.04.061

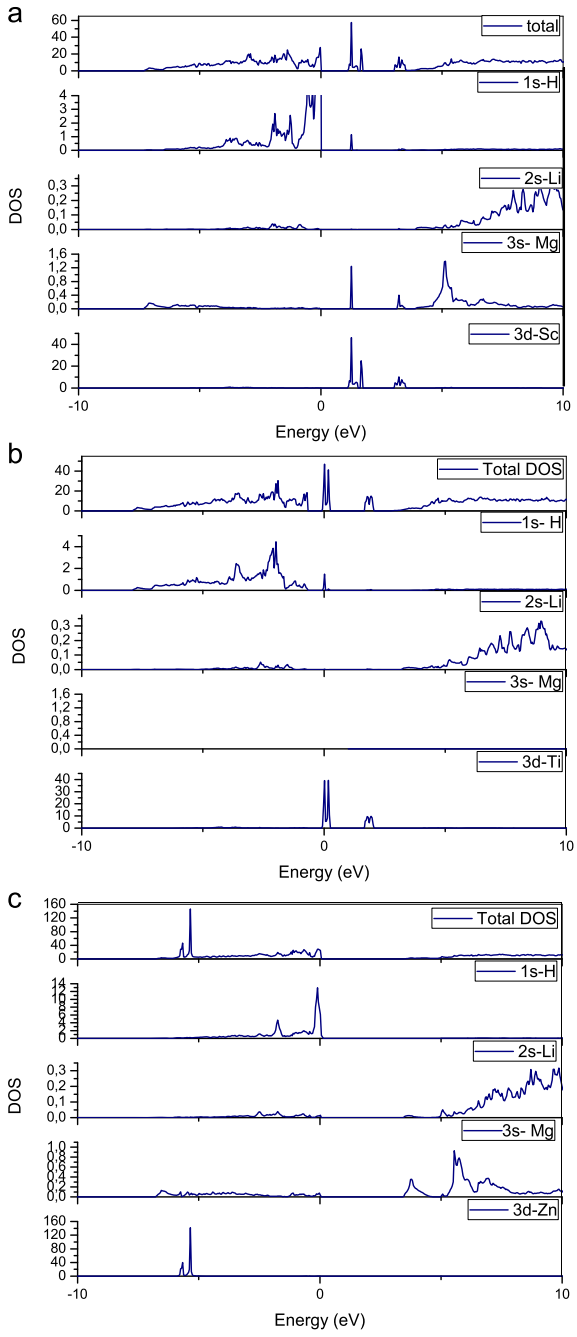

Fig. 2 – Total and partial density of states for (a) $Mg_{14}ScLiH_{32}$, (b) $Mg_{14}TiLiH_{32}$ and (c) $Mg_{14}ZnLiH_{32}$.

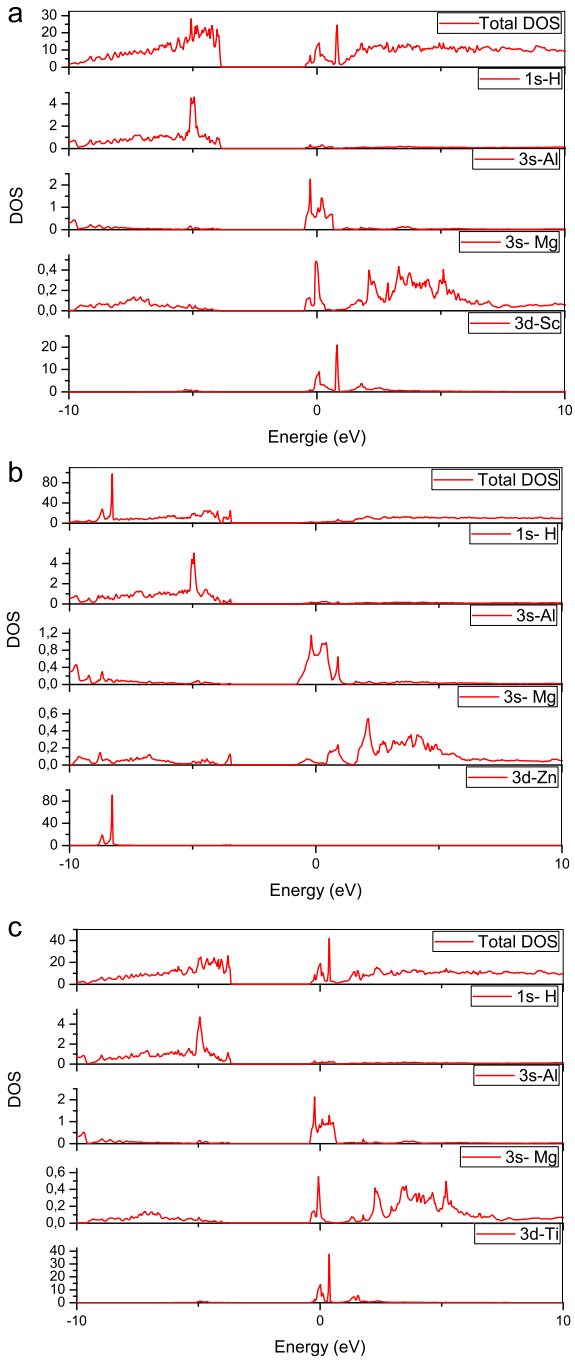

Fig. 3 – Total and partial density of states for (a) $Mg_{14}ScAlH_{32}$, (b) $Mg_{14}ZnAlH_{32}$ and (c) $Mg_{14}TiAlH_{32}$.

These observations may explain the destabilization of the system and then confirm the decrease of heat of formation and desorption temperature previously mentioned.

It is worth noting that, Li and Al help destabilizing the studied systems, yet Al shows better results in term of the decrease of stability than Li, which is probably due to the hybridization between it and the other transition metals, a hybridization that didn't appear in the case of the substitution with Li. To summarize, the highly likely new hybridizations, created between the different elements in the systems, weakened the bonding between Mg and H.

Please cite this article in press as: Bhihi M, et al., First principle study of hydrogen storage in doubly substituted Mg based hydrides, International Journal of Hydrogen Energy (2015), http://dx.doi.org/10.1016/j.ijhydene.2015.04.061

Conclusion

In this work, we have investigated the Hydrogen desorption mechanism within Mg based hydrides using DFT calculations. We have proposed a double substitution, with Al and Li as a second element due to their small weight, firstly to decrease the heat of formation and also the desorption temperature, and secondly to preserve the gravimetric storage capacity of MgH_2. This approach was proposed to overcome the drop of the gravimetry, which occurs in the case of large amount of TM, for single substitution. Through our results we proved the feasibility of this approach, as we observed the destabilization of the systems, which consequently, led to the decrease of the desorption temperature. Furthermore the evaluations of the charge transfer between the different elements, as well as the interpretation of the density of states of the studied systems, allowed us to offer some likely explanations to our results.

REFERENCES

[1] Shang X, Bououdina M, Guo ZX. J Alloys Compd 2003;349:217.
[2] Liang G, Huot J, Boily S, Van Neste A, Schulz R. J Alloys Comp 1999;292:247.
[3] Rivoirard S, de Rango P, Fruchart D, Charbonnier J, Vempaire D. J Alloys Comp 2003;622:356.
[4] Charbonnier J, De Rango P, Fruchart D, Miraglia S, Pontonnier L, Rivoirard S, et al. J All Compd 2004;383:205.
[5] Shang X, Bououdina M, Song Y, Guo ZX. Int J Hydrogen Energy 2004;29:73.
[6] Song MY, Bobet J-L, Darriet B. J All Compd 2002;340:256.
[7] Spassov T, Rangelova V, Solsona P, Baró MD, Zander D, Köster U. J Alloys Compd 2005;398:139.
[8] Shao H, Asano Kohta, Enoki Hirotoshi, Akiba Etsuo. J Alloys Compd 2009;477:301.
[9] Xiao X-B, Zhang W-B, Yu W-Y, Wang Na, Tang B-Y. Physica B 2009;404:2234.
[10] Lakhal M, Bhihi M, Benyoussef A, El Kenz A, Loulidi M, Naji S. Int J Hydrogen Energy 2015;40:6137–44.
[11] Gremaud R, Broedersz CP, Borsa DM, Schreuders H, Rector JH, Dam B, et al. Adv Mater 2007;19:2813.
[12] Moysès Araùjo C, Ahuja R. J Alloys Compd 2005;404–406:220.
[13] Hou ZF. J Power Sources 2006;159:111.
[14] Bouhadda Y, Rabehi A, Bezzari-Tahar-Chaouche S. Rev Des Energies Renouvelables 2007;10:545.
[15] Alapati V Sudhakar, Karl Johnson J, Sholl David S. J Alloys Compd 2007;446–447:23.
[16] Velikokhatnyi OI, Kumta PN. Mater Sci Eng B 2007;140:114.
[17] Bhihi M, Lakhal M, Labrim H, Benyoussef A, El Kenz A, Mounkachi O, et al. Chin Phys B 2012;21:097501.
[18] Lakhal M, Bhihi M, Labrim H, Benyoussef A, Naji S, Belhaj A, et al. Kinetic Monte Carlo and density functional study of hydrogen diffusion in magnesium hydride MgH2. Int J Hydrogen Energy 2013;38(20):8350–6.
[19] Bhihi M, Lakhal M, Naji S, Labrim H, Belhaj A, Benyoussef A, et al. First principle calculations for improving desorption temperature in Mg16H32 doped with Ca, Sr and Ba elements. Bull Mater Sci 2014;37:1731–6.
[20] Shelyapina MG, Fruchart D, Wolfers P. Electronic structure and stability of new FCC magnesium hydrides Mg7MH16 and Mg6MH16 (M [Ti], V, Nb): an ab initio study. Int J Hydrogen energy 2010;35:2025–32.
[21] Ramzan M, Lebegue S, Ahuja R. Transition metal doped MgH2: a material to potentially combine fuel-cell and battery technologies,. Int J Hydrogen Energy 2010;35:1037–10376.
[22] Satyapal S, Petrovic J, Read C, Thomas G, Ordaz G. The U.S.Department of energy's national hydrogen storage project:progress towards meeting hydrogen-powered vehicle requirements. Catal Today 2007;120:246–56.
[23] http://www.fplo.de.
[24] Koepernik K, Eschrig H. Phys Rev B 1999;59:1743.
[25] Perdew JP, Wang Y. Phys Rev B 1992;45:13244.
[26] Bortz M, Bertheville B, Bottger G, Yvon K. J Alloys Compd 1999;287:L4–6.
[27] Nakamura H, Nguyen-Manh D, Pettifor DG. J Alloys Compd 1998;281:81.
[28] Kittel C. Introduction to solid state Physics. New York: Wiley; 1986.
[29] Friedlmeier GM, Bolcich JC. Int J Hydrogen Energy 1988;13:467.
[30] Klose W, Stuke V. Int J Hydrogen Energy 1995;20:309.
[31] Yamagychi M, Akiba E. In: Cahn RW, Haasen P, Kramer EJ, editors. Materials science and technology, vol. 3B; 1994. p. 333.
[32] Maark TA, Hussain T, Ahuja R. Int J Hydrogen Energy 2012;37:9112.
[33] Kelkar T. S.Pal, D.G. Kanhere. ChemPhysChem. 2008;9:928.
[34] Zeng Q, Su K, Zhang L, Xu Y, Cheng L, Yan X. J Phys Chem 2006;35:1385.
[35] Vajeeston P, Ravindran P, Kjekshus A, Fjellvåbg H. Phys Rev Lett 2002;89:175506–11.
[36] Yu R, Lam PK. Electronic and structural properties of MgH2. Phys Rev B 1988;37:8730.
[37] Isidorsson J, Giebels IAME, Arwin H, Griessen R. Phys Rev B 2003;68:115112.

Please cite this article in press as: Bhihi M, et al., First principle study of hydrogen storage in doubly substituted Mg based hydrides, International Journal of Hydrogen Energy (2015), http://dx.doi.org/10.1016/j.ijhydene.2015.04.061

Bull. Mater. Sci., Vol. 37, No. 7, December 2014, pp. 1731–1736. © Indian Academy of Sciences.

First principle calculations for improving desorption temperature in $Mg_{16}H_{32}$ doped with Ca, Sr and Ba elements

M BHIHI[1], M LAKHAL[1], S NAJI[1,2], H LABRIM[3], A BELHAJ[4], A BENYOUSSEF[1,5,6], A EL KENZ[1,*], M LOULIDI[1], B KHALIL[1], O MOUNKACHI[5], M ABDELLAOUI[1] and E K HLIL[7]

[1]LMPHE (URAC 12), Faculté des Sciences, Université Mohammed V-Agdal, Rabat 10000, Morocco
[2]Department of Physics, Faculty of Science, Ibb University, Ibb 1120, Yemen
[3]Centre National de l'Energie, des Sciences et des Techniques Nucléaires, Rabat 10000, Morocco
[4]Département de Physique, Faculté Polydisciplinaire, Université Sultan Moulay Slimane, Béni Mellal 23000, Morocco
[5]Institute of Nanomaterials and Nanotechnology, MAScIR, Rabat 10000, Morocco
[6]Hassan II Academy of Science and Technology, Rabat 10000, Morocco
[7]Institut Néel, CNRS-UJF, 38042 Grenoble cedex 9, France

MS received 26 June 2013; revised 25 December 2013

Abstract. **Using ab initio calculations, we predict the improvement of the desorption temperature and the hydrogen storage properties of doped Mg-based hydrides such as, $Mg_{15}AMH_{32}$ (AM = Ca, Sr and Ba) as a super cell $2 \times 2 \times 2$ of MgH_2. In particular, the electronic structure has been obtained numerically using the all-electron full-potential local-orbital minimum-basis scheme FPLO9·00-34. Then, we discuss the formation energy calculations in terms of the material stabilities and the hydrogen storage thermodynamic properties improvements. Among others, we find that the stability and the temperature of desorption decrease without reducing significantly the high storage capacity of hydrogen. Moreover, it has been observed that such a doping procedure does not affect the electronic behavior as seen in MgH_2, including the insulator state in contrast with the transition metal hydrides, which modify the electronic structure of pure MgH_2.**

Keywords. **Electronic structure calculations; MgH_2; formation energy; hydrogen storage capacity; DFT; first principle calculations.**

1. Introduction

The magnesium (Mg) based hydride is one of the most attractive materials for hydrogen storage applications due to its high gravimetric and volumetric capacities (7·65 wt% and 110 g H_2/l, respectively) for the stochiometric binary MgH_2 (Shang *et al* 2003; Lakhal *et al* 2013). However, it has rather slow hydrogen absorption. The desorption kinetics as well as high dissociation temperature 573–673 K essentially reduces its application for hydrogen storage (Liang *et al* 1999). Various attempts have been made to improve the absorption and the desorption characteristics of magnesium hydride. Experimentally, it has been reported that mixing magnesium or magnesium hydride with small amounts of transition metals (TM) including their oxides radically accelerates the hydrogen kinetics (Mintz *et al* 1978). However, a slight decrease of the desorption temperatures has been observed (Song *et al* 2002; Rivoirard *et al* 2003; Charbonnier *et al* 2004; Shang *et al* 2004; Spassov *et al* 2005; Shao *et al* 2009; Xiao *et al* 2009).

In addition, the study of the electronic structure of Mg-based alloys hydrides is done to predict further modifications destabilizing the corresponding hydrides by lowering the desorption temperature and enhancing the hydrogen kinetic characteristics. Several theoretical studies have been carried out to clarify the mechanisms with the help of alloying effects on the thermodynamic properties of the magnesium-based hydrides. The obtained results are in good agreement with the experimental literature (Moysès Araùjo and Ahuja 2005; Hou 2006; Alapati *et al* 2007; Bouhadda *et al* 2007; Gremaud *et al* 2007; Velikokhatnyi and Kumta 2007; Xiao *et al* 2009; Bhihi *et al* 2012).

The aim of this work is to contribute to the improvement of hydrogen storage properties including absorption and desorption temperatures by studying the electronic structure of Mg-doped hydride with 2nd group ($Mg_{15}AMH_{32}$ where AM=Ca, Sr and Ba) using ab initio calculations based on the DFT techniques. As far as we know, it is the first time that such Mg-doped hydride material is considered to reduce the stability of the system. It is worth noting that the usual way has been devoted to exploring only the transition metals. Using an explicit calculation based on FPLO code, the formation energy and their hydrogen storage thermodynamic properties are explicitly computed. In particular, we discuss the hybridization between orbitals using density of state techniques. It follows that the doped system is less stable than

*Author for correspondence (elkenz@fsr.ac.ma)

the pure MgH_2. Moreover, it has been shown that such a doping procedure allows the system to preserve the same electronic behavior as seen in MgH_2, including the insulator state in contrast with the transition metal hydrides, which usually modify the electronic structure of pure MgH_2.

2. Calculation method

In this paper, we use ab intio calculations based on the all-electron full-potential local-orbital minimum-basis scheme FPLO9·00-34 (www.fplo.de, Koepernik and Eschrig 1999). This has been done to solve the Kohn–Sham equations using the scalar-relativistic scheme. The parameterization of the exchange-correlation energy has been done within the generalized gradient approximations (Perdew and Wang 1992). To ensure a high accuracy in our computations, we have used both self-consistent criterions of the energy and density together with a precision of 10^{-8} Ha and 10^{-6} Ha^{-1} $Å^{-3}$, respectively. To accurately perform Brillouin zone integrations, we have considered a $12 \times 12 \times 12$ K-point mesh. The valence basis state sets are $(3s, 3p)$ and $(1s)$ for Mg and H, respectively. Lattice parameters 'a=b and c' have been optimized for each doped Mg-based hydride ($Mg_{15}AMH_{32}$) using the relaxation method, which will be discussed in the next section. Such parameters may be modified depending on the doped elements.

3. Results and discussion

3.1 *Structural parameters and relaxation*

We first relax the structural parameters using the relaxation method presented in our previous work (Bhihi *et al* 2012). In this calculation, we assume that the experimentally stable rutile structure of MgH_2 (*P42/mnm*, space group No. 136) is obtained with the Wyckoff position of Mg and H $2a$ $(0, 0, 0)$ and $4f$ $(0·304, 0·304, 0)$. First, we consider the lattice parameters as $a = b = 4·501$ Å and $c = 3·01$ Å (Bortz *et al* 1999). Before performing the calculation, we start by relaxing our parameters; see figure 1. Indeed, we minimize the total energy to optimize such parameters. The calculated equilibrium values agree with results obtained by other groups (Bouhadda *et al* 2007; Bhihi *et al* 2012). Our results are given in table 1.

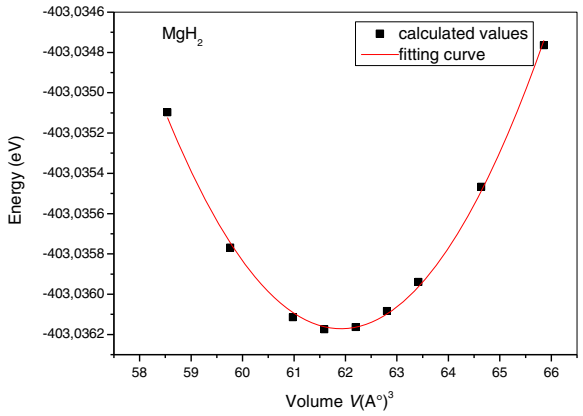

Figure 1. Total energy as a function of volume (V) of primitive cell.

In order to reduce the overall doped atom concentrations, larger primitive supercells with $2 \times 2 \times 2$ stacked original MgH_2 unit cells have been used. In this atomic representation, one Mg atom, among the 16 existing in the supercell, is replaced by alkaline metal AM (AM = Ca, Sr and Ba) atoms. This corresponds to a 6·25% doping concentration. The concentration 12·5% has also been considered, see table 2.

This has been considered to investigate the influence of substitution on the total energy and the electronic structure. This new system will involve a special crystal symmetric structure (*Cmmm* space group no. 65) with 17 non-equivalents site; see figure 2. This structure will allow us to compute the minimal total energy of the doped system to predict the heat of formation. The latter is needed to determine the stability of hydrides.

3.2 *Hydrides stability: heat of formation*

In this study, the heat of formation ΔH of Mg-based hydride, which is the most important thermodynamic parameter, has been calculated and used in order to predict new materials adopted to hydrogen storage. This can be obtained from the fact that it allows determining the heat of the hydrogenation reaction ($\Delta H < 0$ hydride is stable and vice versa), and deducing the temperature of desorption of the hydrogen in the studied system. We recall that the quantity ΔH of the hydride can be defined as the difference between the sum of total energy of products and the reactants (Xiao *et al* 2009):

$$\Delta H_{\mathrm{HF}} = \sum E_{\mathrm{tot}}\,(\mathrm{products}) - \sum E_{\mathrm{tot}}\,(\mathrm{reactants}). \quad (1)$$

The reaction related to the formation of the hydride MgH_2 and $Mg_{15}AMH_{32}$ is as follows:

$$\mathrm{Mg} + \mathrm{H_2} \rightarrow \mathrm{MgH_2}, \quad (2)$$

$$15\mathrm{Mg} + \mathrm{AM} + 16\mathrm{H_2} \rightarrow \mathrm{Mg_{15}AMH_{32}}. \quad (3)$$

Table 1. Minimal total energy for optimized parameters of MgH_2.

Minimal energy E_{min}(Ry)	a=b (Å)	c/a	Reference
−403·03609	4·524	0·66874	This work
−403·042937	4·519	0·66873	Bouhadda *et al* (2007)
−403·04777	4·585	0·6572	Bhihi *et al* (2012)
–	4·5176	0·6686	Maark *et al* (2012)
402·39 (i.e. 5474·854 eV)	4·5124	0·6701	Zhang *et al* (2010)
–	4·495	0·6685	Li *et al* (2006)
–	4·533	0·6686	Liang (2003)

Table 2. Total energy, heat of formation and desorption temperature of $Mg_{15}AMH_{32}$ (AM: alkaline metal).

System	Concentration (%)	Total energy (Ry)	Heat of formation kJ/mol (H_2)	Desorption temperature (K)
$Mg_{16}H_{32}$		−6448·577	−62·57	460·12
$Mg_{15}CaH_{32}$	6·25	−7408·684	−60·82	447·19
$Mg_{14}Ca_2H_{32}$	12·5	−8368·791	−59·05	434·24
$Mg_{15}SrH_{32}$	6·25	−12407·445	−48·17	354·23
$Mg_{14}Sr_2H_{32}$	12·5	−18366·3144	−33·85	248·90
$Mg_{15}BaH_{32}$	6·25	−22326·185	−20·79	152·84
$Mg_{14}Ba_2H_{32}$	12·5	−38203·8	−9·83	72·29

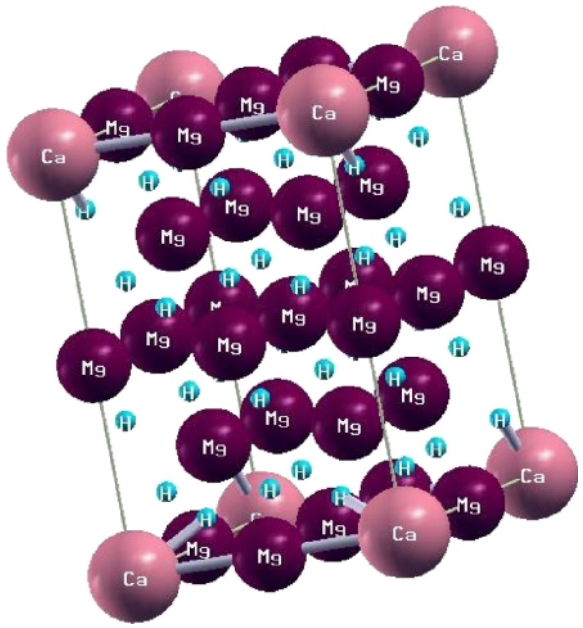

Figure 2. Crystal structure of $Mg_{15}AMH_{32}$ in primitive cell.

On the basis of these reactions, we have calculated the heat of formation of MgH_2 and $Mg_{15}AMH_{32}$ based on hydride according to the following formulas:

$$\Delta H = E_{\text{tot}}(\text{MgH}_2) - E_{\text{tot}}(\text{Mg}) - E_{\text{tot}}(\text{H}_2), \tag{4}$$

$$\Delta E_{\text{HF}} = E_{\text{tot}}(\text{Mg}_{15}\text{AMH}_{32}) - 15E_{\text{tot}}(\text{Mg}) + E_{\text{tot}}(\text{AM}) - 16E_{\text{tot}}(\text{H}_2). \tag{5}$$

The value of the total energy of the H_2 molecule $E_{\text{tot}}(H_2) = -2{\cdot}320$ Ry has been taken from Shang *et al* (2004) and Nakamura *et al* (1998). The total energies per atom for pure elements have been calculated using the lattice parameters of Mg, Ca, Sr and Ba given in Kittel (1986).

Based on the all-electron full-potential local-orbital minimum-basis scheme FPLO9·00-34 method, the calculated total energy and the heat of formation, in the magnesium hydride for optimized parameters structure, are −6448·577 eV and −82·33 kJ/mol (H_2), respectively. These values are comparable with those obtained experimentally $\Delta H = -74{\cdot}3 \pm 0{\cdot}5$ kJ/mol H_2 (Friedlmeier and Bolcich 1988), −81·2 kJ/mol H_2 (Klose and Stuke 1995), -76.15 ± 9.2 kJ/mol H_2 (Vajeeston *et al* 2002) and $\Delta H = -68{\cdot}00 \pm 9{\cdot}2$ kJ/mol (Liang 2003). Such results, which are in good agreement with the experimental ones and with some theoretical values including $\Delta H = -55{\cdot}648$ to $-65{\cdot}196$ kJ/mol H_2 (i.e. −0·577 to −0·676 eV/H_2) (Zhang *et al* 2010) and $\Delta H = -71{\cdot}1$ kJ/mol H_2, obtained recently in the literature (Liang 2003), validate our modeling approximations and the result obtained in our previous work (Bhihi *et al* 2012). The complete calculations of total energy, as well as the heat of formation of the studied new hydride, are listed in table 2. To reduce such values, in order to get unstable behavior, we have doped the system using the alkaline metals for 6·25% and 12·5% concentrations. For 6·25%, the total energy, and the heats of formation of the studied new hydride are −60.82, −48·17 and −20·79 kJ/mol H_2 for $Mg_{15}CaH_{32}$, $Mg_{15}SrH_{32}$ and $Mg_{15}BaH_{32}$, respectively. The same physical quantities have been given for 12·5%, see table 2. The obtained results show that when we increase the concentration of doping element the stability decreases. This is in agreement with the results reported by Bouaricha *et al* (2000) and Tanniru *et al* (2010) who found that for high concentrations (i.e. of greater than 10% of Al), these kinetics become increasingly important. Moreover, Shang *et al* (2003) have used concentration up to 10% of Nb to obtain good results. Also Shahi *et al* (2013) have used transition metals (TM: Ti, Fe and Ni) with different concentrations, they found that 5 wt% of TM gave the best results.

It follows from these calculations that the concentration also plays a crucial role in decreasing the stability (see table 2). The implementation of the alkaline earth metals to MgH_2 reduces the stability of MgH_2, leading to an improvement of the dehydrogenation kinetics.

3.3 *Desorption temperature*

The thermodynamic properties of the hydrides are described by the standard Gibbs energy:

$$\Delta G = \Delta H - T\Delta S, \tag{6}$$

where ΔH and $\Delta S(\Delta S \approx \Delta S\ (H_2) = 130{\cdot}7$ J/mol K) are the heat formation and the entropy change of the dehydrogenation reaction, respectively. At the decomposition temperature for a constant pressure, the standard Gibbs energy becomes zero. Therefore, the temperature of the dehydrogenation can be estimated according to $\Delta H = T\Delta S$ (Bhihi *et al* 2012).

The calculations presented in this study show that for pure MgH_2 the decomposition temperature is equal to 460·12 K, which is close to other values 573–673 K found in Shang *et al* (2003, 2004) and Bhihi *et al* (2012). On the other hand, alloying MgH_2 with small amounts of alkaline metals can have a great effect in destabilizing the parent compound MgH_2 by lowering the decomposition temperature, without significantly reducing its high hydrogen capacity (see table 3).

It has been observed that the temperature of desorption decreases according to the augmentation Z number of the elements appearing in the second group and in decreasing order of the electronegativity. It follows from figures 3–6 and tables 4 and 5 that the band gap decreases from Mg to Ba. This could be explained by the decreasing of the electronegativity.

3.4 *Electronic structure*

The density of state has been used to understand and explain the nature of metals in the alloys hydride $Mg_{15}AMH_{32}$. In

Table 3. Gravimetric hydrogen capacities of $Mg_{15}AMH_{32}$ (AM = alkaline metal).

System	Gravimetric hydrogen capacities (wt%)
$Mg_{16}H_{32}$	7·65
$Mg_{15}CaH_{32}$	7·38
$Mg_{15}SrH_{32}$	6·66
$Mg_{15}BaH_{32}$	6·04

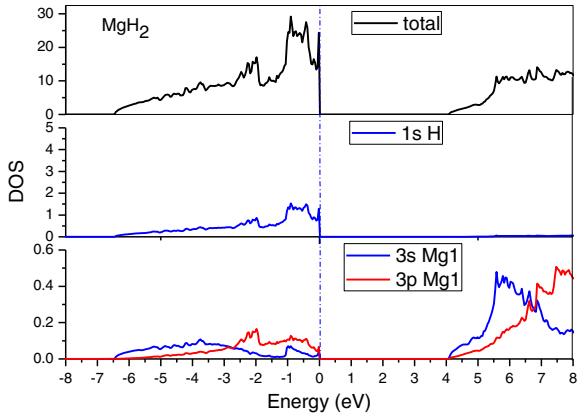

Figure 3. Total and partial DOSs of MgH_2.

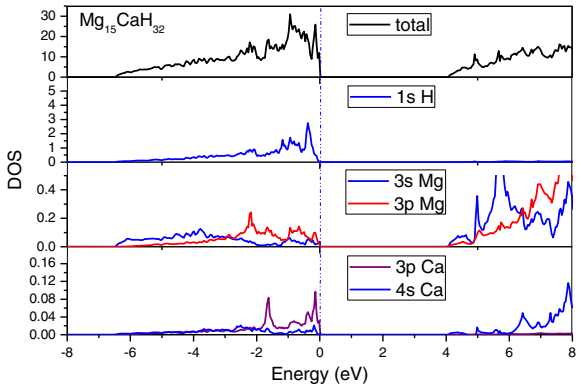

Figure 4. Total and partial DOSs of $Mg_{15}CaH_{32}$.

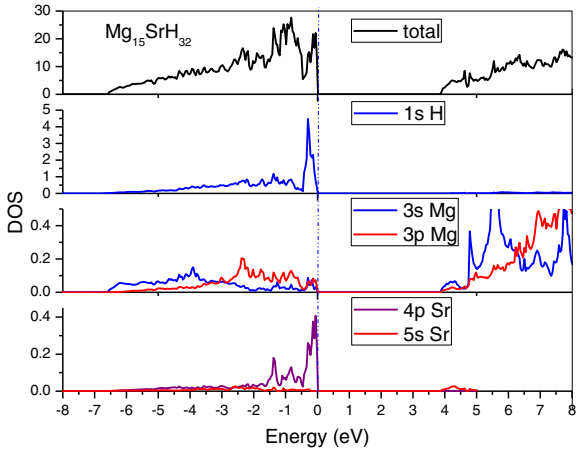

Figure 5. Total and partial DOSs of $Mg_{15}SrH_{32}$.

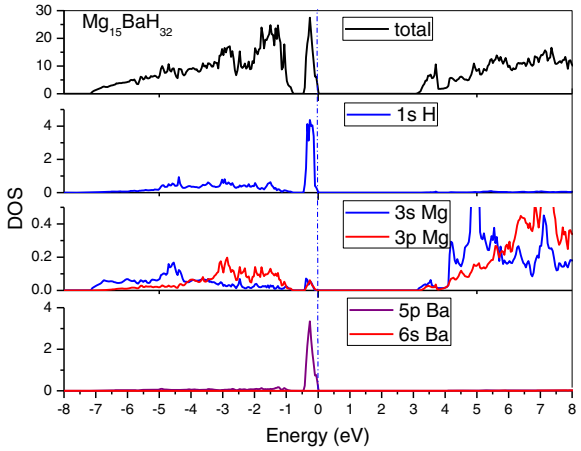

Figure 6. Total and partial DOSs of $Mg_{15}BaH_{32}$.

Table 4. Electronegativity per atom for alkaline metal.

Elements	Electronegativity in Pauling unit
Mg	1·31
Ca	1·00
Sr	0·95
Ba	0·89

Table 5. Energy gap and width of valance band for each system, $Mg_{15}AMH_{32}$ (AM= alkaline metal).

System	Width of valance band (VB) (eV)	Gap energy (eV)
MgH_2	6·426	4·059
$Mg_{15}CaH_{32}$	6·466	4·052
$Mg_{15}SrH_{32}$	6·586	3·850
$Mg_{15}BaH_{32}$	7·147	3·116

particular, it has been explored to clarify their effect on the stability and the kinetics of hydrogen absorption–desorption.

For this reason, the total (DOS) and the partial density of electronic states (P-DOS) of MgH_2, with and without additional metals (AM=Ca, Sr and Ba), have been calculated. Our calculation is plotted in figures 3–6. On the one hand, it follows from figure 3 that there are two parts in the valence band (VB). In the first part, the band with energy range from −1·8 to 0·0 eV is called 'high VB' composed mainly of strongly hybridized H-1*s* and Mg-3*p* states. The second part concerns the band with energy range from −6·42 to −1·8 eV which is called 'lower VB' originating almost from Mg-3*s* and H-1*s* states. While the contribution of the lowest conduction band (CB) is fully from Mg-3*p*, Mg-3*s* and few H-1*s* states. On the other hand, we can observe that the obtained energy gap (E_g) is 4·06 eV, which is typical for an insulating system. Up to a difference of the order of 1 eV, our value and those obtained by the GGA approximation 3·9 eV (Kelkar *et al* 2008; Zhang *et al* 2010), 4·0 eV (Li *et al* 2006) and 4·2 eV (Vajeeston *et al* 2002) are close to the experimental one 5·16 eV given in Yu and Lam (1988). Indeed, this value has been improved by using the GW approximation 5·58 eV (Zhang *et al* 2010).

For MgH_2 doped with alkaline metal, we start by studying the effect of the nature of the alkaline metals (AM) on the electronic structure of MgH_2. To make a comparison between the nature of this metal and MgH_2, we plotted, in figures 4–6, the total and partial DOSs of MgH_2-doped alkaline metals (AM=Ca, Sr and Ba). From these figures, we observe that the overall shapes of the total DOSs for $Mg_{15}AMH_{32}$ (AM=Ca, Sr and Ba) are similar to each other. When doping with alkaline metals, the system preserves the same electronic behavior as seen in pure MgH_2 (Maark *et al* 2012). In particular, the doped system keeps the insulator state. In contrast, the transition metal hydrides modify the electronic structure of MgH_2 which is converted to a metallic structure as reported in Xiao *et al* (2009) and Li *et al* (2006).

The only small difference between different components is seen in the hybridization between H-1*s* and *p* state of metal elements. It becomes more and more localized near the Fermi level according to the following order:

$$\text{Mg} \rightarrow \text{Ca} \rightarrow \text{Sr} \rightarrow \text{Ba}. \tag{7}$$

Moreover, the valence band is mainly attributed to H-1*s* states and the introduction of the doped element has increased the width of the VB according to the above order (7). Comparing the density of states of the second group alkaline metal hydrides including $Mg_{15}CaH_{32}$, $Mg_{15}SrH_{32}$ and $Mg_{15}BaH_{32}$, we find that the $Mg_{15}CaH_{32}$ has the smallest DOS localisation near Fermi level due to the hybridization between Ca-3*p* and H-1*s*. While for $Mg_{15}SrH_{32}$, the hybridization between Sr-4*p* and H-1*s* is more localized than the Ca one. Then, this localization of H orbital becomes very important for $Mg_{15}BaH_{32}$, resulting from hybridization between Ba-5*p* and H-1*s*. This indicates that the localization of H-1*s* states comes from strong local hybridization between AM-*p* and H-*s* states. Also the hybridization between Mg-*s* and H-*s* states, which constitutes the lower VB becomes slightly weaker. This leads to a decreasing of the stability of the hydride. This is consistent with heat of the formation energy calculations listed in table 2. Moreover, we can see that the obtained energy gap (E_g) decreases following the same order as in (7). For each element, the energy gap calculation is summarized in table 5.

4. Conclusions

In this paper, we have discussed the H desorption mechanism within the hydrides using the electronic structure calculations based on the ab-initio method. Among others, we have found that the localization of H-*s* states near Fermi level, obtained from the hybridization between AM and H atoms, is mainly responsible for the gap width tuning and the destabilization of the system. Moreover, the comprehension of hydrogen desorption allowed us to estimate the formation energy and the temperature values of the H desorption. The calculated quantities agree with the experimental data given in Shang *et al* (2003, 2004). Such estimated values allow us to consider that the component $Mg_{15}SrH_{32}$ is the most appropriate material for H desorption near room temperature without losing much in terms of storage capacity. Moreover, we have observed that the stability system decreases in accordance with the decreasing of the electronegativity of the doped elements. In particular, it has been realized that such doping procedures with alkaline metals, in contrast to the transition metals (Li *et al* 2006; Xiao *et al* 2009), do not change the electronic structure as seen in MgH_2 including the insulator state.

Chin. Phys. B Vol. 21, No. 9 (2012) 097501

Hydrogen storage of $Mg_{1-x}M_xH_2$ (M=Ti, V, Fe) studied using first-principles calculations

M. Bhihi[a)], M. Lakhal[a)], H. Labrim[b)], A. Benyoussef[a)c)d)], A. El Kenz[a)†], O. Mounkachi[c)], and E. K. Hlil[e)]

[a)] *Laboratoire de Magnétisme et de Physique des Hautes Energies, associé au CNRST (URAC 12), Département de Physique, B.P.* 1014, *Faculté des Sciences, Université Mohammed V-Agdal, Rabat, Morocco*

[b)] *National Centre for Energy, Sciences and Nuclear Techniques CNESTEN, Morocco*

[c)] *Institute of Nanomaterials and Nanotechnologies, MACsIR, Rabat, Morocco*

[d)] *Hassan II Academy of Science and Technology, Rabat, Morocco*

[e)] *Institut Néel, CNRS-UJF,* 38042 *Grenoble Cedex* 9, *France*

(Received 16 January 2012; revised manuscript received 13 April 2012)

In this work, the hydrogen storage properties of the Mg-based hydrides, i.e., $Mg_{1-x}M_xH_2$ (M=Ti, V, Fe, $0 \leq x \leq 0.1$), are studied using the Korringa–Kohn–Rostoker (KKR) calculation with the coherent potential approximation (CPA) approximation. In particular, the nature and the concentrations of the alloying elements and their effects are studied. Moreover, the material's stability and hydrogen storage thermodynamic properties are discussed. In particular, we find that the stability and the temperature of desorption decrease without significantly affecting the storage capacities.

Keywords: first-principles calculation, formation energy, electronic structure, hydrogen storage

PACS: 75.50.Pp **DOI:** 10.1088/1674-1056/21/9/097501

1. Introduction

Up to date, the magnesium is one of the most attractive materials for hydrogen storage applications due to its high gravimetric and volumetric capacities (7.65 wt.% and 110 gH2/l, respectively) in the form of stoichiometric binary MgH_2.[1] However, its slow hydrogen absorption and desorption kinetics as well as the high dissociation temperature of 573–673 K, essentially limit its application for hydrogen storage.[2] Numerous attempts have been made to improve the magnesium hydrogen absorbing-desorbing characteristics. Experimentally, it has been reported that the mixing magnesium or the magnesium hydride with small amounts of transition metals (TM) or their oxides drastically accelerates the hydrogen kinetics, and a slight decrease of the desorption temperature was observed.[3−9]

Electronic structure studies of Mg-based alloy hydrides are performed to predict further modifications that destabilize the corresponding hydrides by lowering the desorption temperature and enhance the hydrogen kinetics characteristics. Several theoretical studies have been carried out to clarify the mechanisms of the alloying effects on the thermodynamic properties of the magnesium-based hydrides.[10−16] On the other hand, the observed catalytic mechanism is still not adequately explained.

The aim of this work is to study the electronic structures of Mg-based hydrides $Mg_{1-x}M_xH_2$ (M=Ti, V, Fe) with $0 \leq x \leq 1$ by using the Machikaniyama2000 KKR (Korringa-Kohn-Rostoker) code package from Akai of Osaka University.[17,18] The code package is based on the coherent potential approximation (CPA), and provides an intuitive yet accurate approach when combined with the generalized gradient approximation (GGA) methods, and it gives very good results for alloying systems. The obtained results are used to discuss the hydrogen storage thermodynamic properties. In particular, we find that the stability and the temperature of desorption decreases without significantly affecting the storage capacities.

†Corresponding author. E-mail: elkenz@fsr.ac.ma

2. Computational methods

To solve the density functional theory (DFT) one-particle equations, we use the multiple-scattering theory, i.e. the KKR Green's function (KKR-GF) method and the KKR-CPA for low impurity concentrations. The coherent potential approximation is employed to describe the random disordered distribution of impurities. The relativistic effects are taken into account by using the scalar relativistic approximation. The crystal potential is approximated by a muffin-tin potential, and the wave functions in the respective muffin-tin spheres are expanded in real harmonics up to $l = 3$, where l is the angular momentum quantum number defined at each site. In our calculations, 1000 k-points in the irreducible part of the first Brillouin zone are used. For the present KKR-CPA calculations, the package MACHIKANEYAMA2000 coded by Akai[18] is used. In this study, the KKR method within the GGA and the GGA91 for parameterization of the exchange energy[19] is applied. Table 2 shows that the calculated values are in good agreement with those obtained by the Wien2K code.[14,20–22]

The hydride MgH_2 crystallized in the rutile-type structure ($P4_2/mnm$, space group N°136) at ambient conditions.[23] The Wyckoff positions of Mg and H are 2a (0, 0, 0) and 4f (0.304, 0.304, 0), respectively (Fig. 1). The lattice constants used as the input for our calculation are the experimental values, $a = 4.501$Å and $c = 3.01$Å.[23] The lattice constants of Mg, Ti, V, and Fe (Table 1) are taken as reference.[24]

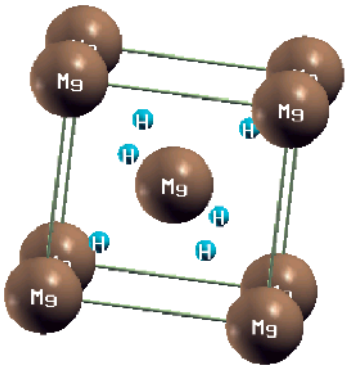

Fig. 1. (colour online) Crystal structure of MgH_2 in the primitive cell.

Table 1. Lattice parameters of simple elements.

Element	Space group	Crystalline structure	a/Å	c/Å
Mg	194–$P6_3/mmc$	Hcp	3.21	5.21
Ti	194–P_3/mmc	Hcp	2.95	4.68
V	227–$Im3m$	Bcc	3.03	3.03
Fe	227–$Im3m$	Bcc	2.87	2.87

3. Results and discussion

3.1. Structural relaxation

We first study the effect of doping on the structure relaxation. The total energy of the system computed by the DFT method depends on the nucleon positions, hence we can minimize the energy functional with respect to the positions. The total energy of MgH_2 as a function of lattice parameter a before and after doping with a certain element (Ti, V, and Fe), has been calculated using the Hellmann–Feynman method[25] in the KKR-CPA method with the GGA91 parameterization.[19] Our results are given in Fig. 2. The equilibrium positions corresponding to the minimal energies for both cases (MgH_2 and MgH_2:TM) are determined by $a_{eq} = 4.585$ Å and the ratio $c/a = 0.6572$. These values are comparable to those obtained experimentally ($a = 4.501$ Å and $c/a = 0.6687$)[22]

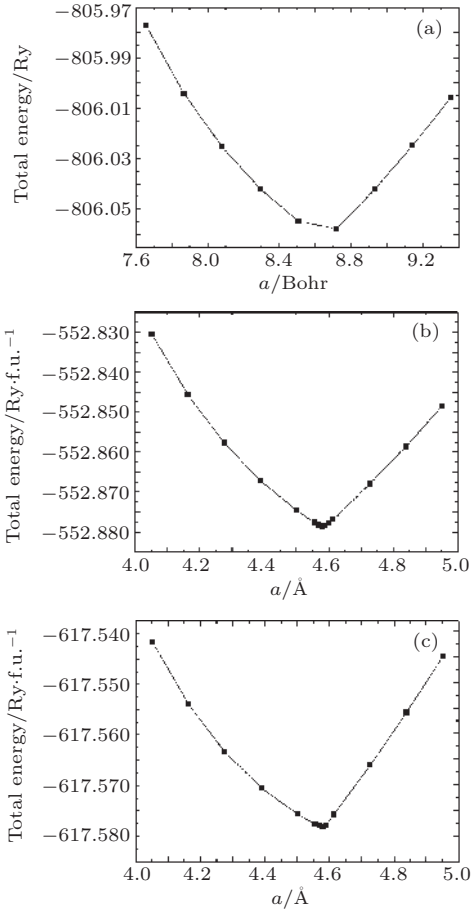

Fig. 2. Total energies of (a) MgH_2,(b) $Mg_{0.9}V_{0.1}H_2$, and (c) $Mg_{0.9}Fe_{0.1}H_2$ each as a function of parameter a of the primitive cell.

and ($a = 4.515$ Å and $c/a = 0.6686$).[26] This means that the volumetric capacity is the same for MgH_2 and MgH_2:TM. This good agreement allows validating our modeling approximations based on the KKR-CPA method with the GGA91 parameterization.

3.2. Hydrides stability: heat of formation

We now evaluate the heat of formation (ΔH) of hydride MgH_2 before and after doping with certain transition metals to study the stability of these hydrides. The heat of formation ΔH is the most important thermodynamic parameter used to identify and classify hydrogen storage materials. This is due to the fact that it can be used to determine the heat of the hydrogenation reaction ($\Delta H < 0$ hydride is stable and vice versa) and deduce the temperature of desorption of hydrogen from the system. The ΔH of hydride can be defined as the difference between the sums of total energies of products and reactants[10]

$$\Delta H_{\rm HF} = \sum E_{\rm tot}(\text{products}) - \sum E_{\rm tot}(\text{reactants}). \quad (1)$$

The reaction related to the formation of hydride MgH_2 reads

$$\text{Mg} + \text{H}_2 \rightarrow \text{MgH}_2. \quad (2)$$

To calculate the heat of formation of reaction (2), we subtract the total energies of the pure element Mg and the hydrogen molecule from that of hydride MgH_2

$$\Delta H = E_{\rm tot}(\text{MgH}_2) - E_{\rm tot}(\text{Mg}) - E_{\rm tot}(\text{H}_2). \quad (3)$$

The value of the total energy of the H_2 molecule, $E_{\rm tot}(\text{H}_2) = -2.320$ Ry, has been taken from Refs. [6] and [27], and that of Mg is calculated and is equal to -400.6670692 Ry, which is comparable to that obtained in Ref. [28].

The calculated enthalpy of formation based on the KKR-CPA method for the magnesium hydride with the optimized and the experimental structure parameters are -85.709 kJ/mol|$cdot$H$_2$ and -79.577 kJ/mol·H_2, respectively (see Table 2). These values are comparable to those obtained experimentally, -74.3 ± 0.5 kJ/mol·H_2,[29] -81.2 kJ/mol·H_2,[30] and -76.15 ± 9.2kJ/mol·H_2.[22] This good agreement allows validating our modeling approximations based on the KKR-CPA method with the GGA91 parameterization.

Table 2. Total energies and heats of formation obtained with experimental and optimized parameters of MgH_2.

Element	Total energy/Ry·f.u.$^{-1}$		Formation heat/kJ·mol^{-1}·H_2	
	Our cal.	Literature	Our cal.	Literature
Mg	–400.6670692	–400.6675[33]	–	–
H_2	–	–2.320[5,26]	–	–
MgH_2[a)]	–403.0477706	–403.042937[13]	–79.577	–74.3 ± 0.5[27]
MgH_2[b)]	–403.0524479		–85.709	

[a)]with experimental parameters, [b)]with optimised parameters

In order to destabilize the MgH_2 systems, transition elements have been introduced, which are known for their role in the destabilization of magnesium hydride[6,28] following the reaction

$$\text{MgH}_2 + xM \rightarrow \text{Mg}_{1-x}M_x\text{H}_2 + x\text{Mg}. \quad (4)$$

Based on this reaction, we can calculate the enthalpies of formation of doped Mg-based hydrides according to the following formula:

$$\Delta E_{\rm HF} = E_{\rm tot}(\text{Mg}_{1-x}M_x\text{H}_2) + x(E_{\rm tot}(\text{Mg}) - E_{\rm tot}(M)) - E_{\rm tot}(\text{MgH}_2), \quad (5)$$

where the total energies per atom for the pure elements are calculated and listed in Table 3. The total energies as well as the resulting heats of formation of the studied hydrides are listed in Table 4. It is shown that the addition of the transition metal to MgH_2 generally reduces the stability of MgH_2, which can lead to an improvement of the dehydrogenation kinetics. This agrees well with the trend observed experimentally[6] and theoretically.[6,28] This destabilization effects on MgH_2 obtained in this work increase in the order of Fe, Ti, and V according to the values of heat of formation of the mixtures. It follows from Eq. (5) that we can control the value of the heat of formation in $Mg_{1-x}M_xH_2$ (M=V, Ti, and Fe, $0 < x < 1$) by varying the concentrations of the doped elements. In fact,

it is shown in Fig. 3 that when we increase the concentration, the heat of formation decreases linearly with a specific slope for each dopant. Consequently, for each doped element, the stability increases until it reaches the one associated with MgH_2 according to its specific concentration C_S in the following order: $C_S(MgH_2{:}Fe)<C_S(MgH_2{:}V)<C_S(MgH_2{:}Ti)$, see Table 5.

Table 3. Total energy per atom for pure elements.

Element	Total energy/Ry·f.u.$^{-1}$
Mg	–400.6670692
Ti	–1707.629854
V	–1898.637153
Fe	–2545.544327

Table 4. Total energy and heat of formation of $Mg_{1-x}M_xH_2$ (M=Ti, V, and Fe) with $x = 0.01$, 0.05, and 0.1.

System	Total energy/Ry	Heat of formation/kJ·mol^{-1}·H_2
MgH_2	–806.104896	–85.709
$Mg_{0.95}Ti_{0.05}H_2$	–936.82869	–18.05273336
$Mg_{0.95}V_{0.05}H_2$	–955.932961	–20.37647298
$Mg_{0.95}Fe_{0.05}H_2$	–1020.63547	–28.11172472

Table 5. Concentration limits (C_S) and gravimetric hydrogen capacities of $Mg_{1-x}M_xH_2$ (M=Ti, V, and Fe).

C_S		31.01%	26.7%	18.57%
Gravimetric hydrogen capacities wt.%	$Mg_{1-C_S}M_{C_S}H_2$	5.994	5.208	6.264
	$Mg_{0.95}M_{0.05}H_2$	7.330	7.289	7.225
	MgH_2		7.658	

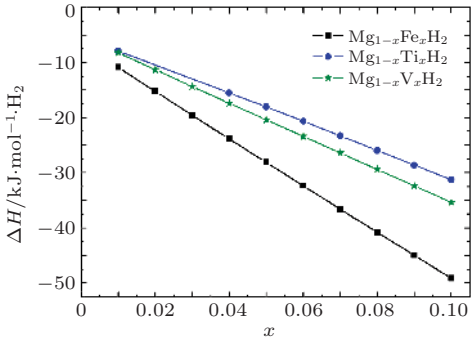

Fig. 3. (colour online) Heat of formation as a function of concentration for MgH_2 doped with Ti, V, and Fe.

3.3. Desorption temperature

The thermodynamic properties of the hydrides are described with the standard Gibbs energy $\Delta G = \Delta H - T\Delta S$, where ΔH and ΔS are enthalpy and entropy change of the dehydrogenation reaction, respectively. For a complex hydride, when the material is heated, the entropy factor slowly overcomes the enthalpy contribution. At the decomposition temperature and under a constant pressure, the standard Gibbs energy is zero. So the temperature of dehydrogenation can be estimated by $\Delta H = T\Delta S$. During heating, the entropy change of the solid is very small compared to that of the gas, so the entropy change during the decomposition reaction is primarily due to the H_2 evolution. At the standard pressure and temperature, for most simple metal hydrides, the entropy is taken to be $\Delta S \approx \Delta S$ (H_2)=130.7 J/mol·K, corresponding to the entropy change due to a mole of gas transforming into the solid.[32] For most of the dehydrogenation reactions, it is estimated that ΔS is in the range of 95 J/mol·K< ΔS < 140 J/mol·K.[33] Therefore ΔH is, to some extent, a reliable predictor of the dehydrogenation temperatures for various metal hydrides.[34]

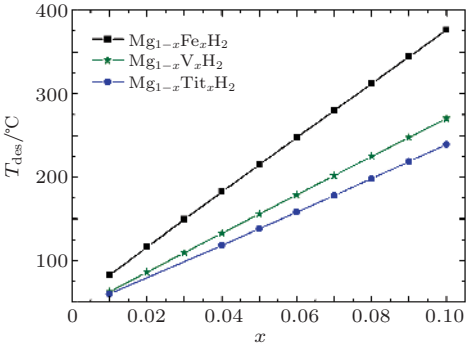

Fig. 4. (colour online) Desorption temperature as a function of concentration for MgH_2 doped with Ti, V, and Fe.

The calculation results of this study show that for the pure MgH_2, the decomposition temperature is

equal to 655.76 K, which is close to values 573–673 K in the other works.[2,6] On the other hand, alloying MgH_2 with small amounts of transition metals can have large effect on destabilizing the parent compound MgH_2 by lowering the decomposition temperature (see Fig. 4) without reducing significantly its high hydrogen capacity (listed in Table 5).

We can show that with the increasing concentration, the temperature also increases until it reaches that of MgH_2, the specific concentrations are $C_{Ss} =$ 31.01%, 26.7%, and 18.57% for MgH_2:Ti, MgH_2:V, and MgH_2:Fe, respectively. Therefore, iron is the best doping element, because it reduces the desorption temperature at a concentration smaller than that in the other doping elements without excessively reducing the storage capacity, see Table 5.

3.4. Electronic structure

The density of state has been used to understand and explain the effect of the nature and the concentration of the transition metal on both the stability and the kinetics of the hydrogen absorption-desorption in $Mg_{1-x}M_xH_2$. For this purpose, the total (DOS) and the partial (PDOS) densities of electronic states of MgH_2 with and without transition metals (M=Ti, V, and Fe) have been calculated.

Figure 5 shows the total density of states of MgH_2 as well as the partial DOS related to Mg-s, Mg-p, and H-s. We find that there are two parts in the valence band (VB). In the first part, the band in the energy range from −0.062 eV to −0.31 eV is called the high VB and composed mainly of strongly hybridized H-s and Mg-3p states. The second part is the band with the energy ranging from −0.31 eV to −0.57 eV, which is called the lower VB and originated mainly from Mg-s and H-s states. While the contribution to the lowest conduction band (CB) are from Mg-p, Mg-s and few H-s states. We can see that the interactions of p (Mg) and s (H) lead the top of the VB to move to a higher energy and make the bottom of the VB move to a lower energy, which increase the width of the VB and consequently decrease the band gap, providing a perfect argument for the discrepancy between our calculation result of 2.745 eV and the experimental results of 5.16 eV in Ref. [35] and 5.6 eV in Ref. [36]. This is related with the result obtained using the GGA approximation, which overestimates the interaction energies between states of Mg and H. So it leads to a large band width and a smaller band gap, and it is well known that the first-principles calculation based on the density functional theory suffers from the errors in the calculated band gap.

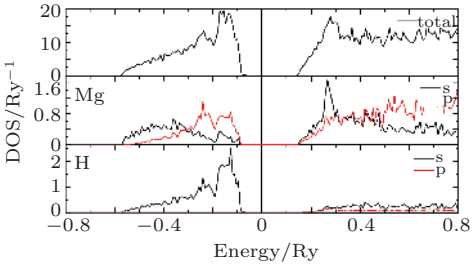

Fig. 5. (colour online) Total and partial DOS of MgH_2 system.

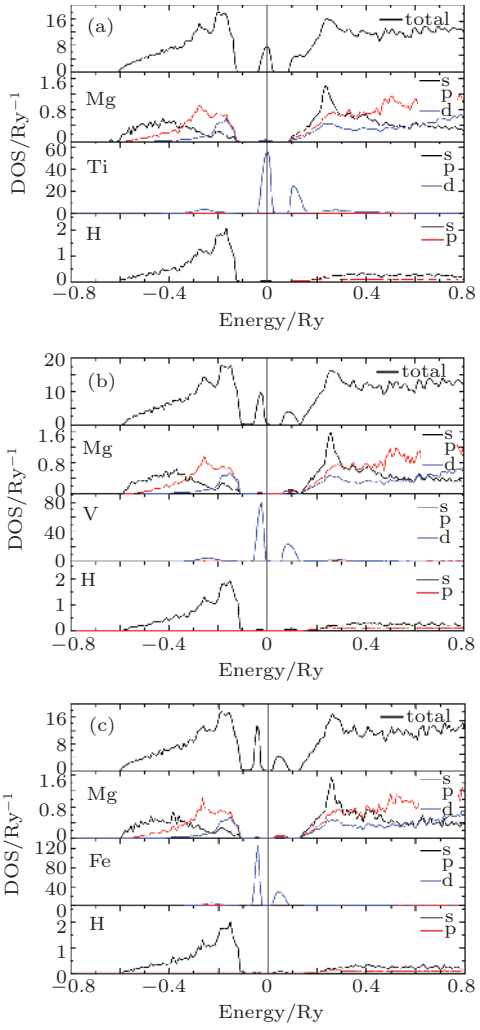

Fig. 6. (colour online) Total and partial DOS of (a) $Mg_{0.95}Ti_{0.05}H_2$, (b) $Mg_{0.95}V_{0.05}H_2$ and (c) $Mg_{0.95}Fe_{0.05}H_2$.

For MgH_2 doped with transition metals (M=Ti, V, and Fe) with concentrations varying from 1% to 10%, we find the same behavior. For this reason, we

plot in Figs. 6 and 7 only the total and the partial DOSs of MgH_2 doped with 5% of M. These figures show that the five orbits of the d state are divided into two energy levels, called t_{2g} and e_{2g}. The t_{2g} energy level is below that of e_{2g}. The appearance of these levels is accord with the crystal field theory in the case of transition metals inserted in the octahedral symmetry,[37] which is the case in our compound. The t_{2g} and e_{2g} states are localized in the band gap. This indicates that there is a weak hybridization between M-d and H-s unlike the case of pure MgH_2, where there is a strong hybridization between H and Mg. Moreover, there is no hybridization between M and Mg, which is consistent with the consideration that no binary MgM exists after releasing the hydrogen.[30]

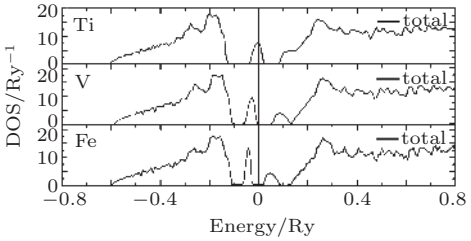

Fig. 7. Total DOS of $Mg_{0.95}M_{0.05}H_2$ (M=Ti, V, and Fe).

Figure 8 shows that the positions of the two levels (t_{2g} and e_{2g}) of the impurity shift to the valence band, and consequently the offset between the energy level t_{2g} and the VB decreases in the order of Ti, V, and Fe. This observation accords with the results of our calculations of heat formation, which increases in the same order. This shows that for all concentrations, the mixture MgH_2:Fe is most stable (MgH_2:Fe>MgH_2:V>MgH_2:Ti) (see Fig. 4).

In order to explain the increases of both the stability and the hydrogen desorption temperature with the increasing concentration of the transition metal in hydrides based on Mg ($Mg_{1-x}M_xH_2$, M=Ti, V, and Fe, $0 \leq x \leq 0,1$), we plot the d states of these transition metals with different concentrations on the same figures (Figs. 8(a)–8(c)). For all systems, we observe that the more the concentration increases, the more the d state of the transition metal shifts to the valance band, which indicates that stability increases with the increasing concentration. This is accord with our calculation of heats of formation for different concentrations.

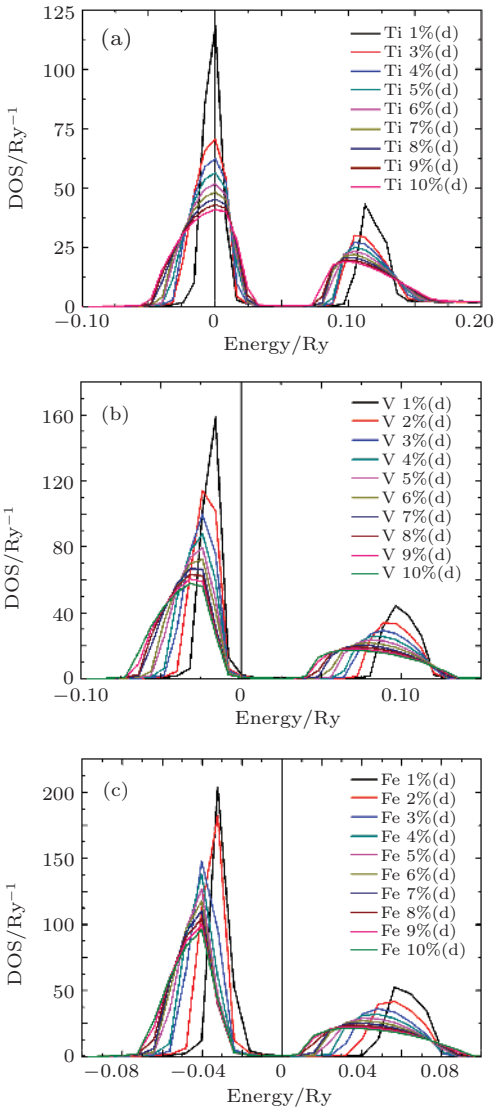

Fig. 8. (colour online) Partial DOSs of d states for the transition metals (a) Ti , (b) V, and (c) Fe in $Mg_{1-x}M_xH_2$ with $0 < x \leq 0.1$.

4. Conclusion

In order to improve the hydrogen storage properties of the Mg-based hydrides, such as $Mg_{1-x}M_xH_2$, (M=Ti, V, and Fe), we have perfomed the first-principles theoretical studies based on the KKR-CPA method. The calculations results of heats of formation for MgH_2 and MgH_2:TM as well as their electronic structures confirm that alloying TM (Ti, V and Fe) can lower the stability of MgH_2. It is favorable for the improvement of the dehydrogenating properties of MgH_2. As a consequence, it can be concluded that alloying MgH_2 with small amounts of transition metals

INTERNATIONAL JOURNAL OF HYDROGEN ENERGY 38 (2013) 8350–8356

Available online at www.sciencedirect.com

SciVerse ScienceDirect

journal homepage: www.elsevier.com/locate/he

Kinetic Monte Carlo and density functional study of hydrogen diffusion in magnesium hydride MgH_2

M. Lakhal [a], M. Bhihi [a], H. Labrim [b], A. Benyoussef [a,c,d], S. Naji [a,e], A. Belhaj [f], B. Khalil [a], M. Abdellaoui [a], O. Mounkachi [c], M. Loulidi [a,*], A. El kenz [a]

[a] Laboratoire de Magnétisme et de Physique des Hautes Energies, associé au CNRST (URAC 12), Département de physique, B.P. 1014, Faculté des sciences, Université Mohammed V-Agdal, Rabat 10000, Morocco
[b] National Centre for Energy, Sciences and Nuclear Techniques CNESTEN, Morocco
[c] Institute of Nanomaterials and Nanotechnologies, MACsIR, Rabat, Morocco
[d] Hassan II Academy of Science and Technology, Rabat, Morocco
[e] Department of Physics, Faculty of Science, Ibb University, Ibb, Yemen
[f] Département de physique, Faculté Polydisciplinaire, Université Sultan Moulay Slimane, Béni Mellal, Morocco

ARTICLE INFO

Article history:
Received 25 January 2013
Received in revised form
12 April 2013
Accepted 30 April 2013
Available online 28 May 2013

Keywords:
Kinetic Monte Carlo
First-principle calculations
Hydrogen storage
Diffusion mechanisms
Activation energies
Time of ad/desorption

ABSTRACT

In this work, we propose a model to investigate the hydrogen storage ab/desorption kinetic properties for the pure MgH_2 using Kinetic Monte Carlo (KMC) simulations. To do such computations, the activation energies for different elementary processes have been estimated. Moreover, the different thermodynamical quantities of interest are determined by performing the ab-initio calculations. Then, we discuss the hydrogen diffusion in magnesium hydride (such as adsorption, diffusion and desorption). More precisely, we study the effect of each elementary mechanism on the diffusion that we characterize through the density distribution of hydrogen atoms including filling ratios, diffusion time, temperature and pressure. Among others, we show that all elementary mechanisms are needed to reproduce a behavior of ab/desorption which correlates well with the experimental results reported in literature. In particular, at high temperature and pressure, the results of simulations indicate that the studied material involves slow kinetics.

1. Introduction

Recently, hydrogen has been considered as one of the most promising energy carriers alternatively to the fossil fuels including coal, oil and natural gas. It faces a significant problem concerning its storage. Indeed, hydrogen storage method should involve high volumetric, gravimetric capacity, a fast sorption rate at relatively low temperatures, and a recycling high tolerance. Alternative methods have been proposed including high pressure gas cylinders, liquid hydrogen, physisorption of hydrogen on materials with a high specific surface area, and hydrogen storage through hydrides (e.g. Boron and Magnesium hydrides). The latter is very promising due to its high hydrogen storage capacities [1–4].

More recently, it has been shown that the magnesium hydride is one of the most attractive materials for hydrogen

* Corresponding author. Tel.: +212 (0)661299306.
E-mail addresses: loulidim60@gmail.com, loulidi@fsr.ac.ma (M. Loulidi).
0360-3199/$ – see front matter
http://dx.doi.org/10.1016/j.ijhydene.2013.04.157

storage applications due to its high gravimetric and volumetric capacities (7.65 wt.% and 110 gH_2/l, respectively) [5]. However, this material shows a slow kinetics, as well as high dissociation temperature 573–673 K, which reduces solid hydrogen storage in normal conditions of pressure and temperature [4,6].

Various attempts have been made in order to improve magnesium hydrogen absorption/desorption properties. Experimentally, it has been shown using mechanical grinding with a small amount of transition metals (TM) or their oxides that the hydrogen kinetic is accelerated and the decomposition temperature of the hydride is reduced [4,5,7,8]. On the other hand, various theoretical calculations have been performed to understand the relevant mechanism dealing with the alloying effects on magnesium hydride thermodynamic properties [9–11]. Based on density functional theory (DFT), we have shown, in a previous work, that alloying MgH_2 with small amounts of transition metals mixture TM (Ti, V and Fe) can drastically decrease the decomposition temperature without reducing significantly its high hydrogen capacity [12]. This has been obtained from the location of the two levels "t_{2g} and e_{2g}" of the impurity (d state) in the band gap. In that work, we have dealt only with the stability properties and the temperature of desorption for Mg-based hydrides such as ($Mg_{1-x}TM_xH_2$, TM = Ti, V, Fe, $0 \leq x \leq 0.1$). More details on such developments can be found in [13–22].

The aim of this work is to present numerical investigations of the hydrogen storage ab/desorption kinetic properties for the pure MgH_2 by combining density-functional theory (DFT) and Kinetic Monte Carlo (KMC) simulations and shed light on the different mechanisms appearing in ab/desorption phenomena. To perform such computations, the activation energies for different elementary processes and thermodynamical quantities we need have been computed by using DFT method. Taking into account of all calculated quantities of interest, we study hydrogen diffusion in magnesium hydride (such as dissociation of H_2, adsorption, diffusion and desorption) using KMC simulations. The effect of each elementary mechanism on the diffusion that we characterized through density distribution of hydrogen, filling ratios, diffusion time, temperature and pressure is analyzed. It is worth noting that this numerical method is adopted to study the time of ab/desorption in MgH_2. Thus, in section 2, we shortly give our calculation methods. Section 3 is devoted to the presentation and the discussion of our numerical results that we compare with those obtained experimentally. In the last section, we give our conclusion.

2. Model and computational methods

2.1. Density functional theory calculations

In order to the calculate different energy barriers, we have used ab-initio calculations based on the all-electron full-potential local-orbital minimum-basis scheme FPLO9.00-34 [23,24] to solve the Kohn–Sham equations using the scalar-relativistic and the full four-component relativistic schemes. The parameterization of the exchange-correlation energy has been done within the generalized gradient approximation GGA [25]. To ensure a high accuracy in our calculations, we used self-consistent criteria for both the energy and the density with precisions of 10^{-8} Ha and 10^{-6} Ha^{-1} $Å^{-3}$ respectively. A mesh of ($12 \times 12 \times 12$) k-points in the irreducible part of the first Brillouin zone was used in our calculations. The total energy is calculated using the scalar-relativistic scheme, for all configurations.

The hydride MgH_2 crystallizes in the rutile-type structure ($P4_2/mnm$, space group N°136) at ambient conditions [26]. The primitive cell has two Mg atoms, one at the origin and the other in the centre of the cell at (1/2, 1/2, 1/2) plus four hydrogen atoms at (x,x,0), (−x,−x,0), (1/2−x, 1/2 + x 1/2) and (1/2 + x, 1/2−x, 1/2) with $x = 0.304$. The initial lattice parameters used, in our calculations, are the experimental values $a = 4.501$ Å and $c = 3.01$ Å [26].

To calculate the activation energies, all hydrogen possible configurations have to be determined. However, in the unit cell model four atoms may move to empty neighbors. To reach the different possible arrangements of H atoms, we should break the usual symmetry $P4_2/mnm$ settings down to the standard setting P1(1) by translating the Wyckoff position coordinates. Based on this symmetry breaking and using combinatorial calculation, we obtain 304 H atom configurations. The activation energies have been obtained from the maximal energy appearing in the possible paths between the initial position and the final one while the energy formation and the desorption temperature have been calculated in $P4_2/mnm$ settings.

2.2. Kinetic Monte Carlo calculation

To investigate the hydrogen diffusion in magnesium hydride, we apply the KMC method [27] to the model we suggest. Thus, the activation energies calculated by DFT method are implemented in our algorithm to determine the rate transition of each elementary process. By defining the relation between simulated time and Monte Carlo steps, we can predict the hydrogen diffusion time (ad/desorption time) in MgH_2 as function of temperature and pressure.

In our model, we consider a supercell containing 160 magnesium atoms and 320 hydrogen atoms. In terms of Miller indices, the hydrogen will be adsorbed or desorbed on the (001)surface. Periodic boundary conditions have been considered along X- and Y-directions. We assume that the gas phase is an ideal gas composed of hydrogen atoms and thus fully described by partial pressures P_{H_2} and temperature T. The rate of hydrogen flux can be obtained using the kinetic theory of gases providing the amount of gas hitting (F) the unit area of a surface per unit time [28].

Absorption and desorption of hydrogen in hydride metals can be done according to three steps: adsorption/desorption, dissociation and diffusion. In order to study the absorption, we consider initially a supercell containing only the magnesium atoms. Then the interstitial sites will be occupied by H atoms at each time step. Such filling of H atoms is based on the above three mentioned processes. The adsorption of H_2 is followed by its decomposition in two H atoms. For such decomposition, one needs to introduce energy barriers controlling the dissociation processes. The calculations we performed show that the barrier energy of H_2 dissociation at the surface (001) of Mg atoms is of order 0.8 eV. It is in good

agreement with the energy barriers 0.75–1.18 eV obtained in the literature [29–31].

Each hydrogen atom has eleven nearest neighbors (N.N): seven in the same plane, two in the upper adjacent plane and the remaining two ones are located at the lower adjacent plane (Fig. 1). After dissociation, the H atoms can move from an interstitial site to another one depending on the corresponding activated energies. It is the diffusion process.

In the algorithm we developed, various possible events including processes of diffusion to the free neighbors, adsorption and desorption are considered. At each KMC step one of the above process is randomly selected with a probability

$$P_i = \frac{R_i}{R} \tag{1}$$

The rate transition R_i associated to the ith jump process and the total rate transition R are given respectively by:

$$R_i = \upsilon_0 \exp\left(\frac{E_i^a}{K_B T}\right) \tag{2}$$

$$R = \sum_{i=1}^{N} R_i \tag{3}$$

where υ_0 describes the jump frequency (usually set to 10^{13} Hz) and the activation energy of ith jump process taken from first-principles calculations (see section 2.2). The time of hydrogen atoms displacement is incremented by Δt, which is defined as the inverse of the total rate transition:

$$\Delta t = -\frac{\ln(u)}{R} \tag{4}$$

where u is a uniformly distributed random variable between $0 < u \leq 1$.

3. Results and discussions

To apply Monte Carlo calculations for studying the kinetic properties of MgH_2, we should implement some thermodynamical parameters and the activation energies. Such quantities are obtained using the DFT method based on ab-intio calculations.

3.1. *Thermodynamic properties of MgH_2 structure from DFT method*

Before discussing the thermodynamics of MgH_2 structure, which includes the desorption temperature and the enthalpy change of formation, we first determine its equilibrium lattice parameters using the relaxation method. Indeed, we optimize the MgH_2 structure by evaluating the total energy as function of the unit cell volume. Using GGA approximation and fitting the obtained values with respect to a generic polynomial of the second order, the equilibrium parameters which correspond to the minimum energy are $a = b = 4.5094$ Å and $c = 3.0163$Å. These values are in good agreement with those obtained in the literature [12,26].

To get the desorption temperature and the enthalpy of formation ΔH, we have to consider the following reaction related to the formation of the hydride MgH_2:

$$Mg + H_2 \rightarrow MgH_2 \tag{5}$$

To calculate ΔH related to the reaction of formation (5) we subtract the total energies of the pure element Mg and the hydrogen molecule from its hydride MgH_2 obtained by relaxing the system:

$$\Delta H = E_{tot}(MgH_2) - E_{tot}(Mg) - E_{tot}(H_2) \tag{6}$$

Using DFT calculation, we find that the total energy of hydrogen is $E_{tot}(H_2) = -2.330$ Ry. It is in good agreement with the one reported in [10,32]. Moreover, the calculated heat of the formation of MgH_2 is $\Delta H = -63.018$ kJ/mol.H_2. It is close to previous theoretical values obtained using different methods: −62.301 kJ/mol.H_2 [9], −75.99 kJ/mol.H_2 [10], −69.51 kJ/mol.H_2 [11], −82 kJ/mol.H_2 [33]. On the other hand, our result is close to the experimental value -76.15 ± 9.2 kJ/mol.H_2 obtained in [34]. We believe that such small difference between different values is due especially to the different methods used in DFT

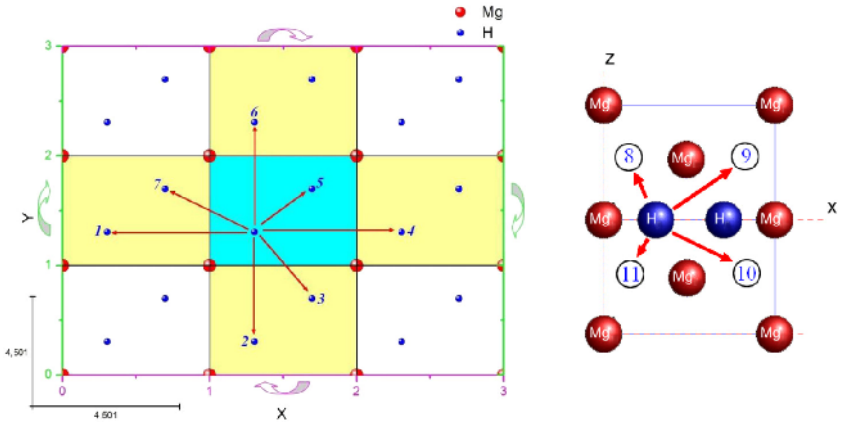

Fig. 1 – Representative scheme of neighbors sites. Left denotes the seven neighbors in the same plane; right shows the four neighbors in the other planes.

calculations. The decomposition temperature T_{dec} can be estimated using the well known thermodynamical relation

$$T_{dec} = \frac{\Delta H}{\Delta S} \quad (7)$$

Taking the above value of ΔH and the value of the entropy $\Delta S \approx \Delta S(H_2) = 130.7$ J/mol.K obtained at standard temperature and pressure [25], we get $T_{dec} = 482.52$ K. It is in agreement with other values reported in [10,12].

3.2. Activation energies

For later use in Monte Carlo simulations, energy barriers (more than 300 activation energies) have been computed. Four situations among them are illustrated in Fig. 2. Particularly, we have found that the energies depend on the surrounding hydrogen atoms and the target-interstitial sites. The barriers get enlarged by increasing the hydrogen atom number in the system. Indeed, DFT calculations reveal that the energies corresponding to the hydrogen atoms motions in the (001) plan are lower than the energies associated with the motion between two parallel (001) plans. Therefore, hydrogen atoms prefer to diffuse along X and Y directions instead of moving vertically.

3.3. Kinetic Monte Carlo study

Having determined the thermodynamic properties of the MgH_2 structure using DFT method, we incorporate all calculated thermodynamical quantities in the KMC method to study the kinetic properties of the magnesium hydride material.

3.3.1. Absorption/desorption times

In order to determine the responsible mechanism of hydrogen storage in magnesium hydride in conformity with the observed behavior in the experiment, we have used several elementary events (adsorption, surface diffusion, diffusion along X-, Y- and Z-direction, and desorption). Along our numerical analysis, we have observed that all the mentioned mechanisms are necessary to reproduce the behavior obtained numerically in literature [5,35].

In Fig. 3, we present the amount of the absorbed and the desorbed hydrogen calculated (in wt.%) as a function of the reaction time using the following equation

$$\rho_m = \frac{xM_{H_2}}{M_{Mg} + xM_{H_2}} 100 \quad (8)$$

where M_{H_2}, M_{Mg} are the molar mass of hydrogen and magnesium respectively and where x is the rate of hydrogen atoms placed at the supercell.

Both absorption and desorption kinetics exhibit a behavior quite similar to that observed in the experimental results with a very small quantitative difference, which is due to the used pressure values being smaller or higher than the experimental one [5,35].

Depending on the initial conditions and to the initial pressure applied on the adsorption (001) surface, the rate of

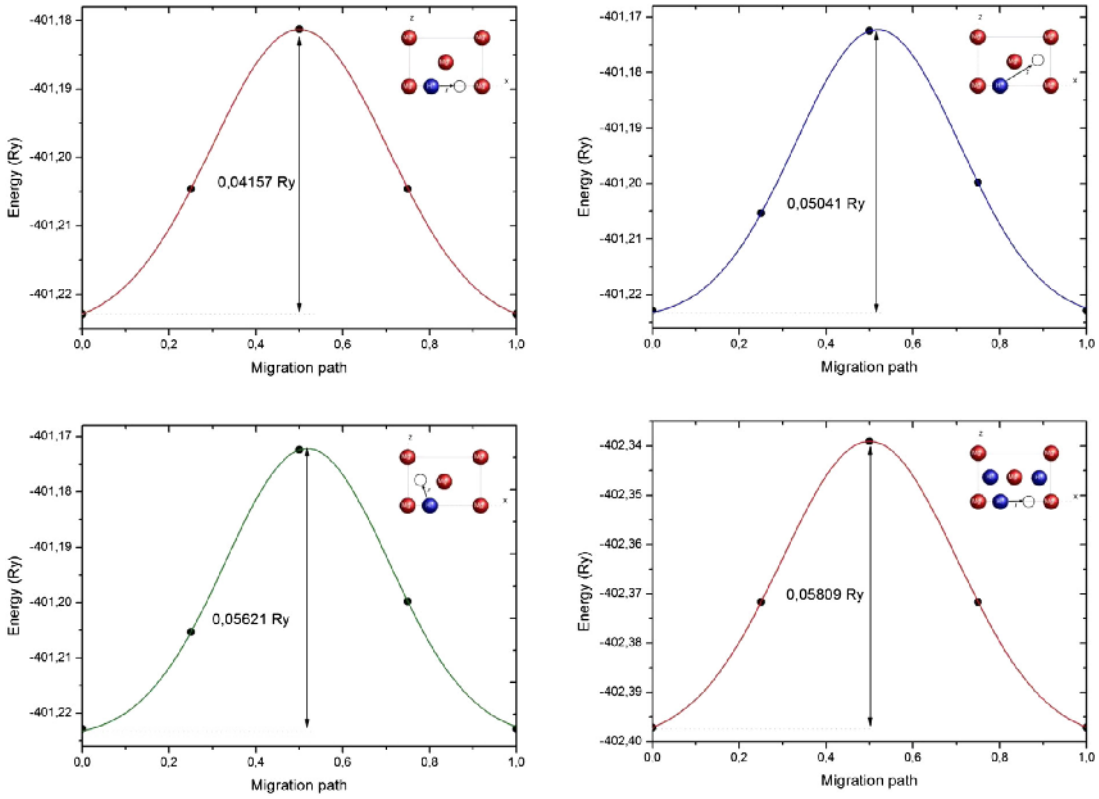

Fig. 2 – Energy curves for an H atom diffusing between two interstitial sites along different paths.

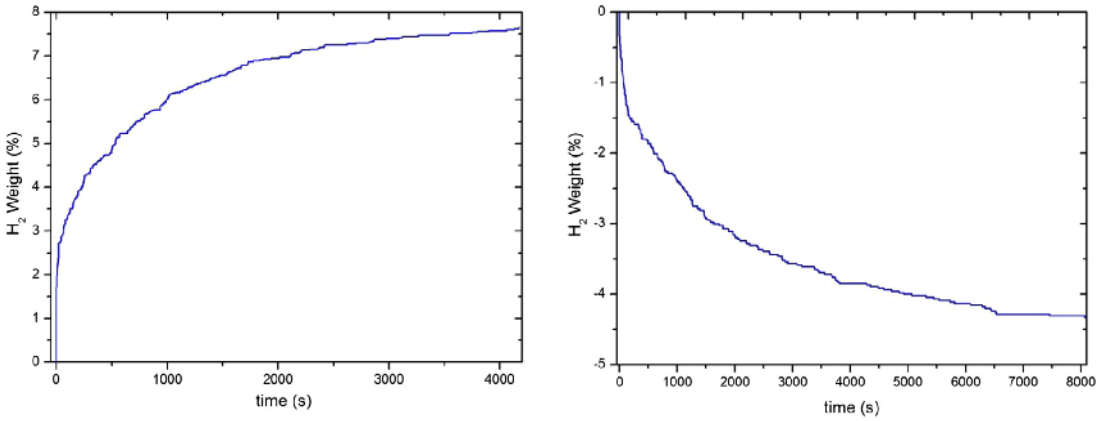

Fig. 3 – Simulation charging/discharging kinetic for the pure MgH_2 at 633 K and 10 bar/1 bar.

hydrogen absorption in our material increases rapidly with respect to time. Once the number of the hydrogen atoms in the system becomes substantial, the activation energies increase. Then, the H atoms move with difficulties to the empty sites. For this reason the amount of hydrogen increases slowly as a function of time until reaching a limit equal to the gravimetric capacity of MgH_2 ($\rho_m = 7.65$ wt.%) where all the empty interstitial sites in the supercell are occupied by hydrogen atoms.

For the desorption process, the system does not completely desorbs all hydrogen atoms which prefer to move inside rather leaving the system. In order to discharge all hydrogen atoms, one needs a high vacuum that we cannot realize within our simulations. The maximal value of dehydrogenation, which depends on the temperature and the applied pressure, remains a little bit constant for a while. It follows that the kinetic of desorption of the hydrogen of our system is very slow in contrast to the absorption mechanism.

The effect of the temperature on such behavior is represented in Fig. 4 for a supercell of ($4 \times 4 \times 5$) and temperature values running from 600 K to 630 K with a step of 10 K. It is shown clearly that higher temperatures lead to significantly

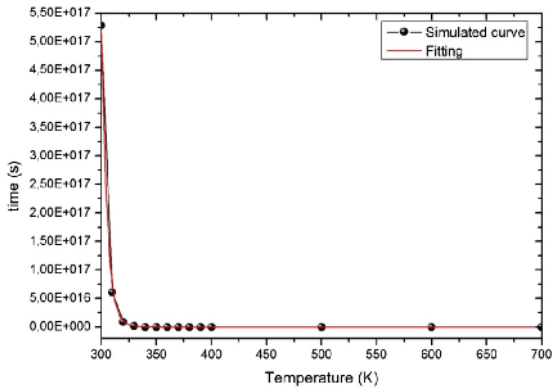

Fig. 5 – Filling time as a function of temperature for 10 bar. Black dots denote the simulation data while the fitted curve is in red. (For interpretation of the references to color in this figure legend, the reader is referred to the web version of this article.)

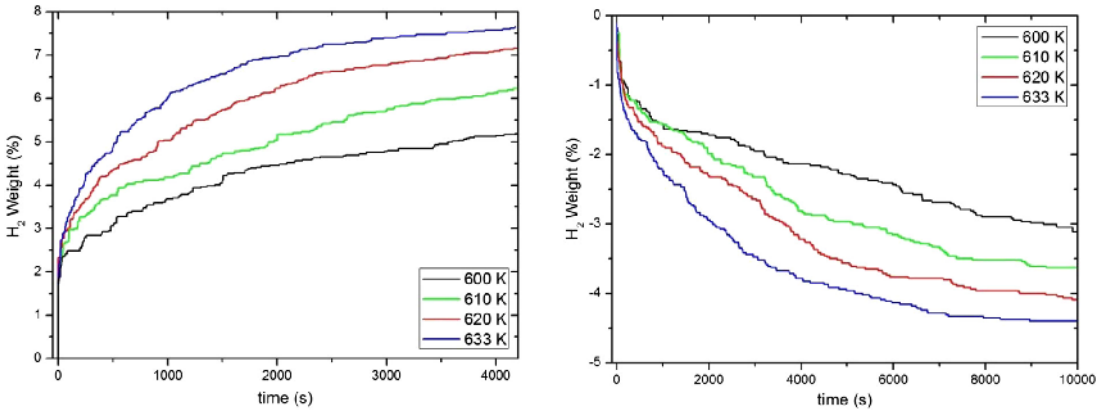

Fig. 4 – Charging/discharging kinetic at different temperature and 10 bar/1 bar.

improved hydrogenation as well as dehydrogenation kinetics since the reaction speed increases by increasing the temperature. This result is in good agreement with the behaviors reported in [36,37]. After a period of 4000 s, the tank already reaches the rate of saturation for a temperature of 630 K, while it hardly exceeds the half size at 600 K. Thus, the filling time depends on the temperature. It decreases exponentially with respect to the temperature as shown in Fig. 5.

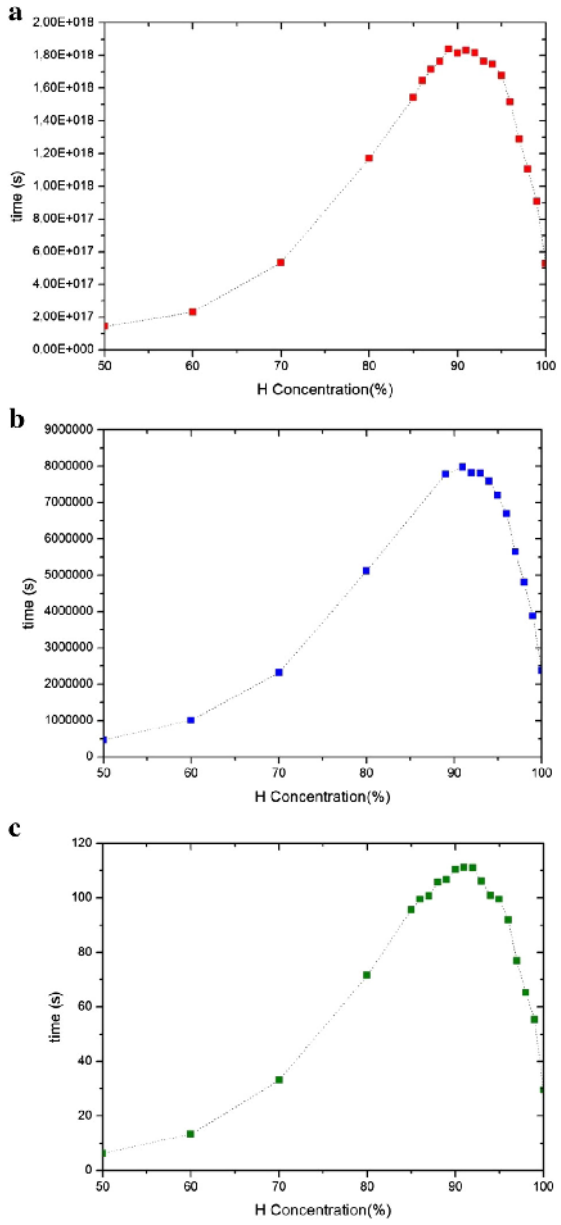

Fig. 6 – Equilibrium time as a function of hydrogen concentration for different temperatures: a-300 K, b-500 K and c-700 K. Dotted lines are plotted for clearness.

3.3.2. *Equilibrium time*

To characterize the equilibrium in our system, the density of H atoms in different plans ($z = 0$, $z = 0.25$,… $z = 1$) is calculated at each Monte Carlo step by

$$\rho(Z) = \frac{n_H(Z)}{n_S(Z)} \tag{9}$$

where $n_H(z)$ represents the number of residing hydrogen and where $n_S(z)$ is the total number of interstitial sites located in the z plan. The system is considered to be in an equilibrium state when the density $\rho(z)$ is uniform; i.e almost the same in all plans z. The equilibrium time, t_{eq} required to reach such equilibrium phase for different hydrogen concentration is the sum of the filling time t_f (the necessary time to introduce the chosen concentration of hydrogen) and the relaxation time t_r (the necessary time to have a homogeneous distribution of hydrogen in the system). We show, in Fig. 6, that t_{eq} increases with respect to the hydrogen concentration until reaching a maximal value corresponding to a concentration of hydrogen atoms close to 90% then it goes down. The same behavior has been observed for different values of temperature (Fig. 6). The increase of t_{eq} is completely obvious. More the hydrogen concentration is high more we need large time t_f to fill the tank. On the other hand, the necessary barriers for the displacement of hydrogen atoms get larger by increasing the hydrogen rate leading to an increment of the relaxation time t_r. We expect that the observed maximum is due to the collision of hydrogen atoms with the upper wall (z_{max}) since the boundary conditions have been applied only on *X* and *Y* directions and not on the *Z* direction. It turns out that the decrease of t_{eq} is due to the decrease of t_r which vanishes for $x = 100\%$ ($t_{eq} = t_f$). Thus, t_r vanishes when all interstitial sites in the supercell are occupied by hydrogen atoms.

4. Conclusion

In this paper, we have suggested a model to study the hydrogen storage ab/desorption kinetic properties for the pure MgH_2 using Kinetic Monte Carlo (KMC) simulations. Different process namely the absorption, desorption and diffusion have been taken into account and all corresponding activation energies have been calculated using ab-initio calculations. After having incorporated all the calculated thermodynamical quantities of interest in our algorithm, we investigated the hydrogen atom diffusion in magnesium hydride and studied the time of ab/desorption in MgH_2. The effects of each elementary mechanism on the diffusion that we characterized through density distribution of the hydrogen atoms, the filling ratios, the diffusion time, the temperature and pressure have been studied. We have shown, within KMC calculations, that the behavior of ab/desorption is in good agreement with the experimental results and the suggested material has slow kinetics at high temperature and pressure. Then, we have revealed that the equilibrium time exhibits a maximum at about 90% of the hydrogen atom rate to fill in the system whose relaxation time vanishes at very high hydrogen concentrations.

Acknowledgments

This work was supported by CNRST in the framework of the national program Dev-RS/04. The authors acknowledge its financial support.

REFERENCES

[1] Züttel A. Materials for hydrogen storage. Mater Today 2003;6:24–33.
[2] Zhou L. Progress and problems in hydrogen storage methods. Renew Sust Energ Rev 2005;9:395–408.
[3] Chen P, Zhu M. Recent progress in hydrogen storage. Mater Today 2008;11:36–43.
[4] Song MY, Kwon SN, Park HR, Hong SH. Improvement in the hydrogen storage properties of Mg by mechanical grinding with Ni, Fe and V under H_2 atmosphere. Int J Hydrogen Energy 2011;36:13587–94.
[5] Cabo M, Garroni S, Pellicer E, Milanese C, Girella A, Marini A, et al. Hydrogen sorption performance of MgH_2 doped with mesoporous nickel- and cobalt-based oxides. Int J Hydrogen Energy 2011;36:5400–10.
[6] Kurko S, Matović L, Novaković N, Matović B, Jovanović Z, Mamula BP, et al. Changes of hydrogen storage properties of MgH_2 induced by boron ion irradiation. Int J Hydrogen Energy 2011;36:1184–9.
[7] Gasan H, Celik ON, Aydinbeyli N, Yaman YM. Effect of V, Nb, Ti and graphite additions on the hydrogen desorption temperature of magnesium hydride. Int J Hydrogen Energy 2012;37:912–1918.
[8] Barkhordarian G, Klassen T, Bormann R. Catalytic mechanism of transition-metal compounds on Mg hydrogen sorption reaction. J Phys Chem B 2006;110:11020–4.
[9] Zhou D, Peng P, Liu J. First-principles calculation of dehydrogenating properties of MgH_2-V systems. Sci China Ser E 2006;49:129–36.
[10] Shang CX, Bououdina M, Song Y, Guo ZX. Mechanical alloying and electronic simulations of (MgH_2 + M) systems (M = Al, Ti, Fe, Ni, Cu and Nb) for hydrogen storage. Int J Hydrogen Energy 2004;29:73–80.
[11] Novaković N, Grbović Novaković J, Matović L, Manasijević M, Radisavljević I, Paskaš Mamula B, et al. Ab initio calculations of MgH_2, MgH_2:Ti and MgH_2:Co compounds. Int Int J Hydrogen Energy 2010;35:598–608.
[12] Bhihi M, Lakhal M, Labrim H, Benyoussef A, El Kenz A, Mounkachi O, et al. Hydrogen storage of $Mg_{1-x}M_xH_2$ (M = Ti, V, Fe, $0 \leq x \leq 0.1$) studied using first principles calculations. Chin Phys B 2012;21:097501.
[13] Yu R, Lam PK. Electronic and structural properties of MgH_2. Phys Rev B 1988;37:8730.
[14] Vajeeston P, Ravindran P, Kjekshus A, Fjellvag H. Pressure-induced structural transitions in MgH_2. Phys Rev Lett 2002;89:175506.
[15] Tsuda M, Diño WA, Nakanishi H, Kasai H. Ab initio study of H_2 desorption from magnesium hydride MgH_2 cluster. J Phys Soc Jpn 2004;73:2628.
[16] Song Y, Guo ZX, Yang R. Influence of selected alloying elements on the stability of magnesium A first-principles dihydride for hydrogen storage applications: investigation. Phys Rev B 2004;69:094205.
[17] Shang CX, Bououdina M, Song Y, Guo ZX. Mechanical alloying and electronic simulations of (MgH_2 + M) systems (M = Al, Ti, Fe, Ni, Cu and Nb) for hydrogen storage. Int J Hydrogen Energy 2004;73:29.
[18] Tsuda M, Diño WA, Kasai H, Nakanishi H. Magnetized/charged MgH_2-based hydrogen storage materials. Appl Phys Lett 2005;86:213109.
[19] Pozzo M, Alfè D, Amieiro A, French S, Pratt A. Hydrogen dissociation and diffusion on Ni- and Ti-doped Mg(0001) surfaces. J Chem Phys 2008;128:094703.
[20] Pozzo M, Alfè D. Hydrogen dissociation and diffusion on transition metal (=Ti, Zr, V, Fe, Ru, Co, Rh, Ni, Pd, Cu, Ag)-doped Mg(0001) surfaces. Int J Hydrogen Energy 2009;34:1922.
[21] Cheng F, Tao Z, Liang J, Chen J. Efficient hydrogen storage with the combination of lightweight Mg/MgH_2 and nanostructures. Chem Commun 2012;48:7334.
[22] Wang LL, Johnson DD. Hydrogen desorption from Ti-doped MgH_2(110) surfaces: catalytic effect on reaction pathways and kinetic barriers. J Phys Chem C 2012;116:7874.
[23] Koepernik K, Eschrig H. Full-potential nonorthogonal local-orbital minimum-basis band-structure scheme. Phys Rev B 1999;59:1743–57.
[24] FPLO Homepage, http://www.fplo.de/.
[25] Perdew JP, Burke K, Ernzerhof M. Generalized gradient approximation made simple. Phys Rev Lett 1996;77:3865–8.
[26] Bortz M, Bertheville B, Böttger G, Yvon K. Structure of the high pressure phase γ-MgH_2 by neutron powder diffraction. J Alloys Compounds 1999;287:L4–6.
[27] Kratzer P. Monte Carlo and kinetic Monte Carlo methods. ArXiv:0904.2556; 2009, ArXiv:0904.2556.
[28] Broom DP. Hydrogen storage materials: the characterisation of their storage properties. Springer; 2011.
[29] Vegge T. Locating the rate-limiting step for the interaction of hydrogen with Mg(0001) using density-functional theory calculations and rate theory. Phys Rev B 2004;70:035412.
[30] Du AJ, Smith SC, Yao XD, Lu GQ. First-principle study of adsorption of hydrogen on Ti-doped Mg (0001) surface. J Phys Chem B 2006;110:21747.
[31] Pozzo M, Alfe D. Hydrogen dissociation on Mg(0001) studied via quantum Monte Carlo calculations. Phys Rev B 2008;78:245313.
[32] Nakamura H, Nguyen-Manh D, Pettifor DG. Electronic structure and energetics of $LaNi_5$, α-$La_2Ni_{10}H$ and β-$La_2Ni_{10}H_{14}$. J Alloys Compounds 1998;281:81–91.
[33] Pozzo M, Alfe D. Structural properties and enthalpy of formation of magnesium hydride from quantum Monte Carlo calculations. Phys Rev B 2008;77:104103.
[34] Yamagychi M, Akiba E. In: Cahn RW, Haasen P, Kramer EJ, editors. Materials science and technology, vol. 3B. New York: VCH; 1994. p. 333.
[35] Patah A, Takasaki A, Szmyd JS. Influence of multiple oxide (Cr_2O_3/Nb_2O_5) addition on the sorption kinetics of MgH_2. Int J Hydrogen Energy 2009;34:3032–303.
[36] Zaluska A, Zaluski L, Ström-Olsen JO. Nanocrystalline magnesium for hydrogen storage. J Alloys Compd 1999;288:217–25.
[37] Zaluska A, Zaluski L, Ström-Olsen JO. Synergy of hydrogen sorption in ball-milled hydrides of Mg and Mg_2Ni. J Alloys Compd 1999;289:197–206.